ANALYSIS OF CYCLIC PERFORMANCE OF STIFFENED STEEL PLATE SHEAR WALLS

OMID HADDAD

FACULTY OF ENGINEERING
UNIVERSITY OF MALAYA
KUALA LUMPUR

2017

ANALYSIS OF CYCLIC PERFORMANCE OF STIFFENED STEEL PLATE SHEAR WALLS

OMID HADDAD

THESIS SUBMITTED IN FULFILMENT OF THE REQUIREMENTS FOR THE DEGREE OF DOCTOR OF PHILOSOPHY

FACULTY OF ENGINEERING
UNIVERSITY OF MALAYA
KUALA LUMPUR

2017

UNIVERSITY OF MALAYA

ORIGINAL LITERARY WORK DECLARATION

Name of Candidate: OMID HADDAD

Matric No: KHA100052

Name of Degree: Doctor of Philosophy

Title of Project Paper/Research Report/Dissertation/Thesis:

ANALYSIS OF CYCLIC PERFORMANCE OF STIFFENED STEEL PLATE SHEAR WALLS

Field of Study: Structure Engineering

I do solemnly and sincerely declare that:

(1) I am the sole author/writer of this Work;
(2) This Work is original;
(3) Any use of any work in which copyright exists was done by way of fair dealing and for permitted purposes and any excerpt or extract from, or reference to or reproduction of any copyright work has been disclosed expressly and sufficiently and the title of the Work and its authorship have been acknowledged in this Work;
(4) I do not have any actual knowledge nor do I ought reasonably to know that the making of this work constitutes an infringement of any copyright work;
(5) I hereby assign all and every rights in the copyright to this Work to the University of Malaya ("UM"), who henceforth shall be owner of the copyright in this Work and that any reproduction or use in any form or by any means whatsoever is prohibited without the written consent of UM having been first had and obtained;
(6) I am fully aware that if in the course of making this Work I have infringed any copyright whether intentionally or otherwise, I may be subject to legal action or any other action as may be determined by UM.

Candidate's Signature Date: 12/17/2018

Subscribed and solemnly declared before,

Witness's Signature Date:

Name:

Designation:

ANALYSIS OF CYCLIC PERFORMANCE OF STIFFENED STEEL PLATE SHEAR WALLS

ABSTRACT

Steel plate shear wall (SPSW) is a structural system, which is used to resist lateral loading such as wind and earthquake. SPSWs consist of a relatively thin steel plate connected to boundary columns and beams. The infill plates can be stiffened or un-stiffened. The main objective of this research is to study the behavior and energy absorption of stiffened SPSW with various configurations of stiffeners under lateral loading. Experimental and numerical methods were deployed to achieve the main objectives. In experimental study, five quarter scale specimens were tested. Two specimens were un-stiffened and, three specimens were stiffened with cross, circular and diagonal stiffeners on one side of steel infill plate. The cross-section areas of stiffeners were kept constant. A comparison of the predicted behavior of five FE model with the experimental test results indicated that the finite element method is able to provide a reliable prediction of the overall behavior of SPSWs subjected to cyclic loading. Using the parametric studies on the FE models, the behavior and sensitivity of cyclic performance to the value of different slenderness of infill plate, thickness of stiffeners and their position on the SPSWs were investigated. It was found that the energy dissipation, seismic performance factors and cyclic performance of stiffened SPSWs were not sensitive to the stiffeners thickness and their configuration. One-side cross-stiffened models and double-side diagonally stiffened models exhibit considerable increases in the strength compared to the un-stiffened infill plate. Furthermore, using the stiffeners resulted in 30% increase in the ductility reduction factor and 20% increase in the response modification factor for stiffened SPSWs.

Keywords: steel plate Shear wall, cyclic loading, stiffener, finite element model, seismic performance factors

PENYIASATAN PADA PRESTASI CYCLIC BAJA KELULIAN BAJA STEEL

ABSTRAKT

Dinding ricih plat keluli (SPSW) adalah sistem struktur, yang digunakan untuk menahan beban sisi seperti angin dan gempa bumi. SPSW terdiri daripada plat keluli yang agak nipis yang disambungkan kepada lajur dan balok sempadan. Plat infill boleh menjadi kaku atau tidak tegar. Objektif utama penyelidikan ini adalah untuk mengkaji tingkah laku dan penyerapan tenaga SPSW yang sengit dengan pelbagai konfigurasi pengukuh di bawah beban sisi. Kaedah eksperimen dan berangka telah digunakan untuk mencapai matlamat utama. Dalam kajian eksperimen, lima spesimen skala suku telah diuji. Dua spesimen adalah plat aluminium dan keluli yang tidak tegar, manakala tiga spesimen yang lain diperketatkan dengan silang, pekeliling dan pepenjuru pepenjuru di satu sisi plat infill keluli. Kawasan keratan rentas keratan terus dipelihara. Perbandingan tingkah laku yang diramalkan daripada lima model FE dengan keputusan uji eksperimen menunjukkan bahawa kaedah elemen terhingga dapat memberikan ramalan yang boleh dipercayai terhadap tingkah laku keseluruhan SPSWs yang tertakluk kepada pemuatan kitaran. Menggunakan kajian parametrik pada model FE, tingkah laku dan kepekaan prestasi siklik terhadap nilai kelembapan yang berlainan pada pinggan infill, ketebalan pengetus dan kedudukannya pada SPSWs telah disiasat. Telah didapati bahawa pelesapan tenaga, faktor-faktor prestasi seismik dan prestasi kitaran bagi SPSWs yang tegar tidak sensitif kepada ketebalan dan konfigurasi mereka. Model satu-sisi rentas tegar dan model dua belas yang berserabut mempamerkan peningkatan yang ketara dalam kekuatan berbanding plat infill yang tidak sengit. Selain itu, menggunakan faktor pengukuh menyebabkan peningkatan 30% dalam faktor pengurangan kemuluran dan peningkatan 20% dalam faktor pengubahsuaian tindak balas untuk SPSW yang tegar.

Kata kunci: plat keluli Lembaran geseran, pemuatan cyclic, stiffener, model unsur terhingga, faktor prestasi seismik

ACKNOWLEDGEMENTS

I would like to offer my sincere thanks to who helped me during the completion of this thesis. Their assistance is highly appreciated, and without their valuable cooperation, I was unable to accomplish my research. To my late mother and my wife, Bayan, I offer my gratitude for their encouragement and support.

I would like to thank both supervisors (Dr. Hafizah Ramli and Dr. Zainah Ibrahim) for their support and valuable guidance during my study. In addition, the UMRG Program Research Grant (Project number RG 142-12AET) and PPP Grant (Project number PV060/2011A) from the University of Malaya, Kuala Lumpur, Malaysia, provided funding support for the experimental program of this research.

TABLE OF CONTENTS

LIST OF FIGURES

LIST OF TABLES

LIST OF SYMBOLS AND ABBREVIATIONS

a	infill plate length
A_b	cross-sectional areas of the storey beam
A_c	cross-sectional areas of the storey column
a_{subp}	subpanel length of stiffened infill plate
b_{subp}	subpanel width of stiffened infill plate
BI	damping factor
C_d	displacement amplification factor
D	Diameter of the circular perforation
d	height of the panel
E	modulus of elasticity
E_I	internal energy
E_{FD}	frictional energy
E_{KE}	kinetic energy
E_V	energy absorbed by viscous dissipation
E_{TOTAL}	total energy
E_W	work done by external forces
F_{yp}	yielding stress of infill plate
F_u	ultimate stress of infill plate
h	frame storey height
h_n	height of the building calculated from the base to top level
h_s	height of the stiffeners
I_c	moment inertia of column
I'_{st}	moment of inertia for stiffeners cross section computed from the mid of infill
K	horizontal force factor (chapter 2)
K	shear buckling coefficient (chapter 3)
K_{Panel}	stiffness of the solid steel panel
K_{pref}	stiffness of the perforated steel panel
L	frame bay width
L_c	clear distance between the holes

L_e	distance of center holes to the free edge
m	mass
M_{fp}	bending moment due to normal stresses associated with the tension field on the boundary frame members
P_{cr}	critical shear load
P_{si}	resultant force from infill plate yielding
R	response modification factor
R_S	strength factor
R_R	redundancy factor
R_μ	ductility reduction factor
R_ξ	damping factor
S	distance between the holes
s	smaller value between the subpanel length a_{subp} and subpanel width, b_{subp}
S_{diag}	diagonal strip width
T	fundamental period of the vibration
t_p	the infill plate thickness
t_s	thickness of stiffeners
t_{wi}	thickness of infill plate
V	design base shear
V_E	base shear force calculated by elastic analysis (base shear force exerted on a structure if it remained entirely elastic
V_y	base shear force at yielding of structure
V_{yp}	ultimate shear strength of the solid steel panel
$V_{yp.perf}$	ultimate shear strength of the perforated steel panel
V_S	base shear force at first plastic hinge
V_W	design base shear force
W_{xci}	web tension stresses component
W_{yci}	web tension stresses component
x	number of horizontal or vertical stiffeners
Y	allowable stress factor
α	angle of inclination of the tension strips calculated from vertical

Δ_m	target displacement
Δ_U	ultimate displacement
Δ_y	yielding displacement
Δt_{stable}	stable time increment
Δ_S	displacement at first plastic hinge
δ_y	yielding stress of infill plate
δ_{ty}	yielding stress of infill plate
δ_{nom}	nominal (engineering) stress obtained from tensile test
δ_{true}	true stress
θ	angle of inclination of tension field stress from vertical
φ	aspect ratio of subpanel of stiffened infill plate
μ	ductility of the structure
ρ	density of the material
Ωo	over strength factor
ω_{max}	highest frequency of the system
ε_{ln}^{pl}	logarithmic plastic strain
ε_{nom}	nominal (engineering) strain obtained from tensile test
ω_h	column flexibility parameter
ξ	fraction of critical damping

Angle of inclination	Tension field inclination
DSPW	Ductile Steel Plate Wall
FE	Finite Element
Infill plate	Sheet plate surrounded by boundary frame member
LYS	Low Yield Steel
M-PFI	Modified Plate Frame Interaction
PFI	Plate Frame Interaction
SPW	Steel Plate Wall
SPSW	Steel Plate Shear Wall
SPF	Seismic Performance Factor

CHAPTER 1: INTRODUCTION

1.1 GENERAL

Steel plate shear walls (SPSW) are a structural system which resists lateral loading (wind, earthquake and explosion) forces. The concept of using the SPSW as the main lateral loading resisting element in a building structure appeared in the 1970's. SPSW consist of infill steel panels (a relatively thin steel plate) connected to boundary columns [Vertical Boundary Elements (VBEs)], and beams [Horizontal Boundary Elements (HBEs)] over the full height of the frame. They have been used in a large number of building structures in the United States, Canada, Mexico, Japan, Taiwan and other countries.

The infill plates can be stiffened or unstiffened. In addition, the surrounding steel frame may use either simple or moment resisting beam-to-column connections. A properly designed SPSW has high ductility and strength, high initial stiffness, excellent energy dissipation capacity and stable hysteresis characteristics. These specifications make them a good choice for high-risk earthquake zones. In comparison to commonly used reinforced concrete shear walls, SPSWs are much lighter, which reduces the gravity loads and seismic loads to be transferred to the foundation. Furthermore, the use of SPSW allows for the use of a single trade on site, the steel erection crew, which is a benefit compared to reinforced concrete shear walls with steel frames. These considerations can significantly reduce construction costs. Because of their simple and fast construction, SPSWs have also been used in strengthening of existing steel and concrete structures. When compared to

braced frames and moment resisting frames, SPSWs incorporate all the advantages of both systems without the disadvantages.

The design philosophy for SPSWs prior to the 1980s was to prevent shear buckling of the infill plate by using either thick infill plates or by adding stiffeners to the infill plate. After the work of Thorburn et al. (1983), the design philosophy in most building standards changed to the use of thin unstiffened infill plates. In SPSWs with thin unstiffened infill plates, axial coupling of column loads is the principal mechanism for resisting the overturning moment, while the shear is resisted primarily by a diagonal tension field that develops in the infill plates after they have buckled. This design philosophy is adopted in the current Canadian (CAN/CSA-S16-01) and American (AISC 2005) steel design standards.

Both the American and Canadian steel design standards require SPSWs to be designed according to a capacity design approach. The capacity design of structures involves pre-selecting a localized ductile fuse/s to act as the primary location for the dissipation of seismic energy. The structure must be designed so as to force the inelastic action to be concentrated at that fuse/s. In SPSWs, yielding in the infill plates and plastic hinging at the end of the beams are considered as the ductile fuses.

Based on capacity design principles, AISC 2005 enlisted three different capacity design approaches for the design of SPSWs. These are nonlinear pushover analysis; indirect capacity design approach, adopted from CAN/CSA-S16-01; and combined linear elastic computer programs and capacity design concepts. Berman and Bruneau (2008) proposed another capacity design method for the design of boundary columns. These capacity design methods have never been studied under real seismic loadings and, thus, there is a need

for seismic evaluation of all the capacity design approaches available in the literature.

1.2 PROBLEM STATEMENT

Despite the work done so far for design and analysis methods of SPSWs and excellent performance of SPSWs, increasing acceptance of the SPSWs for lateral load bearing system is limited relative to the other structural system. The reasons can be categorized in the below:

The minimum infill plate thickness required for handling and welding purposes may be thicker than that required for a seismic design. When the capacity design approach is used, the thicker plate will induce relatively large design forces on the surrounding frame members, requiring larger beams and columns to develop the yield capacity of the infill plate. In order to overcome this problem and the practical concern for utility placement to pass through an opening in the infill plate, circular openings can be made in the infill plate. Therefore, there is a need to find a viable solution for having openings in the infill plates in any location which is necessary, because all standards involve only flat infill plate. However, since the thickness of the infill plate is thin, and they are very vulnerable to fire, they need to be protected from the fire.

The main concerns are the analysis procedure of the whole structure due to seismic load, which is the method for calculating lateral earthquake load that should be applied to the structure and then to the SPSWs. The seismic force resisting system is designed to resist the induced forces and dissipate the energy causing the acceleration of the structures. Among several procedures for seismic force calculation, the Equivalent Lateral Force (ELF) procedure and the Modal Analysis procedure (Response Spectrum Analysis) due to the

simplicity and reasonable result are accepted widely by structural designers. Both analysis procedures use four important seismic factors; the Response Modification coefficient, R: the Over-strength Factor, Ω_0; the Deflection Amplification Factor, C_d; and the Reliability or Redundancy Coefficient, Rμ. These parameters are included in both Canadian (CAN/CSA-S16-01) and American (AISC 2005) steel design standards but only for flat SPSWs and there isn't any parameter for SPSWs with opening or stiffener.

Vian (2005) conducted experimental work on a pattern of multiple regularly spaced circular perforations in the infill plate, and Purba (2006) proposed an equation to determine the shear strength of a perforated infill plate with the specific perforation pattern proposed by Vian (2006). They have investigated the methodology and behavior of SPSWs, however, further work is needed to determine the overall parameters for the calculation of lateral loading for the structural systems that include SPSWs. In addition, current design codes (NBCC 2005, NEHRP 2003) provide the same period formula for seismic design for both reinforced concrete shear walls and SPSWs, which are known to have different dynamic properties. Hence, this empirical period formula needs to be evaluated.

The research described herein includes investigation and derivation of proper response modification coefficient and over strength factor for SPSWs with different stiffeners. Furthermore, because of the high expenses involved in the full experimental programs to evaluate the capacity design methods, an analytical or numerical tool that can accurately predict the monotonic, cyclic and dynamic behavior of SPSWs is also needed.

1.3 RESEARCH OBJECTIVES

The main objective of this research is to study the behavior and energy absorption of stiffened SPSW under lateral loading. The specific objectives of this study include:

1) To examine experimentally the behavior of stiffened SPSWs with different stiffeners configurations in terms of elastic stiffness, energy absorption and cyclic behavior of stiffened SPSWs, and propose the best configuration of the stiffeners.
2) To develop finite element model for stiffened SPSWs with different stiffeners configurations under the effect of cyclic and monotonic displacement.
3) To investigate the effect of geometric properties of stiffened SPSWs with different stiffeners configurations on the cyclic behavior of stiffened SPSWs through parametric studies.
4) To propose seismic performance factors (response modification factor, over strength factor, ductility reduction factor and displacement amplification factor) of stiffened SPSWs with different stiffeners configurations.

1.4 SCOPE AND LIMITATION OF THE RESEARCH

In the experimental part of this research, five (5) quarter-scale tests on the single-story SPSWs specimens were conducted under quasi-static cyclic loading. The aspect ratio of all the specimens was equal to unit. In the second phase of this study, a nonlinear finite element model was developed in order to simulate accurately the monotonic and cyclic behaviors of the SPSWs. The validated numerical model was then used for a parametric study of the SPSWs.

Therefore, the presented results described here are limited to the single story SPSW with aspect ratio equal to unit. The variations involved are the infill plate thickness, stiffeners configuration and their location.

1.5 THESIS OUTLINE

This thesis comprises of six (6) chapters. Chapter 1 introduces the study involve in the thesis with some research background, objectives, problem statement and scope of the thesis.

To understand the research that has been done on the steel shear walls, a detailed study of the literature is crucial. A review of previously available research on the SPSWs is summarized in Chapter 2. The definition of seismic performance factors and selected methodology is also described in this chapter.

Chapter 3 describes the design of the five (5) specimens of SPSWs that was used for the experimental test. The details of the five specimens is described in this chapter. The results of the quasi-static cyclic test that have been conducted on the designed specimens are also presented in this chapter. Based on the output of the experimental program, the behavior of the five specimens is compared. The comparison was done in the aspect of overall performance, hysteresis curves, load-displacement curves, elastic stiffness, ultimate strength and energy dissipation. In addition, the analytical method for the analysis of steel plate shear walls, known as the plate frame interaction (P.F.I) method, has been evaluated based on the experimental test results.

In Chapter 4, the necessary technique for finite element modeling of the tested specimens is described. Using the experimental results, the numerical models of the five specimens were validated. It was concluded that the performance of the specimens successfully captured by FE models, therefore,

the obtained technique of FE modeling was used as a basis for parametric study in Chapter 5.

In Chapter 5, twenty two (22) FE models covering the objective of the present study, was analyzed under monotonic and cyclic loading. For deep investigation, all necessary data was collected from these FE models. Based on the stiffeners configuration, the performance of all models was compared in detail and the advantages of every stiffeners configuration were described. The seismic performance factors calculated for all FE models were also described in this chapter. The sensitivity of the seismic performance factor to the objective of the parametric study investigated and tentative values for the seismic performance factors of the stiffened models were proposed.

Finally, conclusions and recommendations for future research in SPSWs are given in Chapter 6.

CHAPTER2: LITERATURE REVIEW

2.1 INTRODUCTION

Structural systems are designed to sustain two types of loads; gravity and lateral loads. Gravity loads include the self-weight of the building and its contents, while lateral loads result from the action of wind, seismic and blast forces on the building. The latter has prime importance in the design of buildings with greater height-to-width ratio, where wind loads are significant, and also for buildings built in areas of high seismic risk.

Steel Plate Shear Wall (SPSW) is a structural system, which resists lateral loading (wind, earthquake and explosion) forces. Sometimes, the term steel shear wall (SSW) or steel plate wall (SPW) can be used to refer to it.

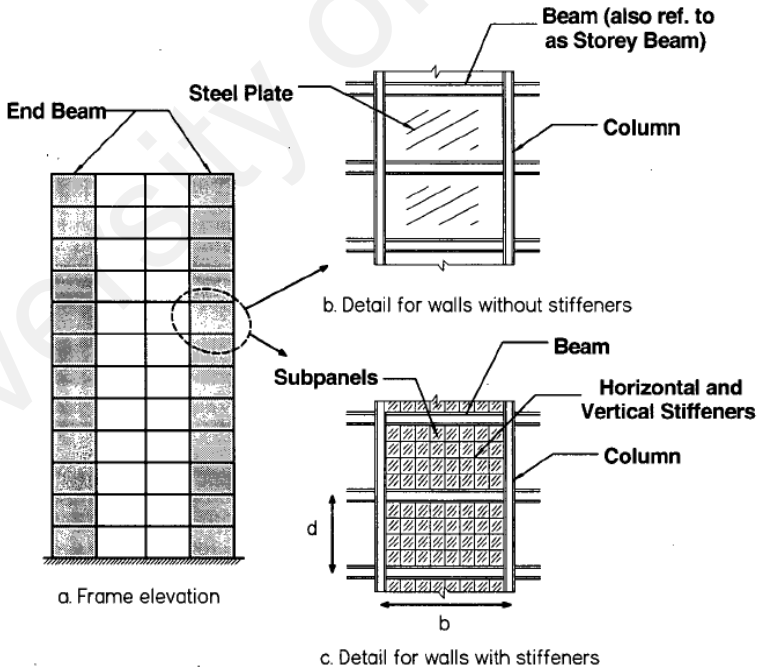

Figure 2-1 Unstiffened and Stiffened steel plate wall (Kharazi, Oct 2005)

The concept of using the SPSWs as the main lateral loading resisting element in a building structure appeared in the 1970s. It has been used in a large number of building structures in the United States, Canada, Mexico, Japan, Taiwan and other countries. SPSWs consist of infill steel panels (a

relatively thin steel plate) that are connected to boundary columns, called Vertical Boundary Elements (VBEs), and beams, called Horizontal Boundary Elements (HBEs) over the full height of the frame. The infill plates can be stiffened or unstiffened. In addition, the surrounding steel frame may use either simple or moment resisting beam-to-column connections; i.e., the connection may only transfer shear forces or a combination of shear and bending moment respectively (Figure 2-1 and Figure 2-2).

In earlier days, SPSWs were treated like vertically-oriented plate girders, in which the infill steel plates perform as the web, the columns represent as parallel flanges and the story beams act like stiffeners (Figure 2-3). Although the plate girder theory seems appropriate for the SPSW design, the presence of axial forces and the relatively high bending strength and stiffness of the beams and columns that form the boundary elements of the wall, make the SPSW different from the plate girders. These boundary members are

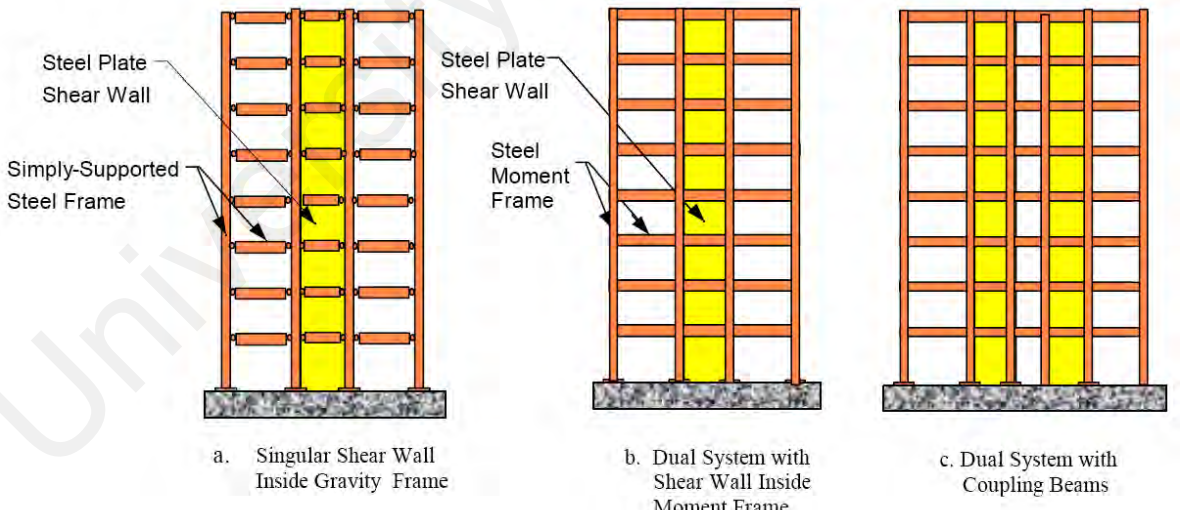

Figure 2-2 typical shear wall system

expected to have a significant effect on the overall behavior of a building incorporating this type of system and several researchers have focused on this topic of SPSWs.

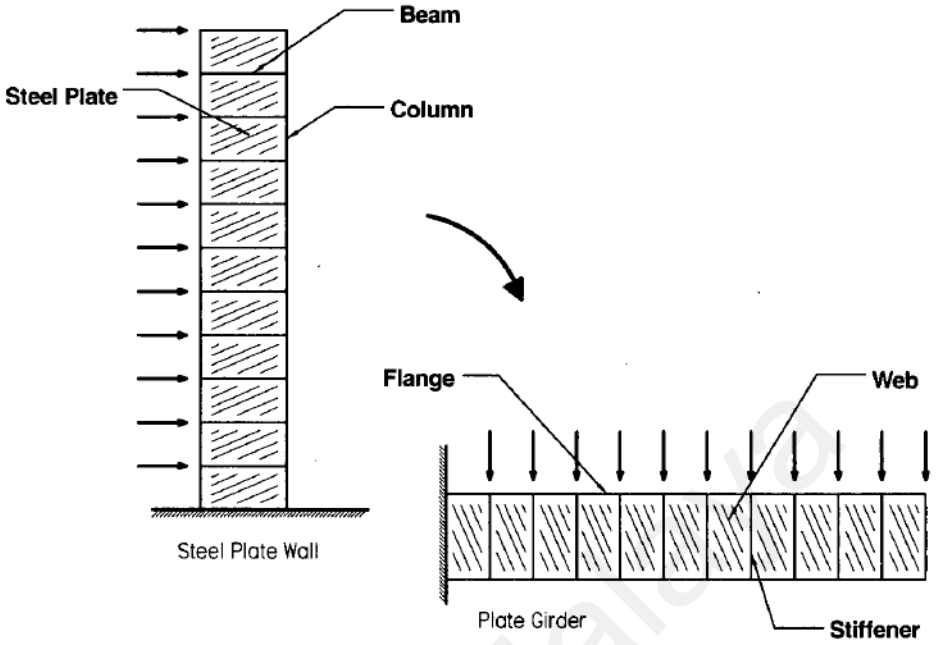

Figure 2-3 steel plate wall idealized as a vertically oriented cantilever plate girder

A properly designed SPSW has high ductility and strength, high initial stiffness, excellent energy dissipation capacity and stable hysteresis characteristics. These specifications make them a good choice for use in high-risk earthquake zones. In comparison to commonly used reinforced concrete shear walls, SPSWs are much lighter, which reduces the gravity loads and seismic loads to be transferred to the foundation. Furthermore, the use of SPSWs allows for the use of a single trade on the site, the steel erection crew, which is a benefit compared to reinforced concrete shear walls with steel frames. These considerations can significantly reduce construction costs. Because of their easy and fast construction, SPSWs have also been used in strengthening existing steel and concrete structures. When compared to braced frames and moment resisting frame, SPSWs incorporate all the advantages of both these systems without the disadvantages.

Before the 1980s, the design philosophy for SPSWs was to prevent shear buckling of the infill plate by using either thick infill plates or by adding

stiffeners to the infill plate. After the work of (Thorburn et al., 1983), the design philosophy in most building standards changed to the use of thin unstiffened infill plates. In SPSWs with thin unstiffened infill plates, the axial coupling of column loads is the principal mechanism for resisting the overturning moment, while the shear is resisted primarily by a diagonal tension field that develops in the infill plates after they have buckled. This design philosophy was adopted by current Canadian (CAN/CSA-S16-01) and American (AISC 2005) steel design standards.

The advantages of SPW among other structural systems can be listed as follows:

- The well designed and constructed SPSWs have very ductile behavior with stable hysteric behavior and can dissipate significant energy. These specifications make them very appropriate for high-risk earthquake zones.
- Owing to the formation, the tension field action in the infill plate, the SPSW has significant initial stiffness, which is very effective for limiting wind drifts; because the tension field performs like diagonal braces.
- SPSWs have lower weight compared to the concrete shear wall. This can reduce the demand on columns and foundation. Furthermore, as the seismic load is proportional to the mass, this can reduce the seismic loads.
- The construction process of an all-steel structure can be significantly faster compared to the reinforced concrete structures and by using SPSWs allows for the use of a single trade on the site. The steel erection

crew, can use this advantage to decrease the erection and construction costs of the project.

- The field inspection process and quality control can be improved by using shop-welded, field bolted SPSW.
- Structural elements occupy a considerable area in the lower floor of high-rise concrete buildings, by using SPWs the cross section of shear walls that decrease, Therefore, the area of the floor can be saved and this is an advantage for architects.
- Construction of the concrete structure in a cold region can be complicated and expensive. Steel construction using SPSWs can be an appropriate solution for overcoming this problem.
- For seismic retrofitting of structures, simple, convenient and rapid methods are vital, which make the SPWs a favorable option for this purpose.
- Properly designed SPWs act like fuse, that prevents the plastic hinges from forming in the columns. These serve as sacrificial elements to protect the frame elements, thus enabling the in-filled panels in the structural frames to be easily repaired afterwards.

Some of the advantages of using SPSWs compared to the conventional bracing system are:

- Neglecting the limitations of using conventional bracing system relating to the allowable height of the structures, using the conventional bracing seems to be non-economical and un-reasonable for high-rise buildings (Figure 2-4).
- Compared to bracing system, SPSW has the advantages of economy, rapid and easy constructability, fewer detailing requirements. Whereas

most of the bracing system needs special details and technologies which some time need particular training for crews.

- SPSW has stable ductile behavior relative to singular bracing element (Figure 2-5).

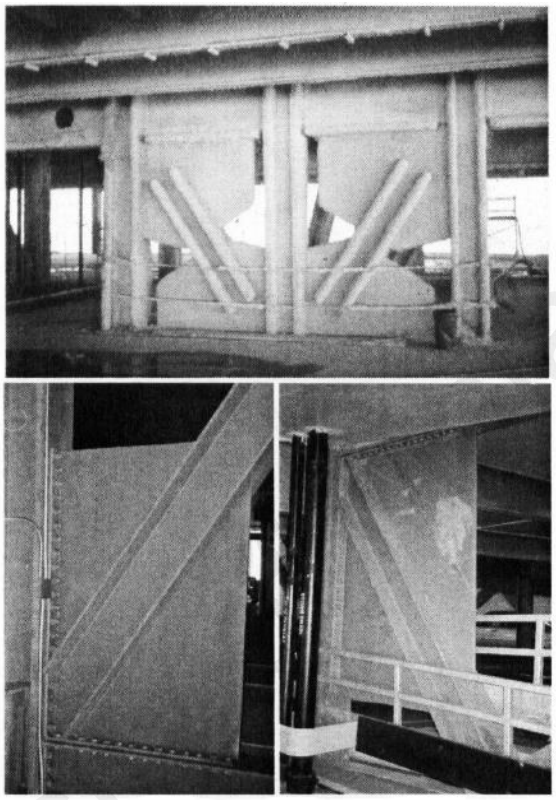

Figure 2-5 Example of excessive brace connection in high rise building ((Kharazi et al., 2005)

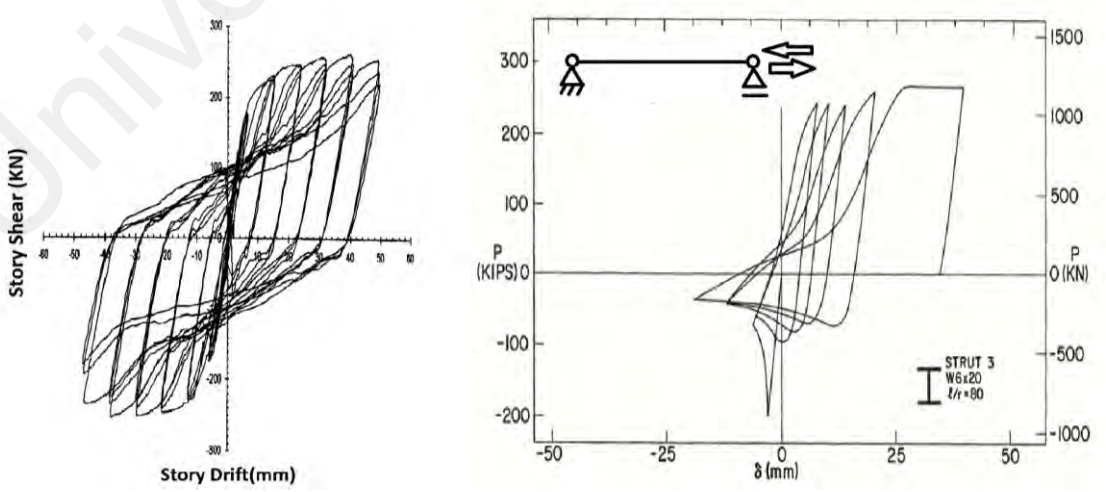

Figure 2-4 Comparison of hysteric curve for SPW (left) and singular bracing element (right) (Lubell et al., 2000)

In general, SPSWs are categorized based on their performance, selection of structural and load-bearing system, and the presence of perforations or stiffeners.

2.2 PREVIOUS RESEARCH

Brief summaries of experimental and analytical studies of steel shear walls conducted by researchers in the world who have studied the pre- and post-buckling of SPWs are listed in the following:

2.2.1 Pioneering Research on SPSWs

To investigate the behavior of stiffened thin plated SPSWs and comparing its performance with the stiff concrete shear walls, Takahashi et al. (1973) conducted a series of experimental and numerical research. They considered the two phases by conducting quasi-static cyclic tests. In the first phase, 12 one-story quarter scale specimens and in the second phase, 2.0 two-story full-scale one bay specimens were tested.

The overall width and height of the specimens of the first phase were equal to 2100 mm and 900 mm respectively and, the investigated parameters were the spacing and width of stiffeners on both sides or one side of the steel panel together with the strength, hysteric curve and post-buckling behavior of the steel panels. Except for one specimen, all other specimens had only vertical or horizontal and vertical stiffeners welded on one or both sides of the infill plate. The boundary frame consists of pine connected stiff members (which allow the members to rotate but the connection could not resist the moment) to create a pure shear force in the infill plates, as all the specimens were cyclic loaded along their diagonal direction. The results of the first phase showed that

all the specimens were able to undergo large deformation with ductile and stable behavior. The specimens with stiffeners on both sides exhibited better performance compared to those SPSWs with one side stiffeners. In most specimens, the hysteric curves were S-shaped except for a few cases where specimens were heavily reinforced with stiffener (Figure 2-6).

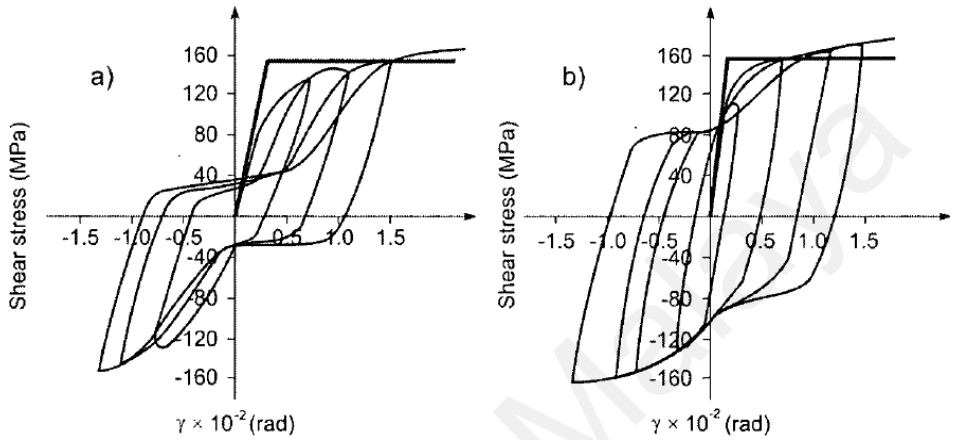

Figure 2-7 Hysteric behavior of a) unstiffened and b) heavily stiffened steel plate wall (Takahashi et al., 1973)

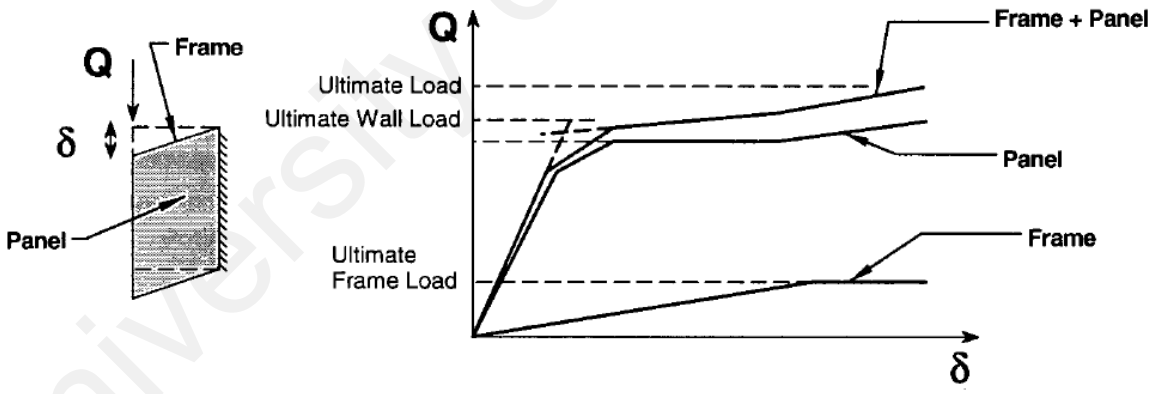

Figure 2-6 Monotonic load-displacement behavior of an SPW showing contributions by frame and web plate by Mimura and Akiyana (1977)

Using the outcomes of the first phase and in the connection to a proposed 32-stories practical building design, Takahashi et al. (1973) designed the test specimens of the second phase. The loading included the cyclic horizontal on two full-scale one bay SPW specimens. The selected design criterion ensured achievement of a full shear yield strength before the occurrence of global out-of-plane buckling. However, the buckling of the sub-panel was accepted once the elastic limit of the infill panel was exceeded.

Takahashi et al. (1973) concluded that the conventional shear theory, where the horizontal shear is transferred by beam action alone, can be used to measure the stiffness and yield strength of the stiffened shear panels, and using this method leads the development of shear yield strength of the subpanel before buckling of the infill plates.

Mimura and Akiyana (1977) proposed an analytical method to predict the cyclic and monotonic behavior of steel shear walls. In the proposed model, the overall strength of SPSWs was assumed to be calculated by the load required to produce elastic buckling in the infill panels in addition the post-buckling strength of the infill plate and boundary frame. To evaluate the buckling shear load of infill plate, the simply supported boundary condition was assumed. In the case of the loads beyond the elastic critical-buckling limit, it was assumed the applied load could be resisted by tension field action. Based on the research done by Wagner (1931), they proposed an equation to compute the angle of inclination. Figure 2-7 shows that the proposed monotonic load-displacement behavior of an SPW, established based on the elastic-perfectly plastic behavior of materials. Based on the load-displacement behavior, a theoretical hysteresis model was developed as shown in Figure 2-8.

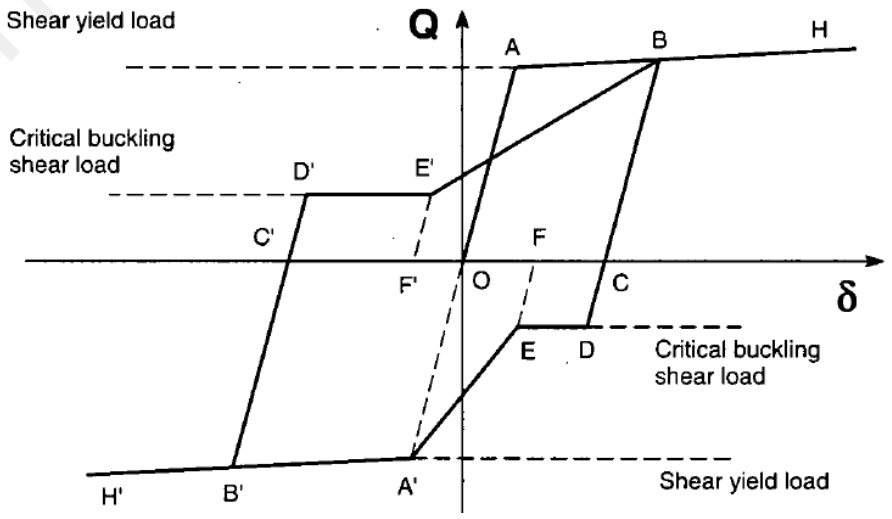

Figure 2-8 Hysteresis model for SPSWs as proposed by Mimura and Akiyana (1977)

Based on Wagner's theory of pure diagonal tension (Wagner, 1931), Thorburn et al. (1983) introduced an analytical method for unstiffened SPWs. Considering that the theory of pure diagonal tension neglected the shear forces suffered by un-buckled infill plate, the analytical models were found to be unable to estimate the pre-buckling shear forces. In the well-defined model, known as the "strip model", the infill plate was replaced by a series of pin-ended inclined strips in the corresponding direction of principal tensile stress in the infill plate. These strips are just able to transmit the tension forces. The sectional area of each strip is equal to the infill plate thickness multiplied by the width of the strip. For one-story one-bay steel plate, which is confined by columns and beams under pure shear, and by using the principle of least work, the angle of inclination of the tension strips was derived as the equation (2-1).

$$\boldsymbol{tan^4\,\alpha} = \left[\frac{1+\frac{L\,t_p}{2\,A_c}}{1+\frac{h\,t_p}{A_b}}\right] \qquad (2\text{-}1)$$

where L is the frame bay width, h is the frame story height, t_P is the infill plate thickness and A_b and A_c are cross-sectional areas of the story beam and column, respectively.

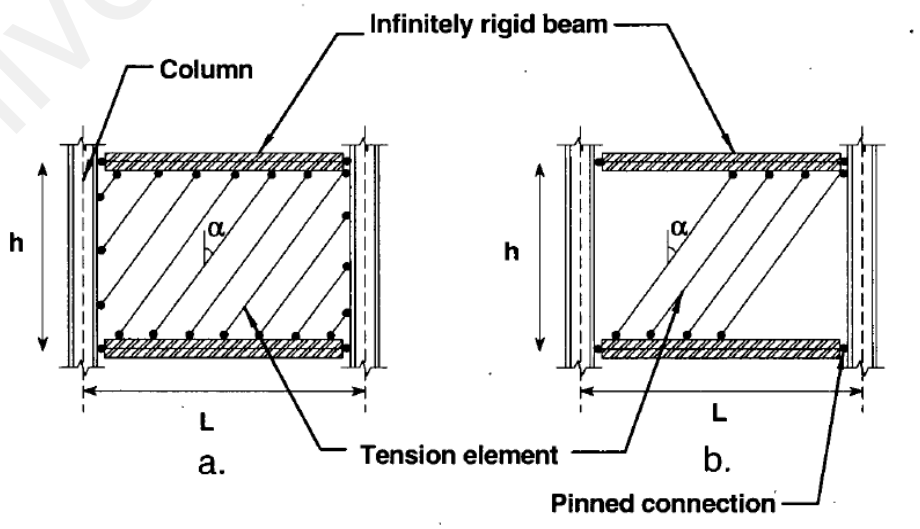

Figure 2-9 Strip model for modeling SPWs by Thourburn et al.(1983) for a)complete tension field action, and b)partial tension field action.

The model includes the infinite rigid beams which were pinned to continuous columns. Two extreme cases were considered for column's rigidity (Figure 2-9). The first case involves the infinite stiff columns, which ensures a uniformly distributed tension field over the entire panel. In the second case, the columns were completely flexible which resulted to no anchorage to form the tension field zones. The researchers also conducted a parametric study to investigate the influence of infill plate thickness, panel width, panel height, and column stiffness on the strength and stiffness of the panel. The study showed that the parameters studied are interrelated and can influence the resulting tension field.

To evaluate the strip model proposed by Thorburn et al. (1983), Timler and Kulak (1983) tested a large-scale single-story SPSW specimen. Without the presence of gravity loads, the specimens were tested three times under cyclic loading to its maximum serviceability drift limit, and it was then further tested under monotonic loading to failure (Figure 2-10). The built-in joints for the interior beam-to-column connections and true pin-joints were considered

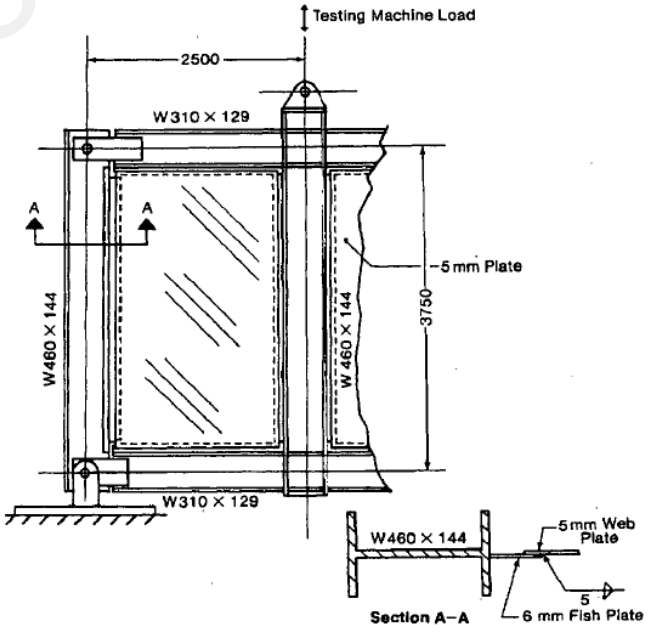

Figure 2-10 SPW configuration tested by Timler and Kulak (1983)

for exterior beam-to-column connections.

The researcher found that, at the yield load level, the overall distribution and magnitude of principal stress along the center-line of infill plate were close to the analytical results. However, the difference in the angle of inclination of principal stress along the center-line of the infill plate became considerable as it approached the ultimate shear strength. Despite the ultimate strength was affected by the failure of fish plates welding but, based on the obtained load-displacement curve, the ductility of 3.5 and over-strength factor of more than 2 were reported. The researcher concluded that the simplified analytical strip model, developed by Thorburn et al. (1983), was satisfactory in predicting the overall load deflection response of the specimen, although the predicted elastic stiffness of the specimen was slightly higher than the measured value. By considering the bending effect of columns, Timler and Kulak (1983), derived a formula to calculate the angle of inclination of the tension strips in the multi-story system, as shown in Equation 2-2. This equation was later implemented in Appendix M of Canada's national standards on Limit States Design of Steel Structures, CAN/CSA-S14-S16.1-94 (1994).

$$\boldsymbol{tan^4\,\alpha} = \left[\frac{1+\frac{L\,t_p}{2A_c}}{1+h\,t_p\left(\frac{1}{A_b}+\frac{h^3}{360\,I_c\,L}\right)}\right] \qquad (2\text{-}2)$$

To verify the inclined tension-bar model proposed by Thorburn et al. (1983), a full-scale single-story unstiffened SPW specimen was tested under quasi-static, fully reversed cyclic and monotonic loading (pushover loading) by Tromposch and Kulak (1987). This specimen was similar to the SPW tested by Timler and Kulak (1983), but with different dimensions and configurations. To stimulate the effect of gravity loads applied to the structure, an axial pre-load was applied to the columns by high strength pre-stress rods anchored at both ends of the columns, which was removed at the monotonic loading stage. The

inclined tension bar model was found to be adequate in predicting the strength and ultimate capacity of unstiffened SPSW specimen. The effect of beam-to-column connection, initial column axial-loads, and residual stress induced in the infill plate due to the welding process was significant when predicting the load-displacement response of the SPW panel.

The hysteresis loops developed by the specimen were pinched but remain stable. To predict the hysteresis behavior of an unstiffened SPW, an analytical method was developed based on the model described by Mimura and Akiyana (1977) as shown in Figure (2-11).

Based on further parametric studies it was concluded that frames with fixed beam-to-column connections could dissipate as much as three times more energy as that dissipated by frames with simple pinned beam-to-column connections. The benefits of post-buckling strength and the relatively stable hysteresis characteristics of unstiffened thin steel panel were clearly demonstrated.

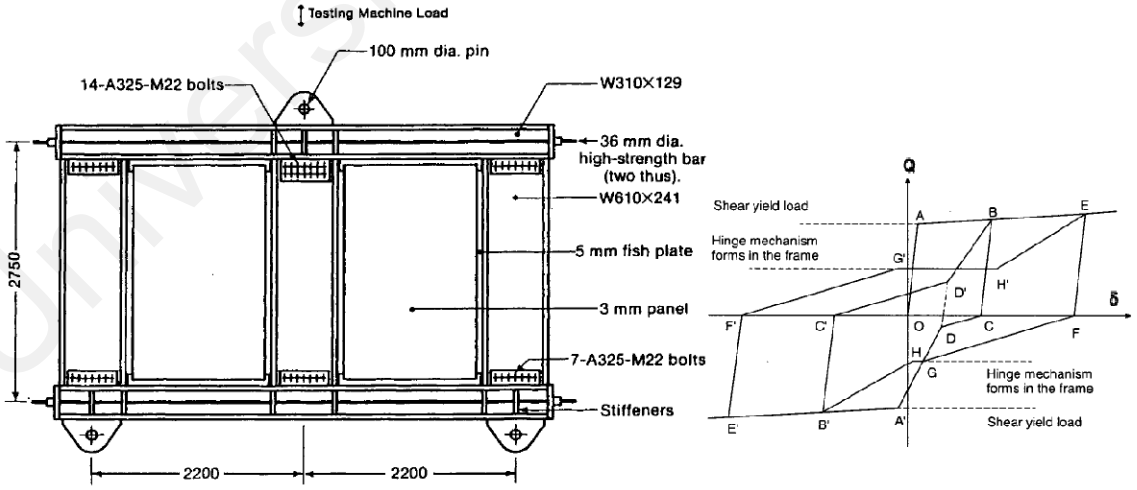

Figure 2-11 SPW specimen tested (left) and Hysteresis model proposed (right) by Tromposh and Kulak (1987)

To investigate the hysteresis characteristics, Roberts and Sabouri-Ghomi (1991) performed a series of tests on small-scale unstiffened steel plate shear panels with and without the opening. The opening was of circular shape

which was located in the center of the panel. Quasi-static cyclic loading tests were conducted on sixteen specimens with panel dimensions of either 300 by 300 mm or 450 by 300 mm, panel thickness of either 0.54 mm, 0.83 mm or 1.23 mm, with 0.2% to offset the yield stress value of either 152 MPa or 219 MPa, and diameter of the central circular openings *D* of 60, 105, or 150 mm. The plate edges of the panel were clamped by two rows of 8 mm diameter high-tensile bolts between pairs of rigid pin-ended frame members. Each panel was tested by applying tension or compression loads in the diagonal direction of the panel at two diagonally opposite corners, which was pinned together. All panels exhibited a stable but pinched hysteresis loop and the ductility value of the specimens reached more than 7. The schematic of the test specimen is shown in Figure 2-12. The results were compared with the results presented in Roberts and Sabouri-Ghomi (1991) findings for a similar specimen but with a solid panel. The ratio of stiffness and ultimate strength of perforated and solid panels are plotted in Figure 2-12, where the stiffness and ultimate strength of panels decrease linearly as the size of the perforation increases. To estimate the stiffness and ultimate strength of the perforated steel panel, researchers recommended that a conservative linear reduction factor of $(1-\frac{D}{d})$ to the stiffness and ultimate strength of the similar solid panel can be applied in Equation 2-3. The researcher concluded by applying the linear reduction factor of $(1-\frac{D}{d})$ to the stiffness and ultimate strength of the solid steel panel, while the stiffness and ultimate strength of perforated panel can be conservatively estimated.

$$\frac{V_{yp.\,perf}}{V_{yp}} = \frac{K_{perf}}{K_{Panel}} = \left[1-\frac{D}{d}\right] \tag{2-3}$$

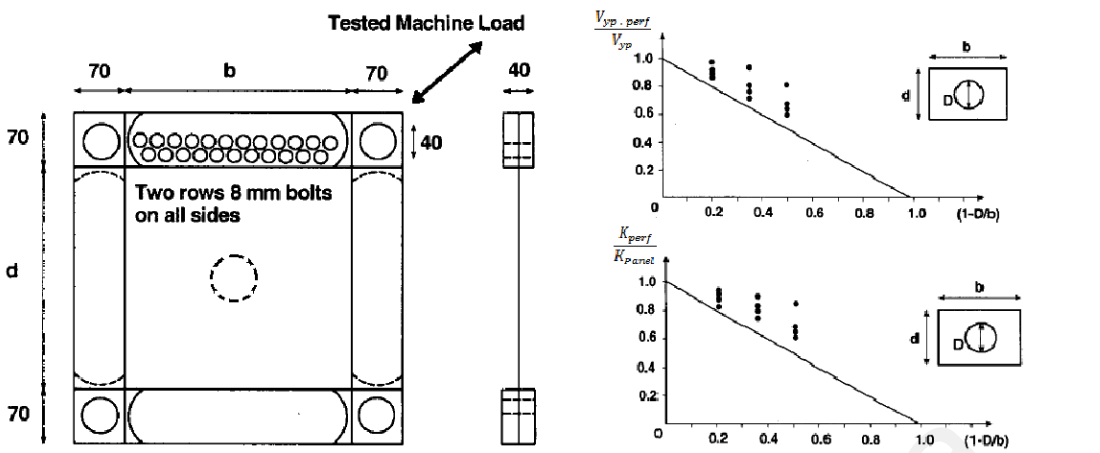

Figure 2-12 detail of specimens tested by Sabouri-Ghomi and Robert (1991) (left) and Effect of circular opening on strength and stiffness of steel shear panel (right)

Also, the researchers observed that there is reasonable agreement between experimental and theoretical hysteresis of the perforated panel. The theoretical hysteresis behavior of the perforated panel was obtained by scaling the hysteresis obtained for a solid panel value using Equation 2-3. This was considered to give a conservative assessment due to the omission of strain hardening in the model and the simply supported boundary conditions.

Based on the research results, Robert and Sabouri-Ghomi (1991) proposed an elastic perfectly plastic model for estimating the hysteresis characteristic of the specimens. In addition, they recognized that the rigid beam-to-column connection resisted a portion of the applied shear load. Sabouri-Ghomi and Robert (1992) then applied their proposed hysteresis model in a non-linear, and dynamic time-history analysis of the thin-plated SPWs. Their method idealized the thin-plated SPW as a vertical cantilever, plate-girder beam with associated story mass and dynamic load concentrated at each story level, which included both bending and shear deformation within each panel. This analytical model was a base for the method called Plate-Frame Interaction (PFI) which was proposed by Sabouri-Ghomi, Ventura and Kharazi (2004).

Caccese, Elgaaly and Chen (1993) conducted a series of experimental and analytical test on the unstiffened SPSWs. Six quarter-scale three-story SPSW specimens of different plate thickness and beam-to-columns connection, without the presence of gravity load on columns, were tested at the roof level under cyclic horizontal loading and monotonic loading. Two objectives of the study were on the effect of the panel's slenderness ratio, and beam-to-column connections on the overall behavior of unstiffened SPW. The dimension of the tested specimens is shown in Figure 2-13, while the thickness of the infill plate was 0.76 mm, 1.9 mm and 2.66 mm. The six specimens included:

- One moment frame
- Three specimens built with moment-resisting beam-to-columns connections and infill plate thickness of 0.76 mm, 1.9 mm and 2.66 mm
- Two specimens fabricated with shear beam-to-columns connections and infill plate thickness of 0.76 mm and 1.9 mm.

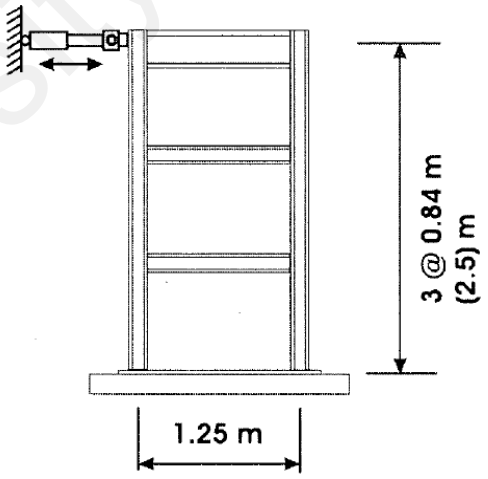

Figure 2-13 Test setup for SPSWs with different connectivity and web panel thickness (Caccese et al., 1993)

Once the cyclic loading is completed, if the specimen was intact, it was monotonically pulled until the actuator displacement limit was reached. Significant pinching and ductility were observed during the cyclic behavior of specimens. Except for the slenderest steel plate specimens, the rigidity of

beam-to-column connection was found to have a minor effect on the overall load-displacement diagram for each specimen. Based on their findings, this was due to the continuous weld joining infill plates to the surrounding beams and columns that acted as moment-resisting connections even without welding the flanges of beams to columns. The amount of energy dissipated by the specimens was mainly affected by the thickness of the infill plate. To investigate the performance of SPW specimens, up to their ultimate strength under monotonic loading, the researcher developed two computer-based analytical models. Based on their analytical studies, they concluded: (i) slender unstiffened plates can achieve a significant post-yield strength, prior to the formation of plastic hinges and the instability in the columns was found to be more desirable; (ii), less slender plates tend to be unstable due to column buckling before the plate can develop full strength. The global overturning moment was found to contribute to high tensile and compressive stresses within the plates along the inside flanges of the columns near the base.

From the testing, Caccese et al. (1993) concluded that in an unstiffened thin-plated SPSW, inelastic behavior began with infill plate yielding and the strength of the system was governed by the formation of plastic hinge in the columns. In a relatively thick-plate SPSW, the failure mode was governed by columns instability, while the only negligible increase occurred in the system strength due to an increase in the wall thickness. They concluded that the building can be designed using a thin SPSW which will respond elastically to a minor lateral load. In the case of severe seismic event, due to column buckling before the development of full strength of the infill plate, walls with less slender plates tend to become unstable. Generally, it was recommended that

thin unstiffened plates be used in order to allow for the plate yielding to occur before column buckling.

Driver (1997) tested the half-scaled four-story SPSW frame using full moment connection under quasi-static cyclic loading. The objective of the experiment was to explore the performance of the multi-story SPW under the effect of intensive cyclic loading. The energy absorption, elastic stiffness, post-yield behavior, yield strength, cyclic instability and influence of moment resisting frame on the shape of the hysteresis loops were highlighted in the research. The specifications of his test setup are shown in Figure 2-14, and no stiffeners were provided for the infill plate. The moment connection of beam-to-columns was constructed by using complete penetration groove welds for beam-flange to columns, and run-off tabs were left in place. The gravity loads were simulated using a vertical actuator at the top of the columns. Equal lateral loads as per requirements of ATC-24 (Applied Technology Council 1992), were applied cyclically at each floor level and 35 load cycles were performed on the specimen with a maximum ductility of nine. To investigate the initial inelastic performance, six cycles were executed prior to reaching the yield displacement at the first story panel. During the three times first story yield displacement, the weld tearing in the top corner of the first story panel and yielding in the beam-to-column joint, was detected. When the story drift nine times from its yield displacement, due to stress concentration, one of the columns was fractured at its connection to the base. The test has revealed that the moment resisting joint did not significantly contribute to the energy dissipation mechanism of the specimen because only minimal whitewash flaking was observed in the beam-to-column joint regions. Despite the

premature failure of the specimen at the column base, the cyclic behavior showed an over-strength of about 1.3 and ductility of more than 6.0.

Driver et al. (1997) developed a finite element model to analyze their test specimens. Beams and columns were modeled with beam elements and infill plates were modeled with shell elements. Initial imperfections based on the first buckling mode of the infill plate were included in the finite element model. Experimentally-obtained residual stresses for the boundary members were also included into the model.

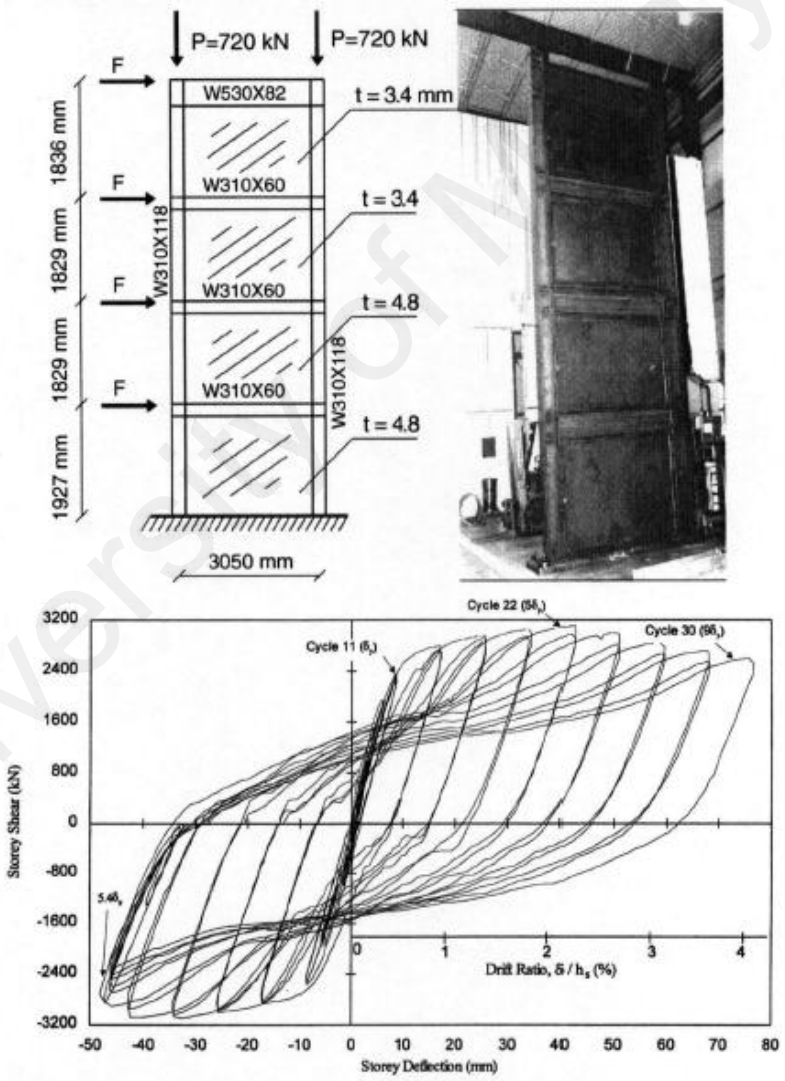

Figure 2-14 Test setup of Driver (1997) and its hysteresis curve

Driver et al. (1997) extended the strip model to include inelastic behavior in the analysis of their test specimen. Each infill plate was replaced by 10 diagonal pin-ended strips. Inelastic behavior in both the inclined tension

strips and in the boundary members were modeled. Although the strip model slightly underestimated the elastic stiffness of the test specimen, excellent agreement was obtained with the ultimate strength.

Lubell, Ventura and Prion (1997) at the University of British Columbia, conducted the quasi-static cyclic testing on two single-story quarter-scale SPSWs specimen (SPSW1 and SPSW2) and one 4-story specimen (SPSW4). The specimens are depicted in Figure (2-15) and (2-16). In all the specimens, the beam-to-column connections were moment resisting connections. The main objective of the quasi-static test was to investigate the formation of diagonal tension field, overall strength, post-buckling stiffness, hysteresis behavior and the effect of beam and column's rigidities. All beams and columns were S75x8 sections, and all infill plates were 1.5 mm thick. The only difference between the SPSW1 and SPSW2 specimens was that the top beam of the specimen SPSW2 consisted of two S75x8 sections, that are fully welded together. This was done to better anchor the tension field developed in the infill plate. For the same reason, a S200x34 section was used at the top beam of the SPSW4 specimen. The specimens SPSW1 and SPSW2 were similar to the first story of four-story specimen SPSW4. During fabrication of SPSW1, it was found that

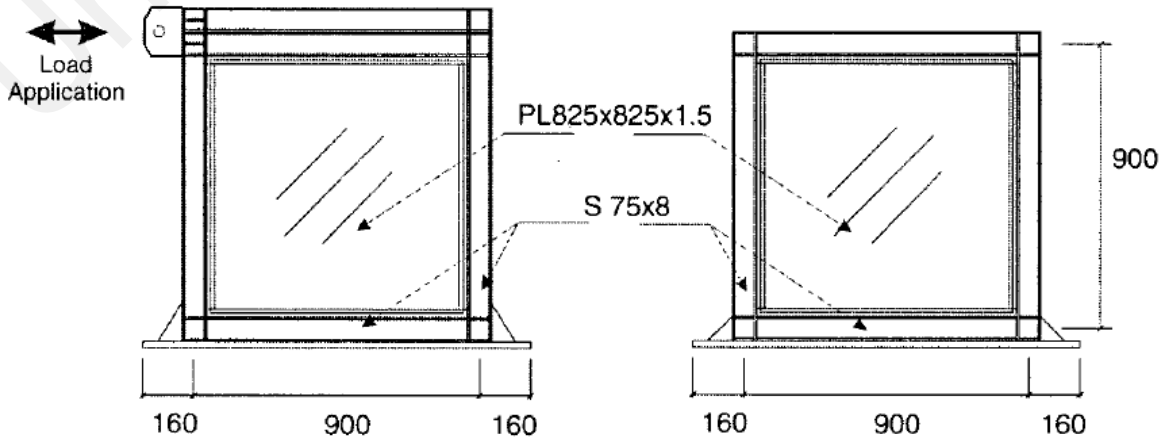

Figure 2-15 Specimen schematic of SPSW2 (left) and SPSW1 (right) (Lubell, 1997)

the initial out-of plane displacement of the infill plate was 26 mm. By taking more caution, the maximum out-of-plane displacements for SPSW2 and SPSW4 were reduced to 5 mm.

All the specimens were tested under quasi-static cyclic loading with the displacement history defined based upon the procedures recommended in ATC-24 (Applied Technology council 1992) guidelines. The single story specimens were loaded at the top of the panel and for the SPSW4 specimen; equal lateral loads were applied in each story. Also for the 4-story specimen, a constant gravity load of 13.5 kN was applied in each story.

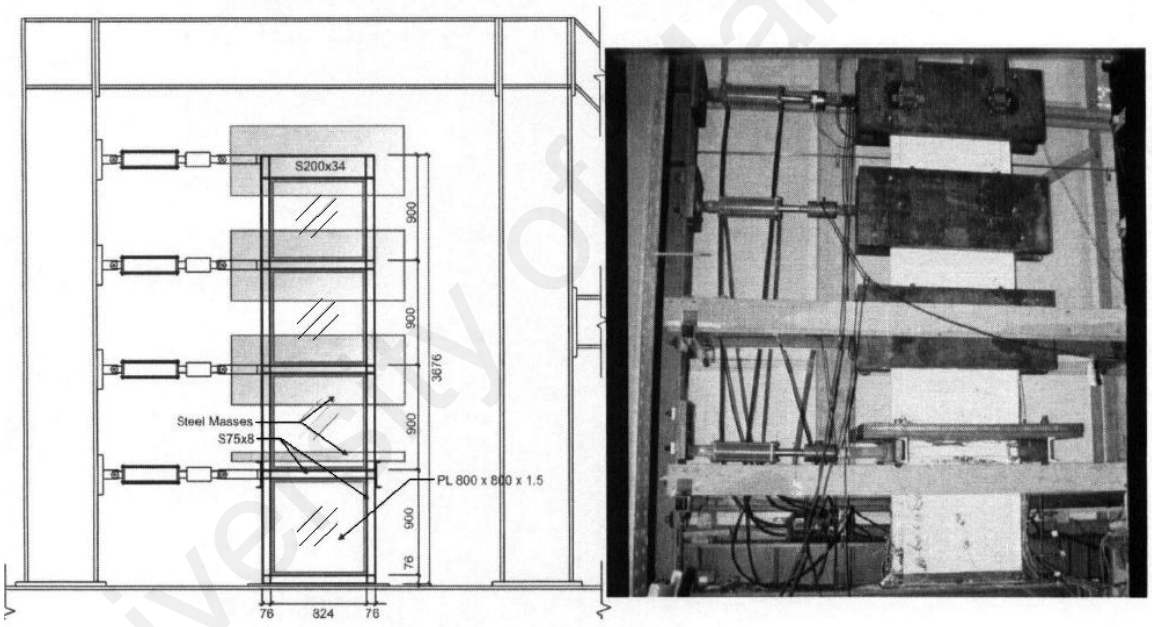

Figure 2-16 Test setup of specimen SPSW4 (Lubell, 1997)

All the specimens showed well-defined load–deformation envelopes, high initial stiffness, and stable hysteresis behavior. Single story specimens underwent significant inelastic deformations providing an approximate ductility of 6.0 and approximate over-strength of 1.5. Specimen SPSW2 showed a significant increase in stiffness and capacity compared to the SPSW1 specimen, which is mainly due to the use of a stiffer beam in SPSW2 and a large initial out-of-plane deformation in SPSW1. A significant "pull-in" of the

columns was observed for all specimens due to their low flexural stiffness. A less desirable yielding sequence was observed for specimen SPSW4 where columns yielded before the significant yielding in the infill plates. This resulted in a state of global instability and termination of test at a first story displacement of $1.5\delta_y$, where δ_y is the yield displacement at the first story. The researchers stated that an increased overturning moment in the multi-story specimen resulted in high axial forces and moments in the columns, thereby altered the yielding sequence (columns yielding before infill plates). Thus, they recommended that design standards should require that SPSWs be analyzed as a whole, as the behavior of a single isolated panel is different from a panel in a multi-story SPSW. Furthermore, the researcher concluded that for both one-story specimens, the infill steel plates significantly reduced the demand on the moment-resisting frame by producing redundant diagonal story braces that decrease the rotational demand on the beam-to-column connection.

Lubell et al. (2000) also conducted a series of numerical analysis of the test specimens using a nonlinear frame analysis program. The capacities of all the test specimens were predicted reasonably well, but the elastic stiffness was significantly overestimated for the SPSW1 and SPSW4 specimens. Based on the results obtained from the analysis, Lubell et al. (2000) concluded that the design standard at that time, CAN/CSA S16.1-M94, did not address the design-related issues like the effect of large overturning moments, the influence of the aspect ratio, and the potential for undesirable yielding sequences of the shear wall components for multi-story SPSWs.

2.2.2 Research on the Characterization of SPSWs Behavior

Rezai, Ventura and Prion (1999), at the University of British Columbia, conducted a series of shake table tests on a quarter-scale four-story SPSW with

a similar dimension to Lubell's four-story SPSW-4 (Lubell et al., 1997). The column and story beams were selected as B100x9 and S75x8 sections respectively. The top end beam and base beams were made of S200x34 and W100x19 respectively. The aspect ratio of the steel shear panel was equal 1:1 and thickness of infill plate was 1.5 mm. To simulate the dead load, the weight of 6800 kg was provided as each story weight of the test setup, which half of it distributed evenly to the specimen.

The main objective of the shake table test program was to collect and make available the necessary data related to the seismic performance of multi-story SPW resulting from intense input excitations. The specimen was braced in the out-of-plane direction. Before doing the shake table testing, Rezai (1999) conducted a low-amplitude vibration test on the 4-story specimen to determine its frequency. The fundamental frequency of the shake table specimen was obtained as 6.1 Hz in the longitudinal direction. The test specimen was subjected to a number of site-recorded and synthetically generated ground motions with varying intensities.

The researcher found that the first mode was the primary mode of vibration with very little contribution from higher modes. Based on the load–displacement curve of all four story levels, the researcher found that the majority of the energy was absorbed by the first story. In addition, the first story was dominated mostly by shear deformations, while the top stories acted as a rigid body rotating around the first story. From the obtained load-displacement curves, it was concluded that shear stiffness of the infill plates significantly affected the overall stiffness of SPSW. Furthermore, it was found that the flexural strain generated in the intermediate-level beams was negligible. Thus, it was concluded that loads in the infill plates at the top and bottom of an inter-story beam counteracted each other. The strip model was found to over-predict the elastic stiffness

of the four-story specimens. The angle of principal strain varied between 37 and 2 from the vertical through the center of first story infill plate; but the angle of the principal strain, near the base, varied between 35 and 0 for alternate loadings. Considering the above-mentioned change in the angle of principal strains (different inclination at various location), Rezai et al. (1999) proposed an improved analytical model for the simplified analysis of SPSW (Figure 2-17). To simplify the model, the tension strips were placed diagonally between opposite corners and from the corners to the mid-span of the boundary members.

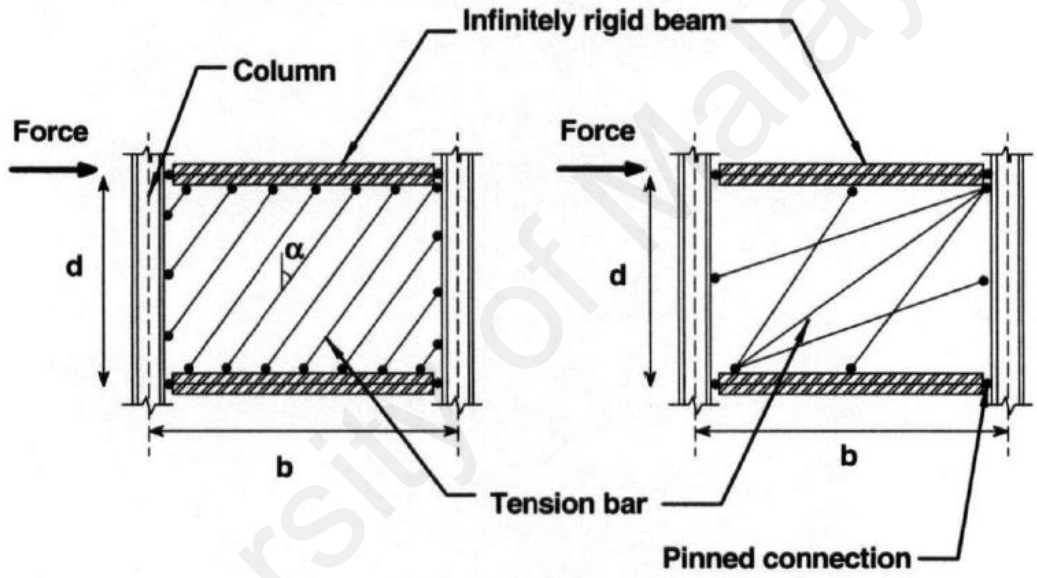

Figure 2-17 Schematic of different strip model (left) and 'Multi-angle strip model 'proposed by Rezai et al. (1999)

The proposed Multi-Angle Strip model predicted acceptable stiffness results for both pushover and dynamic time-history analysis. However, the elastic stiffness can be over-predicted as the overturning moment to the base shear ratio had increased. It was noted that as the overturning moment-to-base shear ratio increases, flexural deformations dominated the response, especially at the upper floors. This transition from shear behavior to flexural behavior was shown to be the weakness of the strip model as it fails to reasonably predict the load-displacement behavior of the structure.

Behbahanifard et al. (2003a) conducted a quasi-static cyclic test on a three-story SPSW specimen, by using the upper three story of the specimen from Driver et al. (1997), in the presence of gravity load, as shown in Figure 2-18. Although the second story infill plate buckled elastically during the previous test, there was no sign of damage (yielding). The history of the loading sequence was similar to that used in the test by Driver et al. (1997). The specimen reached its ultimate capacity at the first story displacement of 7 δy, where δy is the yield displacement at the first story of the three-story test specimen. After that, the strength started to decrease gradually due to the formation of tears in the lower story infill plate. Overall, the specimen showed high initial stiffness, excellent ductility, and high-energy dissipation capability.

A nonlinear finite element model based on the explicit formulation was developed in ABAQUS software to simulate the monotonic and cyclic behavior of both specimens from Behbahanifard et al. (2003a) and Driver et al. (1997). A four node shell element with reduced integration (ABAQUS element S4R) was used for the beams, columns and infill plates. Residual stresses were not included in the finite element model for simplicity. For the cyclic analyses, a kinematic hardening material model was included to simulate the Bauschinger effect. The researchers reported that with the use of ABAQUS/Explicit, convergence was easily achieved. An excellent agreement was observed between the test results and the results from the finite element analysis. However, the capacity was slightly underestimated during the analysis (12% for three-story specimen and 7.8% for four-story specimen).

With the validated finite element model, a parametric study was conducted to investigate some non-dimensional parameters affecting the behavior of a single story SPSW. Ten non-dimensional parameters were identified, from which four are discussed here: aspect ratio$\left(\frac{L}{H}\right)$; ratio of axial stiffness of infill plate to column axial stiffness $\left(\frac{t_p\ L}{2\ A_C}\right)$; a parameter relating to column flexibility parameter, ω_h , as defined in CAN/CSA S16-09; and a parameter related to initial imperfection magnitude. The researchers found that a decrease in the aspect ratio would generally increase the capacity of SPSWs. An increase in the axial stiffness ratio has led to an increase in the stiffness of the shear wall. As the column flexibility parameter decreased, the column lateral stiffness increased relative to the panel stiffness. It was also demonstrated that initial out-of-plane imperfections could significantly influence the initial stiffness of the shear panel. For imperfection sizes larger than 1% of $\sqrt{Lh}$ the stiffness reduction was found to be noticeable and it was recommended that it be accounted for in the design. Thus, it was suggested that

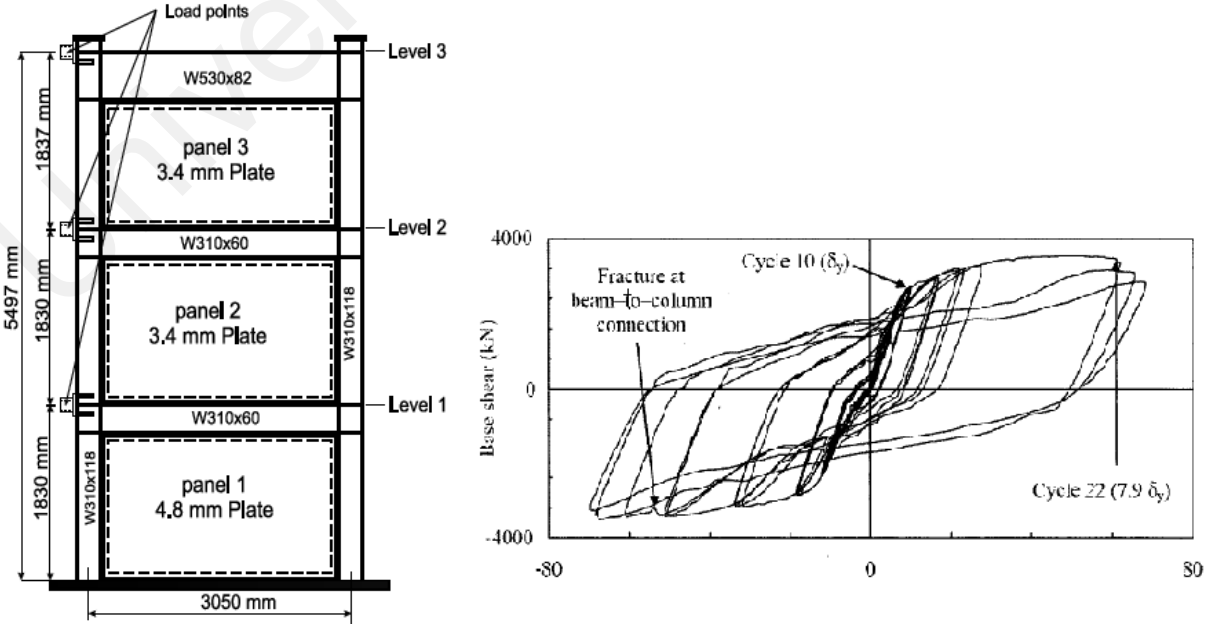

Figure 2-18 Test specimen and hysteresis curve of base shear for the first story of SPSW (Behbahanifard 2003)

imperfections be limited in practice to 1% of $\sqrt{Lh}$. It was concluded that the column flexibility parameter has a significant effect on the behavior of SPSWs.

On reviewing the procedure for the analysis and design of SPSWs recommended by CAN/CSA S 16-01, Berman and Bruneau (2003) found that in some cases this procedure can lead to an un-conservative design which overestimated the expected ultimate strength of SPSWs. Therefore, they proposed a revised method for the design of steel shear walls. In this procedure, using equations derived from plastic analysis of the strip model, which is an accepted model for the representation of SPSWs, the thickness of infill plate is measured. From the methodology point of view, this procedure is similar to the method proposed by Sabouri and Robert (1991). Berman and Bruneau (2003) found good agreement between the ultimate strength obtained from the experimental test, and those predicted by plastic analysis. Also, they investigated the plastic collapse mechanism for various wall configurations. Furthermore, they have identified that the weakness of the existing design procedure, which led to the overestimation of ultimate strength. Based on this investigation, they proposed a new plastic analysis procedure for an estimation of the infill plate thickness, and asserted that this method is considered structural over strength which allows the designer to control the ultimate failure mechanism of SPSWs.

At the University of New York, Vian and Bruneau (2005) presented some results on the steel panel walls and outlined an experimental program. They conducted the test results of three specimens that were made of Low Yield Strength (LYS) steel infill panels and Reduced Beam Section (RBS) at the beam-ends and rigid connection between beam-to-columns. All the specimens had the same boundary frame, but two of the specimens had

perforations for allowing mechanical utilities to pass through. The perforation configuration includes the distributed multiple holes (specimens P) and the second two quarter-scale cut-outs in the top corners of infill panel (specimens CR) which was reinforced to transfer panel forces to the adjacent frame (Figure 2-19).

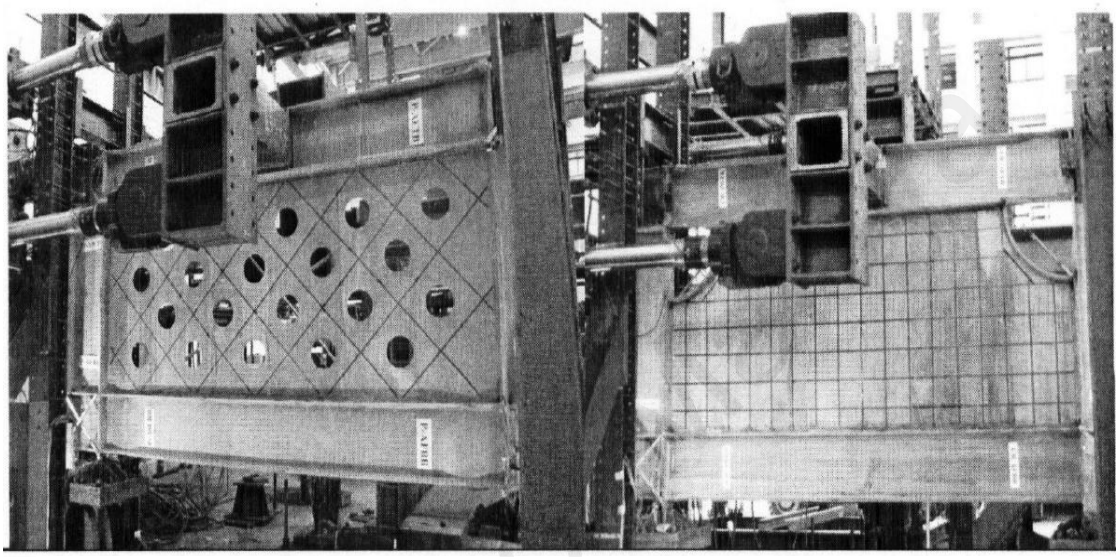

Figure 2-19 Test setup of specimens of Vian and Bruneau (2005), SPSW with circular perforation in web (left) and quarter-circle cut-outs in the web panel corners

Quasi-static cyclic loading was applied for the three specimens. Specimen S2 (with solid infill plate) and P were tested to a maximum inter-story drift of 3%, while specimen CR was tested to a maximum inter-story drift of 4%. The perforated panel reduced the elastic stiffness and overall strength of the specimen by 15% and 19%, respectively compared with the solid panel specimen.

During cyclic testing, all specimens exhibited a behavior in which the beam plastic hinging was located at the connection locations. This showed the effectiveness of RBS connections in SPSW beams and was recommended (Vian and Bruneau, 2005) to control the boundary frame yielding during a significant earthquake. The detailed perforated SPSW specimen (P) exhibited ductile behavior during testing and thus showed that this system is a viable

alternative to a solid panel SPSW, without the need for stiffeners around the perforations. The perforated layout was also recommended for use in SPSW applications where the minimum available plate thickness is larger than required. The cut-out reinforced corner specimen also performed well during testing and appeared to be an effective solution for SPSWs to allow for the passage of utilities.

Vian (2005) also conducted a finite element analysis on the three tested specimens. In general, good agreement was observed between the test results and the hysteresis curves obtained from the analysis. The analytical model of the perforated SPSW was further extended to consider the perforations in the infill plates with diameters of 100, 150, 200 mm. The results were compared with the results for individual perforated strips having the same perforation diameters. It was reported that the elongation predicted by the finite element model of the individual perforated strip and the full SPSW model for monitored maximum strain, was significantly different and thus further research was recommended.

To analyze the shear and bending of ductile SPSW, Kharrazi *et al.* (2005) proposed an analytical model referred to as the Modified Plate-Frame Interaction (M-PFI) model. The objective was to characterize the interaction between structural components, which contribute to the strength and deformation of whole steel plate shear walls. To attain this purpose, the MPFI model separates the behavior of ductile SPSW into three parts: elastic buckling, post-buckling, and yielding. The development of the final equations, can be obtained through several steps. First, a shear analysis was conducted that considered the behavior of the infill panels and frames respectively and then, to obtain the shear behavior of the ductile SPSW, the shear-displacement

relationships for each were superimposed. Second, assuming that the frame and infill plate as a wide flange shape, a bending analysis was conducted. To obtain certain points on the shear load-displacement relationship used for analyzing the behavior of the wall (Figure 2-20), equations were proposed.

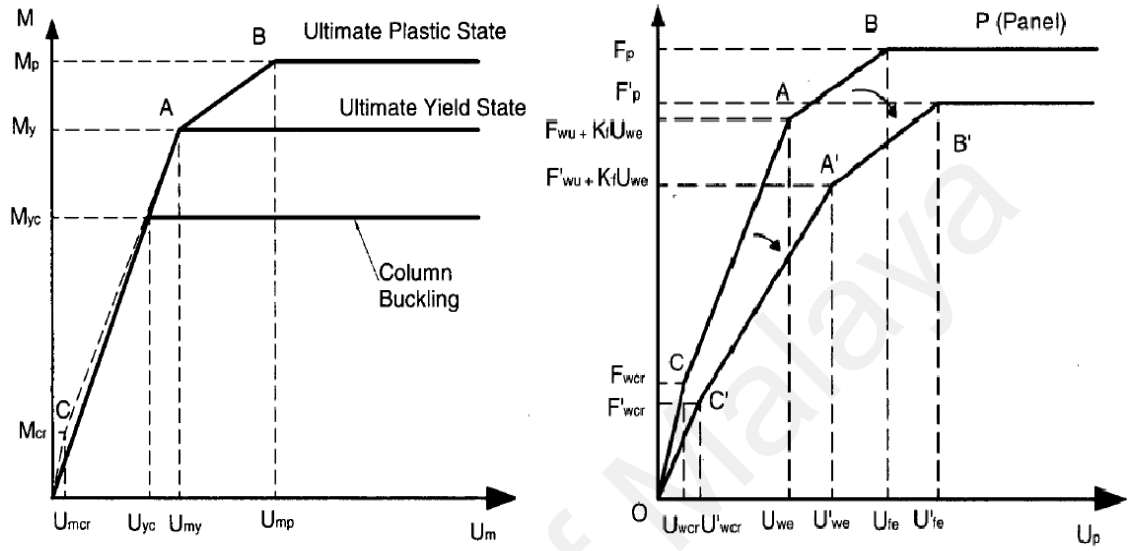

Figure 2-20 M-PFI bending model load-displacement of the panel (web plate and frame) (left); the modified load displacement diagram for shear resistance of the SPSW (Kharrazi *et al.* (2005))

Using the test data from Driver *et al.* (1997) and assuming the angle of inclination equal to 45 degree, Kharrazi *et al.* (2005) evaluated the M-PFI method. A comparison of the results showed that the model overestimated the initial stiffness and initial yielding by 5%. In addition, it underestimated the ultimate capacity of the specimen by about 10%. It is worth to mention that the M-PFI model does not describe the ductility of the SPSW specimen or the actual mechanism, nor does it provide a means for determining the frame forces for use in the design.

Purba et al. (2006) conducted a series of finite element analysis to investigate the behavior of unstiffened thin SPSWs with openings in the infill plate. Two designs, namely the perforated infill plate and the cut-out corner SPSW as proposed by Vian et al. (2005), were investigated.

Nonlinear pushover analysis was carried out for the single-story perforated SPSWs. Variations in the perforation diameter and infill plate thickness were considered in the analysis. Purba (2006) found that the results from the individual perforated strip analysis can accurately predict the behavior of the complete perforated SPSW provided the diameter of the holes is less than 60% of the strip width $\left(\frac{D}{S_{diag}} \quad 0.6\right)$. It was found that no interaction exists between the adjacent strips that could affect the stress distribution within an individual strip. Purba (2006) also examined the applicability of using the equation proposed by Roberts and Sabouri-Ghomi (1992) to approximate the strength of a perforated infill plate with multiple perforations. Based on the results of his analysis, he concluded that the shear strength of an infill plate of a SPSW having multiple regularly spaced circular perforations throughout the infill plate can be calculated by multiplying the shear strength of a solid infill plate by a factor $\left(1 - 0.7\frac{D}{S_{diag}}\right)$. Purba (2006) also investigated two cut-out corner SPSW designs having flat-plate and T-section reinforcement along the cut-out edges. It was observed that there was very slight difference in the shear strength of the infill plate. Thus, the flat plate (with a minimum fish plate) was considered to be adequate to reinforce the cut-out edges.

Veladi et al. (2007) performed theoretical and experimental studies on post-buckling and overall behavior of SPSWs. The main objective of their research was the effect of the aspect ratio on the buckling and post-buckling behavior and force modification factor. In the first part of their research, the available theoretical relations based on the strip model were improved and used to predict the yield displacement and yield strength of a steel panel. In order to evaluate the force-displacement relation and post-buckling behavior of the

specimen, one (1/10) scale specimen was tested under monotonic static loading. Then, six one-story unstiffened specimens with (1/2) and (1/3) scale under cyclic quasi-static loading was tested. The specimens consist of flat infill plate with different thickness and aspect ratio of infill plate, and boundary frames, which were pinned together at the corners (Figure 2-21).

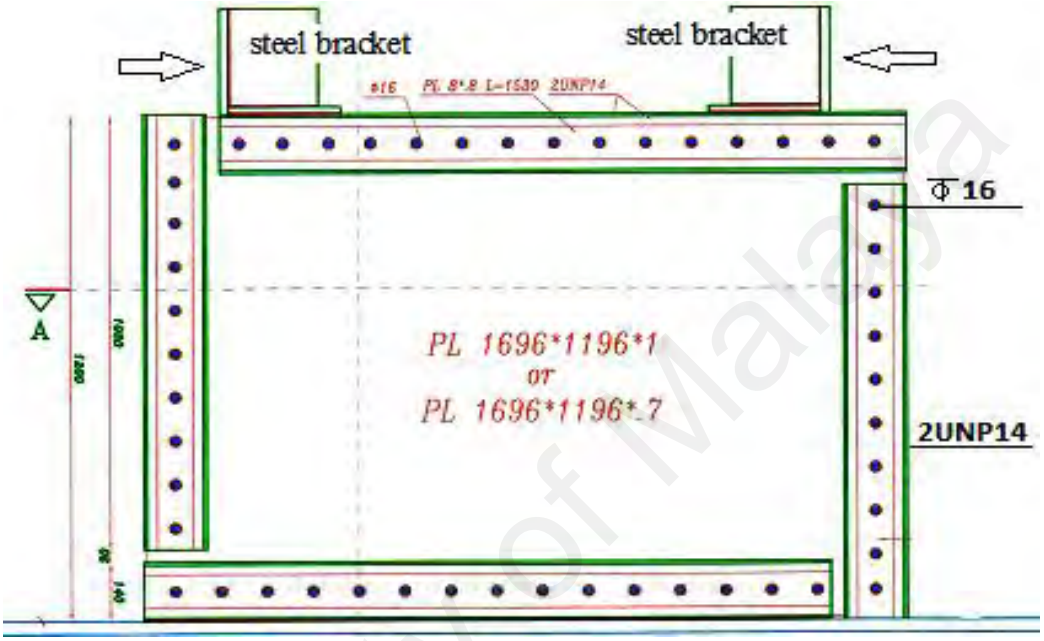

Figure 2-21 Test setup for specimen of Veladi et al. (2008)

It was found that the infill panels surrounded by boundary frame members are able to display a ductile behavior. The drifts corresponding to the yielding and rupture in the panel were 1.7% and 5% respectively. An increase in the thickness had an insignificant effect on the initial stiffness of specimens, but in the range of the same drift, it increased the shear strength of SPSW. Increasing the width of SPSW, considerably increased the shear strength while, it will also decrease the relative displacements of specimens. By increasing the height of the specimens, the absorbed energy and lateral displacement increased, but shear strength decreased. Veladi et al. (2007) concluded that the force modification factor for unstiffened one-story SPW, conservatively can be considered equal 11.0. Good agreement was found between the performances

of test specimens and predicted pre-yielding and post-buckling behavior obtained from the FE analysis.

Bhowmick et al. (2009)studied the behavior of unstiffened steel plate shear walls using nonlinear finite element model at the University of Alberta. With the validated finite element model, the performance of 4-story and 8-story Type D (ductile) and Type LD (limited-ductility) SPSWs with moment-resisting beam-to-column connections, was studied under spectrum-compatible seismic records. The main objective of the study was to propose a design procedure to achieve optimal seismic behavior for SPSWs. The effect of the loading rate on the dynamic behavior of SPSWs was also investigated, as was the $P-\Delta$ effect in terms of its influence on seismic demand in shear and flexure. Bhowmick et al. (2009) also developed a shear strength model for the infill plate with circular perforation at arbitrary location. Finite element analysis showed that the shear strength of an infill plate with circular perforations can be calculated by reducing the shear strength of the solid infill plate by a factor of $\left(1-0.7\,N_r\frac{D}{L\cos\alpha}\right)$. The study on the perforation was limited to the circular perforation's diameters varying from 00 mm to 600 mm. Therefore, the result of this investigation is inapplicable to SPSWs with perforations of other shapes and, the results were not verified by experimental results.

An improved simple formula for estimating the fundamental period of SPSWs was developed by regression analysis of the period data obtained from frequency analysis of series of steel plate shear walls. (T =0.03hn). In addition, the effectiveness of a shear–flexure cantilever formulation for determining fundamental periods and P-D effect of SPSWs was studied. They claimed that

despite the proposed fundamental period is very simple and convenient to use for engineering application, it needs to be verified by experimental works.

Kurban and Topkaya (2009) evaluated the response modification factor, over strength and displacement amplification factor of SPSWs by using the three-dimensional finite element analysis. Forty four unstiffened SPSWs with different number of story, bay width, story mass and infill thickness was considered as the prime variable that influenced the response. The FE models subjected to twenty recorded earthquake signals were analyzed (Figure 2-22). The geometrical and material nonlinearity was included in the analysis. They found there is dependency of ductility reduction and response modification factor to the maximum inter-story drift. The analysis results showed that there

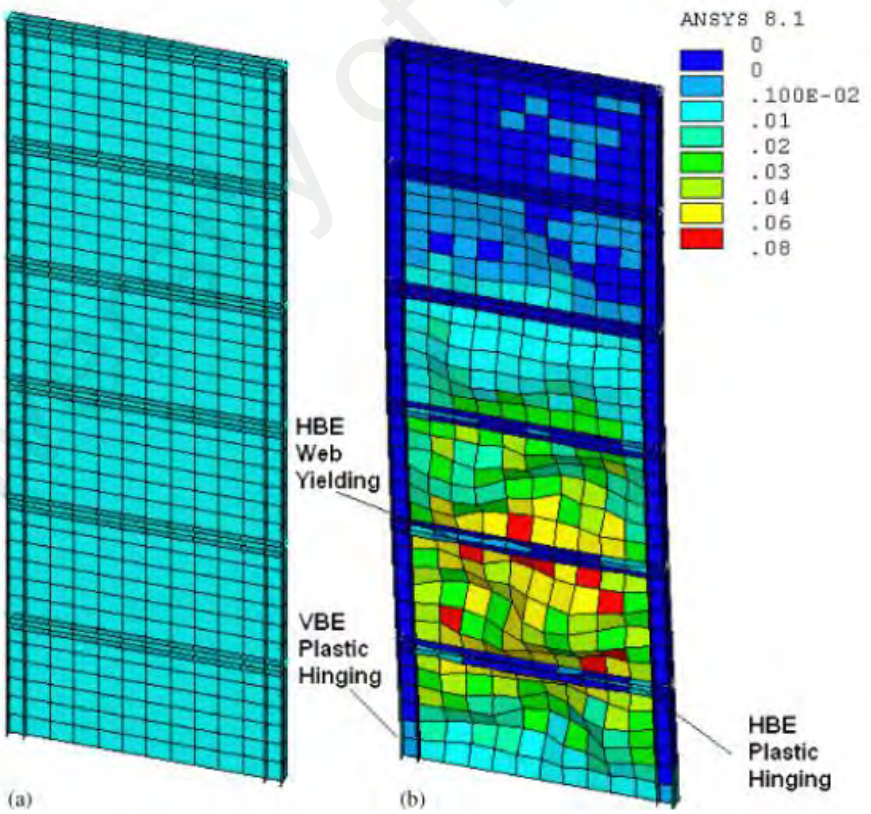

Figure 2-22 Typical Finite Element model of Kurban and Topkaya (2009)

is a correlation of the abovementioned factor with a wide scatter in the values caused by variations in the ground motion characteristics. To quantify the analysis results, the researcher developed the upper and lower bound equations

and the relationship between the response modification factor and displacement amplification factor were established.

2.2.3 Research on the Stiffened SPSWs

Alinia and Shirazi (2009) carried out a numerical investigation, under cyclic loading, to propose a design method for optimal stiffening of the thin steel plate shear walls. The main priority considered for the controlling criteria, was to extend the yielding on the infill plate to wider areas and subpanels. The procedure was applicable for one-side longitudinal and transverse flat stiffeners located in various arrangements of the infill plate, which effectively divides the plate into subpanels and expends tension fields across the infill walls (Figure 2-23). The results showed that using unidirectional stiffeners was more effective than bidirectional cross stiffeners.

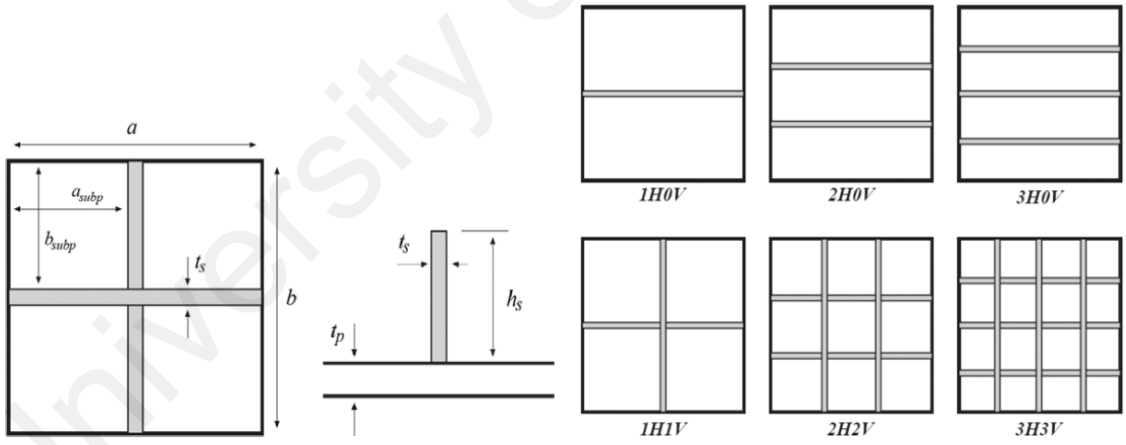

Figure 2-23 Stiffener's arrangement of the numerical study of Alinai (2009)

Gholhaki and Sabouri-Ghomi (2009) studied the effect of the ductility factor on the force modification factors for thin steel plate shear walls. The research was done based upon the results of two cyclic test of three-story ductile SPSW (Figure 2-24) and experimental results of various researchers. One of the three-story specimens was fabricated by fixed column-to-beam

connection and another with simple connection, while in both cases, a low yield steel was used in the infill plates. The aspect ratio of the SPSW in all stories was constant and almost equal to unity. Based on the Uangs method (Uang, 1991) and constant over strength factor, they obtained the value of 10 for force modification factor of SPSWs and concluded that this value is considerably larger than the force modification factor of moment-resisting frames. Furthermore, the performance of SPSWs was found superior compared to the moment-resisting frames.

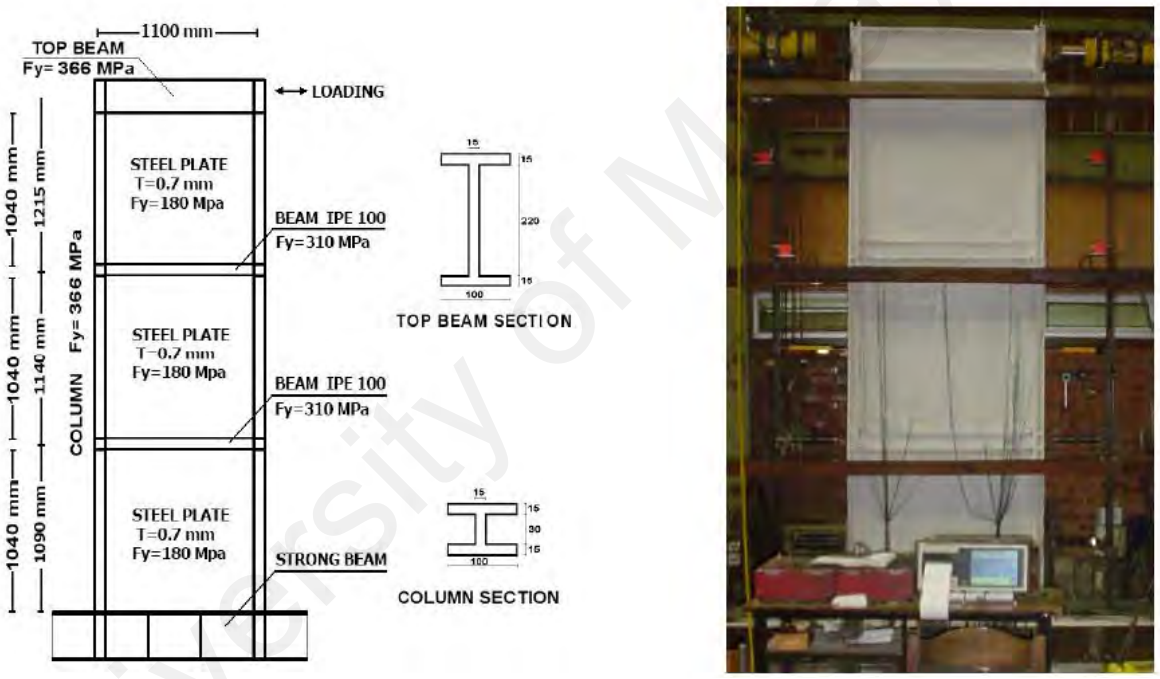

Figure 2-24 Overall configuration of the specimens of Gholhaki and Sabouri-Ghomi (2009)

To investigate the force modification factor and energy dissipation of ductile SPSWs, Sabouri-Ghomi and Asad-Sajadi (2008) conducted an experimental test on three one-story (1/3) scale specimens under cyclic loading. As shown in Figure (2-25), the specimens included two one-sided cross-shape stiffened and unstiffened SPSWs that infill plate fabricated by low yield steel. The third specimen was a bare moment resisting frame fabricated for comparison purpose. The width and height of the specimens were equal to

1590 mm and 1250mm respectively. The obtained ductilities of the stiffened, unstiffened and moment frame were equal to 17.1, 12.9 and 4.9 respectively. The displacement amplification factors obtained on the stiffened, unstiffened and moment frame were equal to 35.9, 29.7 and 7.8 respectively. In addition, the values obtained for the over strength factor of the stiffened, unstiffened and moment frame were equal to 2.1, 2.3 and 1.6 respectively. Using the Uang's method (1991) and considering Newmark and Hall (1982a) for calculation of the ductility reduction factor, the force modification factor for the stiffened, unstiffened and moment frame were equal to 12.2, 11.5 and 4.8 respectively. They found the energy absorption without stiffeners in various displacements is about 20 to 36 percent less than the one with stiffeners.

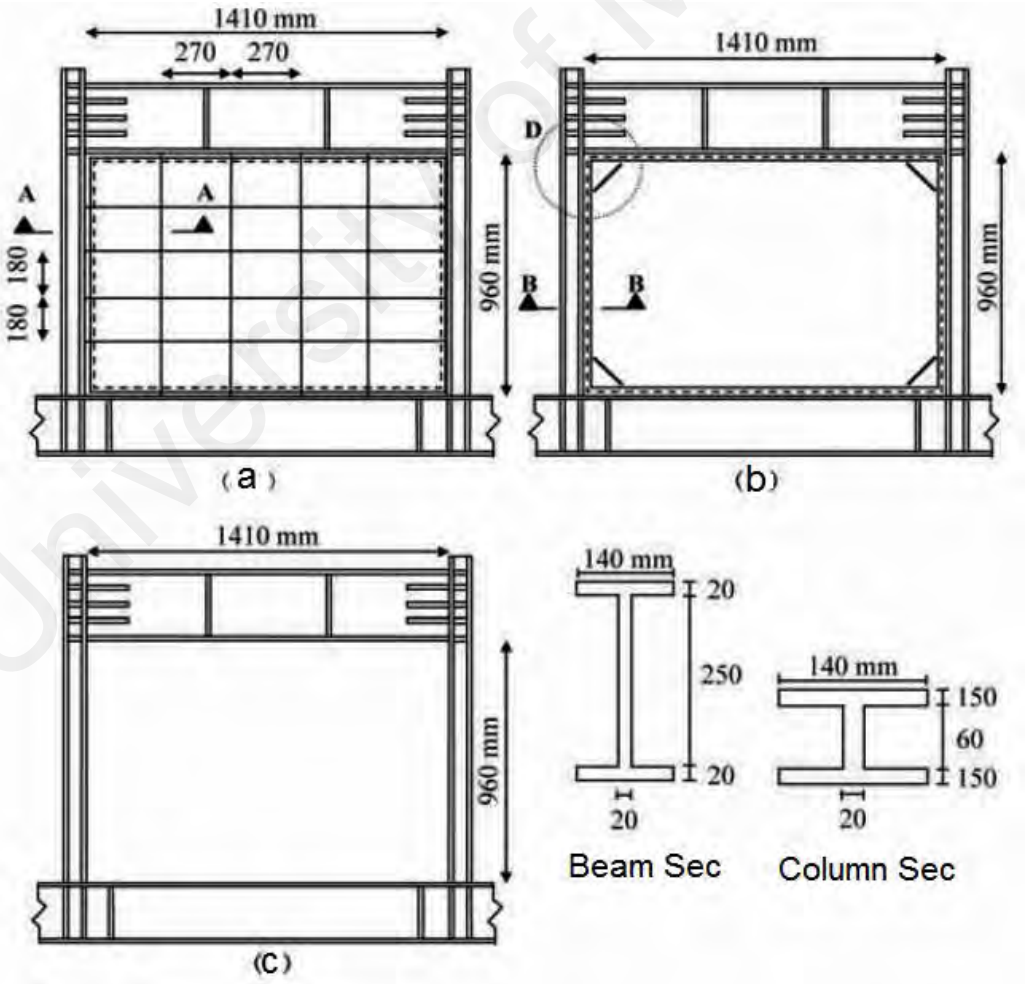

Figure 2-25 Specimens tested by Sabouri-Ghomi and Asad-Sajadi (2008)

Bakhshi, A. and J. Aslani (2012) conducted numerical research on the over strength, ductility and response modification factor of 24 stiffened SPSWs (Figure 2-26). The main objective of the research was to evaluate the effect of some parameters, including the number of stories, infill's thickness and the span of SPSWs on the response modification factor. The models stiffened with transverse flat stiffeners and 2, 4, 6 and 10 story models were considered. In addition, the thickness of the infill plate was equal to 3 and 6 millimeters and, the span of SPSW were 3, 4.5 and 6 meters. Static pushover and nonlinear dynamic analysis was performed on the FE models. The researcher found that the inelastic pushover analysis is more suitable for short period and for regular structures, while for long period structures, nonlinear dynamic is preferable. They concluded that the over strength factor increases as the span decreases, but the effect of the infill thickness and number of stories were negligible on the over strength factor. They obtained the values of 1.7-2.0 for 3 m span, 1.5–1.71 for 4.5 m span, and 1.36–1.63 for 6 m span for the over strength factor. Furthermore, increases in the span resulted to an increase in the ductility factor. The response modification factor varied within the range 7.89 to 12.27. Therefore, using the static pushover analysis, they proposed the values of 7 and 10 for the response modification factor of stiffened SPSWs according to the limit state method and allowable stress method respectively. The response modification factors varied in the range 7.89 to 12.27. Therefore, using the static pushover analysis, they proposed the values of 7 and 10 for the response modification factors of stiffened SPSWs according to the limit state design method and allowable stress design method respectively.

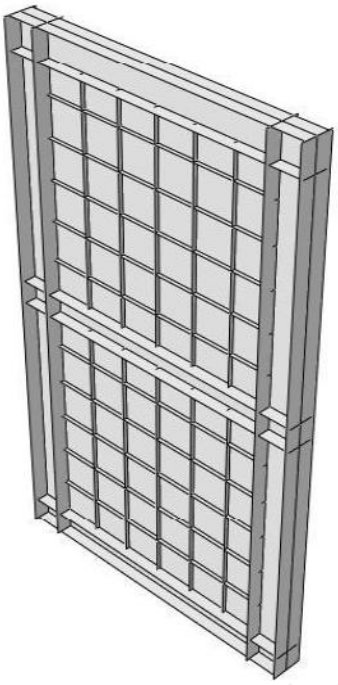

Figure 2-26 Typical FE model of stiffened SPSW of Bakhshi, A. and Aslani (2012)

Nie et al. (2013), experimentally investigated the seismic behavior of stiffened steel plate shear walls, with and without openings. The ductility, energy absorption, stiffness and strength of the specimens subjected to reversed cyclic loading were evaluated. The specimens included three (1/5) scale which;

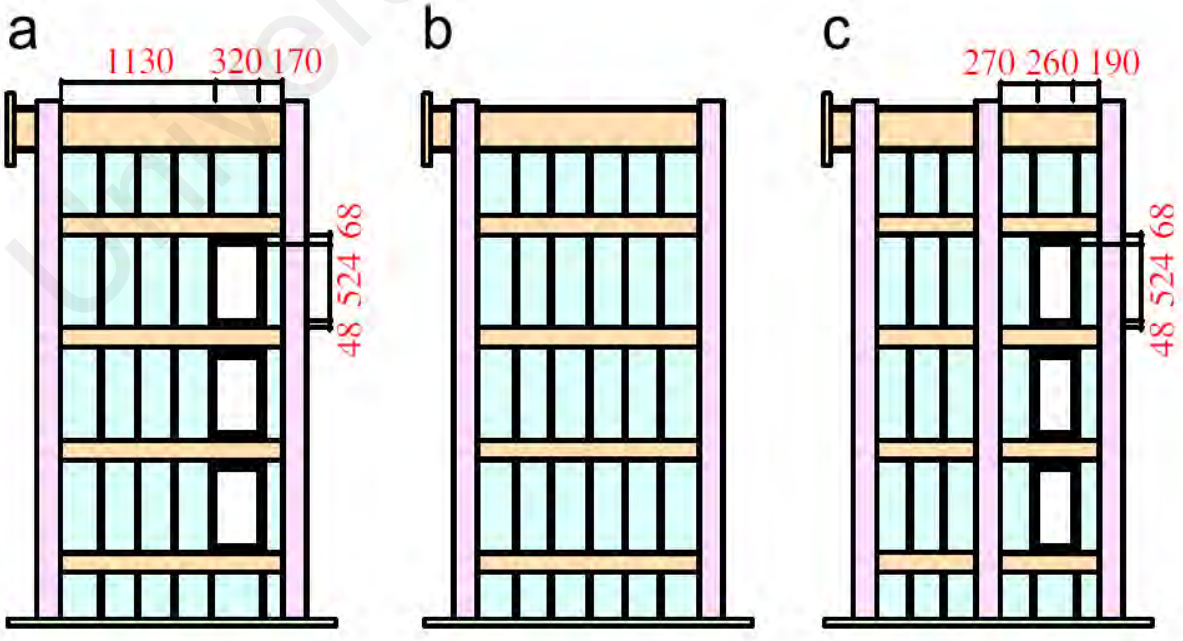

Figure 2-27 Opening loaction and dimension of specimens tested by Nie et. al. (2013)

two walls had rectangle opening, and one wall was fabricated without any opening. To prevent premature buckling of the wall panels under the service load and to provide additional stiffening at the openings, the U-shaped section 24x12x3 stiffeners were welded on both sides of the wall panels. The overall configurations of specimens are shown in Figure 2-27. Based on the test results, the stiffened SPSWs exhibited satisfactory seismic behavior while, in the walls with openings; the strength and stiffness characteristics of the walls were reduced. In the analytical part of the research, using the single-story FE models, the critical factors affecting the shear strength reduction of stiffened SPSWs with the opening were investigated. In addition, Nie et al. (2013) proposed a formula for the determination of the shear strength reduction coefficient. It is worth to mention that, using numerical models, Hosseinzadeh and Tehranizadeh (2012) conducted a similar research on the prospective of the general configuration of models.

Alavi and Nateghi (2012, 2013) conducted an experimental and numerical investigation on the three half-scale single-story SPSWs under the effect of cyclic quasi-static loading,. The objective of the research was to find a method that provides perforation for utility passing without decreasing the stiffness and shear strength. In line with this objective and for comparing the behavior, the fabricated specimens included one un-stiffened and two diagonally stiffened with and without the perforation (Figure 2-28). The perforation was a circular shape with the diameter of 1/3 depth of the panel which cutout from the center of infill plate. The term “special perforated shear walls” was used by the researcher to refer to the diagonally stiffened SPSWs with perforation. They claimed that by means of the proposed stiffening method, the shear strength of the perforated shear walls was achieved which is

close to the un-stiffened wall with the solid panel, and the seismic behavior of the system has considerably improved. In addition, they obtained the ductility of the specially perforated specimen equal to 8.7, which is about 14% greater than the un-stiffened specimen. Based on the numerical studies and for LRFD design method, they proposed the value of 8 and 9 for the response modification factor of un-stiffened and diagonally stiffened steel shear walls.

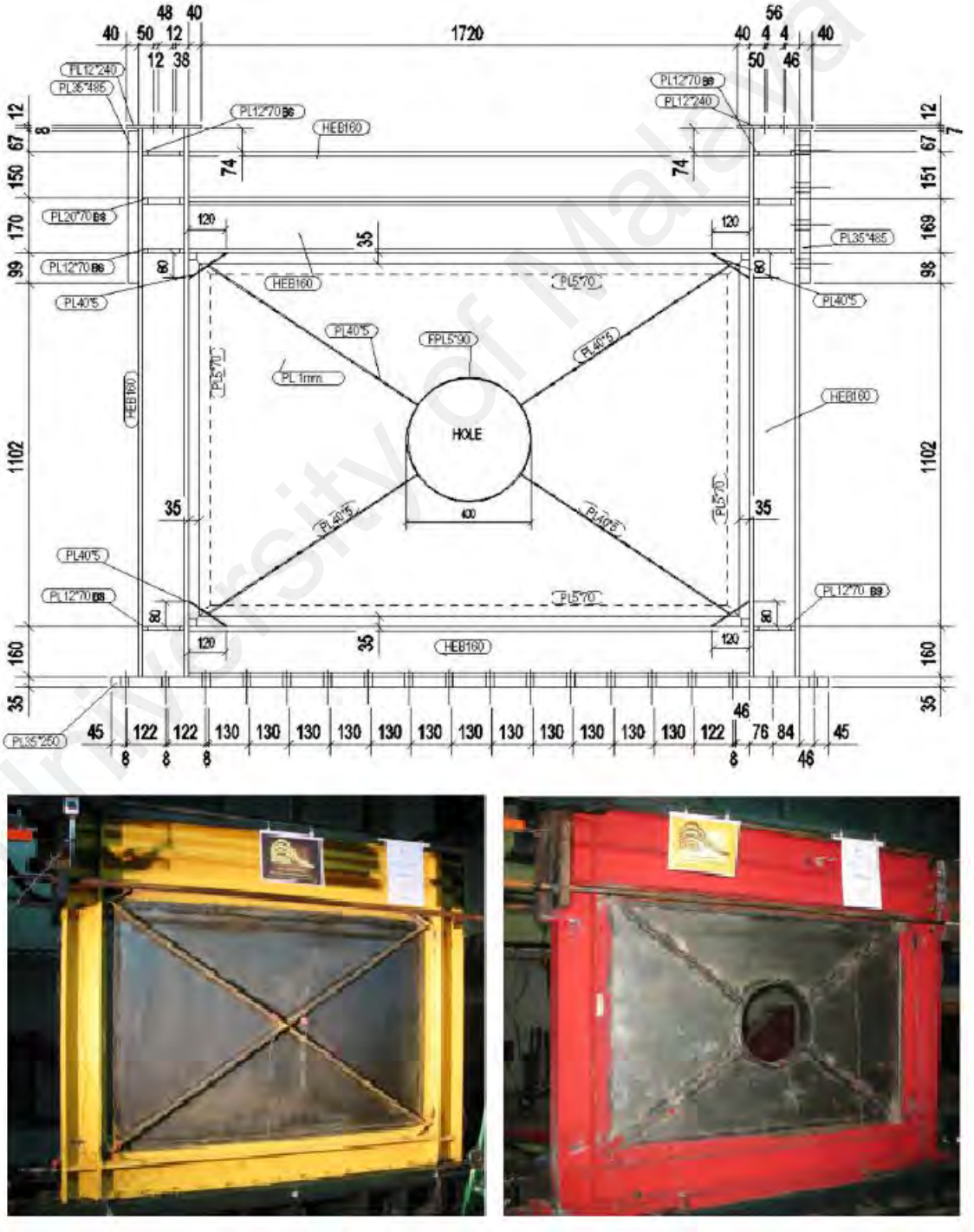

Figure 2-28 Specimens of Alavi and Nateghi (2013)

To investigate the response modification factor of coupled steel shear walls, Abdollahzadeh and Malekzadeh (2013) conducted a numerical analysis. The main objective of the research analysis was focused on the determination of ductility, over strength and response modification factor of coupled SPSWs with various numbers of stories, bay width and coupling beam. For the allowable stress design method and using the static pushover and incremental nonlinear dynamic analysis and based on the situation of the coupling beam, they proposed the values of 11.1, 11.6 and 10.6 for the response modification factor of coupled SPSWs with deep beam, medium beam and for uncoupled SPSWs respectively. For LRFD design method, the above values are equal to 7.9, 8.3 and 7.6 respectively.

In the multi-story SPSW, the ideal performance of the system is that infill plates of different stories will yield simultaneously during the earthquake loading. Such behavior could be gained if uniform inter-story was imposed by the ideally rigid columns. Theoretically, if the SPSW columns are rigid enough and pinned to the base, the infill plates at different stories will yield simultaneously. Qu et al. (2013) concluded that, in the relatively flexible columns, yielding may first occur at a certain story and resulting drift concentration and premature failure of the system (Figure 2-29). The researchers characterized the effect of column stiffness on the system performance and using validated FE models, proposed mathematical models that quantify the effect of column stiffness on the drift concentration of the system. They found that if columns were designed to meet the code-specified minimum stiffness, drift concentration would more possibly occur in the walls with larger length-to- height aspect ratios.

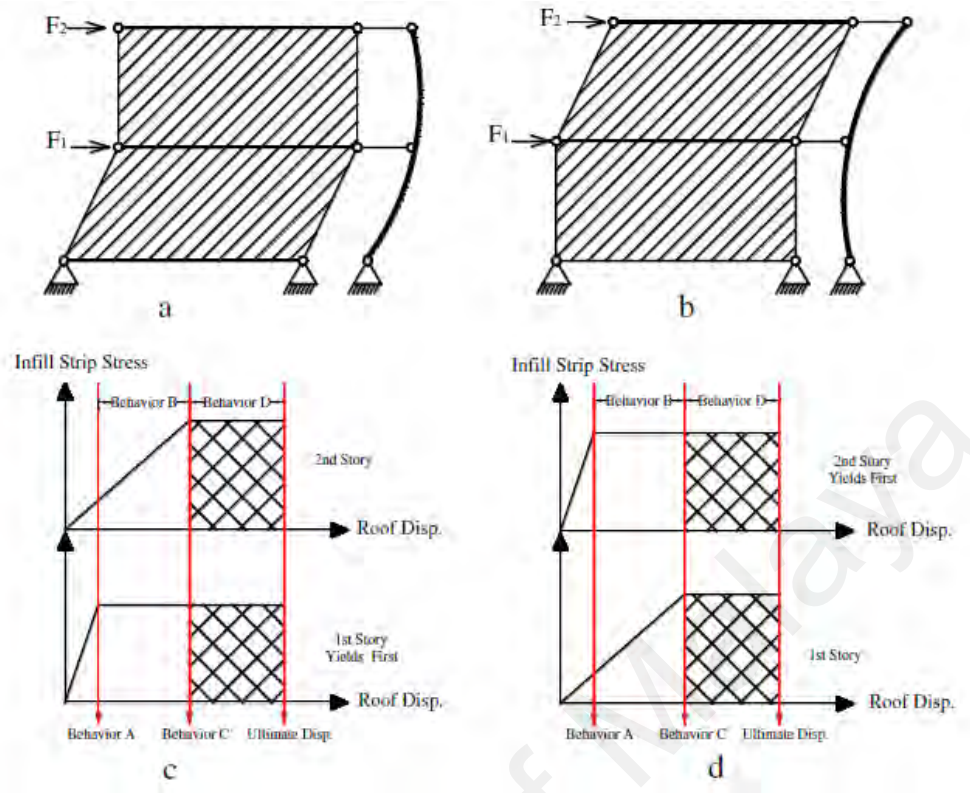

Figure 2-29 Typical behavior of drift concentration at 1st story (left) and 2nd story (right) (Qu et al., 2013)

Zhang and Guo (2014) investigated the effect of pre-compression from adjacent frame columns on the behavior of SPSWs using the FE method. The pre-compression could be produced in the construction process and gravity loads. They found that the pre-compression had reduced the shear capacity of SPSWs and neglecting this issue could be unsafe. The behavior and mechanism of the pre-compression on the SPSW with various aspect ratios are different. They concluded that the axial forces were transferred to the frame columns from the infill plate in shearing and, to account for this effect, a reduction coefficient of shear capacity of the system was proposed.

Sabouri-Ghomi and Mamazizi (2015) conducted an experimental research on stiffened SPSWs with two rectangular openings. An experimental test was performed on three one-third scaled single-story SPSW specimens with two rectangular opening under quasi-static loading. The main objective

was to study the effect of interval between two openings and their distance to the frame columns on the behavior of specimens. The dimensions of the opening were kept constant and its boundaries were strengthened by box profiles (Figure 2-30). The stiffeners were attached to one side of the infill plate. The results indicated that ultimate shear strength, energy absorption and stiffness for all three perforated specimens were similar and, the interval between the two openings had no effect on these parameters.

Figure 2-30 Stiffened SPSW with two rectangular perforation tested by (Sabouri-Ghomi and Mamazizi, 2015)

To obtain a systematic and comprehensive comparison of the steel plate shear wall structures with different construction detail, Meng et al. (2015) conducted a numerical research. The finite element models included eight typical SPSW with different structural construction. As shown in Figure 2-31, two stiffened models which included cross and diagonal models were strengthened by two rectangular section stiffener plates and, the third one was stiffened with a T rib section with cross configurations which modeled on both sides of the low yield point steel infill plate (model SW-T-LYP). The boundary frame specifications were similar as well as the ratio of bay width to the height of SPSW was equal to 1.18 for all models. The ductility, energy dissipation, out-of-plane deformation, hysteretic behavior, failure mode and load-carrying capacity were the interest of this study. All models were analyzed under monotonic and cyclic loading. Meng et al. (2015) concluded that the FE

method had provided a strong tool for assessing the performance of SPSWs and the seismic performance of SPSW can be improved by appropriate construction details. In addition, the proposed T type rib stiffened low yield point steel plate shear wall, can effectively improve the ductility and energy dissipation of SPSWs.

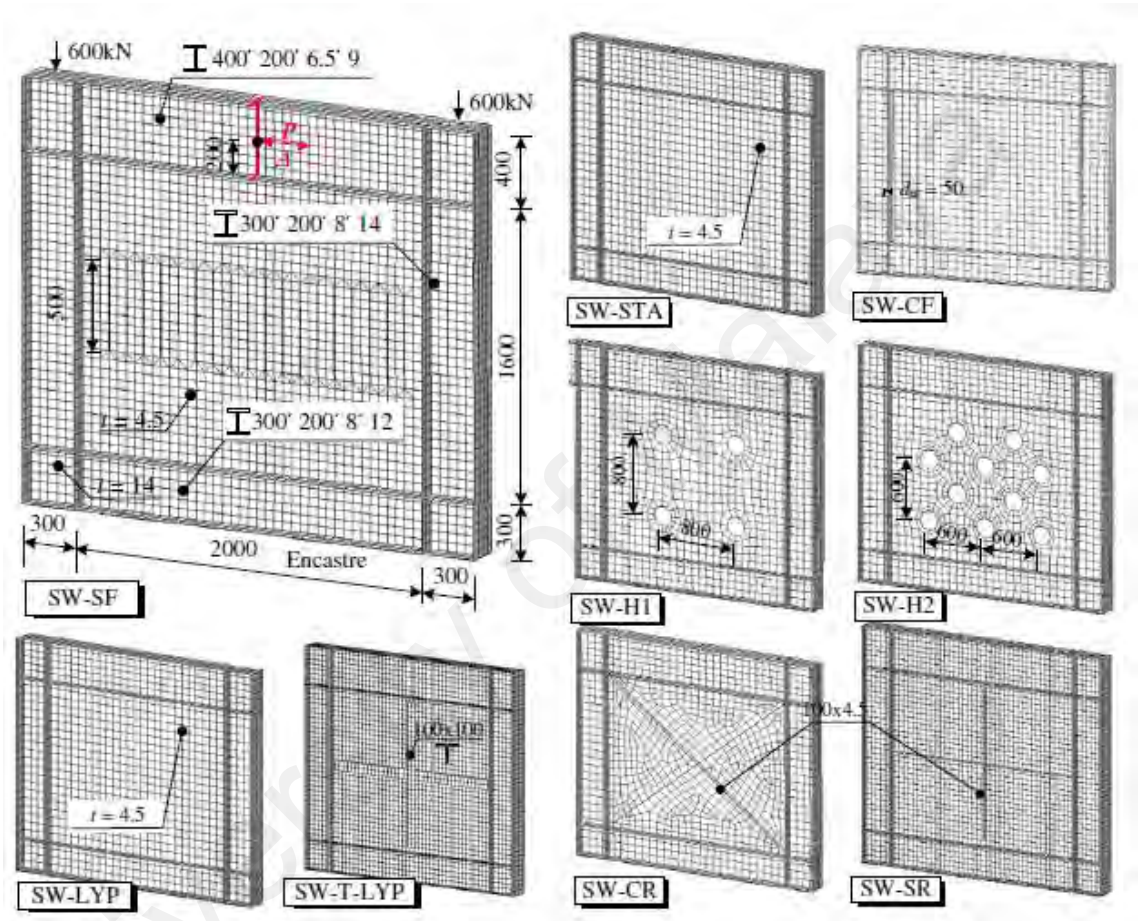

Figure 2-31 Overall configuration of FE models of Meng et al.(2015)

To evaluate the effect of the connection flexibility on the behavior of stiffened and unstiffened SPSWs, Guo et al. (2015) conducted an experimental and numerical research. The hinge, rigid and semi-rigid joint connections of HBE were considered in the research. The experimental test was carried out under cyclic loading on three one-third two-story single-bay specimens all with semi-rigid beam connection (Figure 2-32). These specimens included unstiffened, diagonal stiffened and cross stiffened and, the infill plate aspect

ratio was equal to one. Using the experimental test result, nine FE models of the SPSWs with hinged, semi-rigid and rigid type connection were modeled and validated. The objective of the study was to examine the effect of frame joint forms on the performance of stiffened and unstiffened SPSWs. In the experimental test they concluded that by setting up stiffeners, the yield strength was increased by 20%. The ultimate strength of diagonal stiffened specimens was about 5% larger than the cross stiffened specimens. Based on the numerical analysis, the ultimate capacity of the rigid joint connection was about 15% larger than the hinged joint whereas, such difference was about 5% for semi-rigid joint. The researcher concluded that the effect of joint stiffness on the bearing capacity of SPSW was negligible at elastic stage and suggested a semi-rigid connection on the boundary frame of SPSWs. Author Guo et al. (2017) in a similar research investigated the effect of semi-rigid connection on the behavior of cross stiffened SPSW with various configuration and number of crossed shape stiffeners

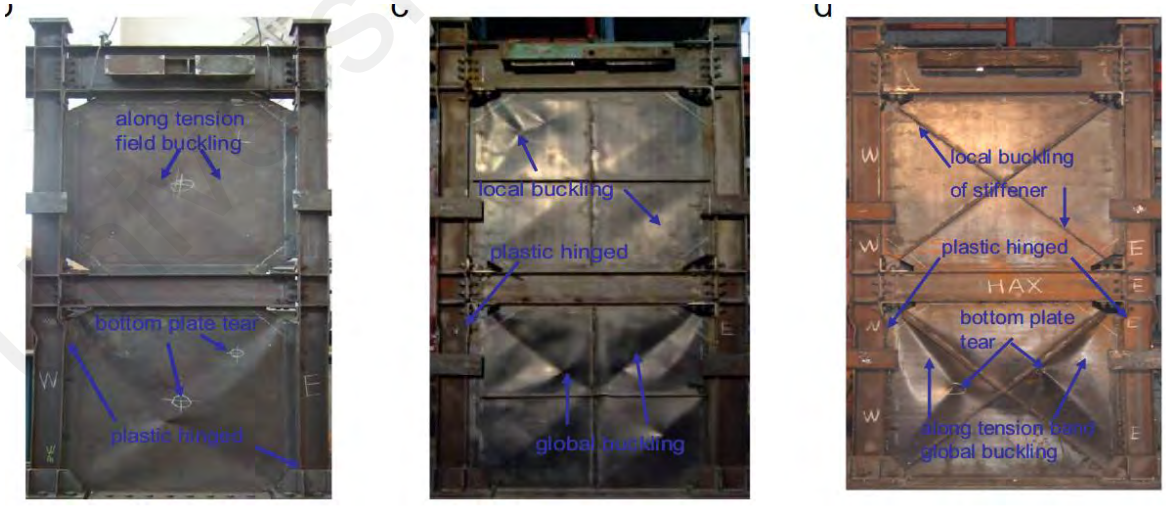

Figure 2-32 Failure mode of specimens tested by Guo (Guo et al., 2015)

To investigate the behavior of stiffened SPSWs by taking into consideration the gravity load effects, Zhao and Qui (2016) conducted the elastic buckling and nonlinear pushover analysis on a set of stiffened and

unstiffened SPSWs. The main objective of the study was the influence of the stiffeners layout on the general behavior of single-story stiffened SPSWs with and without gravity loads (Figure 2-33). The stiffeners include a set of plate or channel sections, which were modeled on one side of the infill plates. They concluded that when gravity loads were considered, the advantages of channel stiffened SPSWs were more outstanding compared to unstiffened SPSWs.

Figure 2-33 Layout of FE models investigated by Zhao and Qui (2016)

Gholipour and Alinia (2016) investigated the width of the bay on the behavior of multi-story code-designed SPSW using FE models. The code recommends the aspect ratio of the panel to be between 0.8 to 2.5. The researcher selected the bay with 3, 6 and 9 meters (aspect ratio equal to 0.83, 1.67 and 2.5 respectively). The number of stories of the models varies between 4 to 19. The main objective of the study was to provide reasonable decision tools for selecting the most proper bay width in the practical project, and to study the impact of the bay width on the performance of multi-story unstiffened SPSWs. The results showed that the proper bay width can reduce

the VBE section in high-rise SPSWs and affected the stiffness, load capacity of the system and deformation mode of the lateral load resisting system. As shown in Figure 2-34 the researchers concluded that bay width influenced the over strength and force modification factor. In Figure 2-34 the horizontal solid line indicates the values that were recommended by ASCE (2010). Furthermore, the researcher concluded that the response modification factor decreases with the number of story in all bay width whereas, it increases with the bay width. The value of 2.5 was suggested for the over strength factor of unstiffened SPSWs. The considerable effect of the aspect ratio of the composite SPSW on the stiffness, ductility and response modification factor was also confirmed by Jiang et al.(2017).

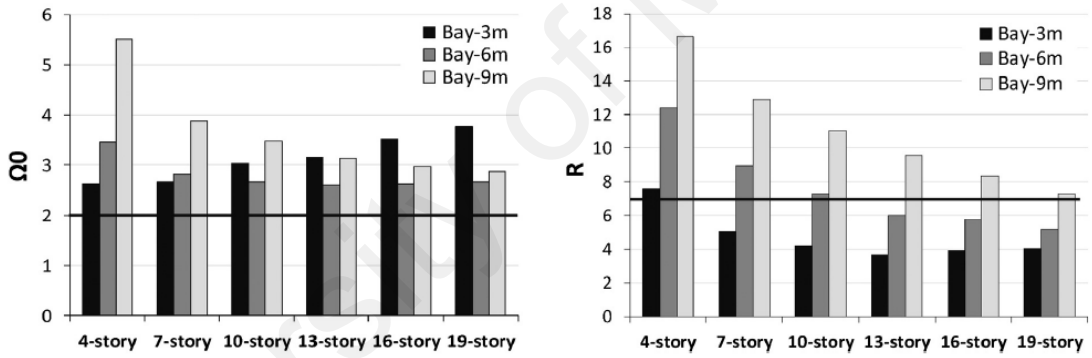

Figure 2-34 The over strength and force modification factor for different story and bay width of SPSW (Gholipour and Alinia, 2016)

Sigariyazd et al. (2016) conducted an experimental and numerical study on the diagonally stiffened SPSWs. The test was carried out on three 1/3 scaled specimens under monotonic loading regime. The first specimen was unstiffened SPSW and the remaining two were diagonally stiffened using different stiffener configurations (Figure 2-35). The yielding and ultimate stresses of infill plate materials were about 20% lower than the material of boundary frame and stiffeners. To prevent any failure due to axial forces, the

triangular plates were used at the connection of the columns to the base. The main objective of the study was to determine the influence of stiffeners on the behavior of specimens. The researchers found that diagonal stiffeners improved the structural behavior, strength and stiffness of the SPSWs. Additionally, equations for calculating the strength and stiffness of the stiffened specimens were provided.

Figure 2-35 Unstiffened and diagonally stiffened specimens of Sigariyazd, et al. (2016)

In an attempt to improve the buckling behavior and hysteresis curves of SPSW, Nooralizadeh, et al. (2017) conducted an experimental research on three sets of stiffened and unstiffened SPSWs under cyclic loading. Based on the stiffener covering area, the sets were divided to unstiffened, partially stiffened and fully stiffened specimens (Figure 2-36). The aspect ratio was equal to one but the dimension and thickness of infill plate were 430 millimeters and 3 millimeters respectively. Using bolts, the folded trapezoidal steel stiffener was connected on one side of the infill plate. The objectives of the research was to find a stiffening method that can eliminate the weaknesses of buckling behavior of SPSWs which includes an early out-of-plane buckling,

un-symmetric hysteresis curve, and low ultimate strength. The findings of the research showed that the hysteresis behavior of stiffened SPSWs improved when compared to unstiffened SPSWs where the ultimate shear capacity of fully-stiffened and partially-stiffened specimens increased 35.4% and 30.4% respectively. Moreover, increasing the stiffener covering area more than the proper ratio was not useful in the buckling behavior. Therefore, they concluded that the stiffeners are not necessary to cover the entire area of the infill plate.

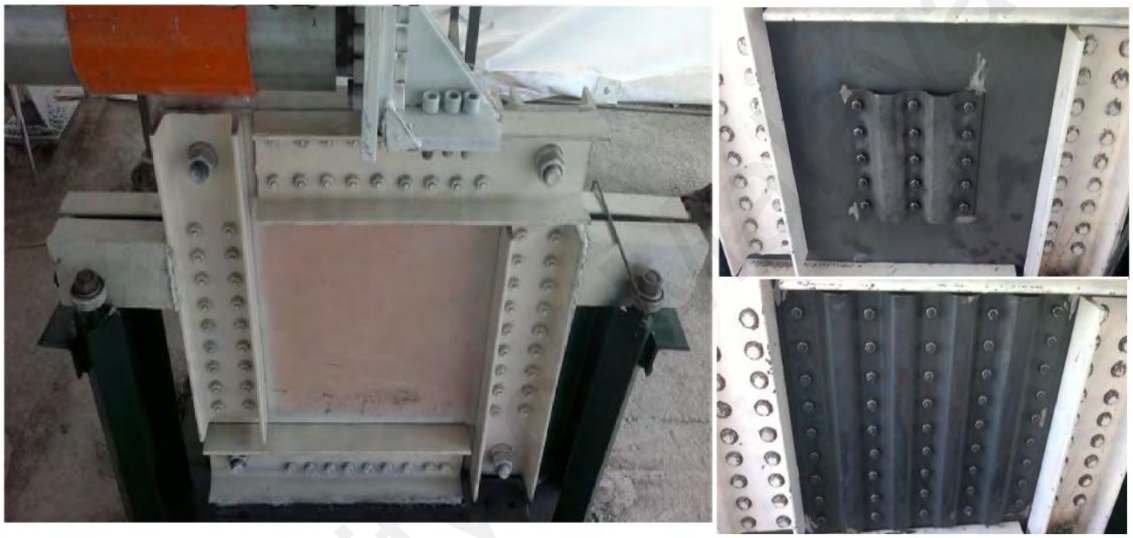

Figure 2-36 Specimens unstiffened, partially stiffened and fully stiffened specimens tested by (Nooralizadeh et al., 2017)

2.3 CONCEPT OF SEISMIC PERFORMANCE FACTORS

2.3.1 Introduction

Response modification *(R)*, over strength *(Ω_o)* and displacement amplification *(C_d)* factors are used in the force-based seismic design procedures. In 1959, the Structural Engineers Association of California (known as SEACO Blue), (SEAOC, 2008) introduced the horizontal force factor *(K)*. By using this factor, a minimum design base shear for limited type of structures was defined; therefore, the *(K)* factor is known as the ancestor of the response modification factor (A.T.C, 1995).

In the context of ATC-63, tentative provisions for the development of seismic regulations for building (A.T.C, 1978), the R (force modification) factors were initially proposed. The R factor was defined as "the ratio of the force level that would be developed in the entirely linear elastic system for design earthquake ground motions to the base shear considered for design". In this report, the *R* factors were proposed based on the judgment and qualitative comparison with the known response of few structures under previously experienced seismic loads. Therefore, most of those seismic resisting systems, which *R* factors prescribed for them within this report, have never been subjected under considerable earthquake shaking, and their real performance was unknown.

Observing the satisfactory performance of structures, has led to the idea that the structures which were designed based on elastic load are able to sustain considerable plastic deformation. Therefore, based on the theory that well-detailed seismic resisting systems are able to undergo large inelastic deformation without collapse (ductile behavior), the concept of the response modification factors was proposed (A.T.C, 1995). The R factor is an empirical response reduction factor that accounts for the over-strength, damping and inherent ductility of the structural system at the displacements greater than the initial yield and approaching the ultimate deformation of a structural system (F.E.M.A, 2003-2006). Engineering practice benefited from these facts of structural behavior and, for the purpose of calculating a design base shear *(V)*, the "*R*" factor was employed to reduce the base shear force (V_E) calculated by elastic analysis using a 5% damped acceleration response spectrum. Both the Equivalent Lateral Force (ELF) and Response Spectrum Method are well known linear static analysis, which the "*R*" factor is utilized to calculate the design base shear. In both the methods, the

inelastic response of structures was approximated by an elastic analysis method just by applying the "*R*" factor.

Various numerical values of response modification factors have been developed and used in different countries. International variability and domestic uncertainty demonstrated the need for a standardized, systematic, and rational procedure for determining the *R* factors. To meet this need, the primary goal of the ATC-63 Project was to establish a methodology for quantitatively determining the *R* factor and the directly related design parameters that affect building seismic response and performance for the usage in seismic design.

As a new structural system, the certainty of the seismic capability needs to be quantified. The ability to use the nonlinear collapse simulation technique leads to link the seismic performance factors to the system performance capability in the probabilistic earthquake. In the current building codes, the seismic performance factors are used to estimate the deformation and strength demands on seismic-force-resisting systems, which are designed using a linear method of analysis, while are responding in the nonlinear range. Despite most of the structural design standards allow for inelastic behavior of structural elements under severe earthquake ground motion, static analysis has protected its prevalence for primary seismic design in practice. As a result, the seismic performance factors have preserved its importance.

The present research focuses on quantifying the seismic performance factors (SPFs), including over-strength factor (Ω_0), displacement amplification factor (C_d) and response modification coefficient (R), for stiffened steel plate shear walls. Using the response modification factor, the reduced seismic forces can be determined through elastic analysis. The displacements determined through the elastic method increases by the displacement amplification factor.

The expected strength can be estimated using the design strength and over-strength factors. In fact, the over-strength factor accounts for the reserved strength from the first plastic hinge to the mechanism stage (instability) of the structural system.

Table 12.2-1 of ASCE (A.S.C.E, 2010) listed the values of 7, 2 and 6 for R, Ω_0 and C_d respectively, and no reliable data is provided for the performance factor for stiffened SPSW. The aim of this investigation is to explore the sensitivity of the seismic performance factor to the stiffeners configuration and stiffeners thickness to provide reliable seismic performance factors for the stiffened SPSWs.

2.3.2 History of Formulation

In the 1980s, using the experimental data obtained from the test on two concentrically and eccentrically braced frames, the researchers from Berkeley described R as the product of three factors that included ductility, reserved strength and viscous damping (Uang and Maarouf, 1996):

$$\boldsymbol{R = R_{\mu} \Omega_0 R_{\xi}} \qquad (2\text{-}4)$$

Where R_{μ} is the ductility reduction factor, (Ω_o) the over-strength factor, and R_{ξ} is the damping factor. The over-strength factor was considered equal to base shear force at the yielding of structure (V_y) which is divided to the design base shear force (V). The ductility reduction factor was calculated equal to the base shear force of the structure that responds entirely elastic (V_E) divided to the base shear force at the yielding of structure (V_y). The value of the damping factor was equal to 1.0.

The Applied Technology Council (A.T.C, 1995) expressed the R factor by the product of three factors as:

$$\boldsymbol{R = R_{\mu} R_S R_R} \quad (2\text{-}5)$$

Where R_{μ} is the period dependent ductility factor, R_S is the strength factor, and R_R is the redundancy factor. As it can be seen, except for the redundancy factor, this equation is similar to the proposed equation by the researchers from Berkeley and their differences are in detail than in concept. In the above equation, the ductility factor ($R\mu$) is the ratio of the base shear force of the structure that responds entirely elastic (V_E) divided to the base shear force at the yielding of structure (V_y). The strength factor (R_S) is defined as the ratio of base shear force at the yielding of the structure (V_y) to the design base shear (V). Therefore, the period dependent ductility and strength factor can be expressed as:

$$\boldsymbol{R_{\mu} = \frac{V_E}{V_y}} \qquad \boldsymbol{R_S = \frac{V_y}{V}} \qquad \boldsymbol{\Omega_0 = \frac{V_y}{V_s}} \quad (2\text{-}6)$$

To consider the regularity of the seismic resisting system and structural integrity, the redundancy factor is proposed. In other words, to consider the sufficiency and reliability of the seismic framing system that uses multiple framing lines in each principal direction of the structure, the redundancy factor is defined. This factor, by reducing the R factor, causes an increase in the demand seismic design load for less redundant structures. To account for the effect of additional viscous damping devices, the damping factor (R_{ξ}) is defined. Considering that, the response modification factors are used in the force-based seismic design procedures, therefore the damping factor was eliminated from the new formulation.

2.3.3 Selected Method for the Calculation of S.P.Fs

To develop rational seismic performance factors in this study, the proposed method by Uang et al. (1991) is used. In the Uang (1991) method, the response of the structural system is replaced by idealized bilinear, which

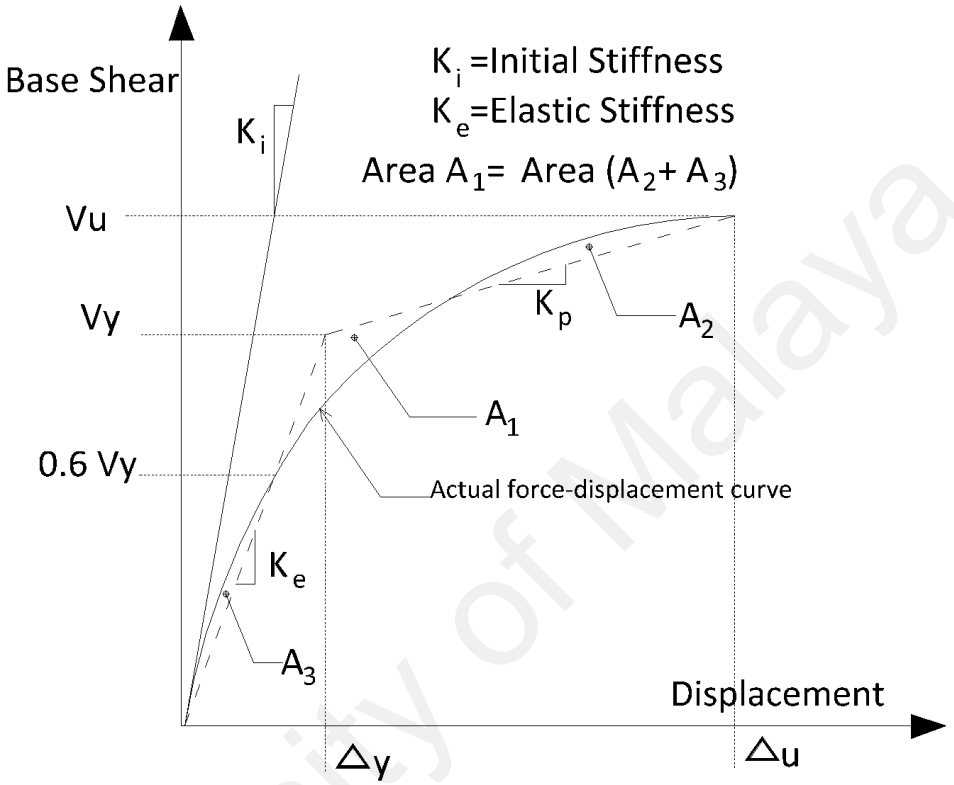

Figure 2-37 Bilinear idealization of load-displacement curves

relates the base shear to the lateral displacement (Figure 2-37). The comprehensive envelope curves and the force-displacement component related to the evaluation of seismic performance factors are depicted in Figure 2-38. In other words, based on the actual envelope and its bilinear idealized load-displacement curve, the seismic performance factors could be evaluated. The code illustration of seismic performance factors according to the Federal Emergency Management Agency (F.E.M.A, 2009a) P695 Quantification of Building Seismic Performance Factors is shown in Figure 2-39. By comparing the methodology outlined by Uang (1991) and FEMA (2009a) it can be seen that both methods are quite similar in the definition of S.P.F .

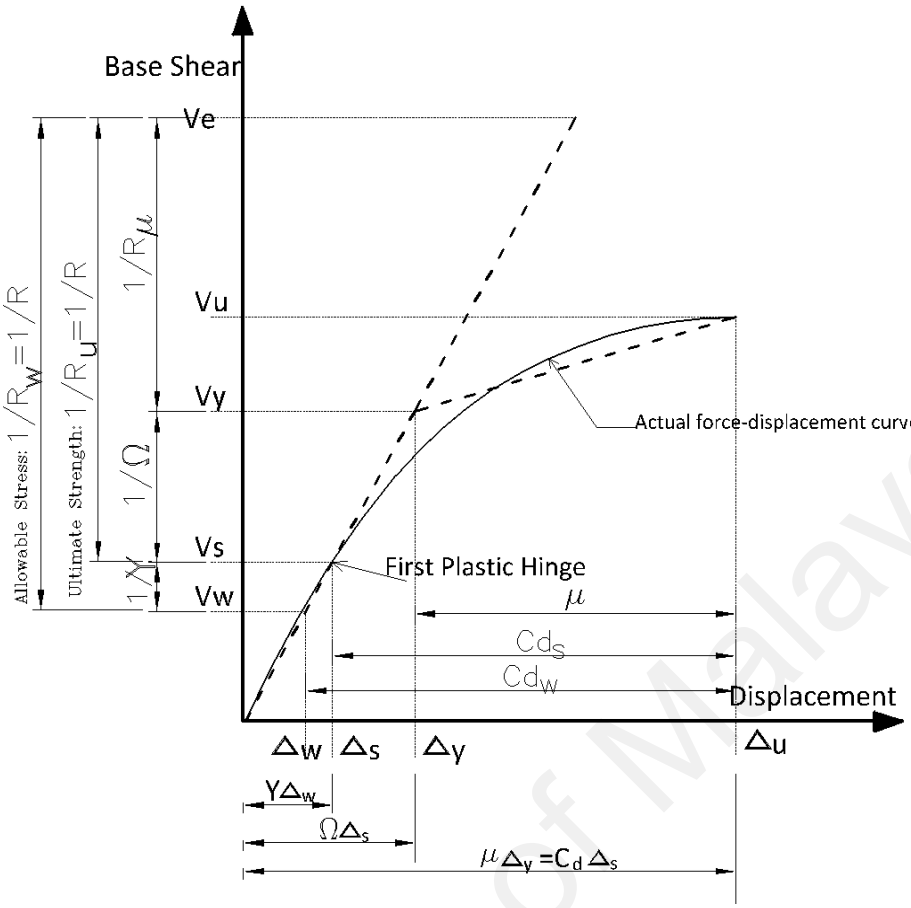

Figure 2-38 Seismic performance factors based on the Uang et al. (1991)

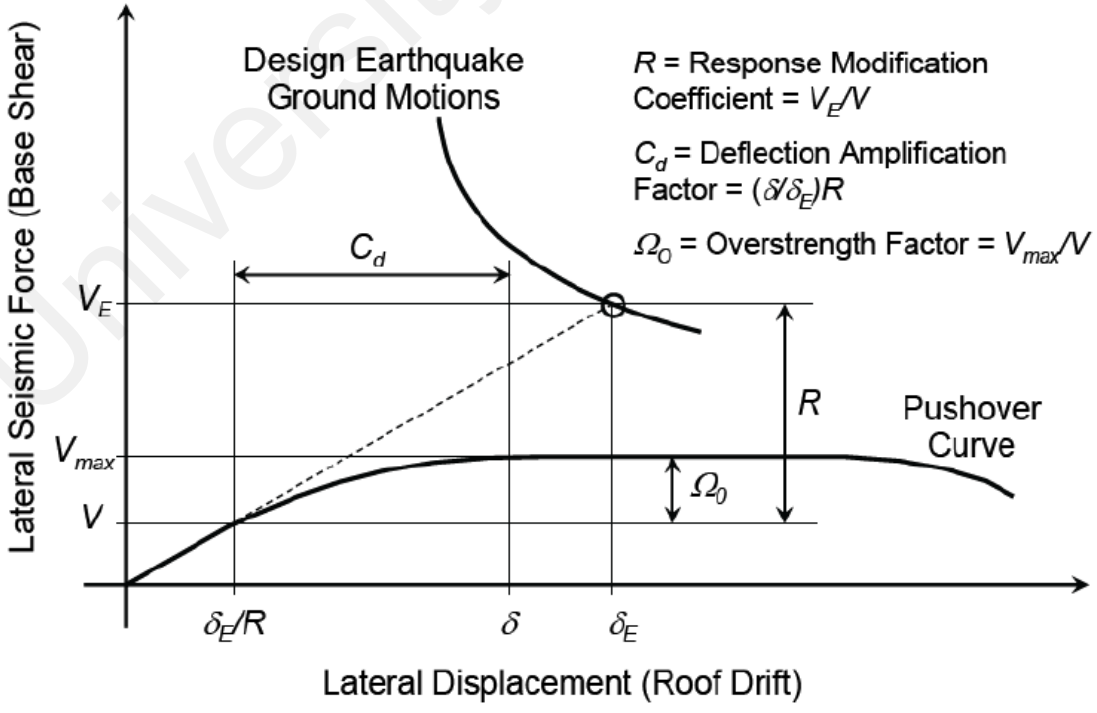

Figure 2-39 Code illustration of seismic performance factors based on the FEMA(2009)

To perform the methodology outlined above, it is necessary to provide a

set of load-displacement curves. These curves can be obtained from experimental tests or numerical modeling, and should be the representative of the range of different SPSWs, which is considered in the study. In the case of numerical models, the load-displacement curve must be able to reflect the strength and stiffness degradation of the structural system. Based on the research done by Ibarra et al. (2005), the post-capping degradation portion of the load-displacement curve is essential to simulate collapse for the numerical models. Ideally, in the case of experimental test, the lateral load is applied until the system reaches a loss of 20% of the base shear capacity. Therefore, for experimental tests or numerical models, which incorporate the strength degradation, the displacement corresponding to the 80% of the ultimate strength is considered to the ultimate displacement (Figure 2-40). The ultimate displacement of the system has the crucial effect on the obtained value of S.P. F.

All significant deterioration mechanism that could lead to the structural

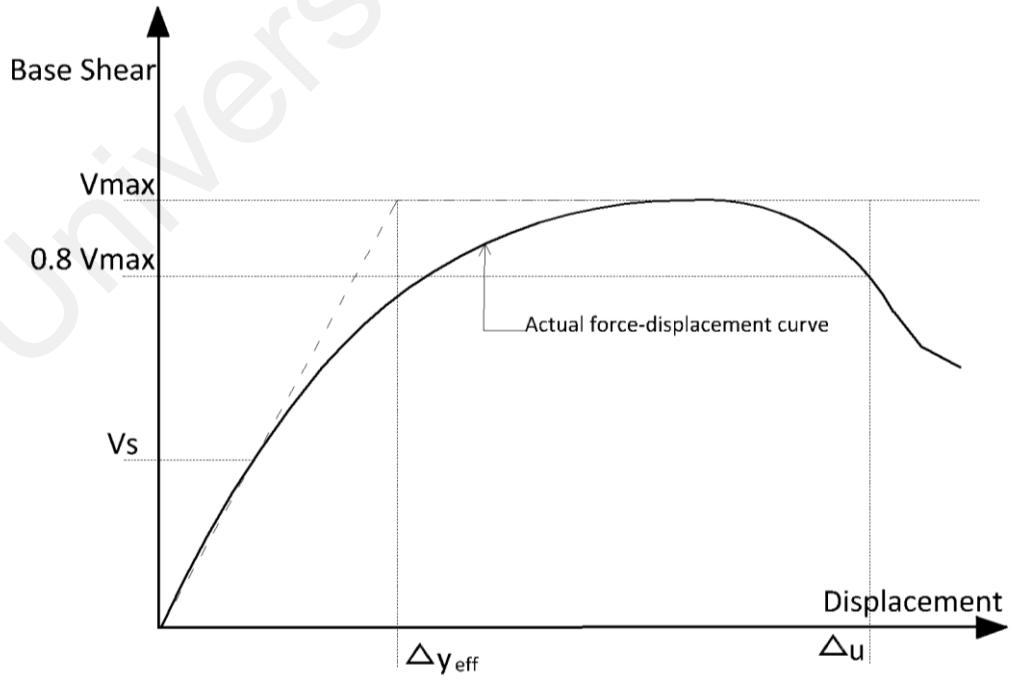

Figure 2-40 Definition of ultimate disablement for load- displacement curves incorporate the strength degradation

collapse should be included in the explicit simulation of the nonlinear system (F.E.M.A, 2009a). The representative nonlinear model of seismic-force-resisting system requires both detailed design information of its assemblies and comprehensive test data on the structural component. Such nonlinear models have substantially less uncertainty in their seismic performance and need a lower safety margin against the collapse compared to the system with less robust data in the equivalent level of safety.

2.3.3.1 Ductility reduction factor (R_μ):

The ductility reduction factor (R_μ) is the ratio of the base shear force of the structure that responds entirely elastic (V_E) divided to the base shear force at the yielding of structure (V_y).

$$\boldsymbol{R_\mu = \frac{V_E}{V_y}} \quad (2\text{-}7)$$

Based on the natural period of vibration and ductility of structures, several equations were proposed for the calculation of the ductility reduction factor. In the present study, the equations proposed by Newmark et al. (1982b) were used throughout the calculation of ductility reduction factors as shown below:

$$\boldsymbol{R_\mu = 1} \qquad \boldsymbol{T<0.03}$$
$$\boldsymbol{R_\mu = \sqrt{2\mu - 1}} \qquad \boldsymbol{0.12<T<0.5}$$
$$\boldsymbol{R_\mu = 1} \qquad \boldsymbol{T>1} \quad (2\text{-}8)$$

Where μ is the displacement ductility. The capacity of the structure to undergo inelastic deformation without collapse is referred as the ductility. The ductility is defined as the ratio of ultimate lateral displacement to the yield displacement:

$$\boldsymbol{\mu = \frac{\Delta_U}{\Delta_y}} \quad (2\text{-}9)$$

2.3.3.2 Over strength factor (Ω_o):

Most buildings had survived past earthquakes that are greater than the designed forces, without considerable damage, had led to the idea that designed structures possess significant reserved strength. The attempts for quantifying this reserved strength resulted to the introduction of over-strength factor. The reserved strength of the structures between formations of the first plastic hinge to the mechanism stage is called over-strength factor. In fact, the over-strength factor is the capability of the structure in the redistribution of internal forces, after entering into the inelastic phase. In addition to the internal force redistribution capability, which is the only reliable source, another important resource of reserved over-strength in the structure could include higher real strength than the nominal design strength of material, bigger size of the structural element compared to the required design dimension, using the simplified conservative models for structure analysis and contribution of non-structural element in the resisting of lateral forces. According to the FEMA (F.E.M.A, 2009a), only non-seismic requirements applicable universally to all structures should be considered when evaluating the potential over-strength relative to earthquake loading. Therefore, only the internal forces redistribution capability could be considered for the estimation of the over strength values.

Based on the reserved strength definition described above, the over-strength factor is considered equal to the ratio of the base shear force at yielding of structure (V_y) to the design base shear force, which first yield of structural element that causes softness in the real envelope of the load-displacement curve (V_s).

$$\boldsymbol{\Omega_0 = \frac{V_y}{V_s}} \qquad (2\text{-}10)$$

2.3.3.3 Response (or force) modification factor (*R*):

The force reduction or response modification factor included several structural key features such as energy dissipation, the ability to sustain inelastic displacement and the capacity to undergo reversed cyclic loading. The *R* factor is quantified by the ratio of maximum base shear force exerted on a structure if it remained entirely elastic to the design base shear force. Therefore, the actual seismic forces are reduced by *R* factor to achieve the design forces. For the LRFD and ASD design method, the *R* factor can be expressed respectively as:

$$\boldsymbol{LRFD} \quad : \boldsymbol{R} = \frac{\boldsymbol{V_E}}{\boldsymbol{V_s}} = \frac{\boldsymbol{V_E}}{\boldsymbol{V_y}} \times \frac{\boldsymbol{V_y}}{\boldsymbol{V_s}} = \boldsymbol{R_\mu \Omega_o} \tag{2-11}$$

$$\boldsymbol{ASD} \quad : \boldsymbol{R} = \frac{\boldsymbol{V_E}}{\boldsymbol{V_w}} = \frac{\boldsymbol{V_E}}{\boldsymbol{V_y}} \times \frac{\boldsymbol{V_y}}{\boldsymbol{V_s}} \times \frac{\boldsymbol{V_s}}{\boldsymbol{V_w}} = \boldsymbol{R_\mu \Omega_o Y} \tag{2-12}$$

These equations show through a force reduction or response modification factor, both the energy dissipation capacity (ductility) and the reserved strength (over-strength factor) are taken into account in the structural design. The allowable stress factor (Y), is used to reflect the difference in the format of material codes and is defined as:

$$\boldsymbol{Y} = \frac{\boldsymbol{V_s}}{\boldsymbol{V_w}} \tag{2-13}$$

For LRFD and strength design method, the value of *Y* is set to 1.0 and for the allowable stress design method, the value of Y is approximately in the range of 1.4-1.5 (Uang, 1991).

The deflection amplification factor (C_d) is defined by the roof drift of the system corresponding to the base shear Δ_E (if the system remained linear elastic for the level of force) and the assumed roof drift of the yielded system and is related to ductility and over-strength as follows:

$$\boldsymbol{LRFD}: \quad \boldsymbol{C_d} = \frac{\Delta_U}{\Delta_S} = \frac{\Delta_U}{\Delta_y} \times \frac{\Delta_y}{\Delta_S} = \boldsymbol{\mu\, \Omega_o} \tag{2-14}$$

$$\boldsymbol{ASD:} \quad \boldsymbol{C_d} = \frac{\Delta_U}{\Delta_W} = \frac{\Delta_U}{\Delta_y} \times \frac{\Delta_y}{\Delta_W} = \boldsymbol{\mu} \times \frac{\boldsymbol{\Omega o}\ \Delta_S}{(\frac{\Delta_S}{Y})} = \boldsymbol{\mu\ \Omega_o\ Y} \qquad (2\text{-}15)$$

2.4 SUMMARY

In comparison with the other lateral load resisting system, the distinctive behavior of SPSWs demonstrated its advantages in the aspect of energy absorption, strength and ductility, stable hysteresis curves and stiffness. An extensive number of researches have been conducted on the performance of un-stiffened steel plate shear walls. Relatively limited research was found on the stiffened SPSWs and comparison of SPSW performance with different stiffeners configuration. Considering such shortcomings, the main objective of this research is to investigate the effect of different stiffeners configuration on the performance of stiffened SPSWs. It is clear that dynamic analysis and shake table testing captures the real performance of stiffened SPSWs. Considering the available facility in the location of research, the quasi-static cyclic loading is selected for the present investigation.

In the analysis of structures under seismic loading, the lateral earthquake load should be applied to the structure and then to the SPSWs. Among several procedures for seismic force calculation, the Equivalent Lateral Force (ELF) procedure and the Modal Analysis procedure (Response Spectrum Analysis) are widely accepted by structure designers due to the simplicity and reasonable results. Both analysis procedures use four important seismic factors i.e. Response Modification coefficient, R, Over-strength Factor, Ω_0, Deflection Amplification Factor, C_d and Reliability or Redundancy Coefficient R_μ. The research described herein includes investigation and derivation of response modification coefficient and over strength factor for SPSWs with different stiffeners configurations. Furthermore, because of the expenses involved in the

experimental programs to evaluate the capacity design methods, an analytical or numerical tool that can accurately predict the monotonic, cyclic and dynamic behavior of SPSWs is needed.

CHAPTER 3: EXPERIMENTAL TEST PROGRAM

3.1 INTRODUCTION

In this chapter, Quasi-static tests are explained. The details of test setup, procedure, protocol, data acquisition, and test results are provided in sub-sections. The tests on the fabricated specimens were conducted at the Construction Research Institute of Malaysia (CREAM) laboratory. The CREAM laboratory facilities are equipped with a 1200mm thick reinforced concrete reaction floor and 1500mm thick reinforced concrete reaction wall. The strong wall was used to apply the horizontal loads on the steel plate shear wall specimens that were anchored at its base to a concrete strong floor.

The main objectives for the tests defined as follow:

1- To obtain the performance data
2- To study post-buckling and post-yield behavior of stiffened and unstiffened specimens
3- To study the influence of different stiffening patern
4- To gather necessary data for Finite Element (FE) modeling
5- To validate the Finite Element models

3.2 DESIGN OF TEST SPECIMENS

Five quarter scale SPSW specimens with different infill plates were fabricated and tested under cyclic loading. Selection of the test specimen was done such that representative SPSW realistic aspect ratio and infill plate thicknesses and its material could be supplied. Simultaneously, the limitation of cyclic actuator and lateral supports was considered. The minimum available thickness for steel and aluminum infill plates was 1.25mm and 1.5 mm respectively. All specimens have the same aspect ratio of infill plate equal to

one. Overall dimensions of the plate are 87 cm with 80 cm center-to-center of connecting bolt hole's (Fig 3-1). In order to prevent tearing at the edge of the walls, all four edges were strengthened by 70 mm wide and 2.50 mm thick plate (Figure 3-1). Typical infill plate detailing is given in Figures 3-1 and 3-2.

The thickness of infill plates is based on the minimum available thickness in the test location area for steel, and aluminum infill plate. For comparison reasons, all stiffened steel plates have the same thickness of un-stiffened plates. The mechanical properties of the material were obtained through standard coupon tensile test.

Two specimens were un-stiffened and they were fabricated from aluminum and mild steel sheet plate. These specimens were named AL-SPSW and US-SPSW, respectively. AL-SPSW is aimed to study the effect of different mechanical properties of infill plate. Three specimens were stiffened steel plate with different shape of stiffening configurations, i.e. cross stiffened (named as CS-SPSW), circular stiffened (CRS-SPSW) and diagonal cross stiffened (DS-SPSW).

3.2.1 Design of Unstiffened Steel Infill Plate

The minimum available thickness for steel infill plate was 1.25 mm. The overall dimension of test specimens was selected such that the cost of fabrication can be decreased effectively, and the capacity limitation of the actuator was considered. Based on the supplier information, both boundary frame member and infill plates were specified to be A572 Gr.50 steel with the minimum yield stress equal to 320 MPa.

In the plate-frame interaction method which is known as PFI method, neglecting the effect of flexural behavior (global bending stress), the shear

load-displacement relation of SPSW is characterized (Sabouri-Ghomi et al., 2005). The shear dominant behavior of SPSW is expected in the ductile SPSW with low number of stories. In such SPSWs, the shear load and displacement relation can be obtained separately and, by superimposing that results, the shear load-displacement diagram of the SPSWs can be defined. In the case of the tested specimens, the hinged boundary frame do not contribute in tolerating of the applied lateral displacement therefore, the shear load-displacement relation of the infill plate defines the characterized behavior of the specimens. The typical characterized behavior of the infill plate based on the PFI method is shown in Figure 3-3. In this figure the points C and D defines the buckling and yielding limits respectively and, the ultimate strength of the infill plate is equal to the yielding load. As shown in Figure 3-3, for an infill plate of width b, height of d and thickness of t_p, the buckling and yielding points are determined by Equation 3-1 to 3-8.

$$\boldsymbol{\tau_{cr} = \frac{k\,\pi^2\,E}{12\,(1-\mu^2)}\left(\frac{t_p}{b}\right)^2 \leq \tau_{wy} = \frac{\sigma_0}{\sqrt{3}}} \quad (3\text{-}1)$$

$$\boldsymbol{simply\ supported\ edge: k = 5.35 + \frac{4}{\varphi^2}} \quad (3\text{-}2)$$

$$\boldsymbol{clamped\ edge: k = 8.98 + \frac{5.6}{\varphi^2}} \quad (3\text{-}3)$$

$$\boldsymbol{F_{wcr} = \tau_{cr}.b.t_p} \quad (3\text{-}4)$$

$$\boldsymbol{U_{wcr} = \frac{\tau_{cr}}{G}.d} \quad (3\text{-}5)$$

$$\boldsymbol{F_{wu} = b.t_p.\left(\tau_{cr} + \frac{C_{m1}}{2}\sigma_{ty}.sin2\theta\right)} \quad (3\text{-}6)$$

$$\boldsymbol{U_{we} = \left(\frac{\tau_{cr}}{G} + \frac{2C_{m2}.\sigma_{ty}}{E.sin2\theta}\right).d} \quad (3\text{-}7)$$

$$\boldsymbol{K_w = \frac{F_{wu}}{U_{we}}} \quad (3\text{-}8)$$

Where t_p, E, μ, σ_0, G, θ are infill plate thickness, modules of elasticity, Poisson's ratio, uniaxial yield stress, shear modules of material of infill plate and angle of inclination of tension field respectively. φ, is the aspect ratio of

the panel or subpanel, which is the greater value between b_{subp}/d_{subp} and d_{subp}/b_{subp}. The critical shear stress, critical shear load, critical shear displacement, shear strength, shear yielding displacement and shear stiffness are shown by τ_{cr}, F_{wcr}, U_{wcr}, F_{wu}, U_{we} symbols respectively. The symbol of σ_{ty} denotes the yielding tension field and determined by equation 3-9.

$$\mathbf{3}.\boldsymbol{\tau_{cr}}^{\mathbf{2}} + \mathbf{3}.\boldsymbol{\tau_{cr}}.\boldsymbol{\sigma_{ty}}.\boldsymbol{sin2\theta} + \boldsymbol{\sigma_{ty}}^{\mathbf{2}} - \boldsymbol{\sigma_{0}}^{\mathbf{2}} = \mathbf{0} \qquad (3\text{-}9)$$

The C_{m1} and C_{m2} are modification factor and the values of $0.8<C_{m1}<1$ and $1<C_{m2}<1.7$ are proposed. Sabouri-Ghomi et al. (2005) proposed the values of 1.0 and 1.2 for C_{m1} and C_{m2}, respectively for ductile steel plate walls with moment connection of beam-column, enough column rigidity and welded steel plate to boundary frame. Sabouri-Ghomi et al. (2005) concluded for specimen with SPSW with pin joints at the end of the beams C_{m1}=0.8 and C_{m2}=1.7 showed best fits of the results of PFI method with the test results of the Timler (1983). In the case of present research with hinged boundary frame, different material classification and bolted connection of infill plate to frame, the definition of proper values of C_{m1} and C_{m2} is the aim of the research.

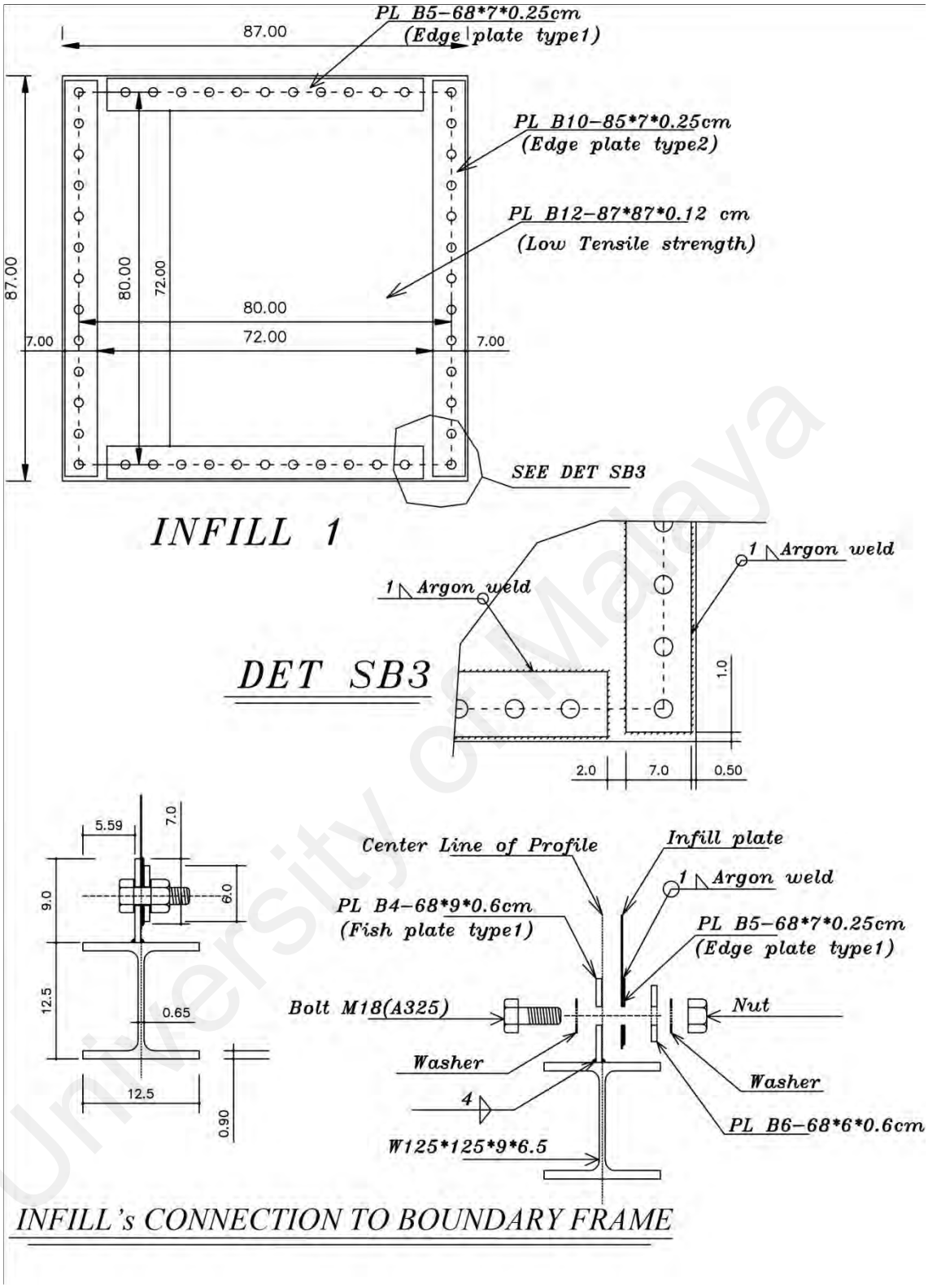

Figure 3-1 Un-stiffened infill detail

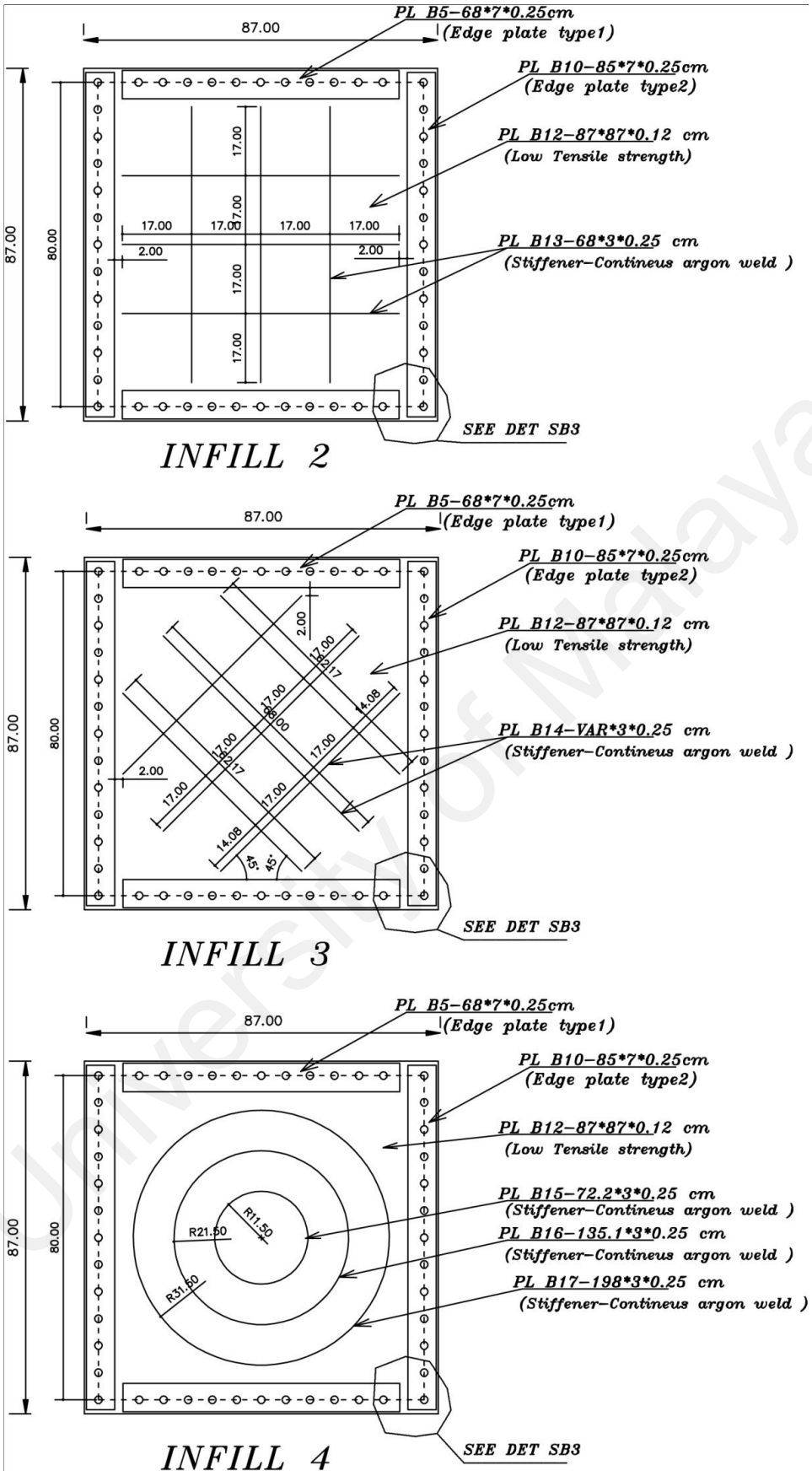

Figure 3-2 Stiffened Infill plates detail

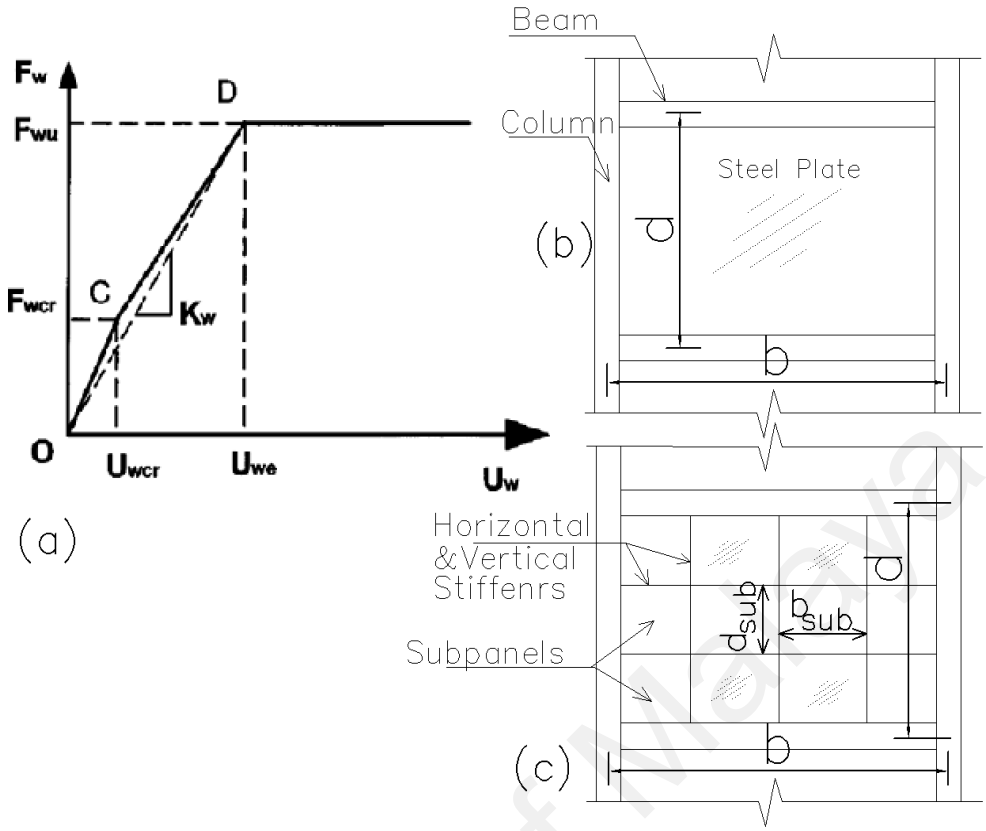

Figure 3-3 (a) Shear load-displacement of infill plate only according to PFI method, (b)and (c) schematic of unstiffened and stiffened SPSW (Sabouri-Ghomi et al., 2005)

3.2.2 Design of Stiffened Steel Infill Plates

A properly designed stiffener with adequate rigidity, induce nodal lines in the stiffened plate. In such plate, the overall buckling mode changes to local buckling of subpanels which restricted by stiffeners. Hence, the elastic buckling strength of such stiffened plate can be computed by considering individual subpanel between the stiffeners and treated as simply supported plates (Alinia and Sarraf Shirazi, 2009). The optimum stiffener arrangement should prevent overall buckling and thus, the critical stress of the stiffened plate would be equal to the critical stress of an individual simply supported subpanel. Meanwhile, for proper stiffened SPSW, steel plate should buckled after the infill plate yielding, therefore based on the PFI method the maximum critical stress of the ($\sigma_0/\sqrt{3}$) could be used for the calculation of the shear

strength and yielding displacement of the infill plate by equation 3-4 and 3-5. This method was used for rectangular subpanels and the precision of such converting of the stiffened SPSW to the subpanels and its applicability for other pattern is a part of the present research.

The critical shear load, F_{wcr} of a plate is thus calculated by the classical Equations (3-4) and (3-10).

$$\boldsymbol{\tau_{cr}} = \frac{\boldsymbol{k\,\pi^2\,E}}{\boldsymbol{12\,(1-\mu^2)}}\left(\frac{\boldsymbol{t_p}}{\boldsymbol{s}}\right)^{\boldsymbol{2}} \qquad (3\text{-}10)$$

Where s is the smaller value between the subpanel length a_{subp} and the subpanel width, b_{subp}, and φ is the aspect ratio of subpanel, which is the greater value of *asubp/bsubp* or b_{subp}/a_{subp}.

Based on the above equations, AISC820 (2007) and the research done by Alinia et al. (2009) Equation 3-11 was used for arrangement of symmetric stiffeners.

$$\boldsymbol{t_s\,h_s^{2.5}} \geq \boldsymbol{1.8}\left(\boldsymbol{1}-\frac{\boldsymbol{x}}{\boldsymbol{10}}\right)\boldsymbol{t_p^{2.5}\,b}\ ,\ \boldsymbol{x} > 1 \qquad (3\text{-}11)$$

Where t_s is the thickness of stiffeners, h_s is the height of stiffeners and x is the number of horizontal or vertical stiffeners. Also, to comply with AISC-820 (2007) and AISC-360 (2010), and reducing the slenderness of the plate, Equations (3-12) and (3-13) were controlled. All stiffeners were connected to the infill plates by proper fillet weld.

$$\boldsymbol{I'_{st}} \geq \boldsymbol{b_{subp}\,t_p^3\,J} \qquad (3\text{-}12)$$

$$\boldsymbol{J} = \boldsymbol{2.5}\,(\frac{\boldsymbol{b}}{\boldsymbol{b_{subp}}})^{\boldsymbol{2}} - \boldsymbol{2} \geq \boldsymbol{0.5} \qquad (3\text{-}13)$$

. To prevent direct transmission of applied load, the stiffeners were designed shorter than the plate length. By applying the Equations (3-14) and (3-15) the weld-ability and local buckling of stiffeners, which proposed by AASHTO (2007) were controlled.

$$t_p \leq t_s < 5t_p \quad (3\text{-}14)$$

$$\frac{h_s}{t_s} \leq 0.48\sqrt{\frac{E}{\delta_y}} \quad (3\text{-}15)$$

The section area of stiffener of other stiffened specimens (CRS-SPSW, DS-SPSW) is similar to the CS-SPSWs and just the stiffeners configuration, and their pattern was changed (Figure 3-2).

3.2.3 Design Connection of Infill Plate to Boundary Frame

A series of fish plates was used to connect the infill plate to the boundary frame. Fish plates are relatively thick steel plates, which are welded to frame member to provide connection place for infill plates. Such plate also increases the stiffness of frame members. To connect infill plates to the fish plate several options could be selected, and it was the subject of numerous researches (Choi and Park, 2009, Schumacher et al., 1999, Hunter, 2010). The majority of researchers used fillet welds for the connection. In the present research, the easy replaceability of infill plate was considered as an advantage. Hence, the bolted connection was designed for connecting the infill plates to fish plates. Such connection also is used by (Choi and Park, 2008) and (Dubina et al., 2012) and in some cases a slight slippage of bolt connections was reported.

According to the clause 17.3 of ANSI/AISC 341-05 (2005), the required strength of web connection to the surrounding HBE and VBE is equal to the expected yield strength in tension by considering the angle of inclination. The web tension stresses component (from infill yielding) is calculated by the Equations 3-16 and 3-17.

$$W_{yci} = \frac{1}{2} F_{yp}\, t_{wi}\, sin2\alpha \quad (3\text{-}16)$$

$$W_{xci} = F_{yp}\, t_{wi}\, sin^2\alpha \quad (3\text{-}17)$$

To prevent tearing or crippling in the bolt holes of the fish plate, the distance between the holes (S) by Equations 3-18, 3-19, 3-20 and distance of center holes to the free edge (L_e) was checked by Equation 3-21.

$$\boldsymbol{S \geq \frac{2P}{F_U t} + \frac{d}{2}} \quad (3\text{-}18)$$

$$\boldsymbol{S \geq 3d} \quad (3\text{-}19)$$

$$\boldsymbol{S \leq 12t \leq 150mm} \quad (3\text{-}20)$$

$$\boldsymbol{L_e \geq \frac{2P}{F_U t} + \frac{d}{2}} \quad (3\text{-}21)$$

According to the Table J3.4M of ANSI/ASCI 360-10 (2010) L_e less than 2.6 cm is not acceptable. Also bearing strength at bolt holes was controlled by using the Equation 3-22 (A.I.S.C, 2010).

$$\boldsymbol{R_n = 1.2\, L_c t\, F_u \leq 2.4\, d\, t\, F_u} \quad (3\text{-}22)$$

Where t is the thickness of plate, d is hole's diameter, F_u is the tensile strength of plate's material and, L_c is the clear distance in direction of the force between the edge of the hole and the edge of adjacent hole, or edge of the plate. The infill plate was connected to the boundary frames by 48 numbers of M18 bolts Grade A325 (Figure 3-4).

3.2.4 Design of Boundary Hinge Frame

Designs of the specimens were done per the following steps:

i. Step1- the inclination angle of tension field of 45 degrees was assumed.

ii. Step2- considering the stresses imposed by yielded infill plate to the boundary member is necessary. To ensure that frame member can sustain the normal boundary stresses associated with the tension field and the assumption of simple supported for beams and columns, Equations 3-23 and 3-24 should be satisfied for columns and beams respectively (Sabouri-Ghomi et al., 2005).

$$M_{fp} \geq \frac{\delta_{ty}.t.d^2}{8} cos^2\theta \quad (3\text{-}23)$$

$$M_{fp} \geq \frac{\delta_{ty}.t.b^2}{8} sin^2\theta \quad (3\text{-}24)$$

By using above equations and the assumed angle inclination in the step1, W100*100*17.2 as a primary evaluation for boundary frame member section was obtained.

For safety reasons and considering the stiffened infill plates which could impose more stresses to the boundary frames; the section of this elements was increased to W125*W125*23.8.

iii. Step3- by using the last profile section, the inclination angle of tension filed by using equation 3-25 was calculated and the equations 3-23 and 3-24 were controlled.

$$tan^4\alpha = \left[\frac{1+\frac{L\,t_p}{2A_c}}{1+h\,t_p\left(\frac{1}{A_b}+\frac{h^3}{360\,I_c\,L}\right)}\right] \quad (3\text{-}25)$$

iv. Step4- A sufficient stiff and strong boundary element better anchors the tension diagonals; therefore, the ultimate strength of infill plate is fully developed. For vertical boundary element, the stiffness is recommended (Sabelli and Bruneau, 2007) by the equation 3-26.

$$I_C \geq \frac{0.00307 t_W d^4}{b} \quad (3\text{-}26)$$

3.2.4.1 Design hinge connection of boundary frame

Hinged boundary frame was used to reduce the complexity of cyclic behavior of SPSWs and the interaction of infill plates with the frame. In this case only infill plates were resisting the lateral displacement and the boundary frame did not contribute in resisting of lateral loads. As illustrated above, frame

members anchored the stresses associated with the infill plate deformations. On the other hand, using such frame is more economical rather than the rigid connection frame. Since every SPSW can be connected to the fish plate of the boundary frame by just a set of bolts, the new specimens can be replaced conveniently and after each test.

To obtain the illustrated mechanism, the hinge connection should be able to rotate freely at the range of maximum test displacement and designed with adequate capacity; otherwise, the test results could be affected. To ensure these goals, connection loading is one of the major key parameters. Using the PFI method (Plate Frame Interaction) and numerical model (SAP2000 model) as a preliminary evaluation of the maximum capacity of shear walls (stiffened specimens), showed that the maximum lateral capacity of the specimens could be around 20 tons. Considering un-predicted conditions, the design load was selected equal to 36 tons.

Design of hinge connection was done as follows:

i. Step1- by using the Equations 3-16 and 3-17 the stresses from yielding of infill plate was calculated.

ii. Step 2- Assuming uniform distribution of above stresses, resultant force from infill plate yielding measured by Equation 3-27 as below:

$$\boldsymbol{P_{si} = W_{yci} * d} \qquad (3\text{-}27)$$

Where *d* is the height of walls

P_{si} = 192*100=19200 kg= 188.2 KN

Meanwhile internal force of the frame in the numerical model was 173.6 KN, which is close to the P_{si}. Thus, the design force for hinge connection equal to 188 KN was selected.

iii. Step 3-Mechanical property of hinge plates was assumed to be $F_{y=}$320 N/mm^2 and F_u=450 N/mm^2. Also main bolt class 8.8(ISO) with mechanical properties $F_{Y=}$660 N/mm^2 and F_u=830 N/mm^2 was selected to be used.

iv. Step 4- By controlling maximum and average shear stresses (Equations 3-28 and 3-29) on the body of the main bolt, its diameter was obtained:

$$\boldsymbol{f_{v_{mav}} = \frac{4}{3}\frac{V}{A} \leq F_v} \quad (3\text{-}28)$$

$$\boldsymbol{f_v = \frac{V}{A} \leq F_v} \quad (3\text{-}29)$$

Where V is shear force of bolt, A is shear section area of bolt and F_v is allowable corresponding stress

v. Step 5- considering crippling on the bolt body, thickness of hinge plates was calculated as follows:

$$\boldsymbol{f_p = \frac{V}{half\ perimeter\ of\ bolt * tickness\ of\ plate} \leq F_p = 0.9F_y} \quad (3\text{-}30)$$

vi. Step 6- considering crippling on hinge plates, another values for thickness of hinge plates was calculated:

$$\boldsymbol{f_p = \frac{V}{project\ of\ bolt\ body\ on\ the\ hole} \leq F_p = \begin{cases} 1.2\,F_u \\ \frac{L_e \cdot F_u}{2d} \leq 1.2F_u \end{cases}} \quad (3\text{-}31)$$

Where L_e is the distance from the hole center to the free edge of plate. By using drawing method and considering free rotate ability of frame member relative together, the minimum obtained value for L_e was equal to 3.91 cm. This value is considered in the required fields.

vii. Step 7- controlling the Equation 3-21 and using minimum available value for $L_{e,}$ lead to another required thickness for hinge plate thickness:

The frame consists of four I-Shape profile W125x125x9x6.5 connected by using high tensile plate and Bolt M30 ASTM A325. Center to center line of the frame members was 102.5 cm and inner frame clear distance is 90 cm (Figure 3-4). Fish plates of 68x9x0.6 cm and 85x9x0.6 cm was welded to the boundary frames.

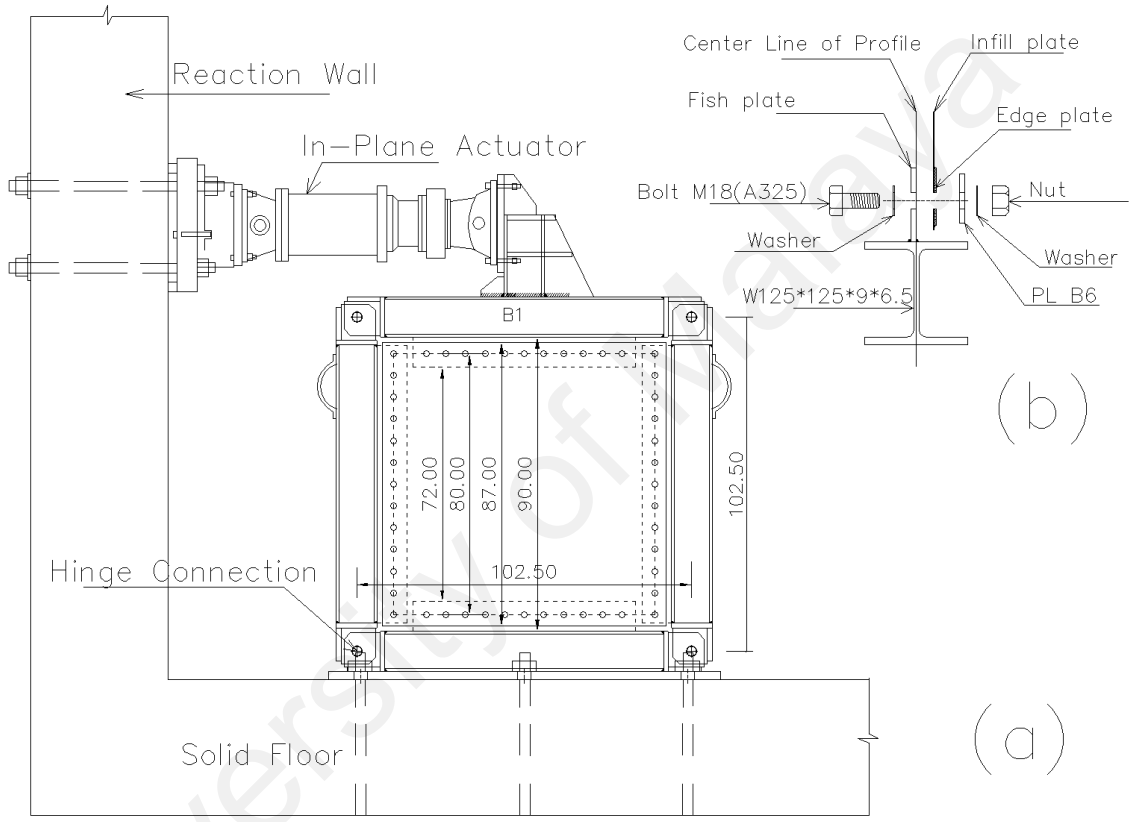

Figure 3-4 Test Setup Design

3.2.5 Summary of Infill Plate Design And Specimens Description

Five quarter-scale specimens were fabricated and prepared for cyclic loading test (Figure 3-5). Two specimens are un-stiffened, and they are fabricated from aluminum and ordinary steel sheet plate. They were named as AL-SPSW and US-SPSW respectively. The three remaining specimens are stiffened steel plate with different shape of stiffening called Cross stiffened steel plate "CS-SPSW", circular stiffened steel plate "CRS-SPSW" and diagonal cross stiffened "DS-SPSW". All specimens have the same aspect

ratio equal to one and overall dimension is 87 cm with 80 cm center to center of connecting bolt holes (Figure 3-5). In order to prevent tearing in the edge of walls due to using of bolts, all four edges were strengthened by 70 millimeters wide and 2.50 mm thick plate. The area section of all stiffeners is 2,5*30 mm. Other specifications of specimens are given in Table 3-1.

Table 3-1 Summary of test specimens

Specimens	Infill Thickness (mm)	Stiffener Thickness (mm)	Stiffeners Pattern	Total Weight (kg)	Infill plate dimension (mm)	Boundary frames
AL-SPSW	1.5	-	-	4.75	870 x870	W125x125x9 x6.5
US-SPSW	1.25	-	-	11.75		
CS-SPSW	1.25	2.5	Cross	14.0		
CRS-SPSW	1.25	2.5	Circular	13.85		
DS-SPSW	1.25	2.5	Diagonal	13.80		

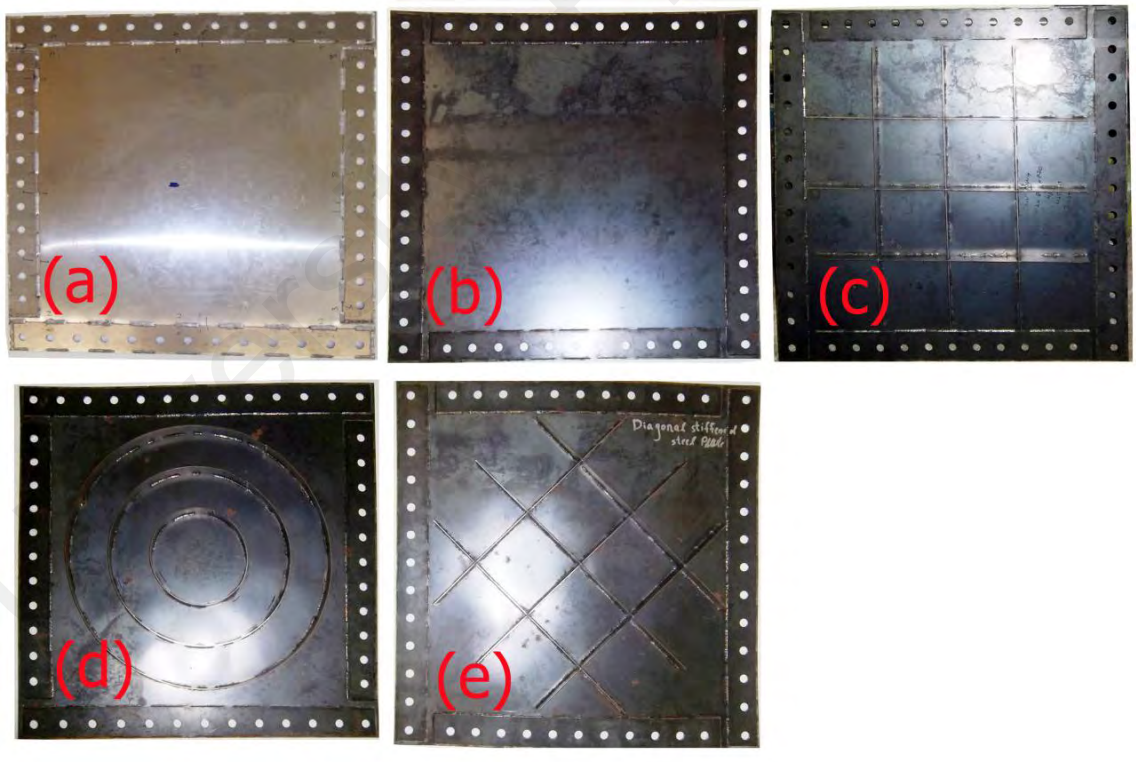

Figure 3-5 Fabricated Specimens a)AL-SPSW, b)US-SPSW, C)CS-SPSW, d)CRS-SPSW and e)DS-SPSW

3.2.6 Coupon Tensile Tests

To determine the actual yield and ultimate stresses of the specimen's components, tensile tests were conducted. For more accurate finite element modeling, also strain-stress curves of used material should be defined. The procedure followed in these tests was outlined in the British Standard (B.S., 2001). According to this standard, the shape and dimensions of the test pieces depend on the shape and dimensions of the metallic product from which the test pieces

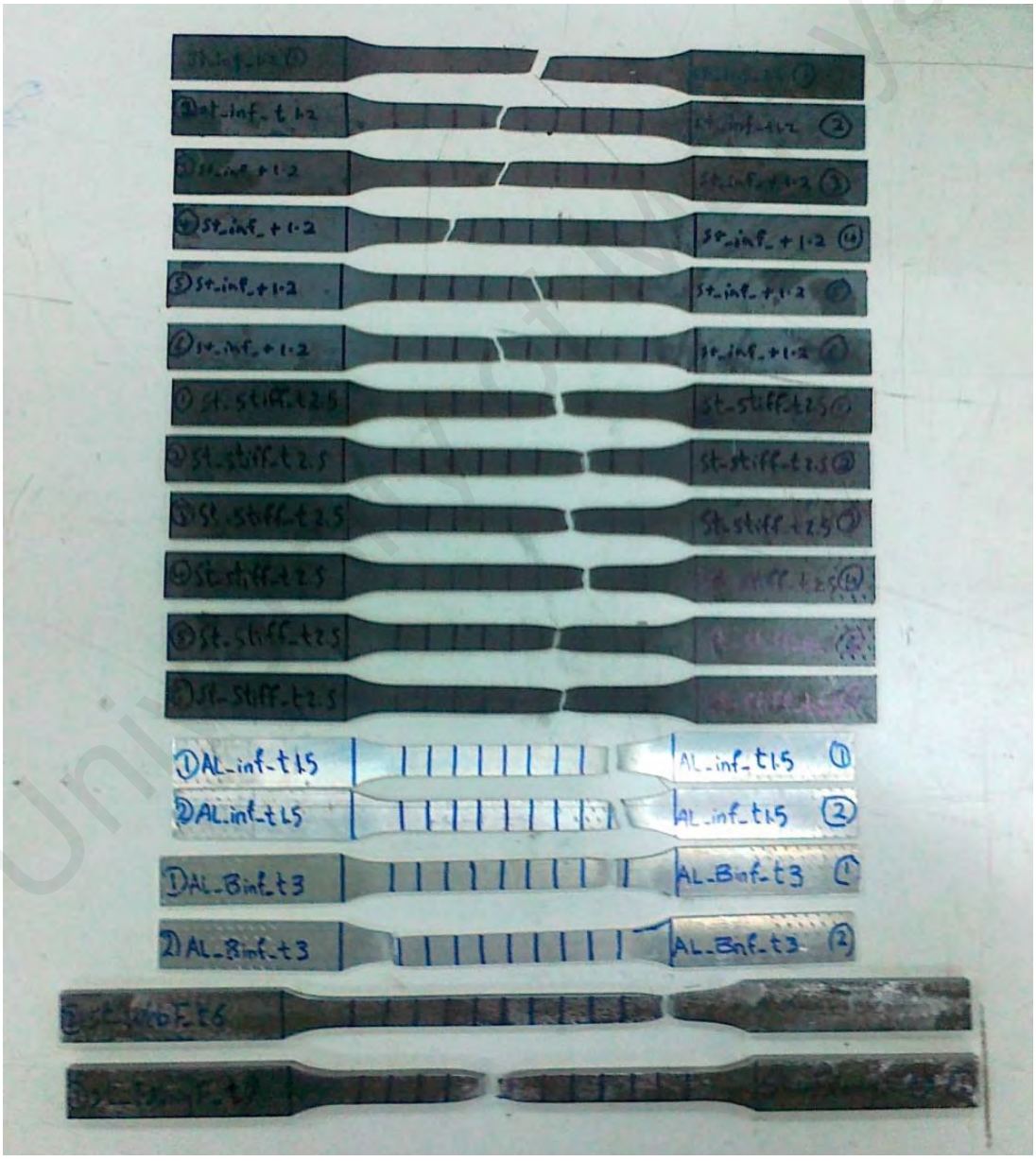

Figure 3-6 Tensile Coupons

Figure 3-7 Tensile Test machine

are taken. It means that different thickness of specimens parts need different shape for coupon test; thus as can be seen in Figure 3-6, the coupon shapes are categorized for thickness smaller and bigger than three milimeters. Tests were performed on a 2000 KN universal testing machine (Figure 3-7). Two test coupons in two orthogonal direction were cut from infill plate sheets and from their strengthening plate sheet. Test coupons of aluminum (1.5 mm thickness) named AL-inf-t1.5 and its strengthening plate (3 mm thickness) named AL-Binf-t3. The coupons test from steel infill plate sheets (1.2 mm thickness) named St-inf-t1.2 and from steel stiffeners sheet plate (2.5 mm thickness) named St-stiff-t2.5. Furthermore, coupon test was cut from web (6 mm) and flange (9 mm thickness) of boundary frame test which named as St-WebF-t6 and St-FlangF-t9 respectively (Figure 3-6). Figure 3-8 shows the stress-strain curves of tensile coupon test and its statistical average value results are summarised the in Table 3-2. It should be noted according to clause 4.9.2 and 4.9.2.2 of British Standard (B.S., 2001) lower yield limit is selected as the yield strength for steel plates. In the case of aluminum, the yield strength was defined by offset method. The yield strength at 0.2% offset for aluminum, is

obtained by drawing through the point of horizontal axis of the abscissa ε= 0.002 a line parallel to initial straight-line portion of the stress-strain diagram. The obtained amount of aluminum yield stress is quite close to the amount which could be obtained by drawing vertical line from ε=0.00 .

Table ვ-2 Coupon tensile test results

Coupon	Member	Thickness (mm)	Elastic Modulus (MPa)	Yield Stress (2) (MPa)	Ultimate Stress (3) (MPa)	Yield strength Ratio =(2)/(3) (%)	Rapture Strain (%)
AL_Inf	Aluminum infill plate	1.5	69	275.67	350	79	16
St_Inf	Steel infill plate	1.2	200	350	430	81	53
St_FlangF	Flange of Boundary Frame	9.0	200	320	427	75	40
St_WebF	Web of Boundary Frame	6.0	200	288	427.9	67	45
St_Stiff	Stiffeners	2.5	200	335	412.2	81	48

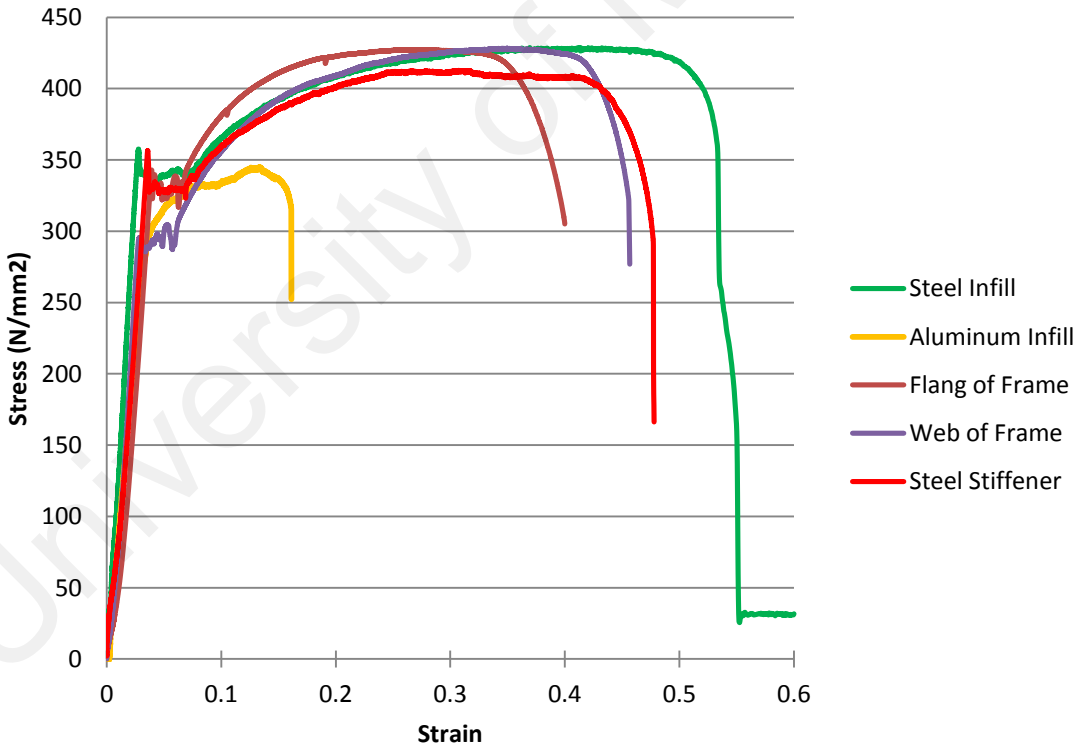

Figure ვ-8 Results of Tensile test of Coupons

3.3 TEST SETUP

To test the specimens after their fabrication, all specimens and boundary frame were transferred to the CREAM laboratory. Once in place, the base plate

of the boundary frames was anchored to the strong floor using high-strength steel anchor bolts. The test setup is depicted in Figure 3-4 and 3-9. This setup was designed to test the specimens as a vertical cantilever beam. In-plane computer-controlled hydraulic actuator was mounted between the boundary frame and reaction wall as shown in Figure 3-4 and 3-9. This actuator with horizontal load capacity of 500 KN and available stroke of ±100mm was employed to apply in-plane loading on the specimens. The actuator was connected to the reaction wall through pin units that were free to rotate in the vertical direction. The actuator was connected to the top beam flanges via loading tabs. The tabs were welded to the top beam flanges. Pin unit that was free to rotate vertically was used to connect the loading tab to the actuator.

To avoid out-of-plane displacements of the SPSW, lateral bracing was provided in the frame top beam levels as shown in Figures 3-9 and 3-10. This system includes an erected frame and rollers which surrounded the specimens and provided the lateral bracing for frames top beam. This brace allows development of expected in-plane specimen movement without offering any restraint or requiring manual adjustments. It also served to correct the small twisting of specimens, which probably induced by welding and fabrication process.

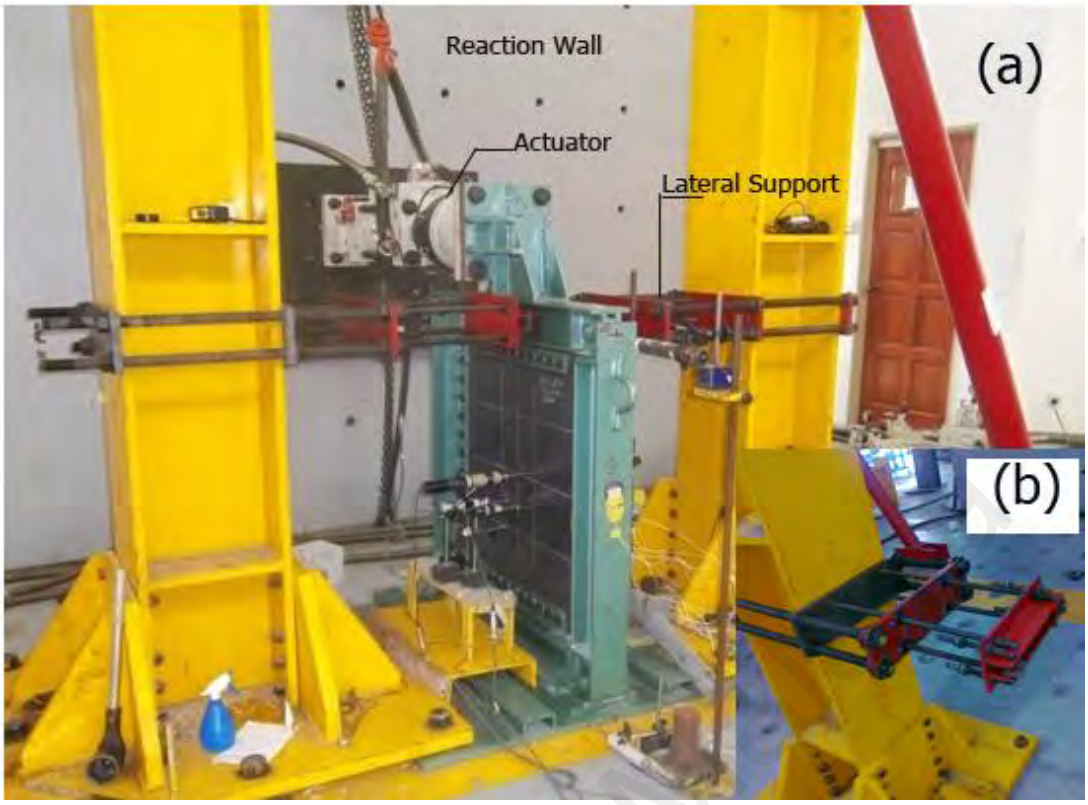

Figure 3-9 (a) Test Setup of Laboratory, (b) Lateral Support

3.3.1 Loading Procedure

It was decided that the specimens be loaded with gradually increasing, fully reversed, lateral cyclic load to failure. This lateral loading consisted of applying horizontal displacement at the top of the boundary frames according to the pre-designed cyclic displacement history. By using a displacement-controlled loading history, experimental tests were conducted using quasi-static cyclic loading. Despite most of the previous researcher used the Applied Technology Council (A.T.C, 1992) recommendations; in this research, the loading strategy for testing was derived by following the method outlined in the FEMA-461 (2007) for experiments using quasi-static cyclic loading. Generally, the above-mentioned two loading protocols have similarity but there are some differences. The displacement amplitudes in ATC must be arranged based on the yielding displacement of specimens, while in FEMA-461; they should be arranged based upon the target displacement. Moreover, numbers of

step in elastic and plastic behavior regions are different in the two protocols. For better comparison of results among the other researchers, the loading history and its amplitudes based on the FEMA-461 (2007) were extracted to be consistent with ATC (1992) protocol, especially in the elastic region. Before the establishment of specimens loading sequences, an estimation of yield displacement was required. By using coupon tension test results, Plate Frame Interaction method (Sabouri-Ghomi et al., 2005) and non-linear numerical model, yielding displacement for un-stiffened steel plate was obtained. Referring to the yielding displacement, the amplitudes of loading histories were measured. According to FEMA-461, at the lowest damage state, at least six cycles must be executed, and it was done by arranging the 6^{th} cycle displacement lower than the yielding displacement. That means, the values of the initial three displacement amplitudes were chosen as 0.315, 0.42 and 0.61 of the estimated yield displacement to ensure observation of multiple elastic cycles prior to the specimen reaching the global inelastic region of behavior. It should

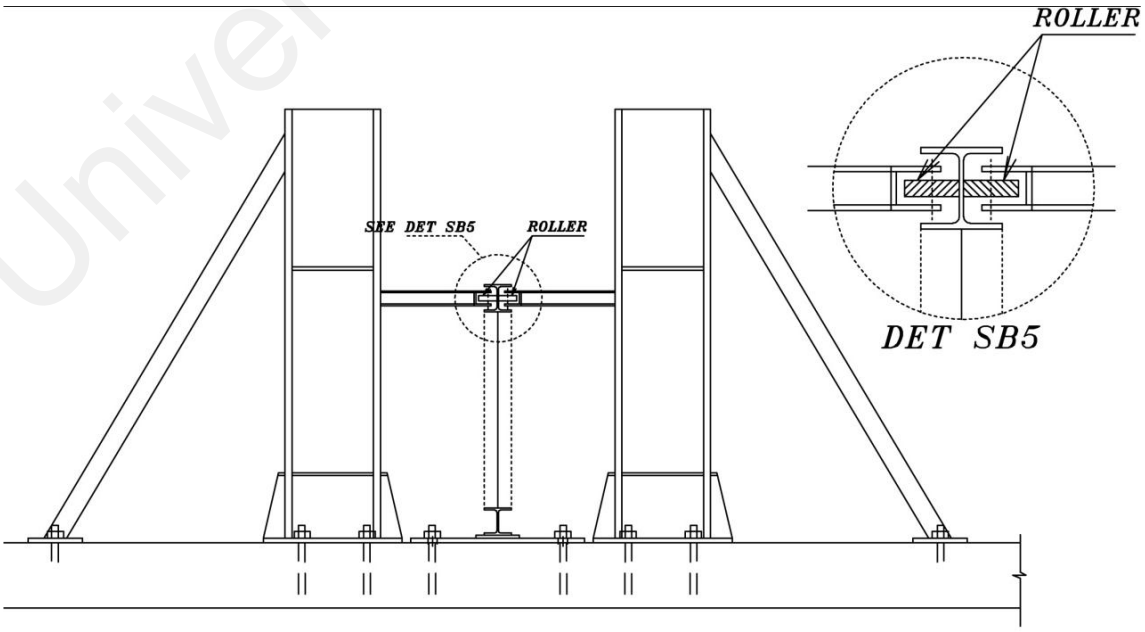

Figure 3-10 Lateral Support Setup Design

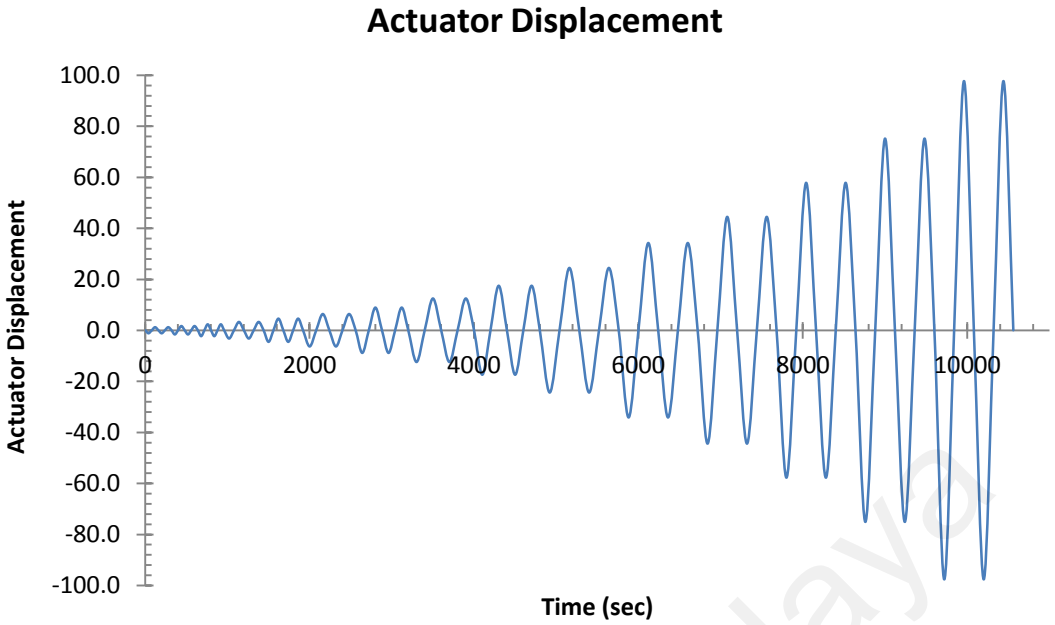

Figure 3-11 Displacement History of Actuator

be mentioned, up to target displacement (Δ_m=34.2mm) step amplitudes equal to 1.4 times of previous step amplitude; after that point, they were increased by 1.3 coefficient. In addition, the loading rate should be small enough that dynamic effects are negligible and at the same time the deformation increment should be sufficiently large, such that material creep is not a significant effect. The displacement history is shown in the Figure 3-11, and it was developed in a way that the next step not be slower than the previous step. As it can be seen, 30 total cycles are provided with maximum displacement of 97.7 mm due to stroke limitation. This displacement history was applied to all specimens and once the damage evidence appeared or actuator stroke reached its limitation, the loading was stopped.

3.3.2 As-built Measurements

Before testing, as-built measurements of specimens were done. These measuremenst includes: infill plate imperfection after installation in the boundary frame test; thickness of infill plate; thickness of strengthening plate;

thickness of stiffeners; frame dimensions; thickness of cross section parts of the frame member. The measurements revealed that there is negligible tolerance within the fabrication process. The amount of infill plate imperfection (which will be employed in the numerical modeling) after installation is shown in Figures 3-12 to 3-16.

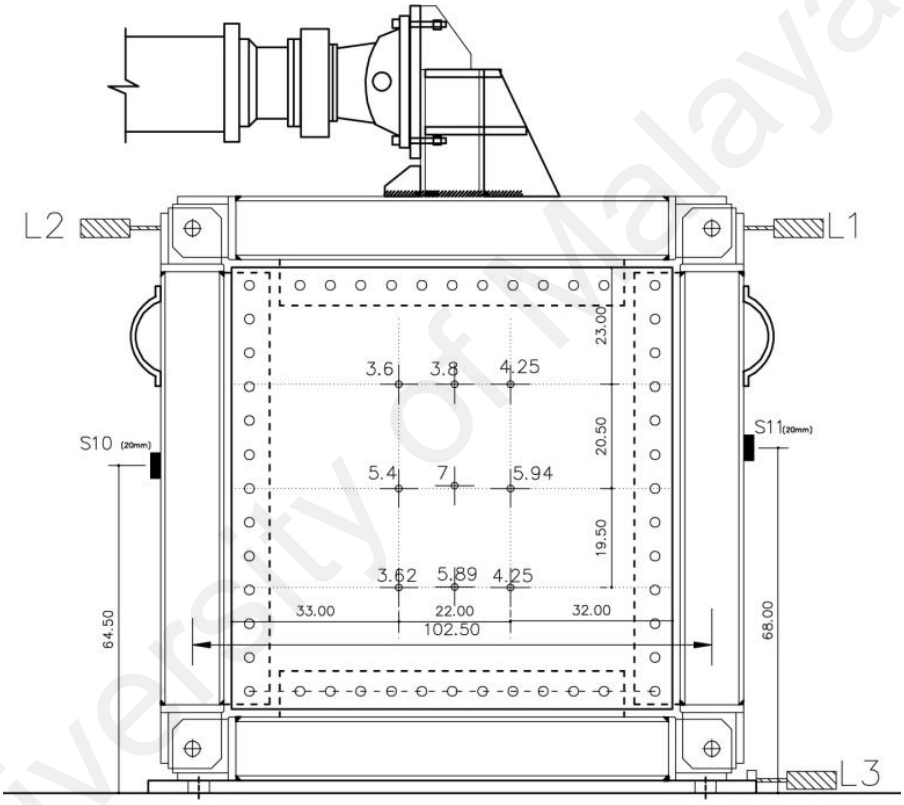

Figure 3-12 Imperfection measurements of AL-SPSW

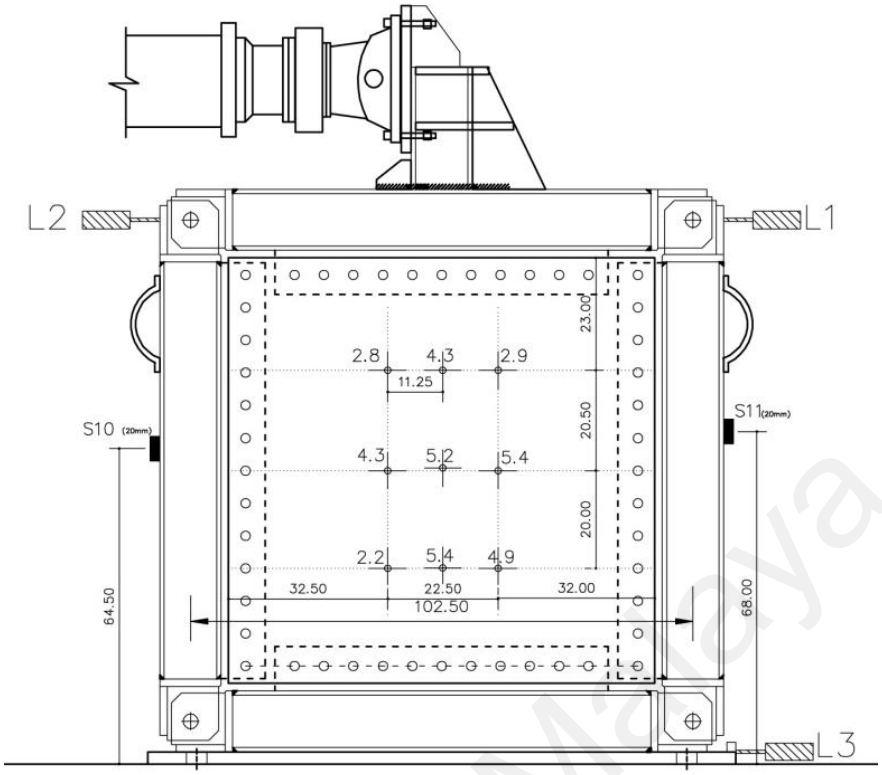

Figure 3-13 Imperfection measurements of US-SPSW

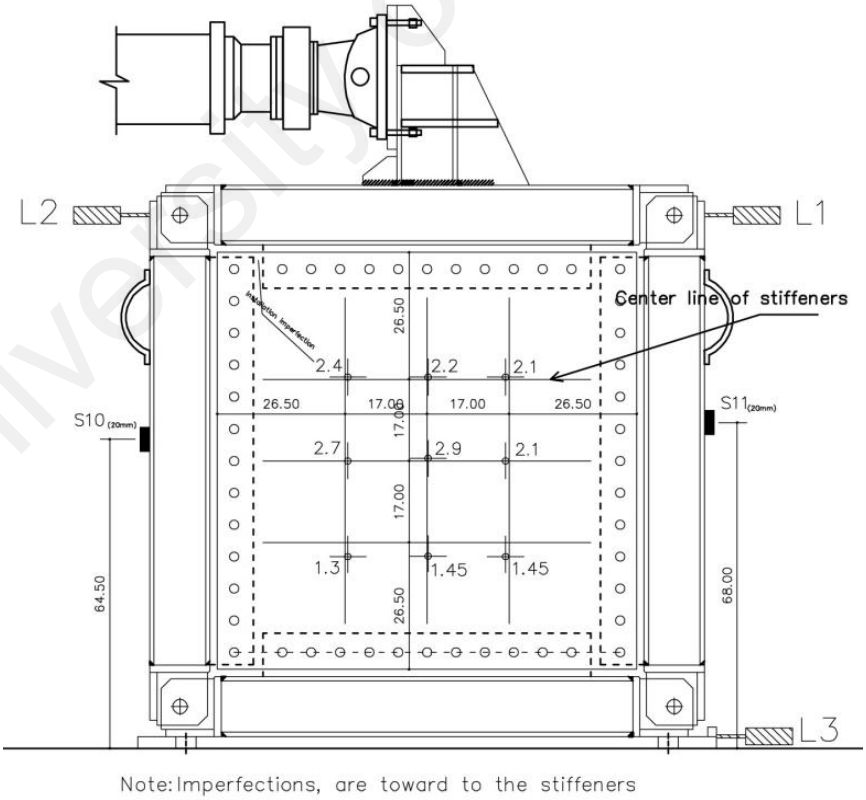

Figure 3-14 Imperfection measurements of CS-SPSW

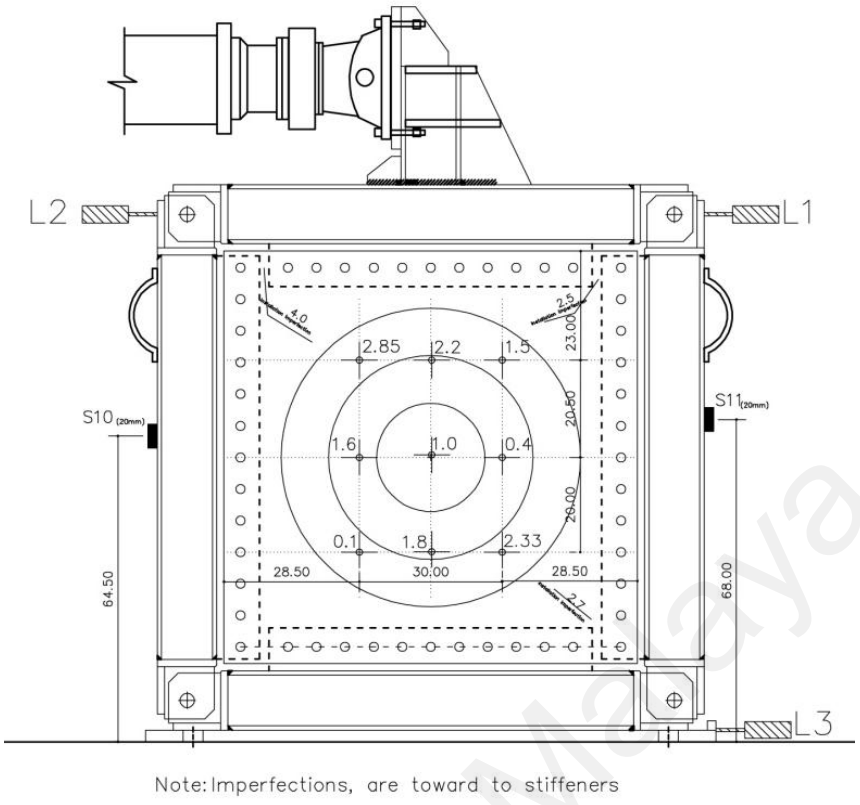

Figure 3-15 Imperfection measurements of CRS-SPSW

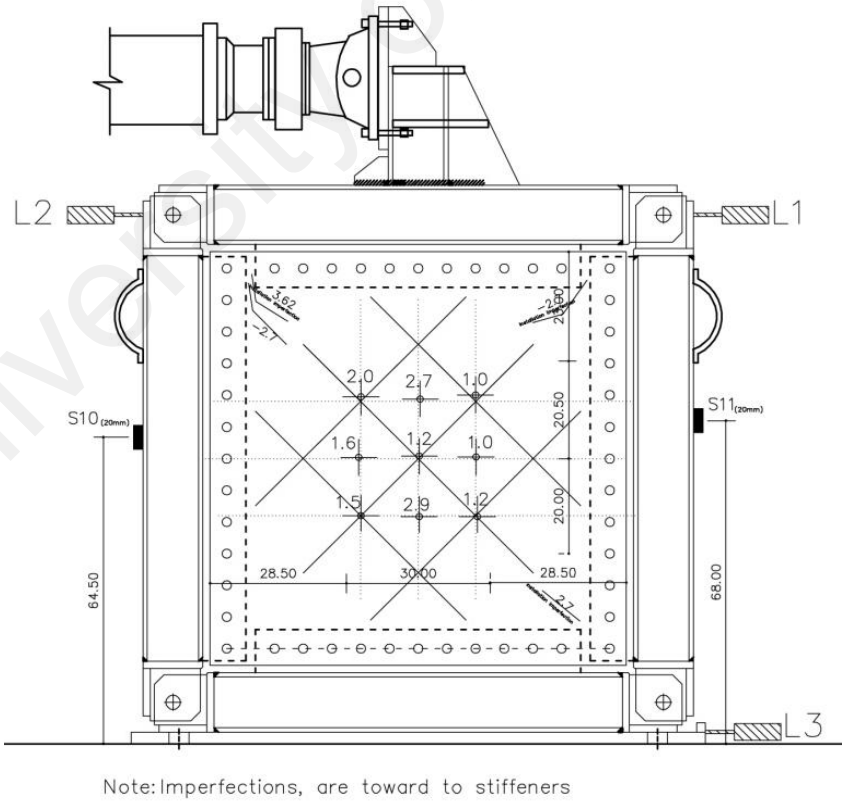

Figure 3-16 Imperfection measurements of DS-SPSW

3.3.3 Instrumentation and Data Acquisition

To collect required data for controlling the test or interpreting of its result, specific measurements were made. The measurements included the applied load, in-plane displacement of frame and its parts, out of plane displacement of infill plates, strain of frame and infill's displacement. All displacements controlled loading was governed by the actuator's displacement sensor. As the main device, the hydraulic actuator contained an integral load cell and displacement measurement sensor.

To measure in-plane displacement of frame, two Linear Variable Displacemetn Transformers (LVDTs) were placed at the level of pinned connection (LVDT 1, 2). In the applied load direction, one LVDT was placed in the base plate, to check the in-plane slipage of base plate (LVDT 3). Therefore, the displacement data of this LVDT could be used for correcting the data, if any slipage occurred. Out-of-plane displacements of infill plates at the various locations, prior to large buckling waves, were recorded by a set of LVDTs. Figures 3-17 to 3-21 showed the location of LVDTs placed on the infills and frame's part.

In order to obtain an estimation of the stress distribution, strain should be measured at the considered locations; so that stress could be calculated by material properties. For this purpose, uniaxial strain gauges which measure strains only in one direction was mounted to the specimens and frame parts. All the strain gauges were single grid electrical resistance gauges with a gauge length of 10 or 20 mm. Following the manufacturer's recommended surface preparation and installation procedures, all gauges were attached using M-Bond 2000 adhesive. Uniaxial strain gauges were placed on the outer flanges

of columns, various positions on the infill plates and its stiffeners. Figures 3-17 to 3-24 shows the instrumentation layout of the specimens.

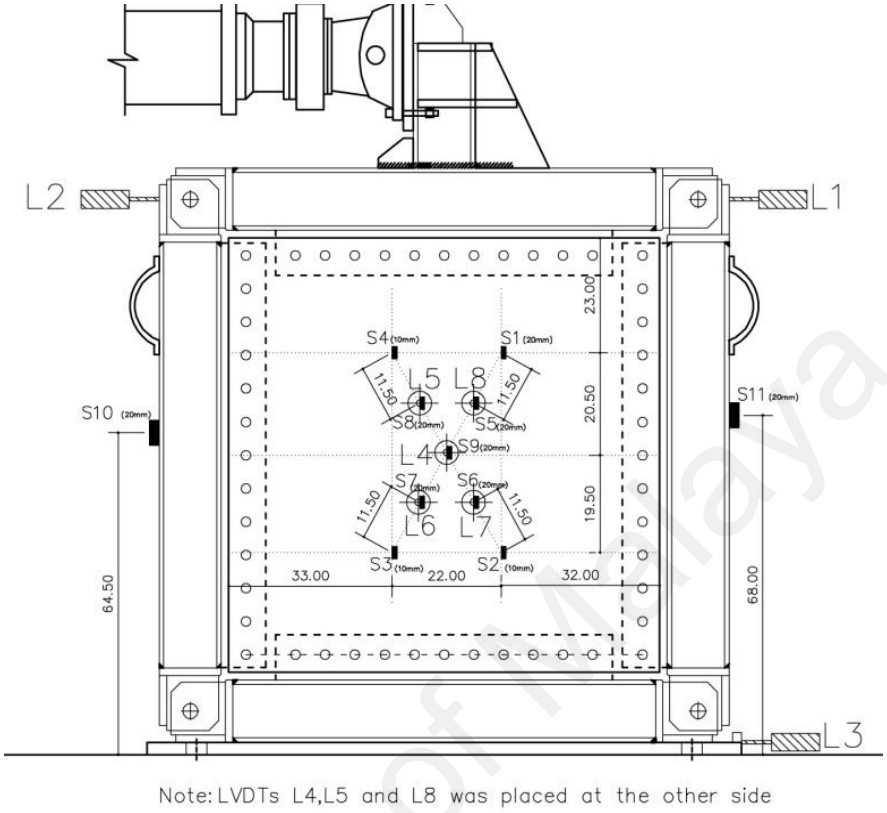

Figure 3-17 Strain gauge and LVDT labels of AL-SPSW

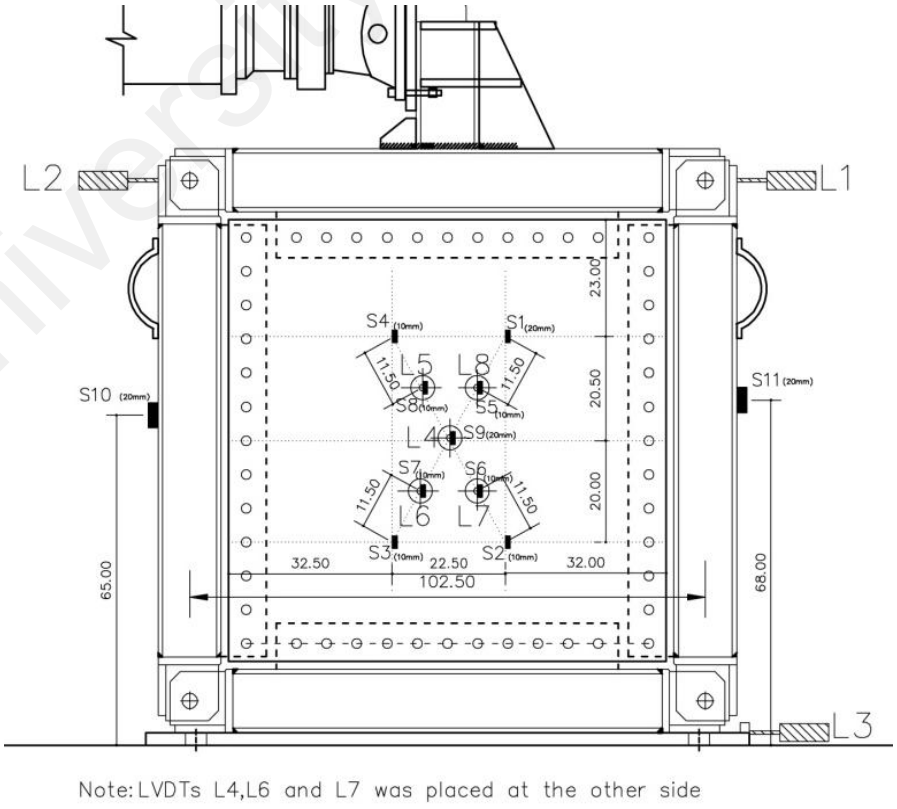

Figure 3-18 Strain gauge and LVDT labels of US-SPSW

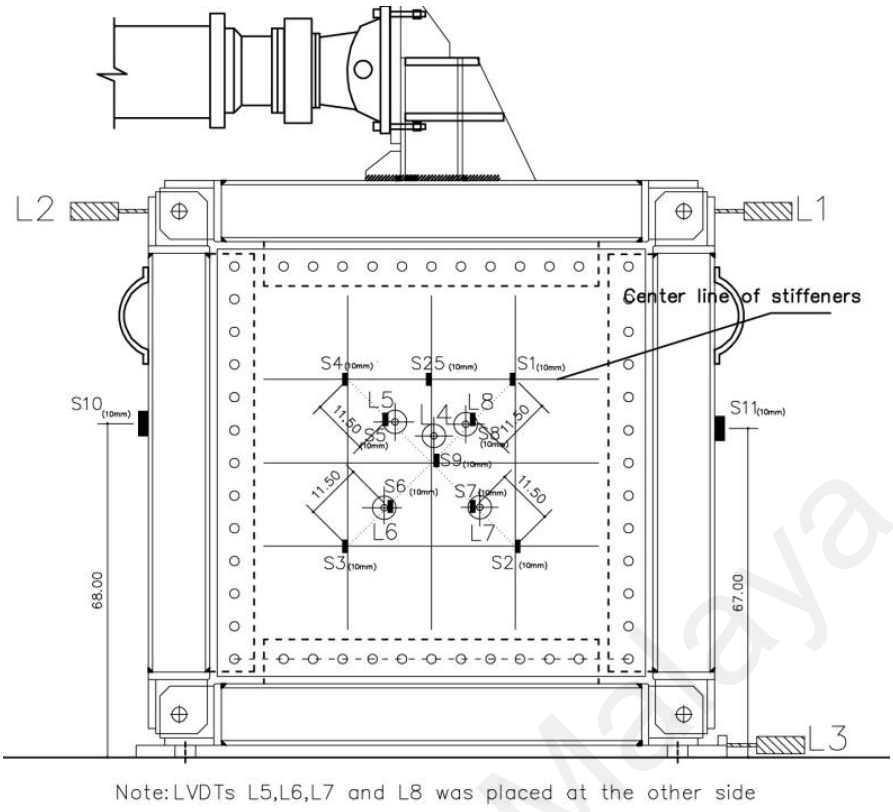

Figure 3-19 Strain gauge of infill plate and LVDT labels of CS-SPSW

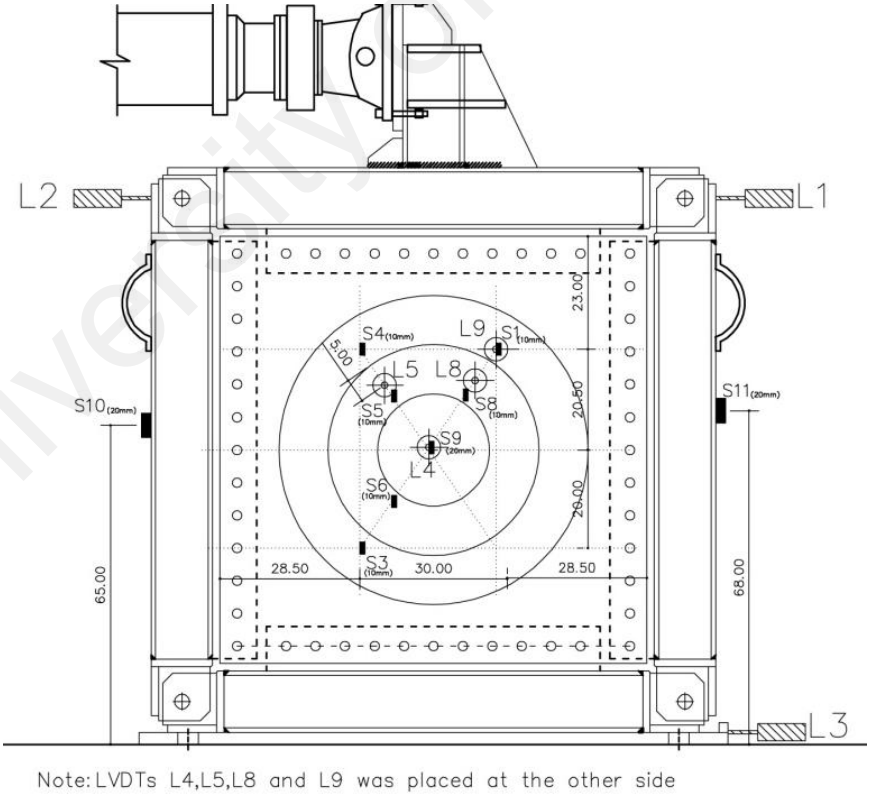

Figure 3-20 Strain gauge of infill and LVDT labels of CRS-SPSW

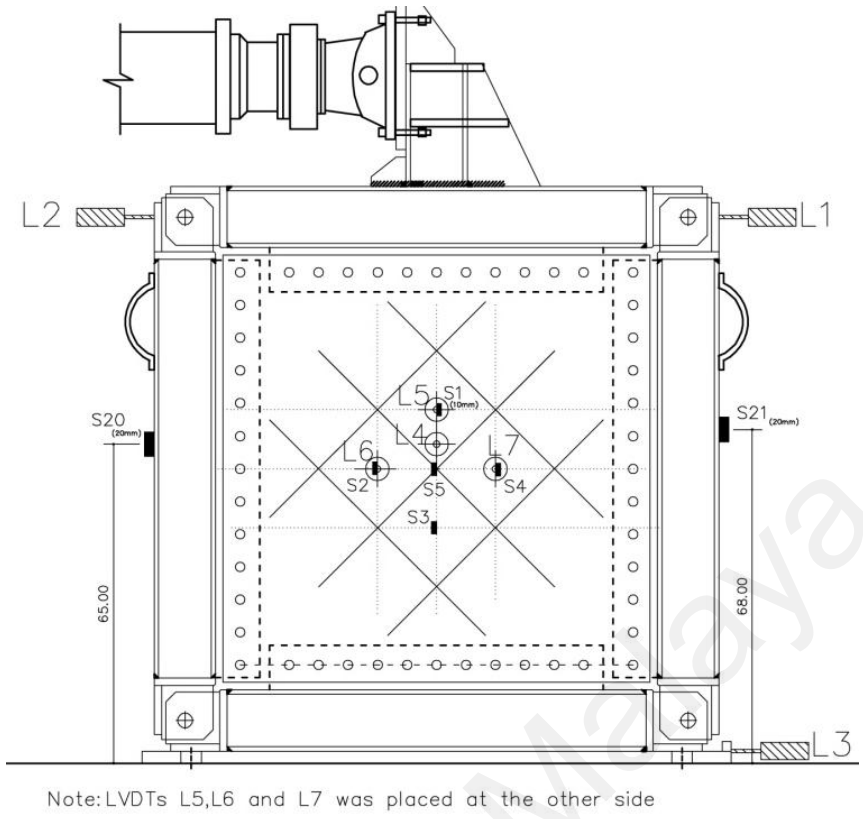

Figure 3-21 Strain gauge of infill and LVDT labels of DS-SPSW

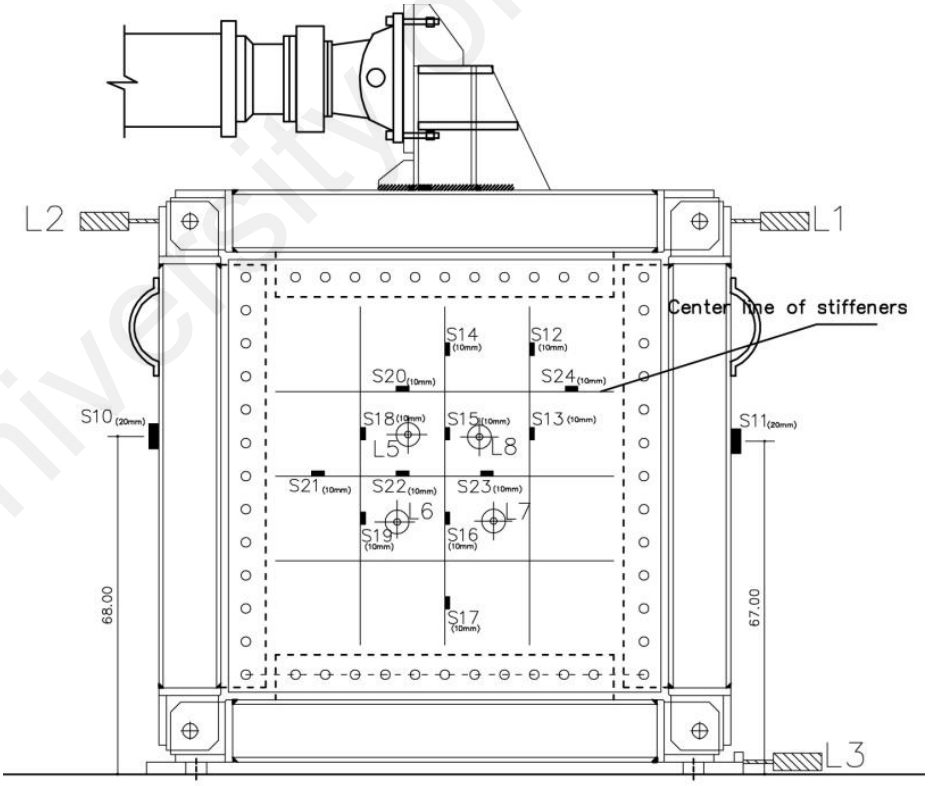

Figure 3-22 Strain gauge of stiffeners CS-SPSW

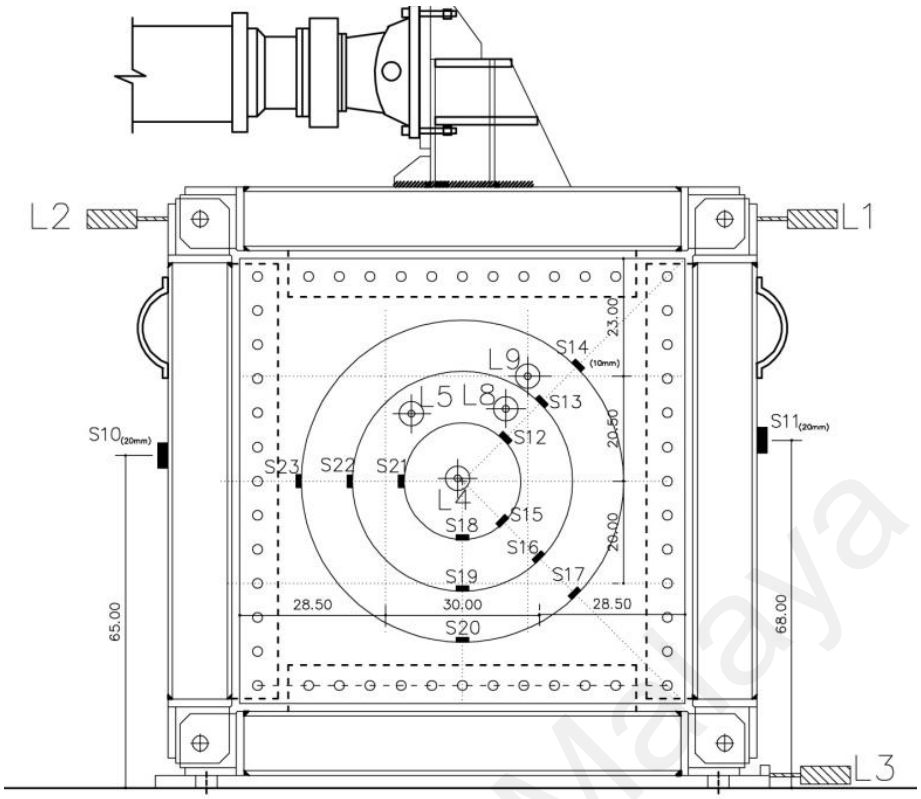

Figure 3-23 Strain gauge of stiffeners CRS-SPSW

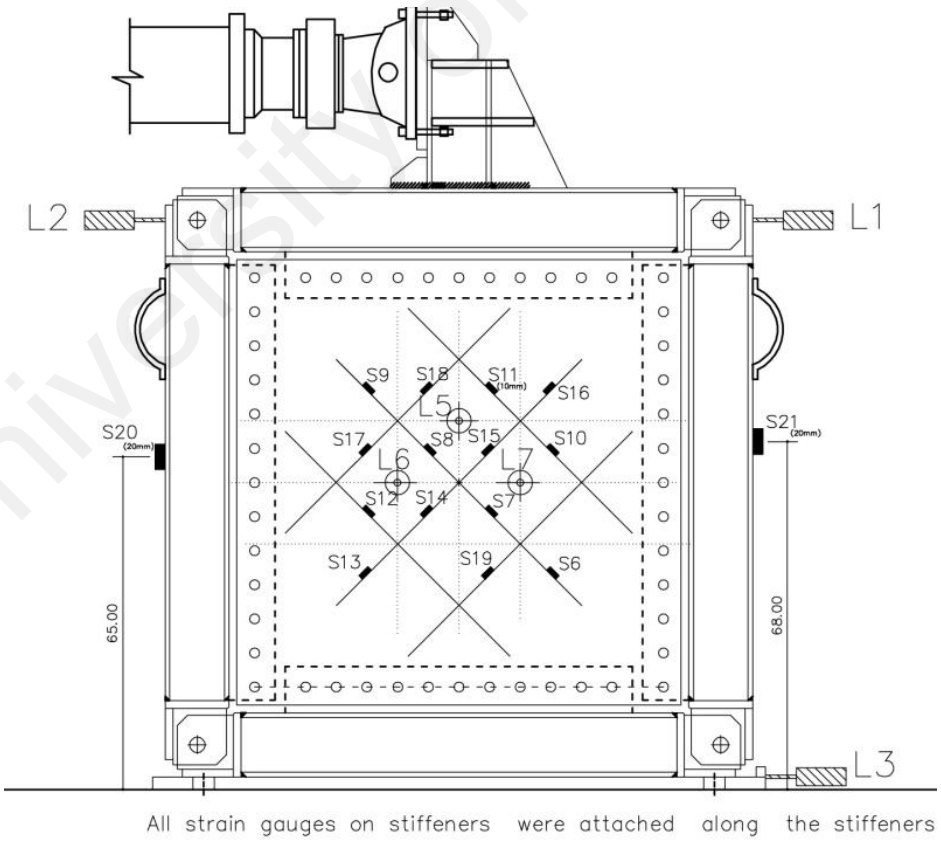

Figure 3-24 Strain gauge of stiffeners DS-SPSW

The data acquisition system consisted of portable DATALOGER with 30 channel and commercial laptop computer. The DATALOGER used "Visual Log TSD7130" software and collected the signal data from load and displacement of actuator; strain gauges and LVDTs; the lobtop was used for recording the converted signal from DATALOGER as the series of numbers. The dataloger has 30 channel for recording and in the case of specimen CRS-SPSW which there were more than 30 channel; two dataloger and two loptop were deployed simultaneously. All data recordings was conducted at a rate of one sample per second. In addition to the cyclic loading applied to specimens, the test procedure included inspection of specimens for tears and yield patterns at different stages during the testing (Figures 3-25 to 3-29).

Figure 3-25 AL-SPSW after test

Figure 3-26 US-SPSW after test

Figure 3-27 CS-SPSW after test

Figure 3-28 CRS-SPSW

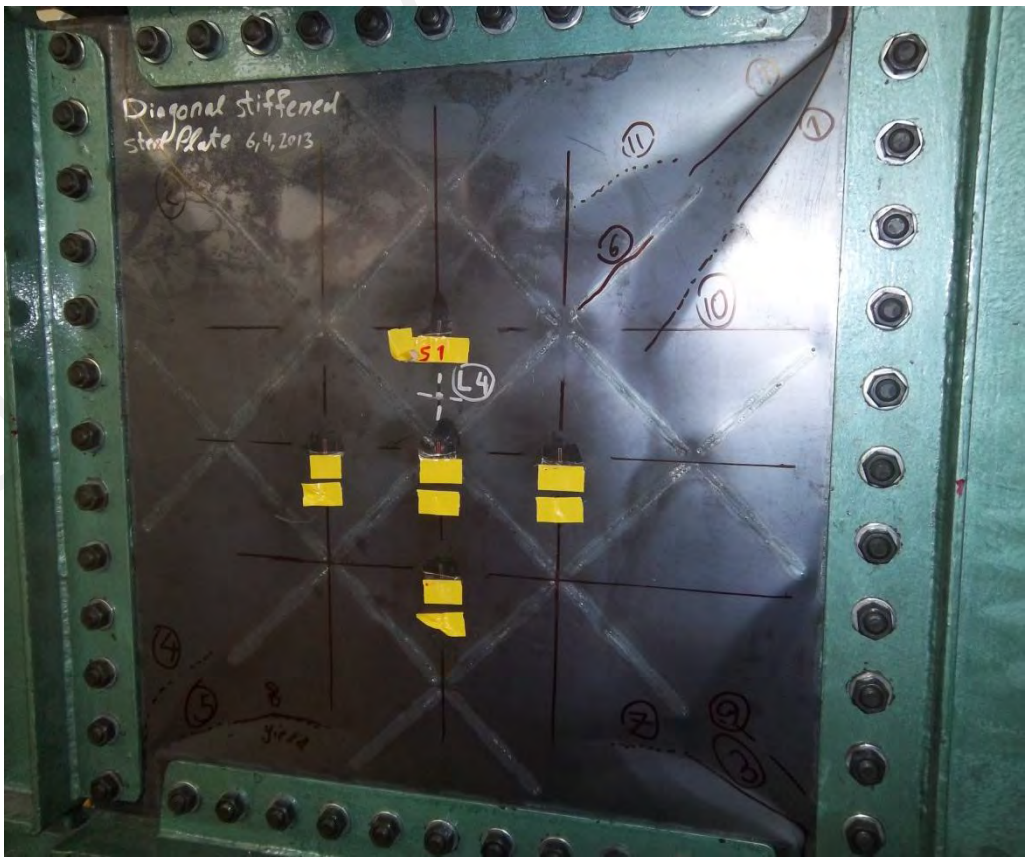

Figure 3-29 DS-SPSW after test

3.4 TEST RESULTS AND DISCUSSIONS

3.4.1 Cyclic Behaviors and Hysteretic Response

Lateral shear displacement according to Figure 3-11 was applied to the top of specimens. The shear load and shear displacement was recorded during the tests. In order to trace required data, several LDVT and uni-axial strain gages were installed on the proper positions. The findings from the cyclic behaviors and hysteresis response are described in the following sub-sections.

3.4.1.1 AL-SPSW

Based on the LVDTs and strain gauges data, the buckling of infill plate was started at the 5th cycle at 0.6 mm displacement (0.069% drift). After that several pop-ups sounds as the sign of buckling sound was heard and it continued during the test. First tension field appeared in the 12th cycle at a displacement of 4.47mm (0.51% drift). Also, a very clear tension field action was observed in the 19th cycle with a displacement of 16.9mm (1.94% drift).

In the 23rd cycle (22.7mm displacement, 2.61% drift) a tearing was seen in the top right corner of the infill plate. This was followed by another tearing in the bottom left and the top left. In the cycle 25, at the displacement of 43.3mm (4.69% drift), the top left tearing was extended. Due to extended tearing of the infill plate, the specimen failed in the 26th cycle, and the loading was stopped.

Referring to the test results, up to cycle 22, there was no significant sign of yielding in the infill plate. The strain gages readings (Figure 3-30) showed that yielding happened in the 23rd cycle at a displacement of 16.6mm (1.92% drift). The maximum load carrying capacity of the specimen was 132.39 KN, which occurred at the displacement 41.5 mm (4.78% drift). The hysteresis curve of the aluminum infill plate, AL-SPSW is shown in Figure 3-31. In Table

3-3, a brief comparison of the theoretical (PFI method) and experimental results are provided.

Table 3-3 Comparison of test results and PFI method for AL-SPSW

Aluminum Infill Plate			
	PFI method	Test Results	
		+	-
Buckling Displacement (mm)	0.1	0.6	0.6
Buckling Load (KN)	3.9	0.89	0.89
Yielding Displacement (mm)	10.8	27.5	23.4
Yielding Load (KN)	166.54	104.1	97.1
Ultimate Load (KN)	166.54	134.18	124.46

+: Positive Loading -: Negative Loading

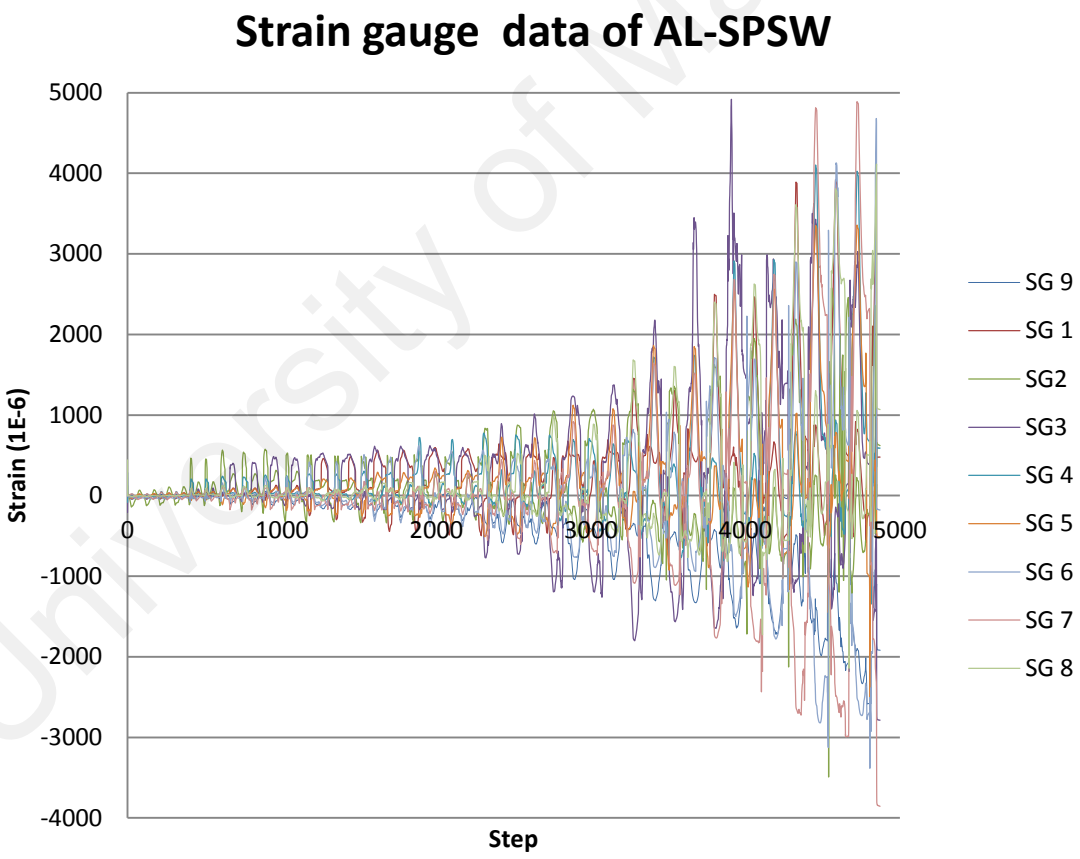

Figure 3-30 Strain gauge data of AL-SPSW

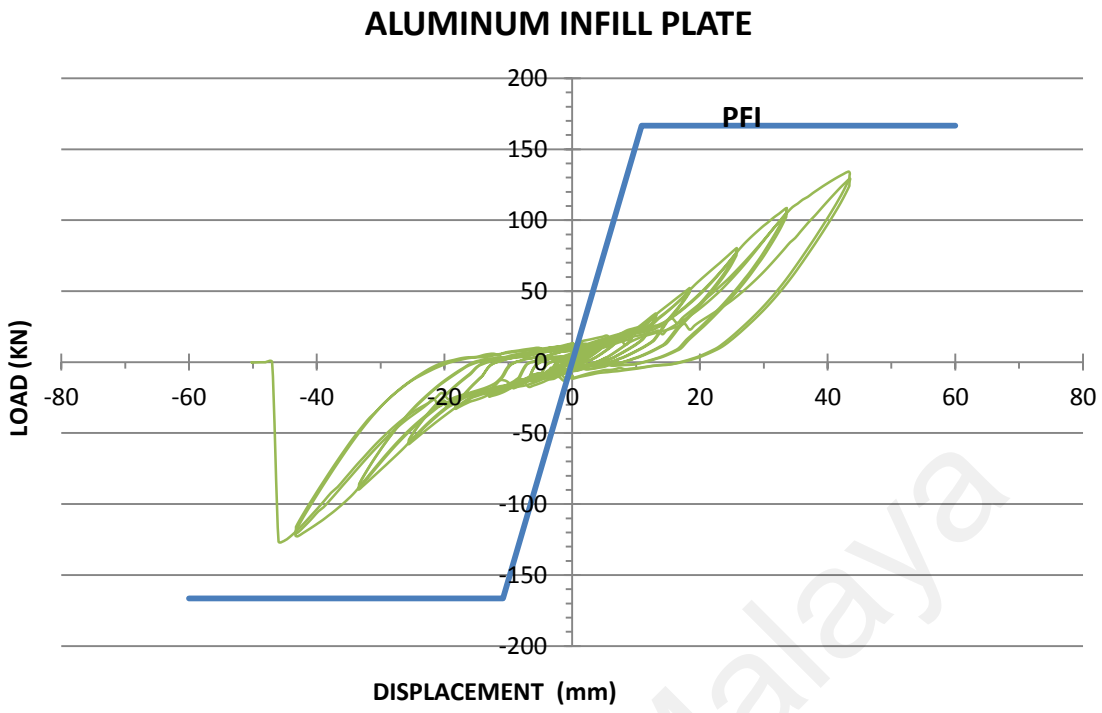

Figure 3-31 Hysteresis curve of AL-SPSW and load-displacement obtained from PFI method

3.4.1.2 US-SPSW

In this specimen, buckling started at the 15th cycle at the center of infill plate, but at the half bottom of the infill plate, buckling started at the 9th cycle at the displacement of 2.26mm (0.26% drift). First sound of pop-up buckling was heard at the 9th cycle at the displacement of 2.5mm (0.29% drift). First buckling wave of tension field appeared at the 16th cycle 6.66mm (0.76% drift). At the 19th cycle with displacement of 17mm (1.95%drift), buckling line was seen at the left top corner and then at the right top corner.

The strain gauges readings (Figure 3-32) showed that first sign of infill plate yielding was occurred at the 23rd cycle at the displacement of 30.4mm (3.49% drift). The maximum load carrying capacity of the specimen was 185.23 KN, which occurred at the displacement of 77.82 mm (8.94% drift). Maximum displacement of the specimen was 78.16mm. Hysteresis curve of the specimen for cyclic loading is showed in the Figure 3-33. There is a good

agreement between the results (ultimate load) of the test with the PFI method, as shown in Table 3-4.

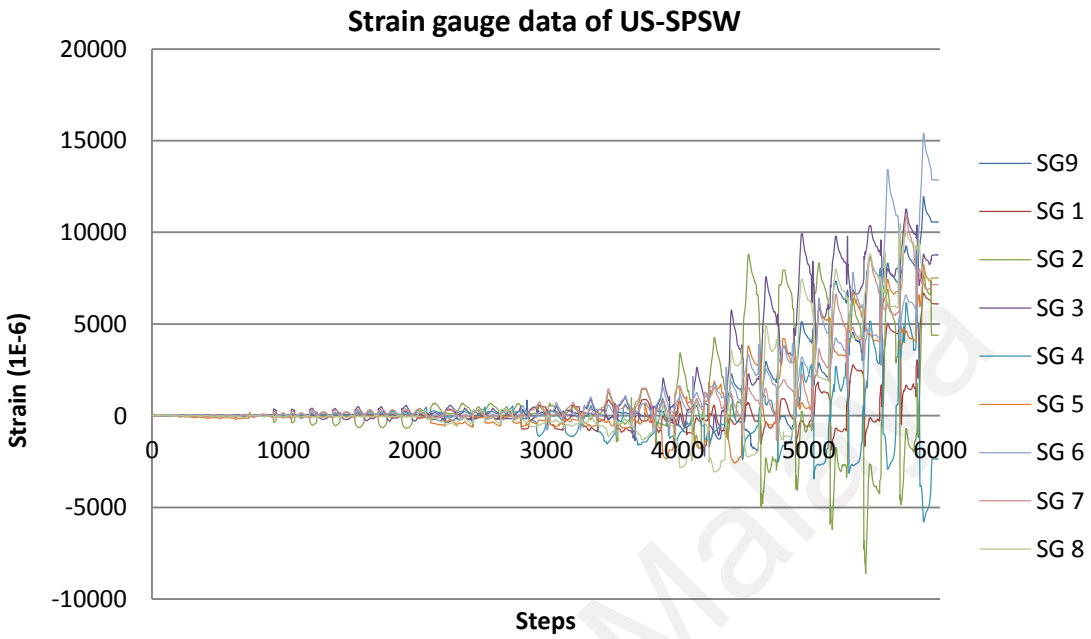

Figure 3-32 Strain gauge data of US-SPSW

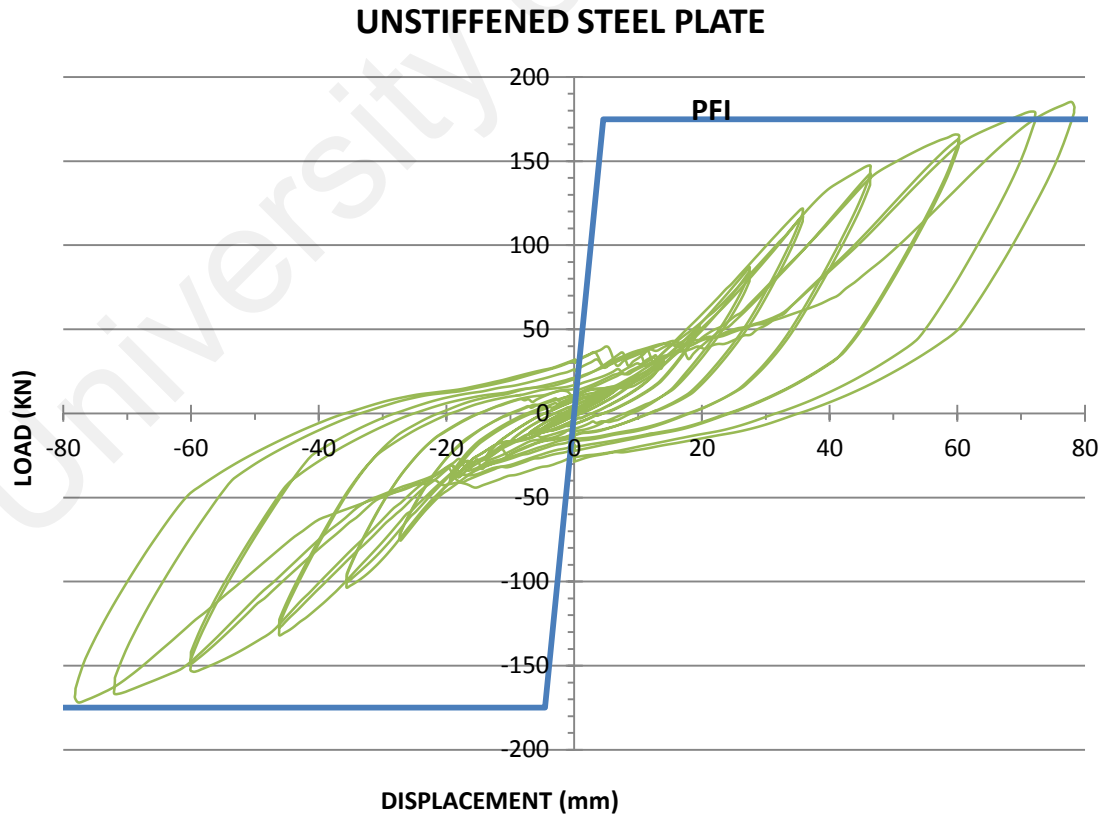

Figure 3-33 Hysteresis curve of US-SPSW and load-displacement obtained from PFI method

Table 3-4 Comparison of PFI method and test results of US-SPSW

Un-Stiffened Steel Plate			
	PFI method	Test Results	
		+	-
Buckling Displacement (mm)	0.067	2.26	2.26
Buckling Load (KN)	6.6	4.57	4.57
Yielding Displacement (mm)	4.60	30.4	29.6
Yielding Load (KN)	174.9	137.1	121.4
Ultimate Load (KN)	174.9	185.23	171.9

+: Positive Loading -: Negative Loading

3.4.1.3 CS-SPSW

To prevent buckling of the base plate, two additional strong supports were installed on both sides of the base plate of the testing frame (Figure 3-34). Due to the installation process, before the loading start, a local primary buckling line at the top right corner (reaction wall at the right) in the gap between the strengthening plates was found.

According to the LVDTs data, in the central sub-panel (LVDT 4, 7, 8) at the 9^{th} cycle at the displacement of 3.1mm (0.36% drift), out of plane displacement suddenly was increased. The pop-up sound of buckling in the 17^{th} cycle at the displacement of 10.2mm (1.17% drift) was heard.

The top right primary buckling in the 18^{th} cycle at the displacement of 4.875mm (0.56% drift) was developed. The sub-panel below the first top right panel buckled in the 21st cycle. As shown in Figure 3-35, the overall tension field buckling of infill plate is turned to local buckling of sub-panels.

Vertical top left stiffener buckled and yielded at the 20^{th} cycle in the displacement of 2.87mm (0.32% drift). First sign of yielding at the infill plate appeared in the 22nd cycle at the displacement of 6.48mm (0.74% drift).

Hysteresis curve of specimens is shown in the Figure 3-36. Maximum load carrying of the CS-SPSW was 179 KN, which occurred at the displacement 42.2mm (4.85% drift). The maximum displacement of the specimen is equal to 56.3mm (6.47% drift). The stiffeners situation could be one of the main reasons of the considerable difference between the PFI and test results. In the PFI method, it was assumed that all subpanel were stiffened at all four edges and they reached their ultimate yielding strength, while in the case of CS-SPSW, there are several subpanels that were stiffened in the three side. As a result, these three side stiffened subpanels couldn't reach their yielding strength.

Table 3-5 CS-SPSW comparison of PFI and test results

Cross-Stiffened steel plate			
	PFI method	**Test Results**	
		+	-
Buckling Displacement (mm)	After yielding	2.87	2.87
Buckling Load (KN)	After yielding	39	39
Shear yield Displacement (mm)	2.0	12.17	12.6
Yielding Load (KN)	200.1	134.58	144.9
Shear Strength (KN)	200.1	179	177

+: Positive Loading -: Negative Loading

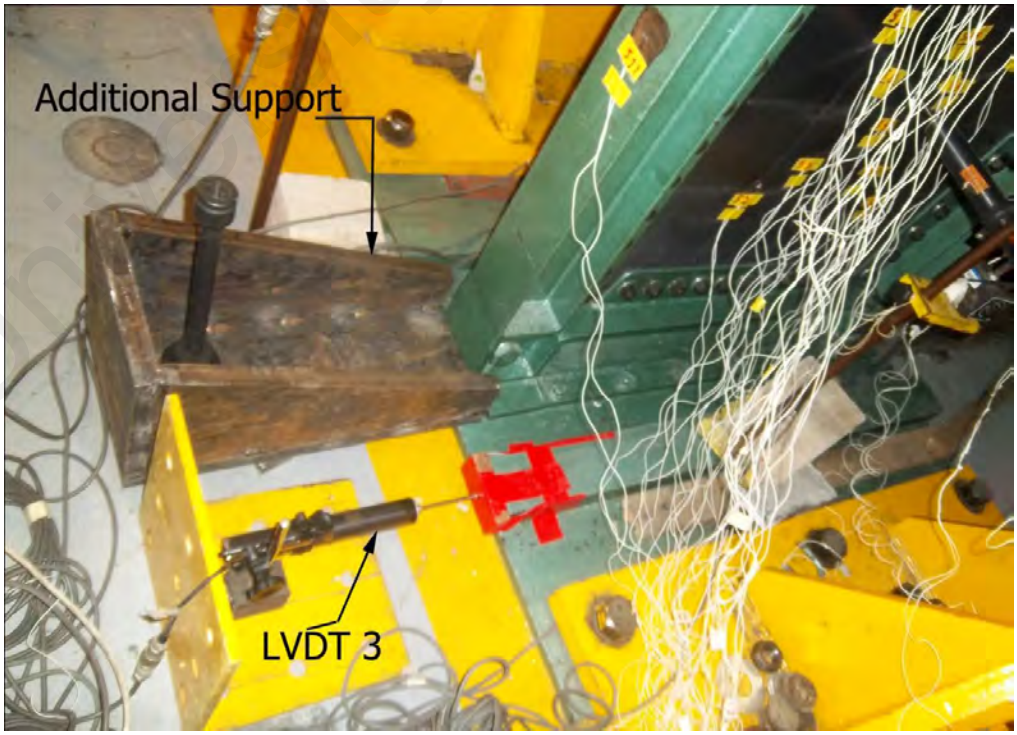

Figure 3-34 Additional support for stiffened specimens

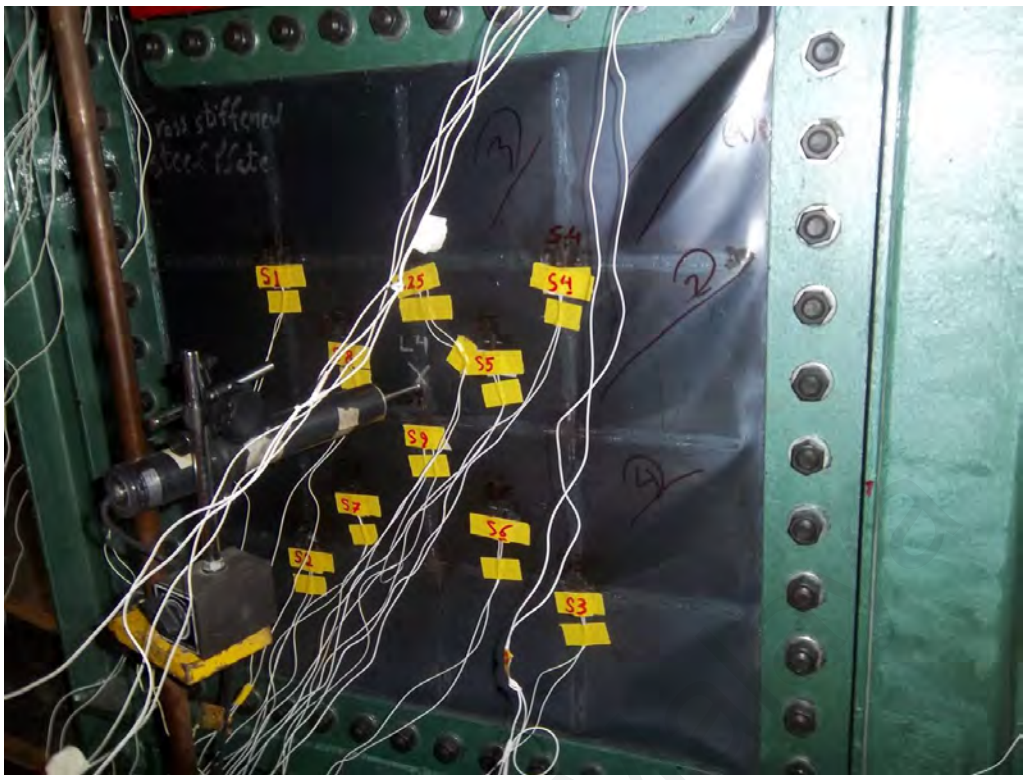

Figure 3-35 Local buckling of sub-panels for CS-SPSW

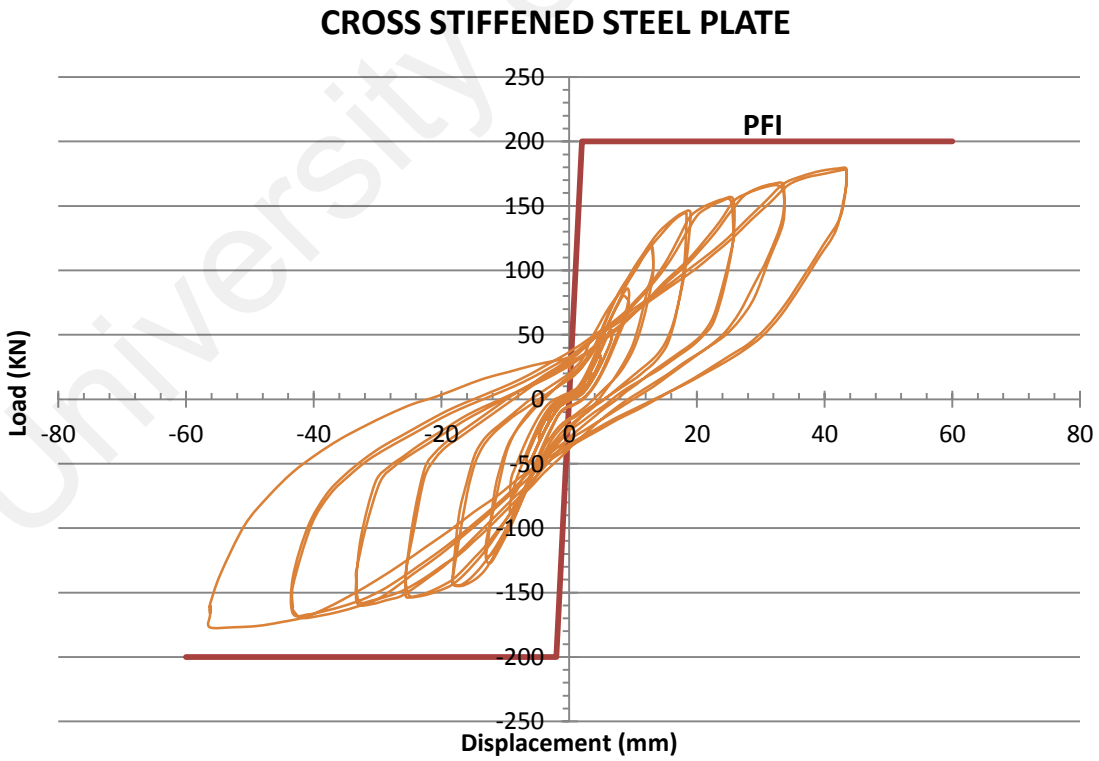

Figure 3-36 Hysteresis curve of CS-SPSW

3.4.1.4 CRS-SPSW

During the installation process of infill plate to the boundary test frame, 3 primary buckling lines in the corners of infill plate was seen. At the 17th cycle, those buckled lines which located in the right half on specimens (reaction wall at the right side) slightly developed.

The LVDT which was installed in the center of infill plate (LVDT4 in Figure 3-37) showed a sudden increase of out of plane displacement in the 13th cycle at the displacement of 5.4mm (0.63% drift). The strain gages which were installed far from the center of infill plate (the order of activity level from little to more: 1, 3, 5& 6 in Figure 3-38) showed more activity among others. As LVDTs which were installed at the same location showed more out of plane displacement (LVDT 9) which could be the effect of special behavior of the specimen.

By considering the strain gages installed on the stiffeners, (SG14, 17, 20 &23 in Figures 3-39) they seemed to be more active compared to the others. That means the outer stiffeners suffer more strain than other locations and as the distance increased from the center of infill plate, this effect will be more considerable, especially at the beginning of the loading. This behavior is more tangible for strain gages in the diagonal direction. The strain gauge 14 and 17 are more active than 20 and 23. According to the Figure 3-38, as a singularity phenomena, the strain in the right column of the test frame suddenly exceeded the yielding strain (SG 10) at the 15th cycle at the displacement of 0.68mm.

It is very clear that tension field action is very vital for dissipating more energy in the steel plate shear walls. In the case of CRS-SPSW the tension field buckling waves appeared as a set of parallel rings between the stiffeners (Figure 3-40). As it can be seen in Figure 3-41, which shows the hysteresis

curve of CRS-SPSW, owing to this special kind of behavior, in the last cycle (27^{th}) the hysteresis loop is expanded and the capacity of the system to absorb more lateral displacement has increased considerably. The maximum load carrying capacity of this specimen was 190 KN at the displacement of 51.4mm (5.9% drift) and the maximum displacement were equal to 53mm (6.1% drift).

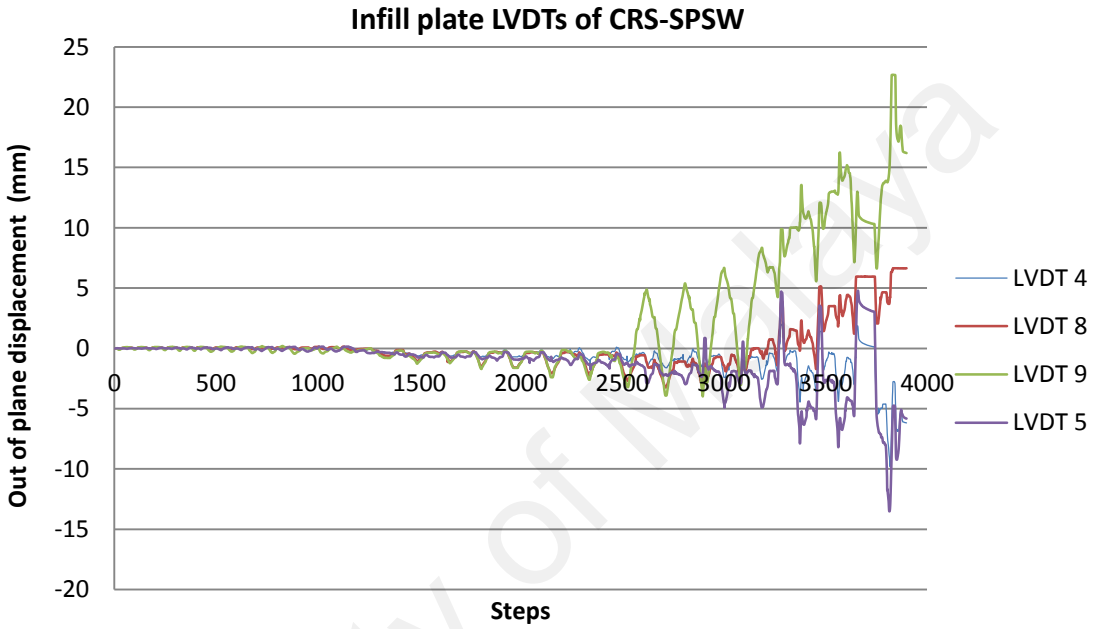

Figure 3-37 Infill plate LVDTs of CRS-SPSW

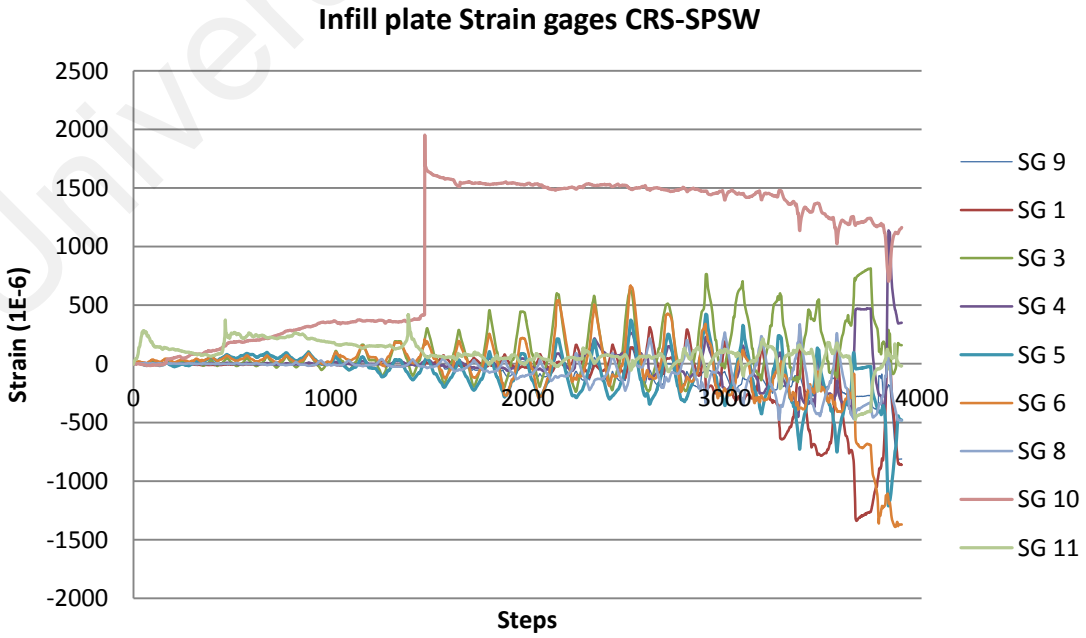

Figure 3-38 Infill plate strain gages of CRS-SPSW

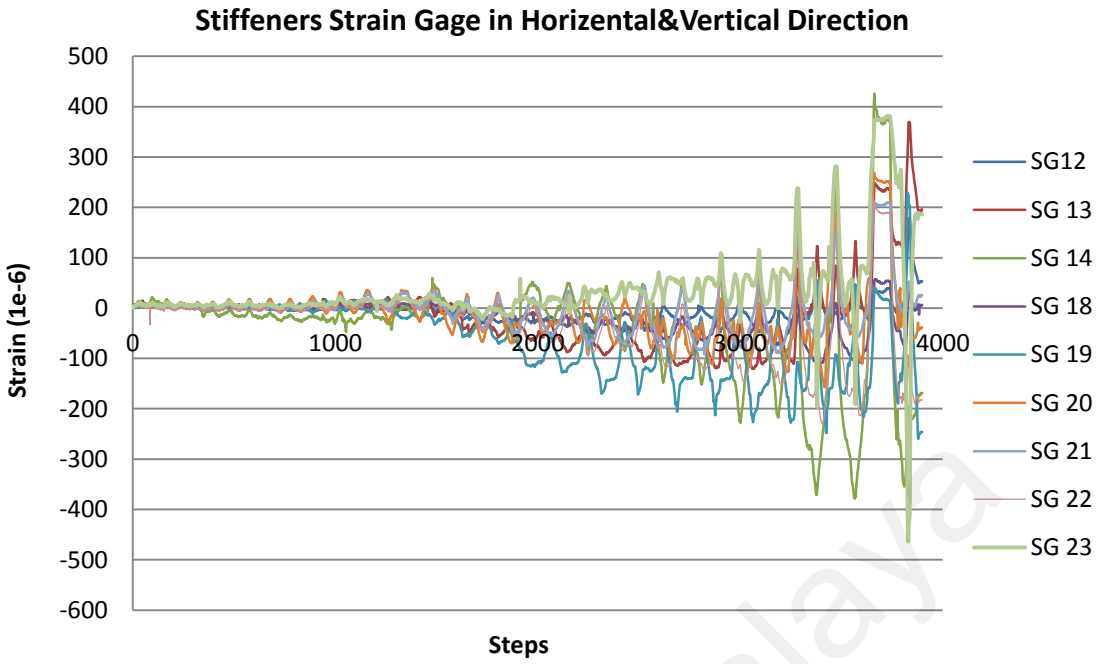

Figure 3-39 Stiffeners strain gauges of CRS-SPSW

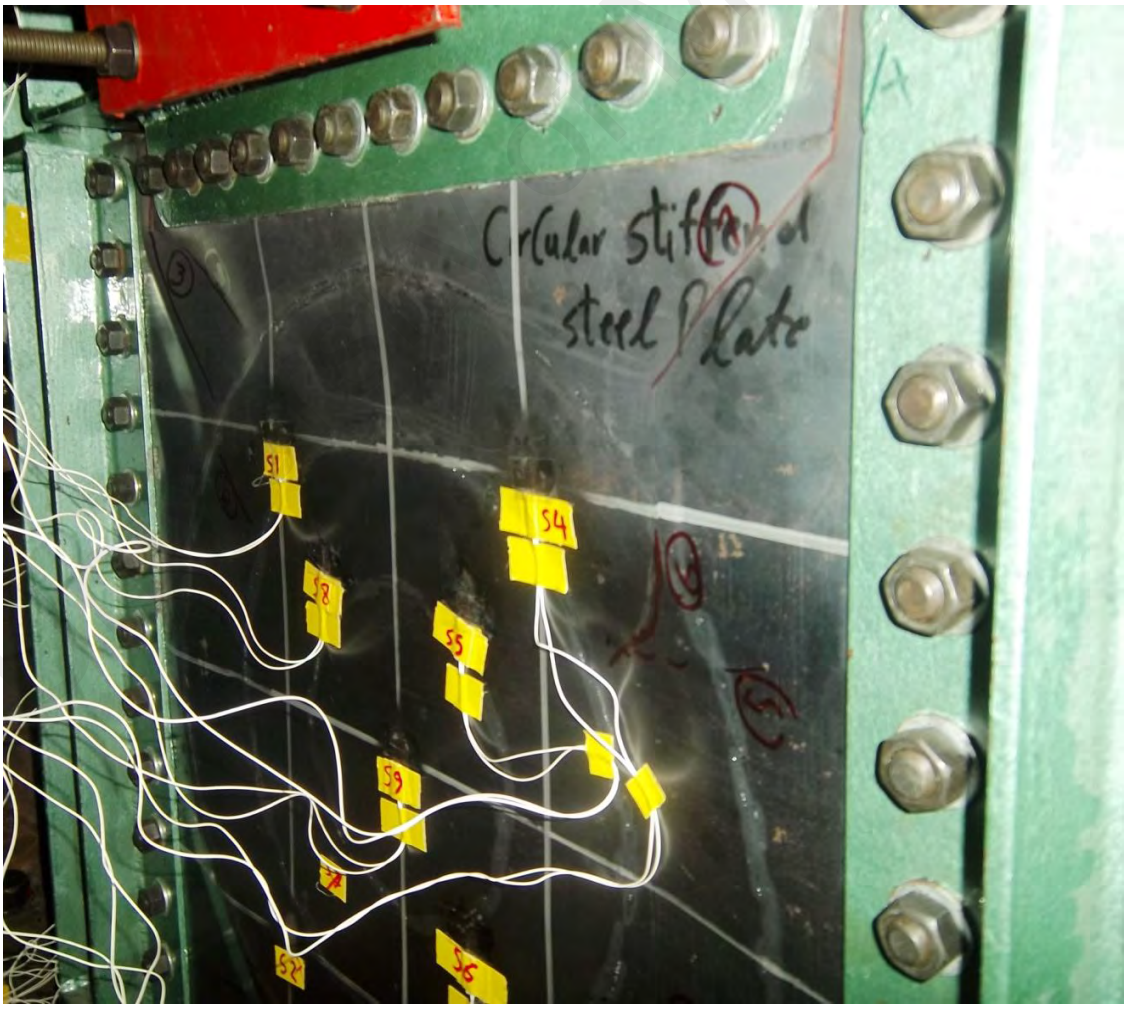

Figure 3-40 Buckling rings between the stiffeners for CRS-SPSW

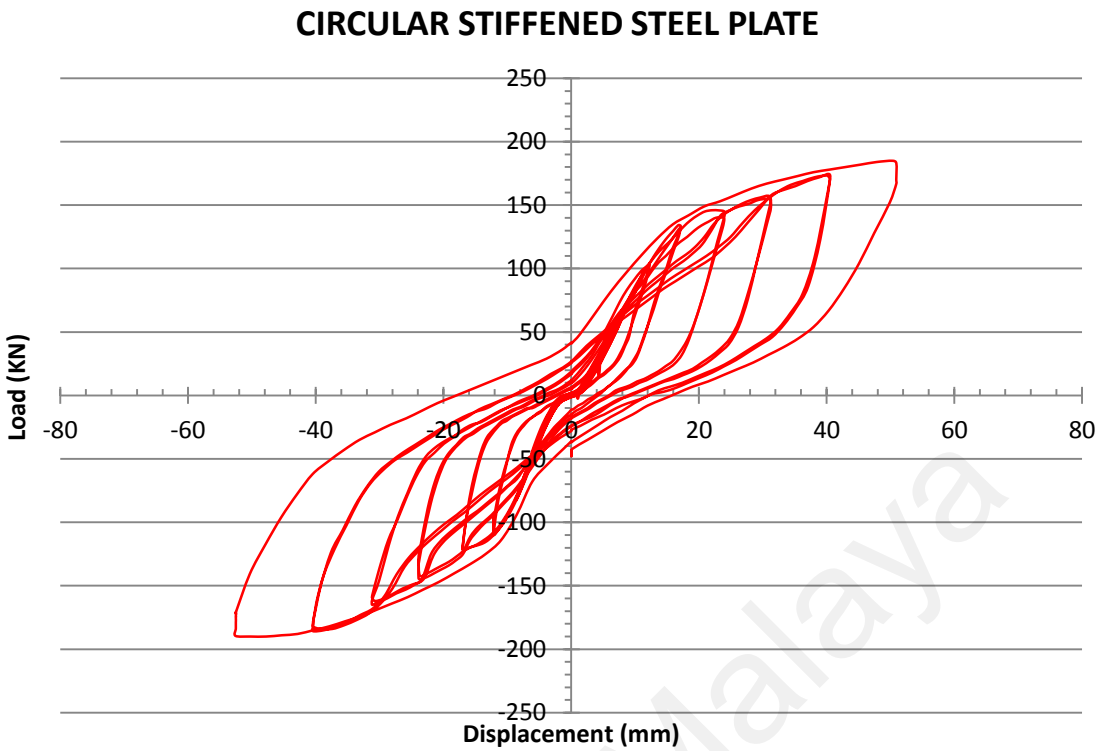

Figure 3-41 Hysteresis curve of CRS-SPSW

3.4.1.5 DS-SPSW

Similar to other specimens, buckling started at the corners of the infill plate. First buckling line inside the sub-panel was developed at 17th cycle in the 12mm displacement (1.38% drift). According to the LVDTs data (Figure 3-42), all four central sub-panels buckled in the 26th cycle at 41.18mm displacement (4.74% drift). The installed strain gages on the stiffeners (Figure 3-44 and 3-45) showed that the stiffeners which do not pass from the center of infill plates are suffering more strain. This behavior was clearer after 24th cycle at displacement 41.2mm (4.74%drift). Additionally, the buckling of the above-mentioned stiffeners has occurred at the same cycle.

The specimen undergone 26 cycles (Figure 3-46) with maximum load carrying of 165 KN at the displacement of 47.37mm (5.44% drift). The maximum displacement of the specimen was equal to 56.19mm (6.47% drift).

The noticeable character for DS-SPSW is that nodal buckling has appeared, but the stiffeners configuration has prevented the formation of tension fields between the stiffeners (Figure 3-47). The effect of this stiffener is quite clear on the hysteresis curve of DS-SPSW which posses un-favorable performance among other stiffened specimens.

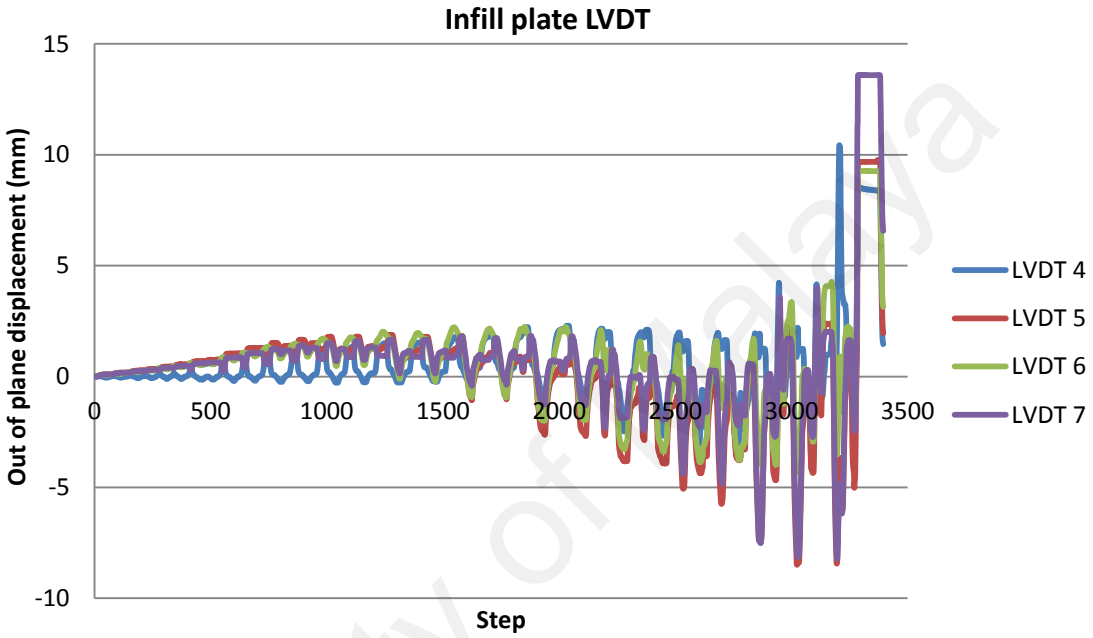

Figure 3-42 LVDT data of DS-SPSW infill plate

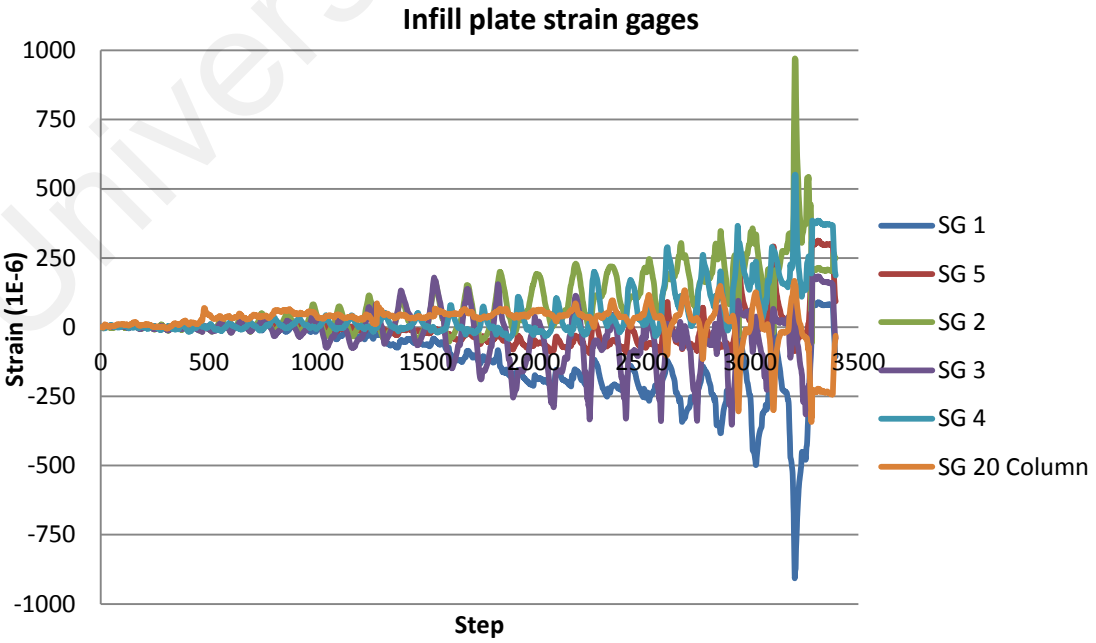

Figure 3-43 Strain gauge data of infill plate of DS-SPSW

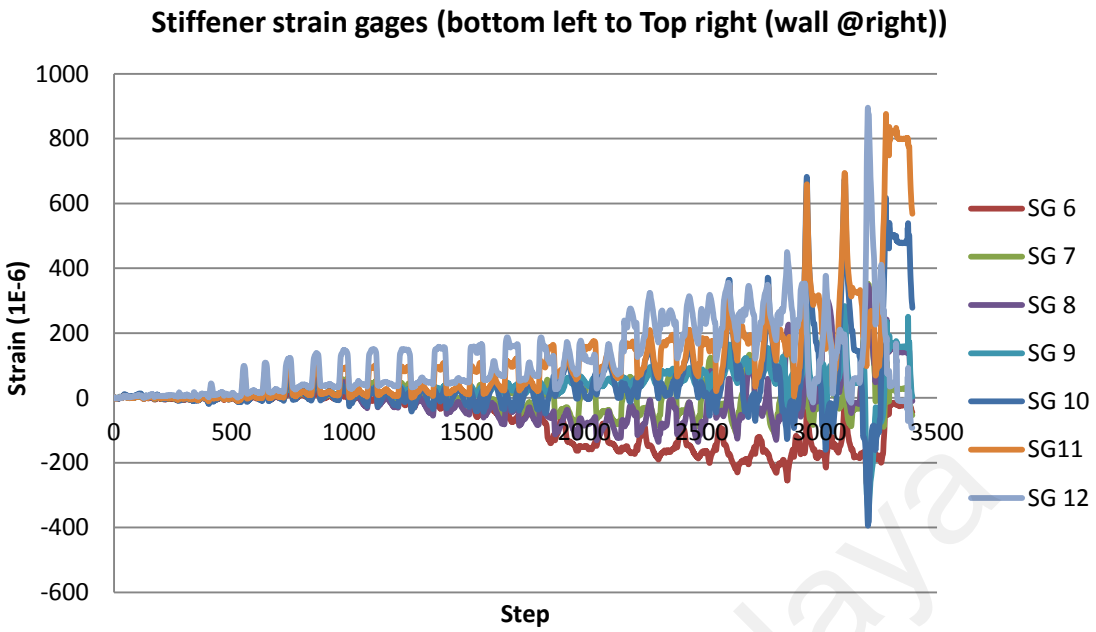

Figure 3-44 Strain gauge data of stiffeners of DS-SPSW

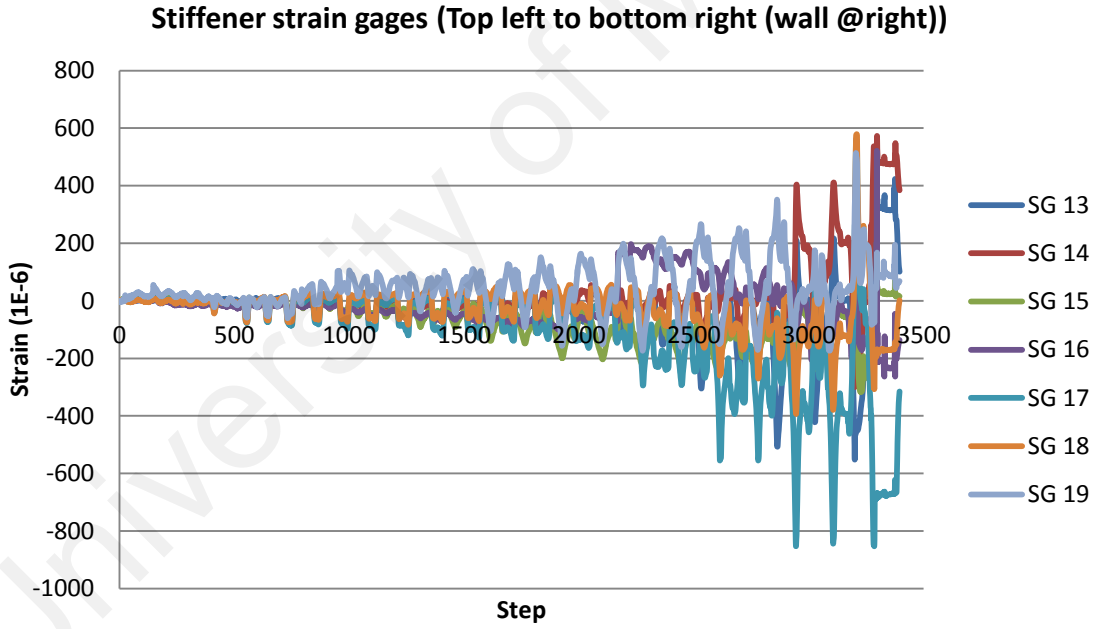

Figure 3-45 Strain gauge data of stiffeners of DS-SPSW

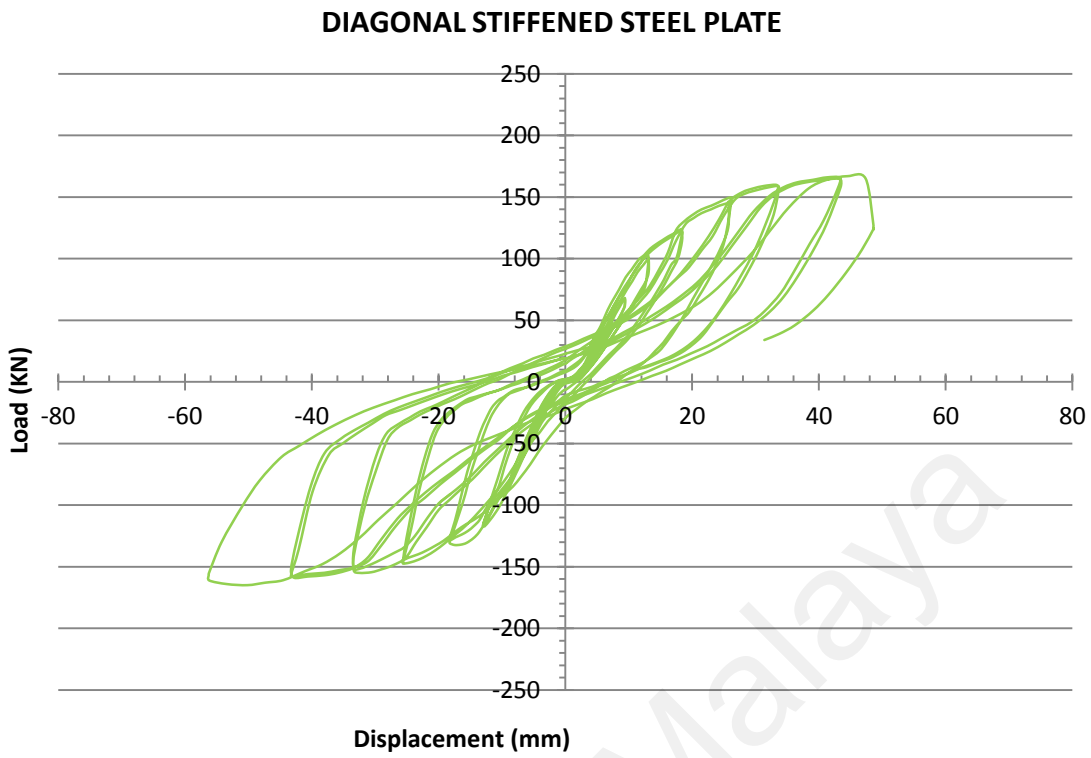

Figure 3-46 Hysteresis curve of DS-SPSW

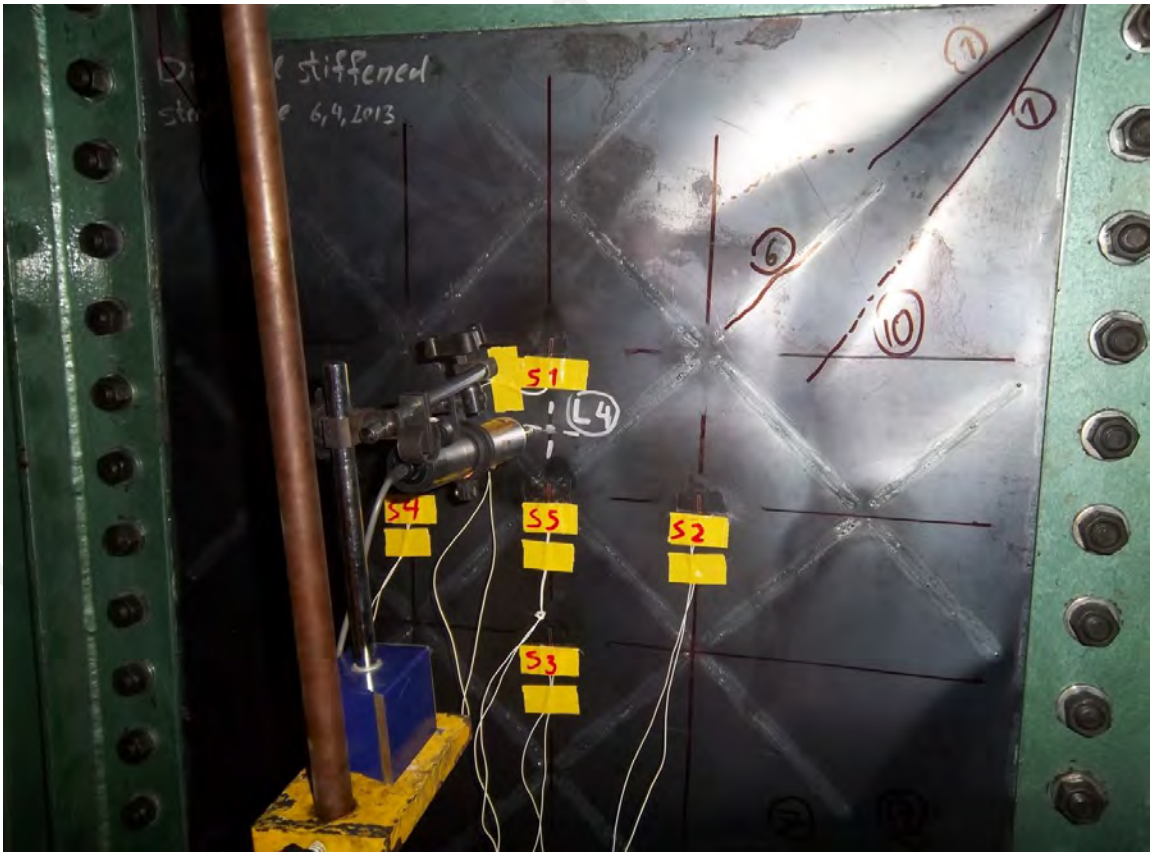

Figure 3-47 Nodal buckling line of DS-SPSW

3.4.2 Comparison of Cyclic Behavior

The envelopes of the hysteresis curves of all specimens are shown in Figure 3-48. By comparing stiffened and un-stiffened specimens, differences in the shape and size of hysteresis curves could be found. It should be mentioned that due to the utilization of hinged connection, boundary frame did not contribute to the resisting of the applied lateral load and only infill plates suffering the applied displacements.

In the case of two the un-stiffened infill plates (US-SPSW and AL-SPSW), in low amplitude displacements (or in the early loading cycles), the slopes of the hysteresis curve are not considerable. In other word, the lateral stiffness of the system is negligible when compared to the other parts of the hysteresis curve. This behavior was also observed in previous studies, which has used hinged boundary frame or thin infill plate (Tromposch, 1987, Roberts and Sabouri-Ghomi, 1992, Veladi et al., 2007, Valizadeh et al., 2012). Pinched hysteresis loops are characteristic behavior of thin steel plate shear walls. In such panels, buckling before yielding occurs and once tension field action (in large amplitude displacement) forms, its performance will improve.

Comparing with the un-stiffened infill, the buckling behaviors of all stiffened specimens are improved and the effect of this behavior could be seen in the hysteresis curves, where the slopes of early loading cycles were increased. Furthermore, similar to research of Alinia et. al. (2007) and Sabouri-Ghomi et. al. (2012), installation of stiffeners had a negligible effect on the shear strength of steel plate, but it affected the stiffness and yielding displacement.

Because of considerably enclosed area, stiffened panels display a superior and larger hysteresis curve and absorb more energy. The hysteresis

loops of stiffened panels are stable and have less displacement compared to the un-stiffened panels, and no degrading was observed. These advantages have distinguished the cyclic behavior of stiffened panels.

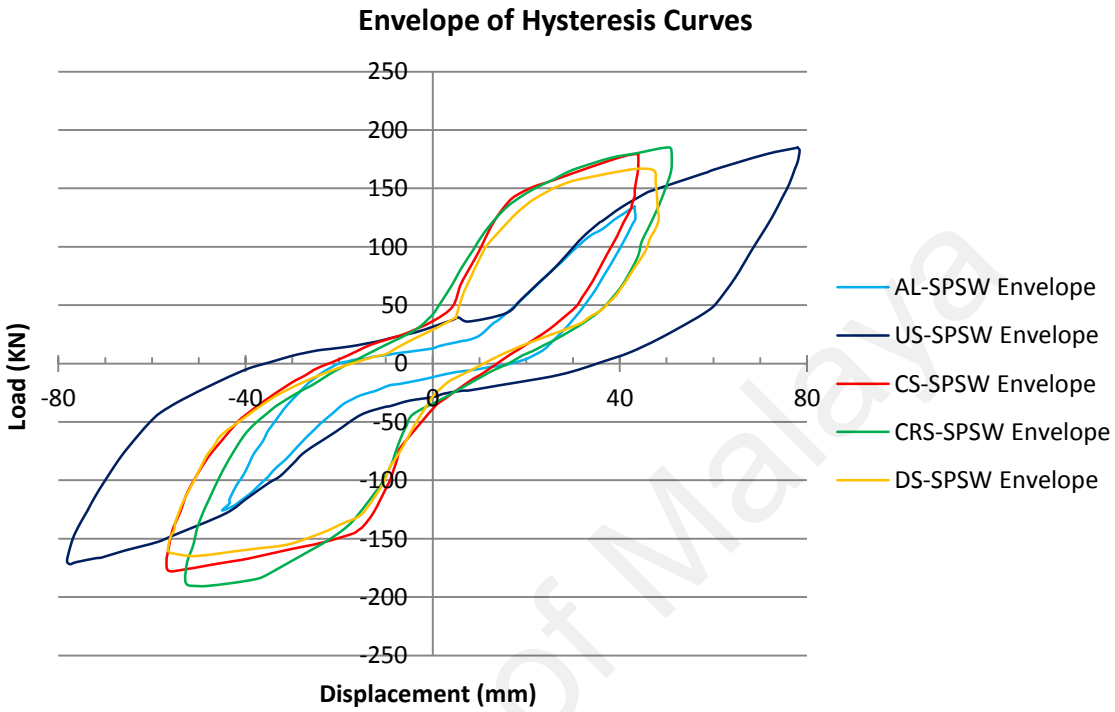

Figure 3-48 Envelope of hysteresis curves of all specimens

3.4.3 Stiffness

By tracing the key point of hysteresis curves, load-displacement curves of test specimens are obtained (Figure 3-49). The results of elastic stiffness are summarized in Table 3-6. The methodology of extracting initial linear stiffness is shown in Figure 3-50. This method is a combination of advices of ATC40 (1996) which is based on equal energy definition, and FEMA440 (F.E.M.A, 2005).

Based on the equal energy curve definition, the enclosed area under the load-displacement curve and ideal bilinear should be equal. By comparing the stiffness of un-stiffened steel plate with others, it can be seen that the stiffeners

changed the shear stiffness considerably, especially for the cross-stiffened (CS-SPSW), where the stiffness increased up to 240%.

Table 3-6 Elastic Stiffness of all specimens

Specimens	AL-SPSW	US-SPSW	CS-SPSW	CRS-SPSW	DS-SPSW
Stiffness (KN/mm) +	3.79	4.5	11.05	9.52	9.45
-	4.16	4.1	11.5	14.12	10.2

+: Positive Loading -: Negative Loading

Figure 3-51 illustrates the stiffness performance of all panels. As can be seen, due to the imperfection, the early buckling of the un-stiffened panel (AL-SPSW, US-SPSW) in few primary cycles, affected the performance. This effect appeared as decreasing in stiffness up to special drift, and once tension field action started; the stiffness increased. These curves were created based on the real slope of the tangent line to the load-displacement curves in the keys point. The horizontal parts are showing the stiffness of panels in the linear part of load-displacements curves. The effect of material types is quite clear on the stiffness of the un-stiffened specimens. According to Figure 3-51, despite the stiffness of AL-SPSW and US-SPSW seems to be close together, but their corresponding yielding drifts are different. The highest amounts of stiffness belong to the CS-SPSW, where its stiffness degradation is not favorable. After yielding, the stiffness degraded in a better trend for DS-SPSW hence, the panel with diagonal stiffeners performed better. The uncommon variation of the stiffness of AL-SPSW and US-SPSW in Figure 3-51 could be related to the hinged boundary frame that did not provide any stiffness for the specimens. In the case of AL-SPSW and US-SPSW, the infill plate buckled at the beginning of the loading and the stiffness degradation started and it was continued until the tension field action started. After the emerging of the tension field, the stiffness of those specimens increased.

3.4.4 Ductility

The ability of a structure to sustain deformations after its initial yield, without any significant reduction in ultimate strength or breaking, is defined by ductility. This factor indicates the capacity of a structure to absorb seismic energy through plastic deformation. Furthermore, for prediction of structural behavior and their ultimate capacity under lateral load, the ductility is one of the most important factors.

In terms of quantity, the displacement ductility is defined as the maximum displacement (Δ_u) divided to the first yield displacement Δ_y (Fig 3-50). The overall ductility's of panels are summarized in Table 3-7, which are calculated based on the definition of ideal bilinear load-displacement of panels.

Table 3-7-Overall ductility of all specimens

Specimens	AL-SPSW	US-SPSW	CS-SPSW	CRS-SPSW	DS-SPSW
Ductility +	1.41	2.29	3.36	3.22	2.99
-	1.34	2.32	4.34	4.81	3.69

+: Positive Loading -: Negative Loading

The ductility's gained in different level of drift are shown in Figure 3-52. All stiffened specimens have shown that their ductility's are increased, and the superior behavior of CS-SPSW is quite clear among other stiffened panels. Despite the aluminum panel's failure occurred in the early cycle of loading, but due to the lower yield stress, its ductility seems to be better compared to the un-stiffened steel plate.

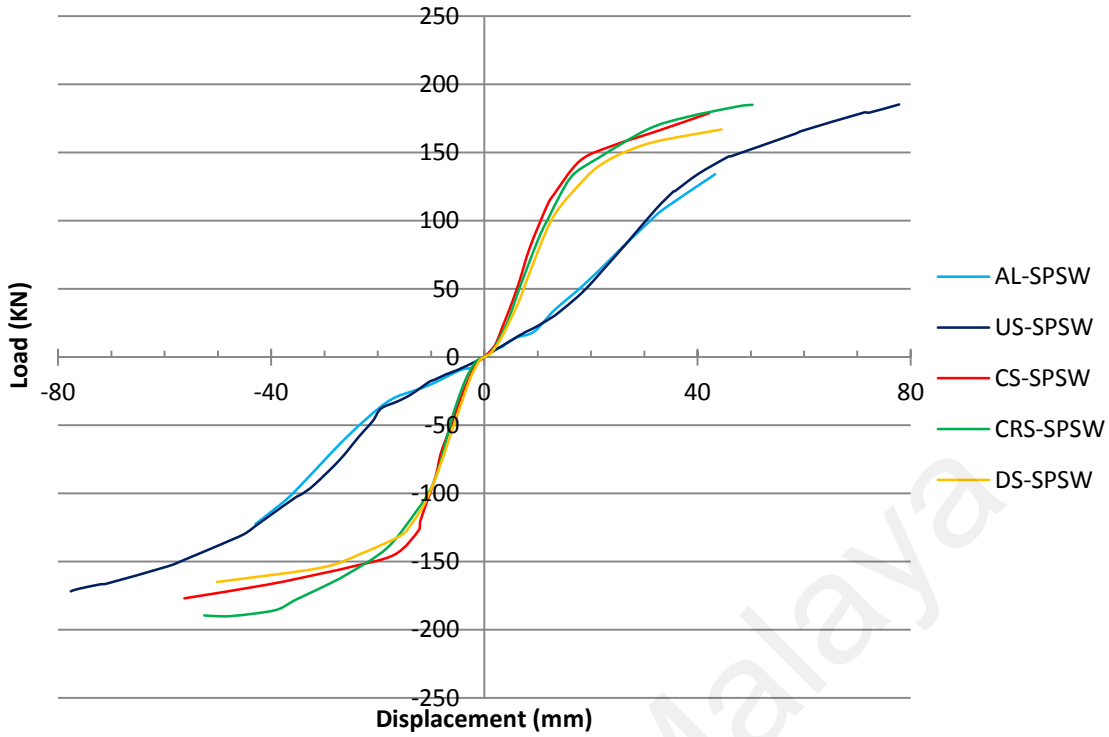

Figure 3-49 Load-Displacement curves off all specimens

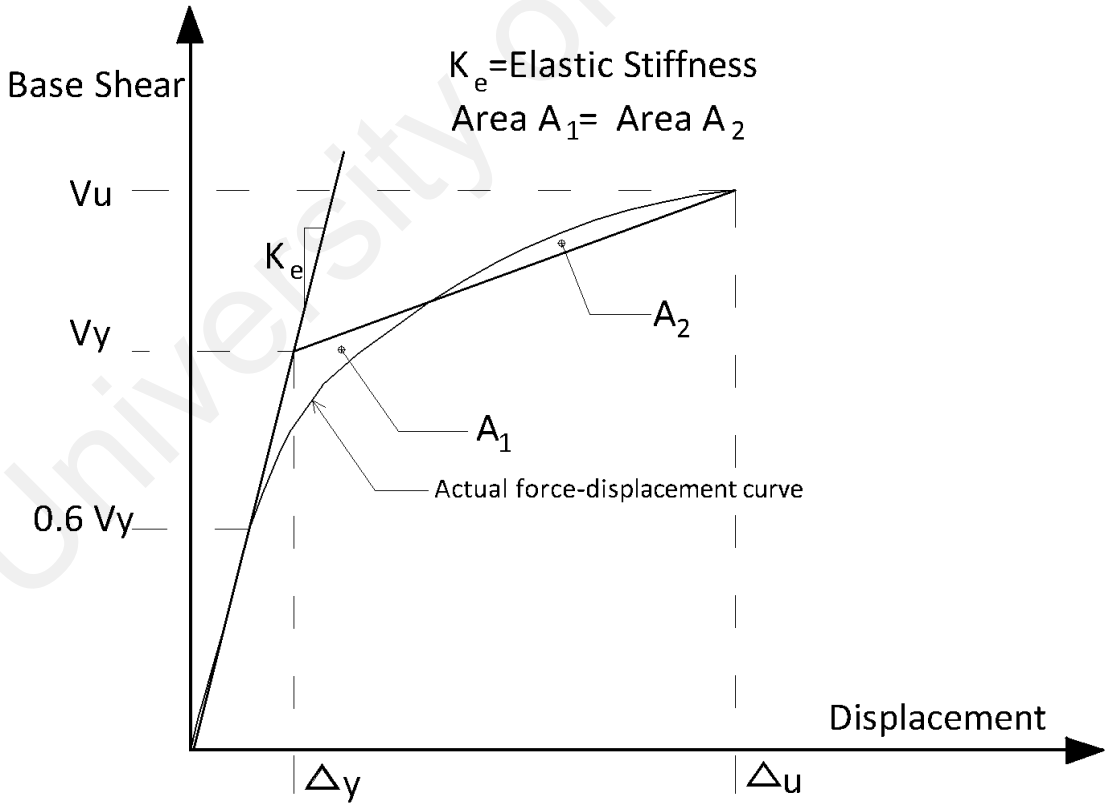

Figure 3-50 Idealization of Load-Displacement cuvre by bilinear

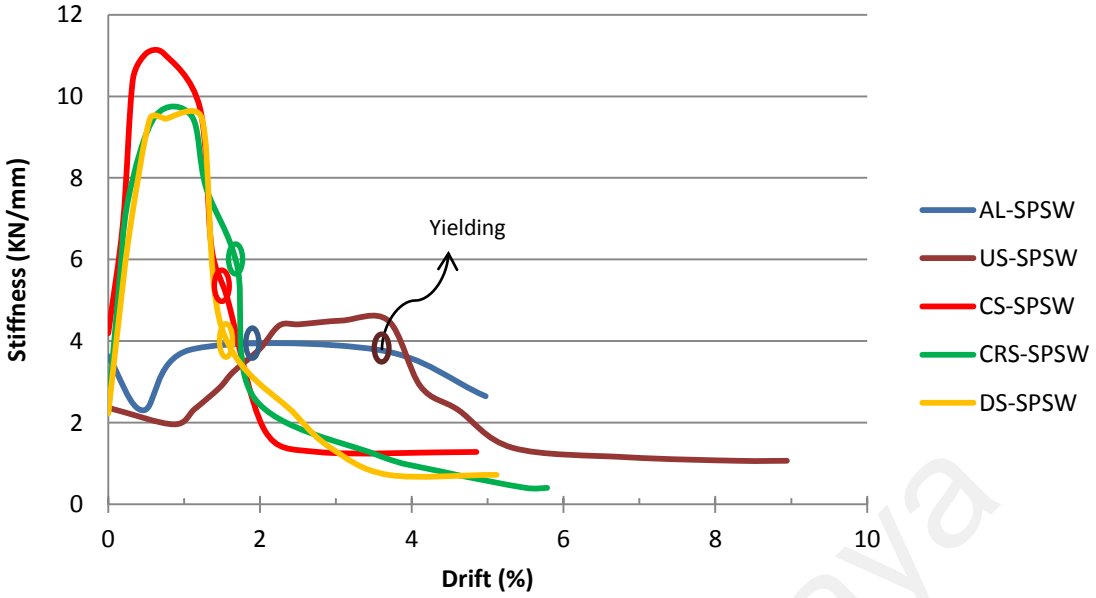

Figure 3-51 Stiffness vs. Drift

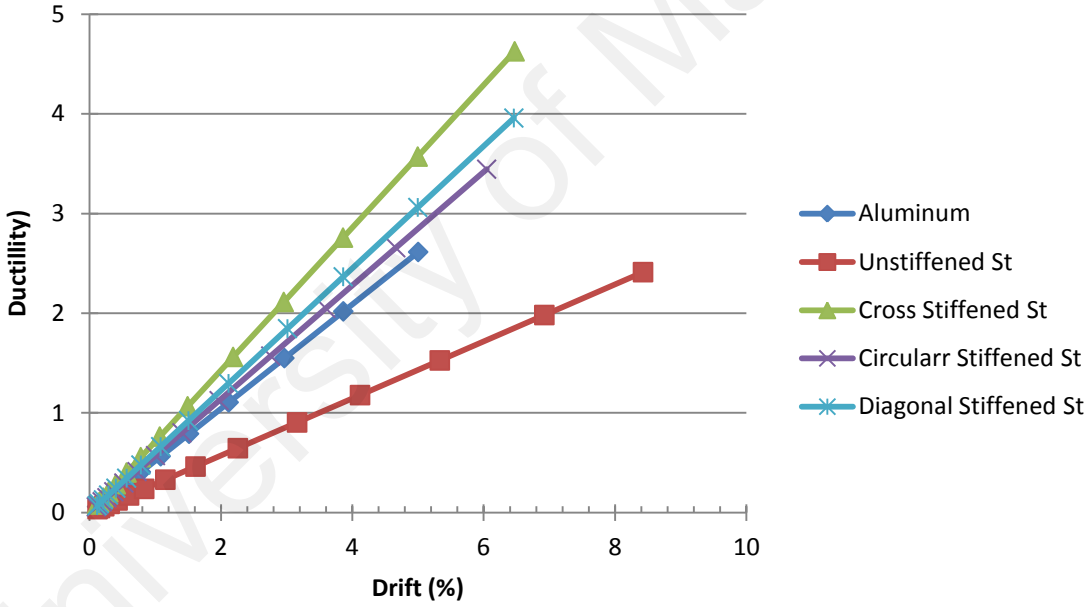

Figure 3-52 Ductility at different levels of drift

3.4.5 Energy Dissipation

The area within the hysteresis curve defined as the energy dissipation capacity (Figure 3-53). Forming the tension fields (Fig 3-54), plastic buckling and stable hysteresis loops is the dominant factor for absorbing more energy in the steel plate shear walls. The dissipated energy per every cycle is plotted in

Figure 3-55. It should be noted that energy dissipation continued to increase through the running cycles, except for AL-SPSW in the last cycles. In every subsequent paired cycles with identical target displacement, un-stiffened panels (AL-SPSW and US-SPSW) absorbed less energy in their second subsequent running cycles. In contrast, such behavior improved for stiffened panels, especially in the case of DS-SPSW, which at the same amplitude running cycle, equal energy was absorbed. The relatively wide hysteresis loops enclosing considerably more area for stiffened panels, are indicative of large energy absorption ability. As can be seen in Figure 3-55, performance of CRS-SPSW in the last cycle is distinctive, which has dissipated larger amount of energy among other panels.

The cumulative dissipated energy versus the drift is plotted in Figure 3-56. In this graph, among distinctive performance of stiffened panel, CS-SPSW has absorbed the greatest amount of energy. Due to long cyclic life of un-stiffened steel panel (US-SPSW), its energy absorption seems to be better. Although the aluminum infill plate (AL-SPSW) failure occurred in early cycles, its energy dissipation ability is similar to the un-stiffened infill plate.

The dissipated energy and displacement ductility levels variation based on the corresponding drift, can be combined in a unique graph, as shown in Figure 3-57. This graph shows another perspective of energy dissipation behavior. From this perspective, using the US-SPSW up to ductility level of 2 seems more effective for energy dissipation compared to other panels. The above-mentioned characteristics behavior of the un-stiffened panel has advantages when the gained ductility level is limited by design considerations. Up to ductility 3.5, CRS-SPSW has shown better performance in absorbing energy. Performance of AL-SPSW is not remarkable and as shown in Figure 3-

57, considerable differences between AL-SPSW and other panels could be seen.

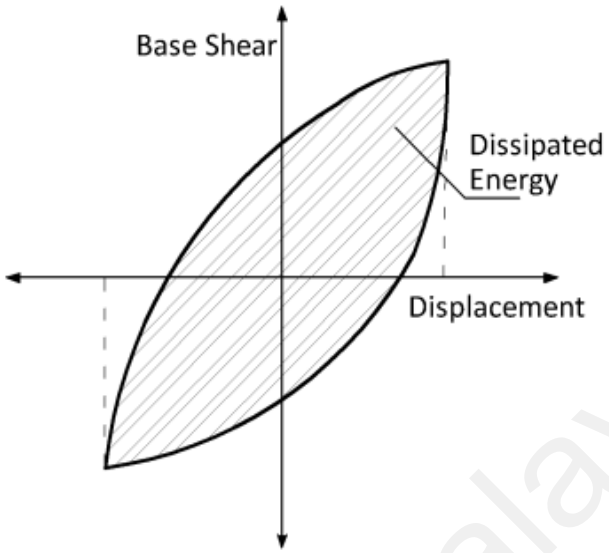

Figure 3-53 Dissipated energy methodology of every hysteresis loop

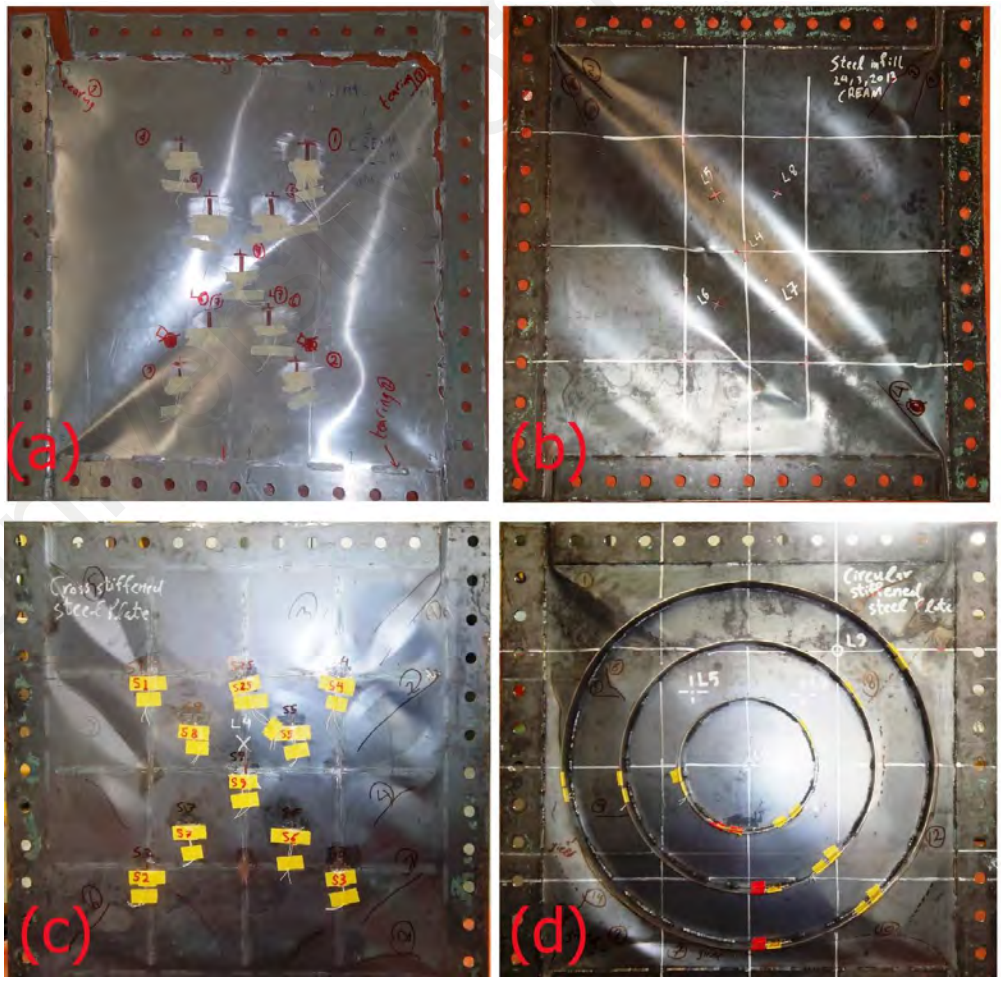

Figure 3-54 Different buckling mode for (a) AL-SPSW, (b) US-SPSW, (C) CS-SPSW and (d) CRS-SPSW

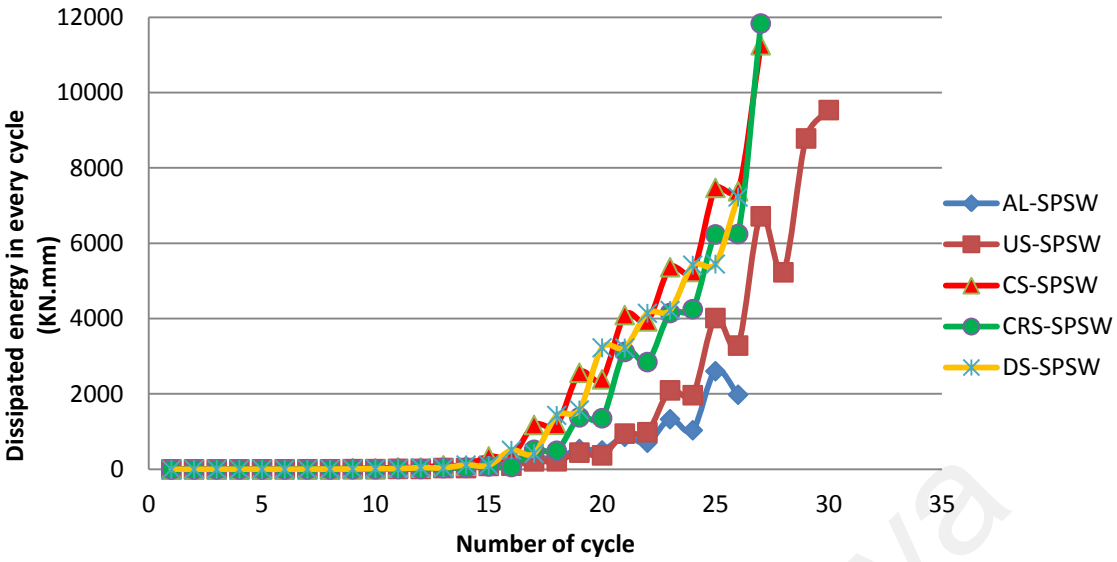

Figure 3-55 Dissipated energy per every cycle of all panels

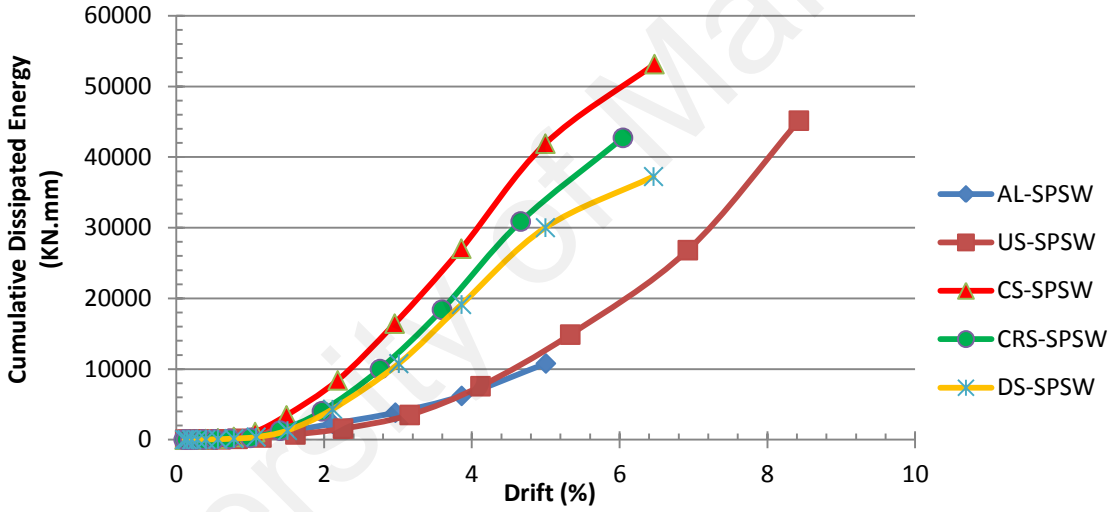

Figure 3-56 Cumulative dissipated energy of panels

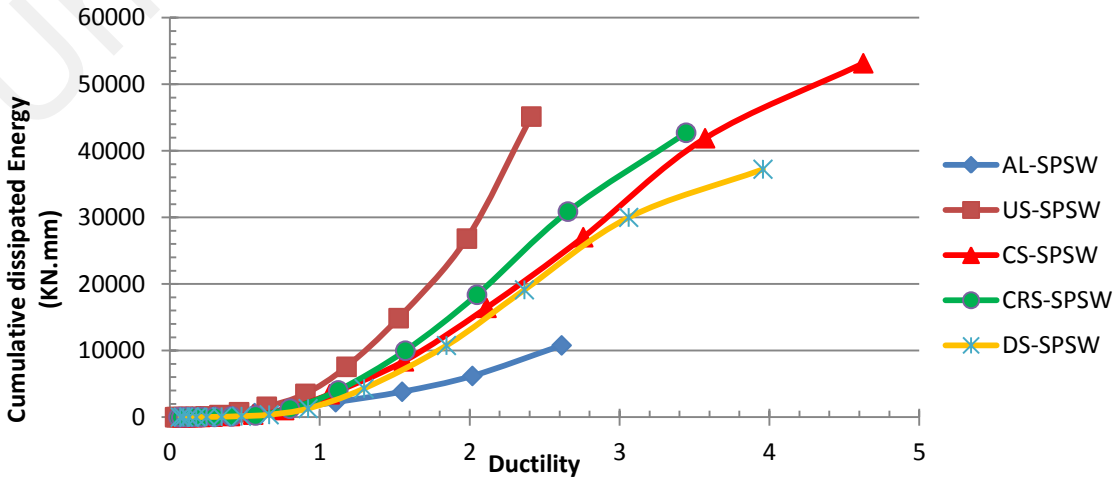

Figure 3-57 Ductility versus cumulative dissipated energy

3.5 SUMMARY

The cyclic behavior of stiffened and un-stiffened SPSWs was examined in this chapter. From a total of five test specimens, two specimens were un-stiffened aluminum and steel plate, whereas another three specimens were stiffened with cross, circular and diagonal stiffeners on one side of steel infill plate. The sectional area of stiffeners was kept constant.

The tests showed that before yielding, aluminum plate (AL-SPSW) exhibit good cyclic performance. Due to the material hardening effect, it was unable to sustain more cycles and brittle failure occurred.

Un-stiffened steel plate performance was very ductile with stable hysteresis curve and no tearing was observed. The PFI method, under estimated just 4.5% of shear capacity of this specimen and there is good agreement between the results. Un-stiffened steel plate possesses excellent deformation capacity, and it reached 9.56% drift without any tearing. Due to outstanding deformation capacity, energy dissipation performance was found more considerable after the drift of 6.47%.

The results of stiffened specimens showed that installation of stiffeners increased the stiffness considerably. The buckling mode was governed by the stiffener configuration. Cross stiffened specimens (CS-SPSW) showed the validity of using suggested equations, which changed the overall buckling of infill plate to buckling of the sub-panel with no major sign of the stiffeners buckling. The PFI method has acceptable precision on the prediction of ultimate strength of cross-stiffened panels and just 10% over estimate the shear strength of CS-SPSW. The ultimate shear strengths of all stiffened specimens were close together, so by converting circular and diagonal stiffened panels to

the ideal cross stiffened pattern; their shear strength could be estimated by PFI equation method.

Comparing with the un-stiffened infills, the buckling behaviors of all stiffened specimens are improved. Because of considerably enclosing area, stiffened panels displays a superior and wide hysteresis curve and more energy absorbed. The hysteresis loops of stiffened panels is stable and has less displacement compared to the un-stiffened panels, and no degrading were observed.

The stiffeners increased the shear stiffness, energy dissipation and ductility considerably, especially for the cross-stiffened (CS-SPSW). The highest amounts of stiffness, dissipated energy and ductility belong to the CS-SPSW, where its stiffness degradation is not favorable. After yielding, the stiffness degraded in a better trend for DS-SPSW and from this aspect, the panel with diagonal stiffeners performed superior. The stiffness of un-stiffened specimens was influenced by the material specifications.

CHAPTER 4: FINITE ELEMENT MODELING

4.1 INTRODUCTION

An experimental investigation was conducted and described in the previous chapter, to better understand the structural behavior of steel plate shear walls (SPSWs). However, quantity and dimensions limit such experimental tests. Thus, the experiment cannot cover all aspects of structural behavior. Additional expenses for conducting other experimental tests can be avoided via the numerical modeling of SPSW behavior under various loading and geometric conditions, a method that can simultaneously cover the wide range of parameters. The objective of the current chapter is to develop a reliable finite element (FE) model under pushover and quasi-static load. The FE models were validated with the test data in Chapter 3. The models were considered because of their accurate simulation of initial stiffness, post-yielding stiffness, ultimate strength, and hysteric behavior.

The commercial general-purpose nonlinear FE program, ABAQUS Ver. 6.11 (Simulia, 2009a), was deployed to develop a numerical model of the SPSWs. The advantages of this software include the capability to solve highly nonlinear engineering problems, an extensive library of elements, and various available geometric boundary conditions.

ABAQUS consists of two main analysis modules, ABAQUS/Standard and ABAQUS/Explicit. In ABAQUS/Standard, an implicit method is used to analyze systems under quasi-static and dynamic loads. In the implicit method, equilibrium is achieved through an iterative procedure, from which the deformed configuration of the structure is obtained. Thus, the equilibrium equation is achieved by iteration. In ABAQUS/Explicit, a nonlinear explicit

dynamic formulation is used to analyze systems under dynamic and quasi-static conditions. In the dynamic explicit method, unbalanced forces between the internal and external forces at the beginning of the increment are considered as the driving forces that act on a mass. From these forces, the deformed state is obtained after a slight increment using the central difference method; thus, no iteration is involved in this technique.

The SPSW was initially analyzed with the static implicit method implemented in ABAQUS/Standard because the tests were conducted under quasi-static conditions. The development of the tension field and shear buckling of the infill plate as the load increased created local instabilities in the infill plates. These instabilities caused difficulty in tracing the solution until the limit point owing to the convergence problems during the solution process using an implicit method. Therefore, in an explicit formulation, the solution was obtained without any iteration, and the explicit version of ABAQUS was used to analyze SPSWs under cyclic loading.

4.2 IMPLICIT FE METHOD

In the implicit method, the incremental solving of a nonlinear equilibrium equation obtains a nonlinear response from the system. The difference between internal node point forces and external applied load is the equation of equilibrium at the end of load increment. To solve the equilibrium equation, an iterative process is necessary because the internal nodal point forces depend on the history displacements of a nodal point. ABAQUS/Standard uses different repetitive methods, including Riks algorithm, Newton–Raphson, and modified Newton–Raphson (Simulia, 2009b, Simulia, 2010).

Local instability in steel shear walls occurs as the tension field re-orients during loading and unloading. This situation is aggravated within the modeling of cyclic loading of SPSWs. Most iterative methods fail to converge in the vicinity of unstable responses owing to the convergence problem of local instabilities.

Sudden out-of-plane deformation of the infill plates due to tension field development during the reverse-loading cycle, accompanied by a loud "popping" sound, was observed in the experimental studies. This phenomenon, which is also known as the "dynamic displacement snapping effect" or "Snap-through," caused serious convergence problems in the analysis of the SPSWs (Figure 4-1). This phenomenon was evident during the pushover analyses, which lasted longer at extreme deformation locations. For most analyses, the size of each increment should be reduced to achieve convergence. An increment size of 10^{-5} was appropriate for the explicit method but not suitable for the multiple-iteration implicit method. Considering the poor performance of the implicit FE method, the dynamic explicit method was chosen to analyze SPSWs because of their quasi-static loadings.

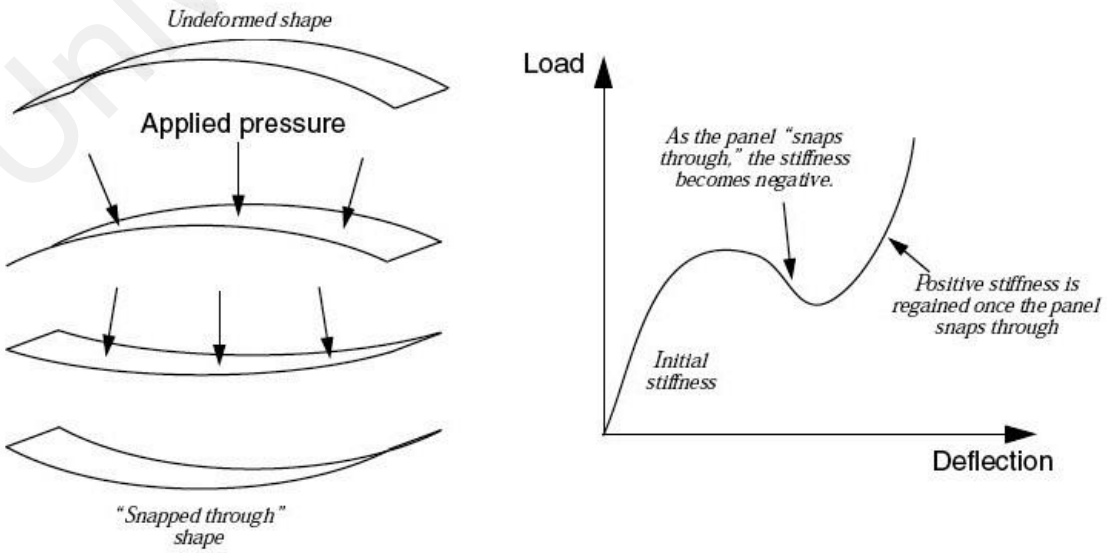

Figure 4-1 Snap-through of large shallow panel (Simulia, 2010)

4.3 EXPLICIT FE METHOD

The explicit dynamic method was developed to analyze the dynamic behavior of a structure during a rapid loading regime. This method can be applied to a wide range of nonlinear mechanical/structural problems. In addition, quasi-static problems such as post-buckling behavior, failure analysis, nonlinear material, and geometry can be solved using the explicit technique. Using the implicit method for these problems may not be successful owing to the convergence difficulties. Therefore, the explicit method was applied to simulate SPSWs in quasi-static loading. During the simulation of SPSWs under quasi-static loading, some consideration should extended to kinetic energy control (Simulia, 2009b, Simulia, 2010). The relevant literatures of explicit formulation method are available in Bathe (1996).

The distinguishing characteristics of the explicit and implicit methods are:

- Explicit methods require a small-time increment size that depends solely on the highest natural frequencies of the model and is independent of the type and duration of loading. Simulations generally take on the order of 10,000 to 1,000.000 increments, but the computational cost per increment is relatively small.

- Implicit methods do not place an inherent limitation on the time increment size; the increment size is generally determined from accuracy and convergence considerations. Implicit simulations typically take orders of fewer increments than explicit simulations. However, the cost per increment of an implicit method is far greater than that of an explicit method because a global set of equations must be solved in each increment (Simulia, 2010).

4.3.1 Definition of Stability Limitations of Dynamic Explicit Method

ABAQUS/Explicit, which is a central difference method, applies a commonly used time-integration method. The central difference method is a conditionally stable algorithm (Bathe, 1996) used as a time integrator. Therefore, the amount of time that a state can be advanced while maintaining a bounded error is restricted by its stability limit. The stable time increment in the presence of damping and the highest frequency of the system is defined as follows:

$$\Delta t_{stable} = \frac{2}{\omega_{max}}\left(\sqrt[2]{1+\xi^2} - \xi\right) \quad (4\text{-}1)$$

Where ξ is the fraction of critical damping in the mode with the highest frequency. To control high-frequency oscillations, in ABAQUS/Explicit, a small amount of damping in the form of bulk viscosity is added to the model. Equation 4-1 shows that the reduction in damping reduces the stable time increment and results in the increased CPU processing time for analysis completion. For large models, obtaining the highest actual frequency is not always feasible. Therefore, ABAQUS/Explicit adopted a conservative and realistic method to determine stability limit. The highest frequency, based on the element-by-element method, is higher than the highest frequency of the global model (Simulia, 2009b, Simulia, 2010), thereby allowing the highest frequency of individual elements within the model to be estimated. The estimated stable time increment that was based on the element-by-element calculation is, therefore, smaller than the global value and exists as a more conservative estimate. The highest frequency of an element was associated with the dilatational mode, and the critical time increment is stated as follows:

$$\Delta t_{stable} = \frac{L_e}{C_d} \quad (4\text{-}2)$$

Where, L_e is the smallest characteristic length of the element and C_d is the dilatational wave speed of the material defined as

$$C_d = \sqrt{E/\rho} \quad (4\text{-}3)$$

Where ρ is the density of the material and E is the modulus of elasticity. Equations 4-2 and 4-3 indicate that a conservative value for the critical time increment is the time that a dilatational wave passes across the smallest characteristic element length. The dilatational wave speed depends on the density and stiffness of materials. Hence, changing the size of FE mesh and material properties results in a change in the critical time increment, which, in turn, changes the required computational time for an explicit analysis. When the material is stiff, the wave speeds are high, resulting in a smaller stable time increment. Then, when the material density is high, the wave speed is insignificant, resulting in an increase in the critical time increment.

Wave speed is constant because the modulus of elasticity is constant for a specific material in the linear portion of analysis. Therefore, the critical time depends only on the smallest FE element size in the nonlinear range. However, the tangent modulus of elasticity decreases and, consequently, the wave speed reduces, resulting in an increase in the critical time increment. The element size should be consistently large to provide an acceptable accuracy of the analysis, given that the critical time increment is approximately proportional to the shortest element dimension (Behbahanifard et al., 2003b, Hibbitt et al., 2000).

4.3.2 Simulation of Quasi-Static Analysis by Dynamic Explicit Method

The explicit FE method is based on a dynamic formulation in which inertial forces resulting from the acceleration and mass of the system exert a considerable effect. Hence, special considerations are necessary in solving a

quasi-static problem using a dynamic explicit procedure. If inertial forces remain negligible and a simulation of the analysis is completed in the shortest time possible, then an acceptable result of the analysis will be obtained. Different methods are available to increase the speed of analysis without considerably reducing the accuracy of the quasi-static solutions. Therefore, if speed is increased to a point that inertial forces are dominated, then the solution will be prone to localizing and the results will differ substantially from the quasi-static solution.

The loads and displacements should be applied as smoothly as possible to prevent any change in acceleration from one increment to the next and obtain an accurate quasi-static analysis. ABAQUS provided a facility called SMOOTH STEP for such cases. Within the smooth step amplitude, the smoothest possible loading amplitude between two points is applied to the system. From this option, each load data pair is connected with curves, the first and second derivatives of which are smooth, and the slopes are zero at each data point (Simulia, 2010, Behbahanifard et al., 2003b). Quasi-static analysis can be performed conveniently using the explicit FE method, where smooth amplitude is applied on the loads. For most structural simulations, a loading duration that is 10 times the period of the lowest vibration mode is suggested to ensure a quasi-static solution (Hibbitt et al., 2000).

During the simulation, a general technique should be used to monitor the energies of a model and evaluate whether the response is quasi-static or not. These energies include internal energy (both elastic strain energy and plastic work) E_I, energy absorbed by viscous dissipation E_V, frictional energy (energy dissipated by frictional forces in a contact problem) E_{FD}, kinetic energy E_{KE},

and work performed by external forces E_W. The total energy E_{TOTAL} and the energy balance equation are defined as follows:

$$\boldsymbol{E_I + E_V + E_{FD} + E_{KE} - E_W = E_{TOTAL} = 0} \quad (4\text{-}4)$$

For a quasi-static simulation, internal energy in the bar is expected to be almost equal to the work performed by external forces. The viscous dissipated energy is usually small, unless dashpots, material damping, or viscous materials are used. The kinetic energy should be negligible given that the velocity of the system (i.e., the mass of the material) throughout the quasi-static simulation is insignificant. Generally, the kinetic energy of the deforming material should not exceed a small fraction (typically 5%–10%) of its internal energy during most quasi-static simulations (Simulia, 2010).

To evaluate the quality of the simulation, the ratio of kinetic energy history E_{KE} to internal energy history E_I must be compared to determine whether the ratio is less than 5%–10% during the analysis. When the ratio satisfies the suggested value, then the reasonability of the energy should be evaluated separately. Generally, smooth energy is expected from a smooth loading history. The last step in verifying the results is controlling the quality of the energy output. Noisy behavior, which results from the smooth loading history, causes the quality of the simulation to be unacceptable. The history of kinetic energy during the analysis should be inspected because the energy ratio cannot demonstrate the noisy behavior. To identify the cause of any high kinetic energy, for cases that do not exhibit quasi-static behavior, the velocity history of some critical nodes must be controlled. This verification technique was applied to the quasi-static simulation of tested unstiffened and stiffened SPSWs in Chapter 3.

4.3.3 Description of the Finite Element Model for Quasi-Static Analysis

4.3.3.1 Element Selection

The infill plate and the boundary members were discretized with shell elements to capture local buckling of the beam and column flanges. Most of the continuum and plate elements in ABAQUS/Explicit are based on an updated Lagrangian formulation (Bathe, 1996). Therefore, at the beginning of each increment, the nodal coordinates were updated to reflect their current positions in space, and all the shape functions and derivatives were re-evaluated using these updated nodal coordinates. This formulation is useful because the deformation magnitude and strains in the infill plates after many cycles are extremely large, such that the shape of the shear wall, especially in the first panel, is changed considerably.

The S4R shell element provided by the ABAQUS element library was selected to model the infill plate, boundary frame, and fish plates. The S4R element is a four-node double-curved general-purpose shell element with a reduced integration point. This element considers large membrane strains and arbitrary large rotations. Each node of the shell element has six degrees of freedom, namely, three translations and three rotations that are defined within a global coordinate system (Figure 4-2). The S4R element can model the

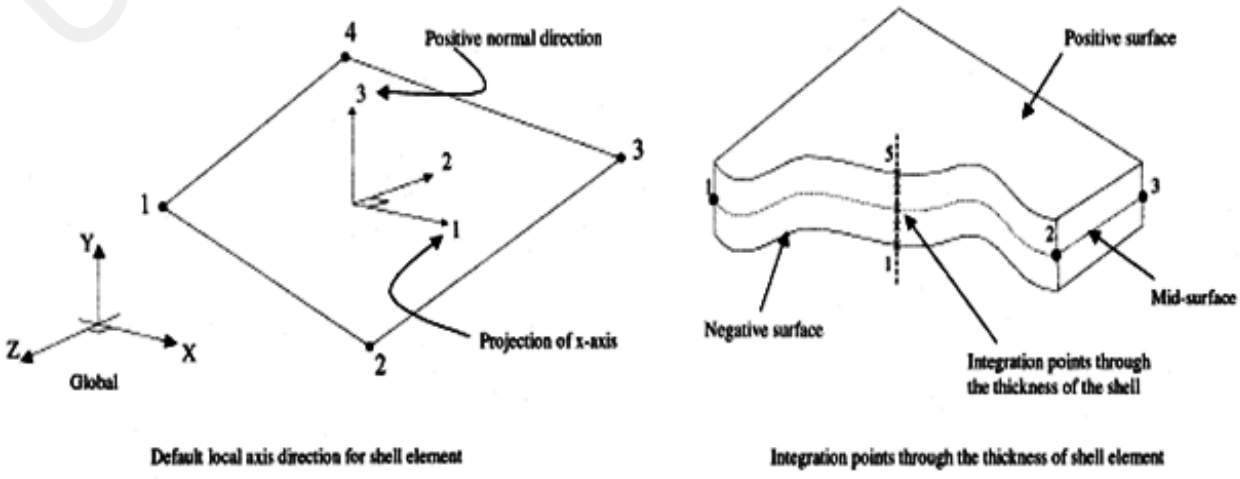

Figure 4-2 Default local axis and integration points for shell element S4

behavior of both thin and thick shells.

The S4R shell element was based on an iso-parametric formulation, which means the same shape functions were used to interpolate the displacement field and the geometry of the element. This element used one integration point on its mid-surface to form the element internal force vector. Reduced integration elements provided more accurate results and significantly reduce operating time if the elements were not distorted. However, given that S4R is a linear reduced element, it may suffer from hourglassing under certain loading conditions. This phenomenon may impact the load application and required mesh size of the SPSW model. Hourglassing is a pattern of zero energy non-physical deformations. ABAQUS/Explicit uses a small artificial stiffness, which is associated with rotation near the normal to the shell surface,

(a) Deformation of a first-order element with reduced integration subjected to bending

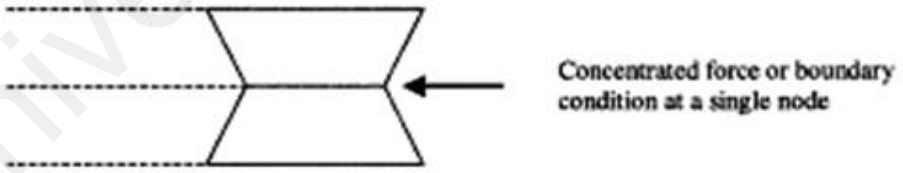

(b) Concentrated force or boundary condition creating hourglass deformation

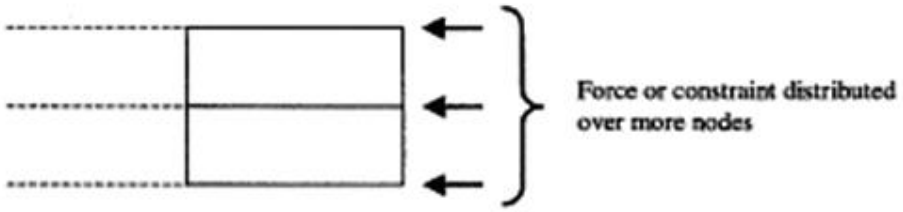

(c) Improved deformation pattern with distributed force or constraint

Figure 4-3 Hourglass mode: (a) shape; (b) common source of hourglass mode; (c) method of improvement

to prevent hourglass modes. The default hourglass stiffness values are small, such that the artificial energy content is negligible. In the present analysis, the default value was sufficient to prevent the hourglass mode.

A number of methods can be used to diagnose hourglassing in an analysis. When examining the deformed shape, hourglassing appears as a pattern of alternating trapezoid deformations (Figure 4-3). If the artificial energy is excessive, then excessive strain energy may be controlling this mode. The most useful approach is to compare the artificial energy to the internal energy. This ratio should be less than 5%–10% during most of the analyses. For modeling beams and columns, at least four elements are recommended in the depth of a web or the width of a flange to prevent hourglassing (Simulia, 2009b, Simulia, 2010). To discourage hourglass modes, all the concentrated loads and boundary conditions are distributed on a number of nodes. The size of the mesh used in modeling the SPSW is sufficiently fine to prevent hourglassing during the simulation, either in the deformed shape or the history of artificial energy.

The default number of integration points through the thickness of the S4R element is five (Figure 4-2), which is usually sufficient to simulate the elasto-plastic response of a shell structure under monotonic loading. For a more complex analysis that involves strain reversal (cyclic loading) and high localized curvatures, more integration points may be required.

4.3.3.2 Geometry and initial imperfection

The imperfections can be defined as camber and sweep of columns and beams and out-of-flatness of the plate. The camber and sweep of the beams and columns and the column out-of-plumb were small and were neglected in the

formulation of the FE model. Despite the assumption that neglecting the fish plate will not affect the overall behavior of SPSWs (Driver, 1997), the fish plate connection tabs were considered in the FE analysis. The behavior of the thin plates subjected to in-plane membrane stresses is affected by the initial out-of-plane deformations. The stiffness of a perfectly flat plate is extremely high under in-plane-shear forces. However, slight initial imperfections substantially reduce the in-plane shear stiffness or the plate. Therefore, initial imperfections of the infill plates were considered in the FE model. The imperfection pattern, which is equal to the measured amounts of the experimental program, was applied to the model.

4.3.3.3 Loading regime and boundary condition

In the experimental test, horizontal displacement was applied to the model by an actuator mounted between the reaction wall and the specimens. To model such loading, lateral displacement was applied to the corresponding portion of the FE model, which was simulated as the loading tab. The history of displacement, which was applied to all models under quasi-static analysis, is shown in Figure 4-4. This displacement history is equal to the displacement history in the physical test, but its repetitive loops were eliminated to shorten the analysis operating time. Its interval loop time was also set to the shortest appropriate period than the necessary energies to satisfy the quasi-static control.

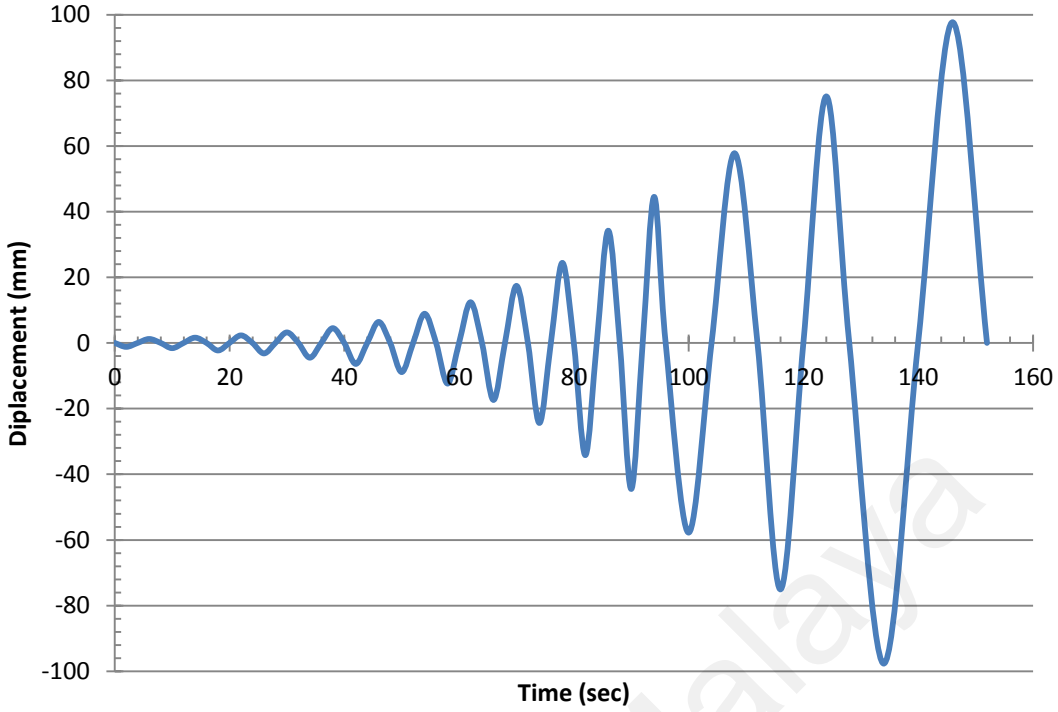

Figure 4-4 History of displacement applied on the FE Models

To simulate the fixed condition of the column-to-base plate connection, the bottom nodes of the bottom flange of the bottom beam were restrained from displacement and rotation in all directions (Figure 4-5). To simulate the constraints imposed by lateral supports in the experimental test, the out-of-plane displacements of the top beam webs were also restrained before cyclic loading. The imperfection, which is equal to the reported amount of the experimental program, was applied to the model. The hinge connection between boundary frames was modeled using the hinge connection element.

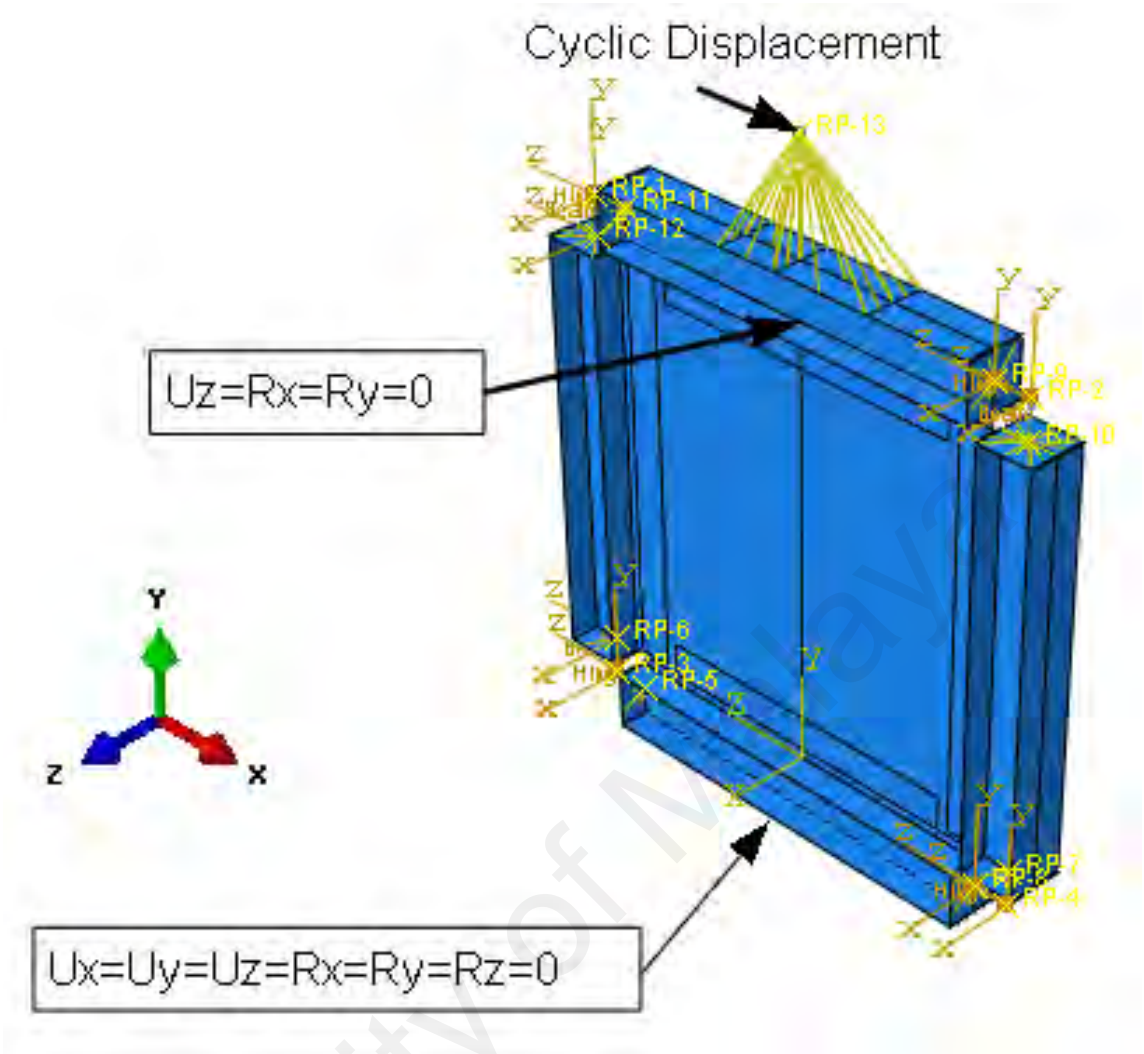

Figure 4-5 Typical boundary condition of FE models

4.3.3.4 Material properties

The material properties obtained from coupon tensile tests are nominal values, namely, engineering stress and engineering strain, which are defined in terms of an initial gauge length and an initial cross-sectional area of the coupon, respectively. FE analysis uses true stress (Cauchy's stress) and logarithmic plastic strain. Hence, stress and strain are measured regardless of the type of analysis. To obtain the true stress (δ_{true}) and logarithmic plastic strain (ε_{ln}^{pl}), the following transformations are applied to the coupon tensile test data:

$$\boldsymbol{\delta_{true} = \delta_{nom}(1 + \varepsilon_{nom})} \quad (4\text{-}5)$$

$$\varepsilon_{ln}^{pl} = ln(1 + \varepsilon_{nom}) - \frac{\delta_{true}}{E} \quad (4\text{-}6)$$

Where E is the modulus of elasticity, δ_{nom} is the nominal (engineering) stress, and ε_{nom} is the nominal (engineering) strain obtained from material tests. To exact simulation of materials of the tested specimens, the slope of linear part of material properties (Figure 3-8) was used.

The material models in ABAQUS/Explicit are based on "incremental" theories in which the mechanical strain increment Δε is decomposed into an elastic portion $\Delta\varepsilon_{el}$ and a plastic portion $\Delta\varepsilon_{pl.}$ An incremental plasticity model is usually formulated in terms of a yield surface, flow rule, and a hardening model. The von Misses yield surface is used in ABAQUS/Explicit to specify the state of multi-axial stress that corresponds to the start of plastic flow. This yield surface assumes that yielding of metals is independent of the hydrostatic stress and has the form of a cylinder, which is centered on the hydrostatic axis in a three-dimensional principal stress space (Simulia, 2010).

The associated flow rule is used to obtain the plastic strain increment. The flow rule states that as the material yields, the inelastic deformation rate (plastic strain increment vector) is normal to the yield surface. Thus, the plastic deformation is volume invariant. This assumption is generally acceptable for most metals.

A hardening rule specifies the evolution of the yield surface during plastic flow. In ABAQUS/Explicit (Simulia, 2010), five types of work hardening models are provided for metals: isotropic, kinematic, Johnston–Cook, user, and combined hardening models. In the isotropic hardening model, the size of the yield surface changes (increases or decreases) uniformly in all directions when plastic straining occurs (Figure 4-6). The isotropic hardening model in ABAQUS/Explicit is nonlinear, and a full range of effective plastic stress versus effective plastic strain can be defined. The Johnston–Cook

hardening model is a particular type of isotropic model where the yield stress is defined as an analytical function of effective plastic strain, strain rate, and

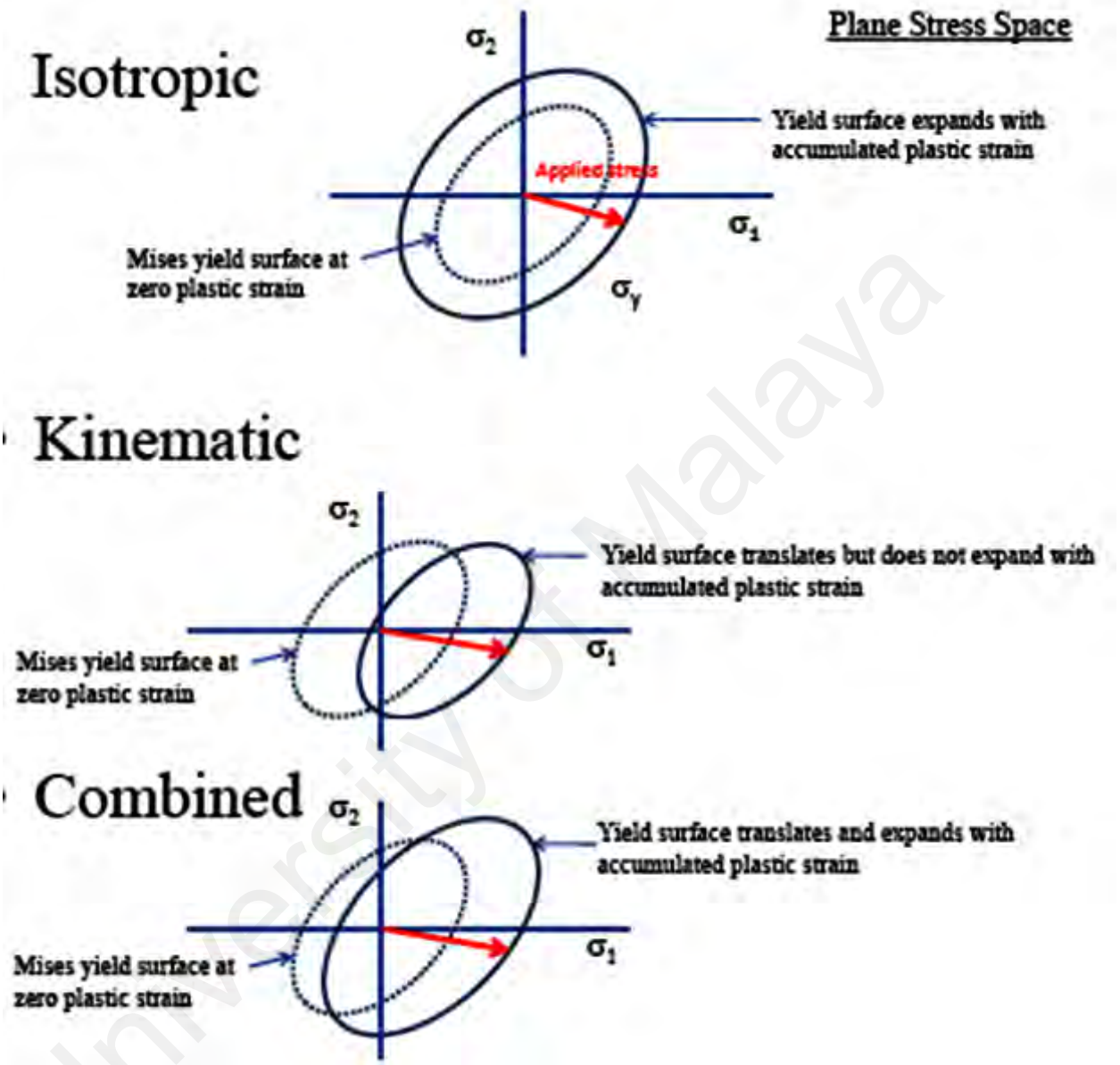

Figure 4-6 ABAQUS metal plasticity

temperature. This hardening rule is suitable for modeling monotonic high-rate deformations of most metals.

The isotropic hardening model is used only for the pushover analysis or the shear wall. However, cyclic loading of the test specimen implies that many strain and stress reversals occur during the process. The Bauschinger effect becomes important and should be considered in the model. The kinematic hardening flow rule is intended to simulate the behavior of metals subjected to

cyclic loading and is typically applied to studies of low cycle fatigue. In this model, the basic concept is that the yield surface translates in stress space without any rotation or changes in size. Specifically, yielding in one direction reduces the yield stress in the opposite direction. Thus, simulating the Bauschinger effect and anisotropy is considered by work hardening (Figures 4-6 and 4-7). In practice, the governing hardening is located between the isotropic and kinematic hardening even when the linear kinematic hardening can consider the Bauschinger effect (Figure 4-8). The nonlinear isotropic/kinematic hardening (combined hardening) model can provide more accurate results in many cases involving cyclic loading. The combined hardening model considers the Bauschinger effect and "cyclic hardening with plastic shakedown" (Figure -9). This phenomenon is a characteristic of symmetric stress-or-strain-controlled experiments. Soft or annealed metals tend to harden toward a stable limit, whereas initially hardened metals tend to soften (Simulia, 2009c).

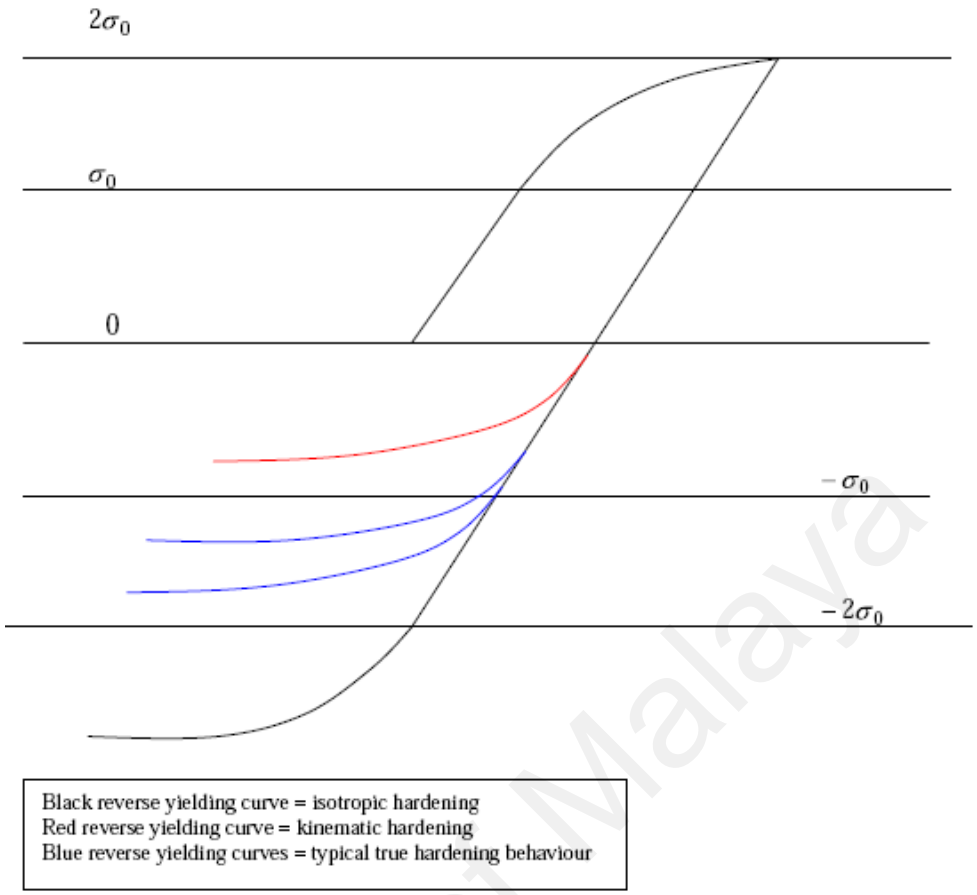

Figure 4-7 Schematic comparison of isotropic, kinematic and typical hardening

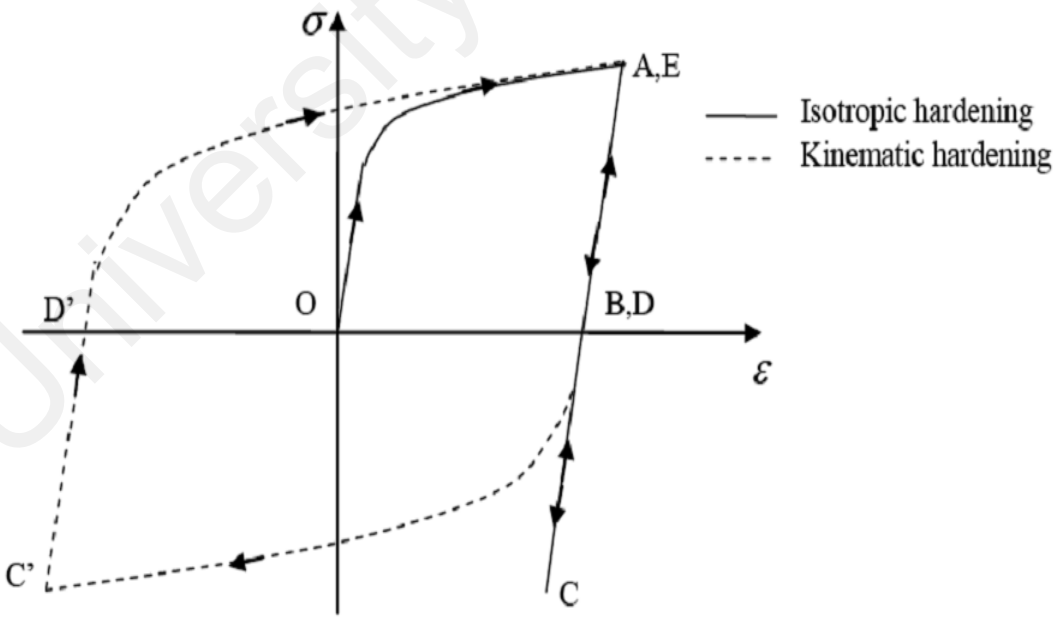

Figure 4-8 The effect of different hardening low on the uni-axial cyclic

4.4 VALIDATION OF FE MODELS

To verify the validation and accuracy of using FE modeling techniques, the results from pushover and quasi-static analyses were compared with each respective experimental outcome from Chapter 3 and the structural characteristic behavior from the theoretical equations. The parameters used to compare between pushover analysis results and experimental and theoretical results included initial stiffness, point of significant yielding, and shear resistance at drift, where peak capacity was obtained from the tests. In the case of quasi-static analysis results, apart from these parameters, additional

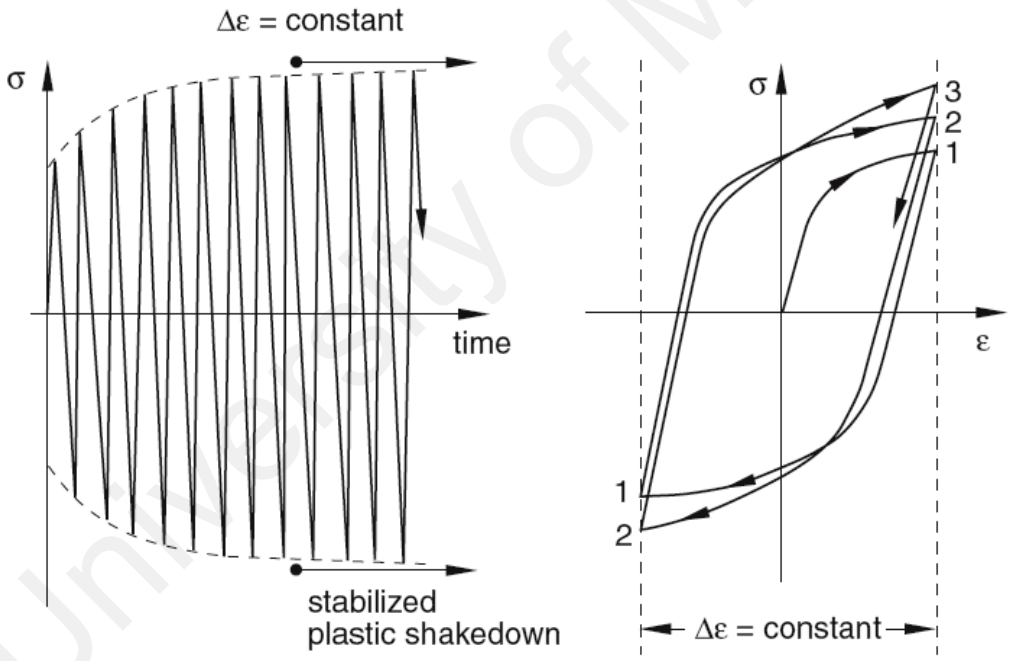

Figure 4-9 Plastic shakedown

comparison was conducted between structural characteristics obtained from quasi-static tests and analysis. The additional characteristics were dissipated energy and pinching and stiffness of hysteresis loops, as well as the deformed shape of models at different stages of cyclic loading.

4.4.1 Energy Histories

Figures 4-10 to 4-14 show the variation in time analysis of the different energies for the whole models during the quasi-static simulation. The external work and internal energy are equal, and the other forms of energy are negligible relative to internal energy. Therefore, the analysis was carried out in a quasi-static condition. The artificial energy was also extremely small compared to the internal energy, indicating that the hourglass mode did not affect the simulation. The kinetic energy during the analysis was negligible, indicating that the loading time was set to the appropriate value, where the inertia forces (from the mass and velocity of the model) were not dominant. The loss of elastic energy of the system during the unloading stages at each loading cycle appeared as waves in the external work and internal energy curves. The pushover analysis of the models was conducted by RIKS technique, which is provided in ABAQUS; the energies of the models may not necessarily be controlled.

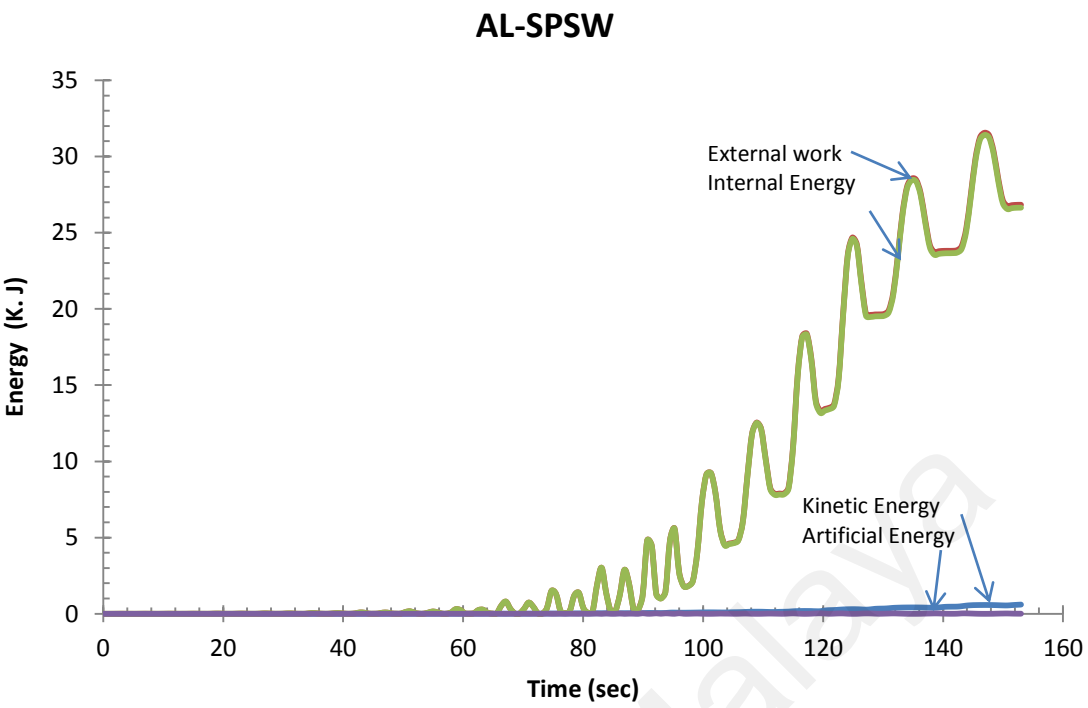

Figure 4-10 History of different energies during cyclic analysis of AL-SPSW

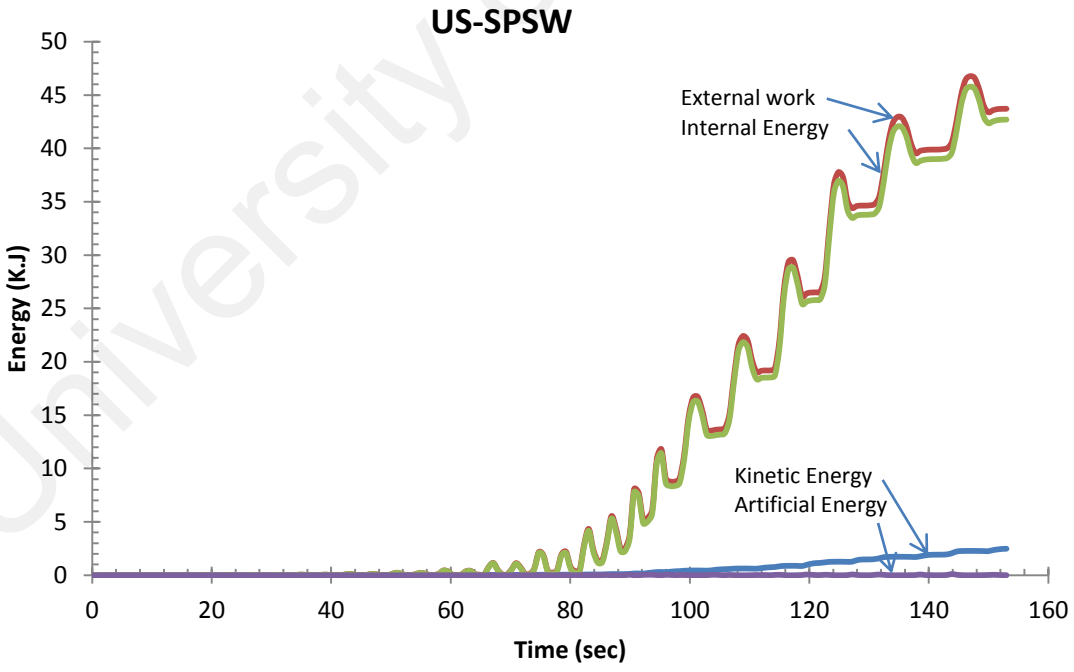

Figure 4-11 History of different energies during cyclic analysis of US-SPSW

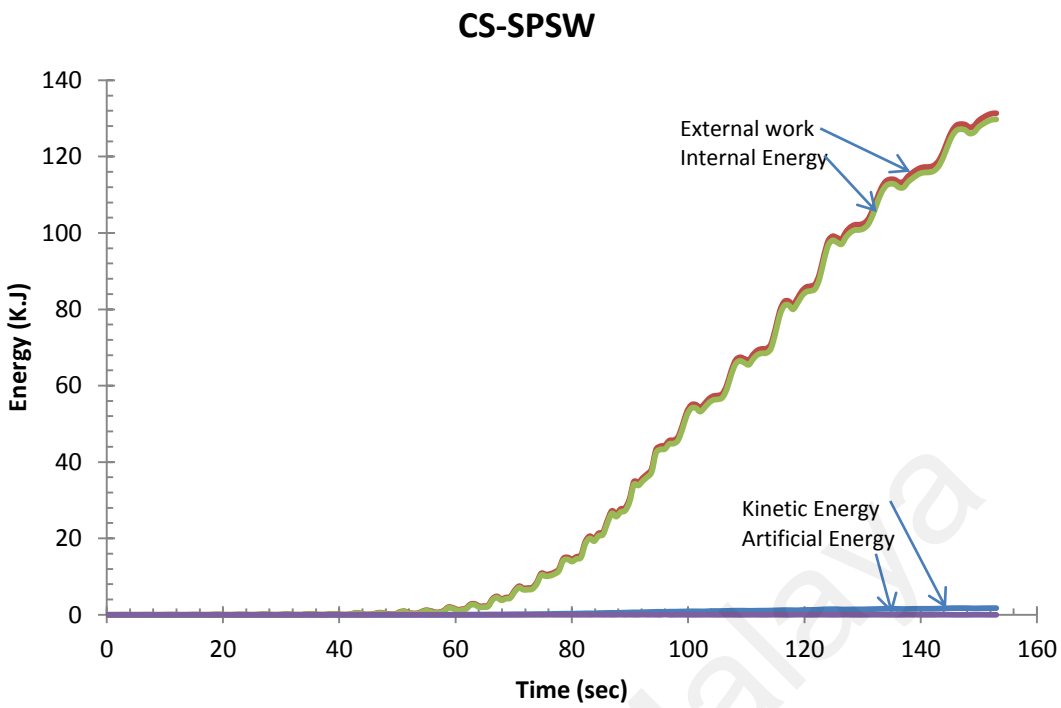

Figure 4-12 History of different energies during cyclic analysis of CS-SPSW

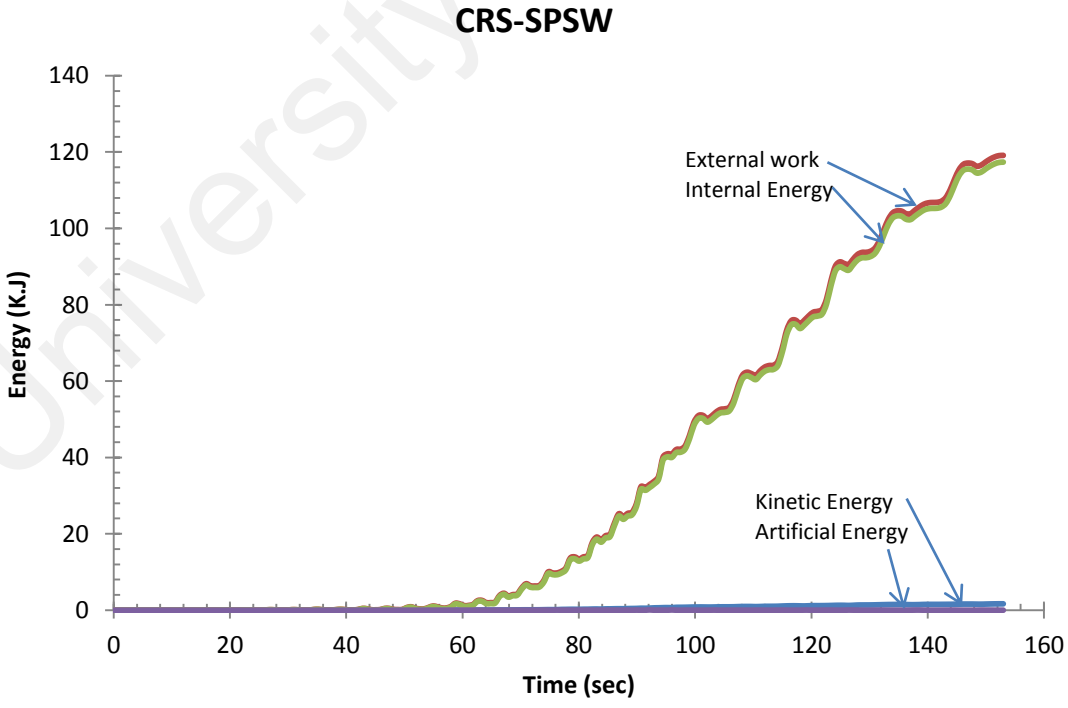

Figure 4-13 History of different energies during cyclic analysis of CRS-SPSW

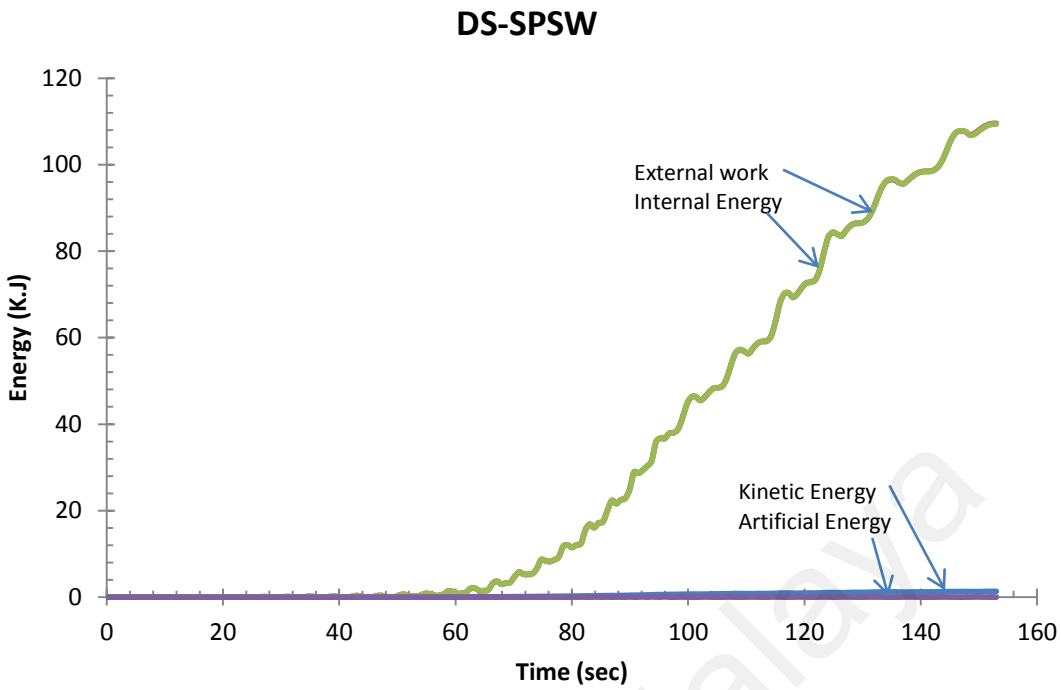

Figure 4-14 History of different energies during cyclic analysis of DS-SPSW

4.4.2 Load-Displacement Curve

Figures 4-15 to 4-19 show that the story shear versus lateral displacement was obtained from pushover analysis and the plate frame interaction (PFI) method, and the load–displacement hysteresis curves were generated from FE analysis and quasi-static test results for all specimens. The response characteristics were used as a basis for comparison and showed that the FE analysis (pushover and quasi-static) and the PFI results were consistent. A discrepancy was observed between the stiffness and the ultimate strength of specimens provided by FE models and the test. The variations between the results for AL-SPSW and US-SPSW (both unstiffened infill plates) are notable. Tearing is one of the most important causes of variation in estimating overall capacity and stiffness. Tearing appeared at the early loading cycles of AL-SPSW and caused the specimen failure. Another possible cause of the slight estimation of the FE results could be the effects of residual stresses that were

neglected in the FE models. The differences in material properties obtained from the tensile test and the actual infill plate properties could be other reasons. The method used to define the material property in FE models was based on the obtained data from the tensile test. For some materials, such as aluminum infill plate, a cyclic tensile test could lead to better results.

The slightly higher predicted stiffness in the models was attributed to the applied loads that were maintained horizontally in the FE model, whereas the loads applied to the test specimens rotated slightly as the test specimen deformed. The resulting vertical component of the load, due to rotation of the hydraulic jacks, reduces the stiffness of the panel.

Despite the pinching captured in FE models, the hysteresis curve obtained from the FE analysis showed less pinching than that observed in the test results. In the thin plate, after reloading in the opposite direction, the stiffness decreased until the tension field started. This behavior appeared as pinched hysteresis curves. Reduction in the stiffness of test results appeared immediately after reloading in the opposite direction. However, such stiffness reduction was delayed in the FE simulation. This behavior could be caused by the eccentricity of infill plate to the boundary frame member due to the presence of fish plates. In the experimental program, the infill plates were connected to the boundary frame by using the fish plates. Therefore, the tension field developed in the infill plates were transferred to the boundary members at an eccentricity equivalent to the average thickness of the fish plate and infill plate. The eccentricity of the force increased the out-of-plane plastic deformation in the infill plate and caused the reduction in stiffness and the increase of pinching in the test results. Eccentricity was not considered in the

FE simulation because of the use of a shell element that all members modeled in their center plane.

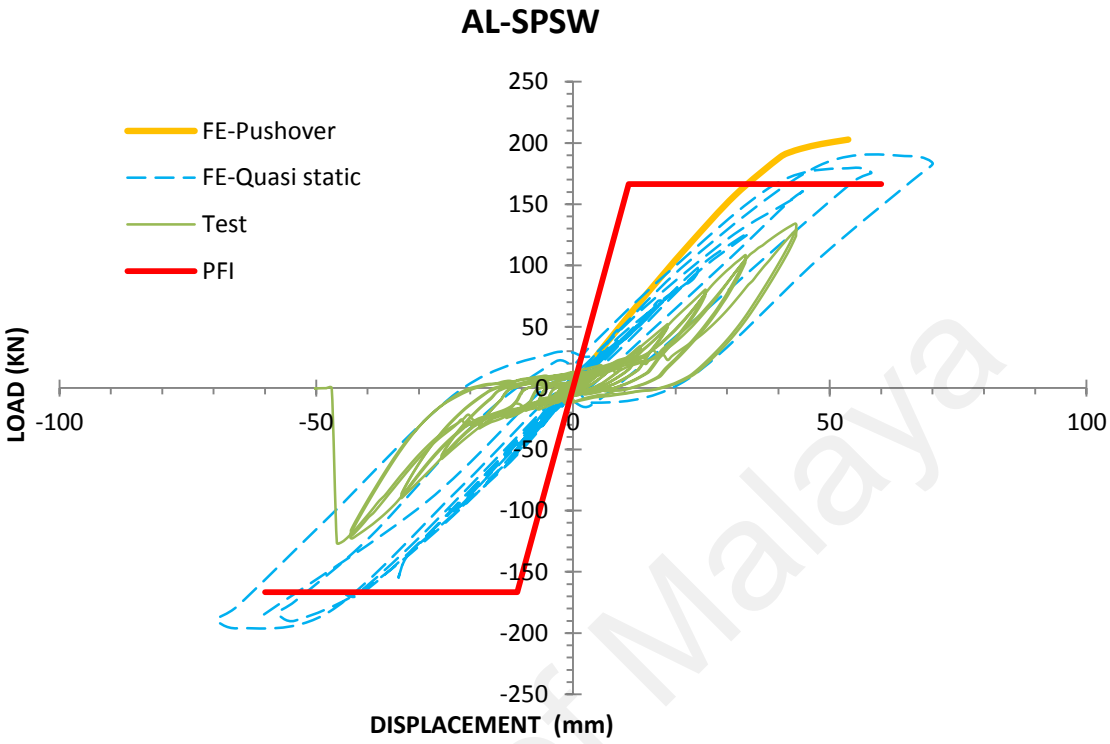

Figure 4-15 Comparison of load-displacement and hysteresis curve of AL-SPSW

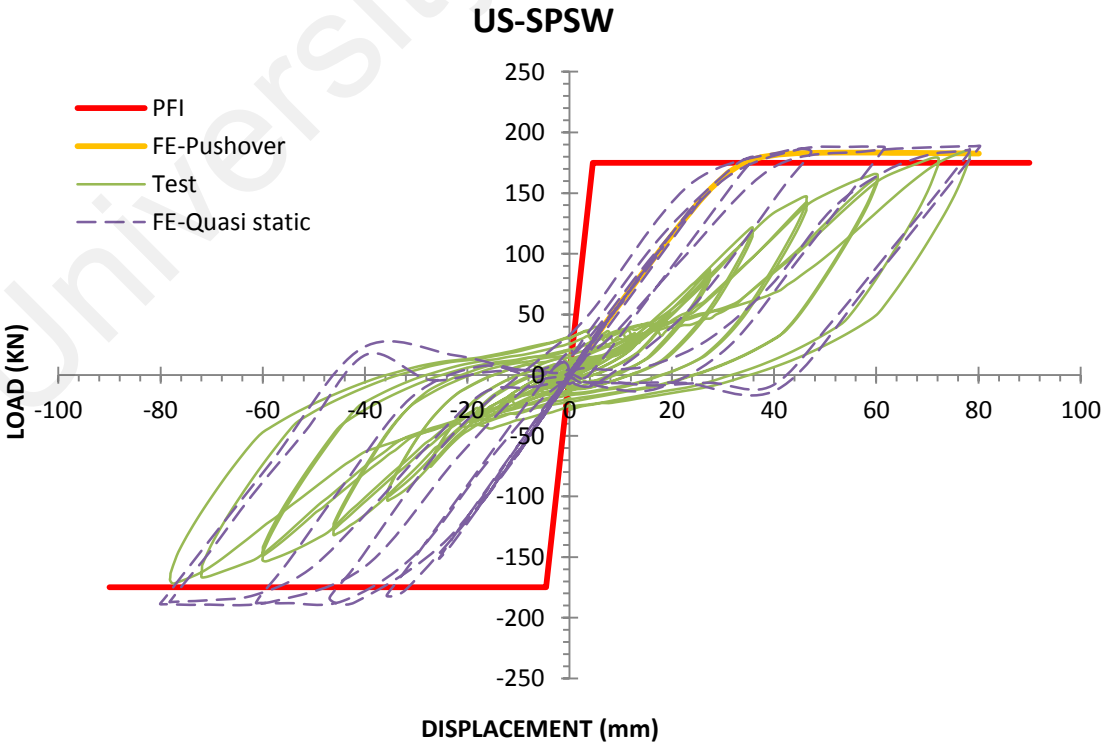

Figure 4-16 Comparison of load-displacement and hysteresis curve of US-SPSW

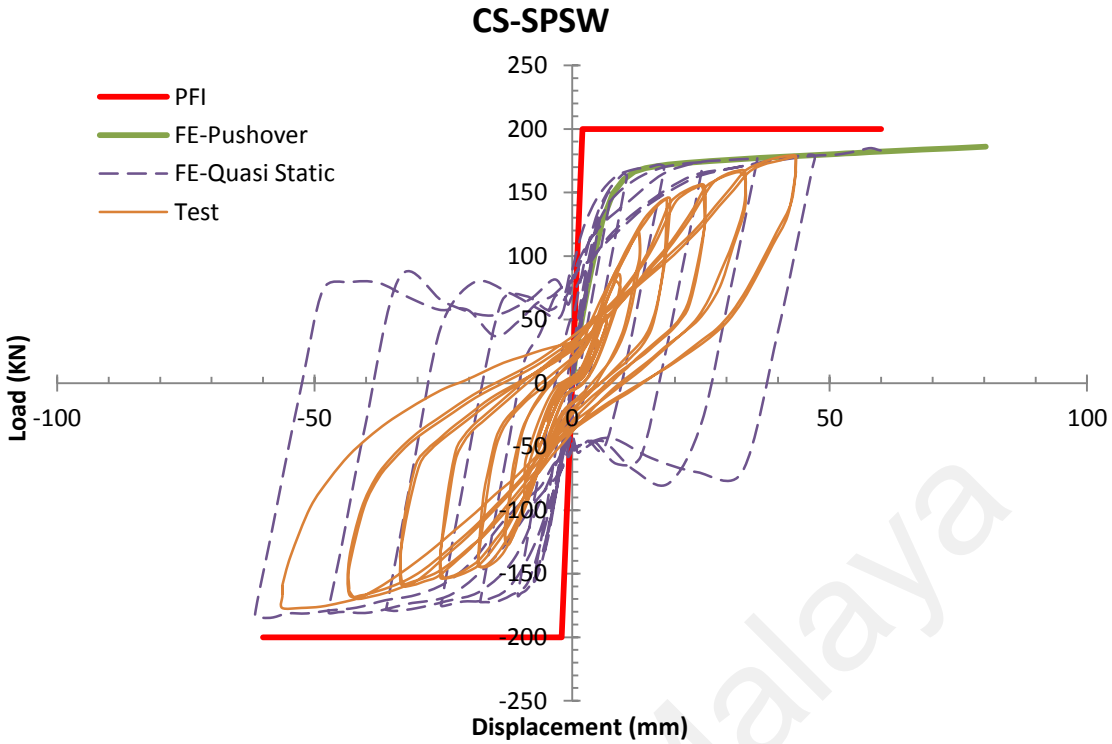

Figure 4-17 Comparison of load-displacement and hysteresis curve of CS-SPSW

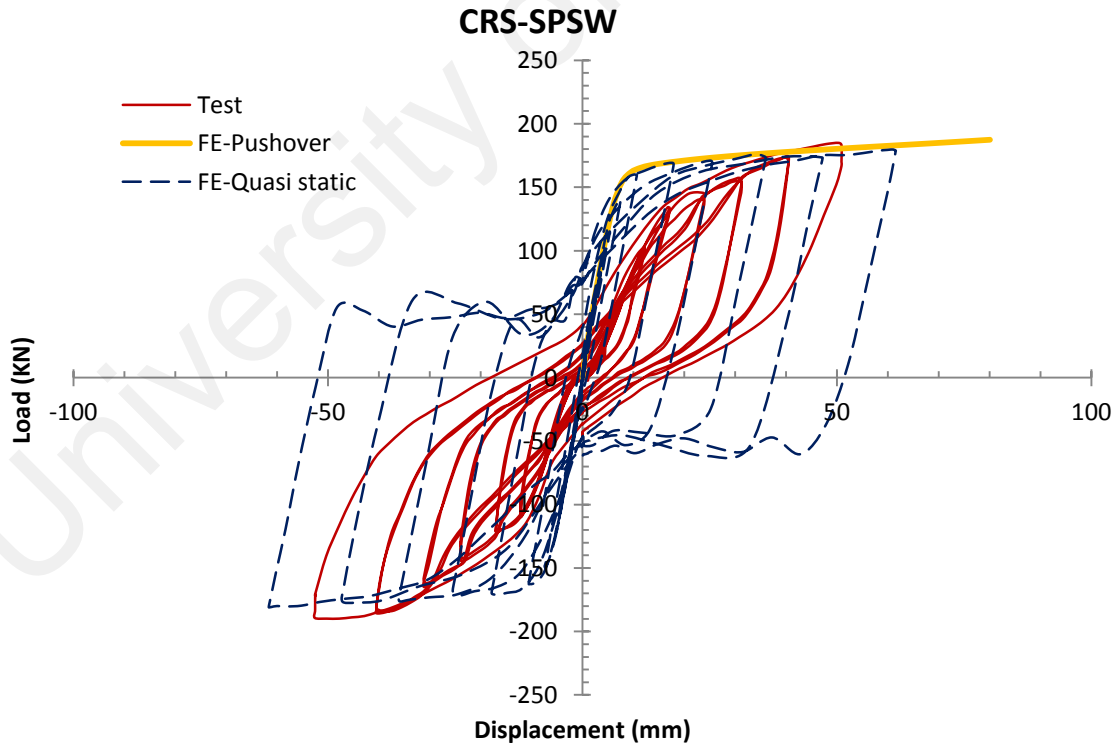

Figure 4-18 Comparison of load-displacement and hysteresis curve of CRS-SPSW

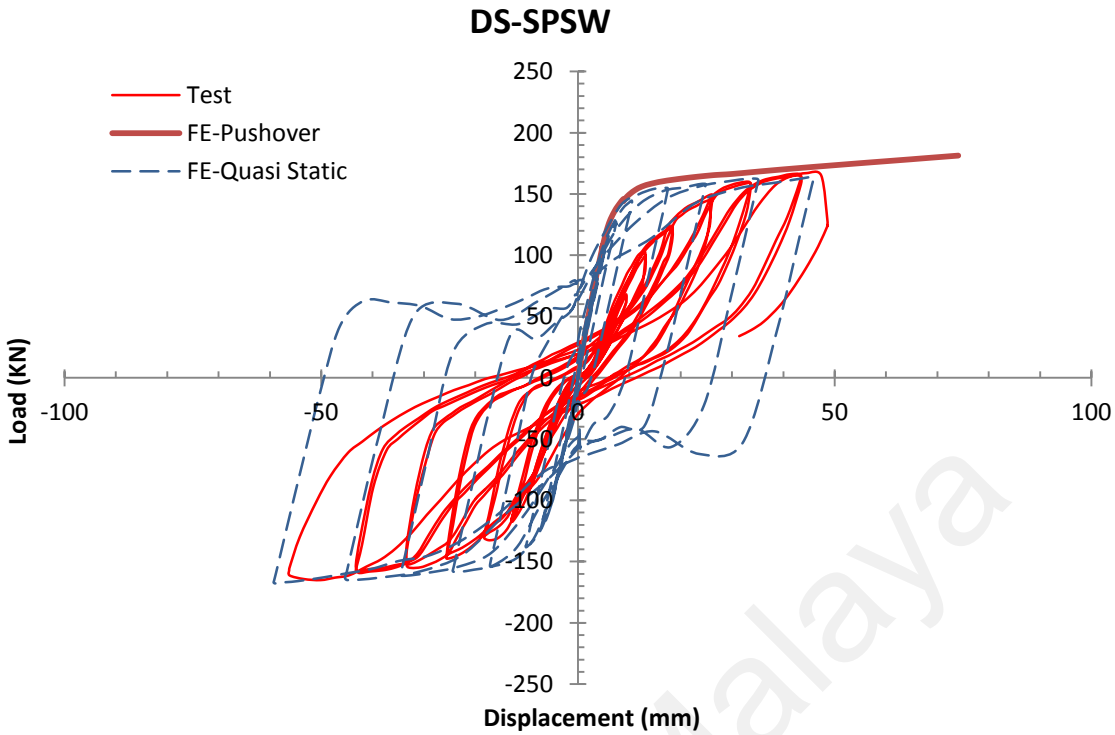

Figure 4-19 Comparison of load-displacement and hysteresis curve of DS-SPSW

4.4.3 Deformed Configuration

The development of a tension field during cyclic loading and redevelopment in the opposite direction was observed during the quasi-static tests. Figures 4-20 to 4-24 depict the behavior that was exactly simulated in the FE models. To evaluate the quality of simulation, the deformed configuration, shape, and number of buckle waves during the cyclic loading were compared, as shown in Figures 4-25 to 4-29. The figures show similarities between FE models and test results.

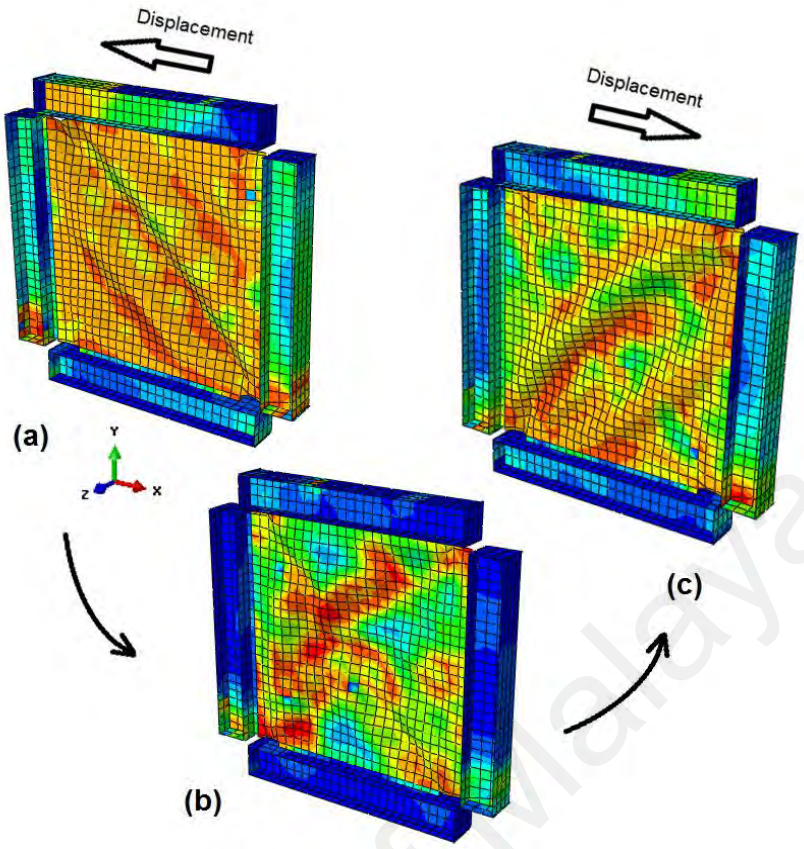

Figure 4-20 Deformed shape of AL-SPSW from quasi-static analysis, a) loading, b)unloading and c)reloading

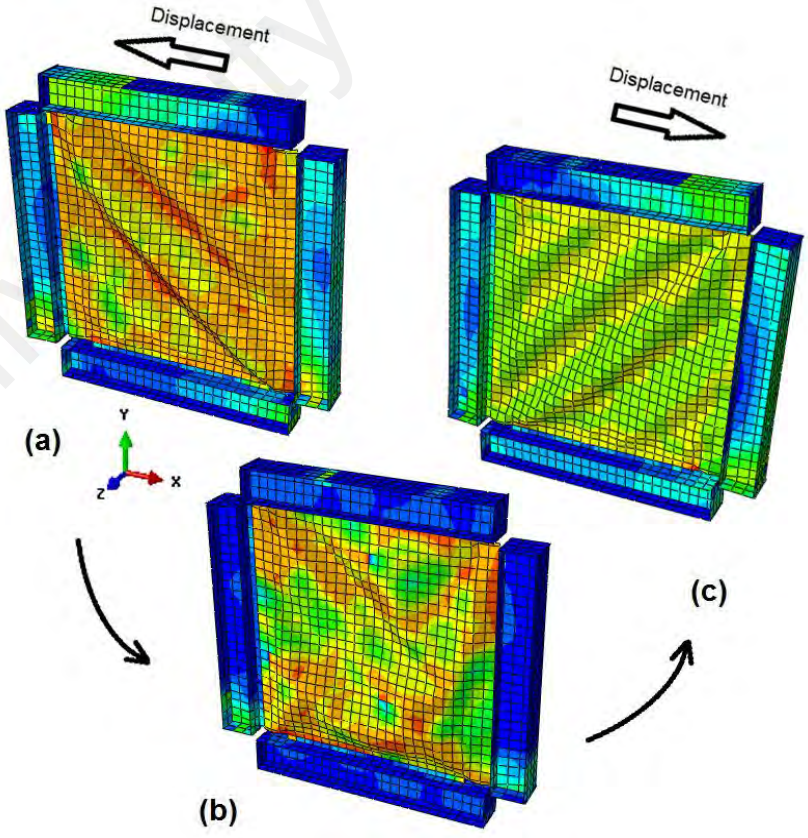

Figure 4-21 Deformed shape of US-SPSW from quasi-static analysis, a) loading, b)unloading and C)reloading

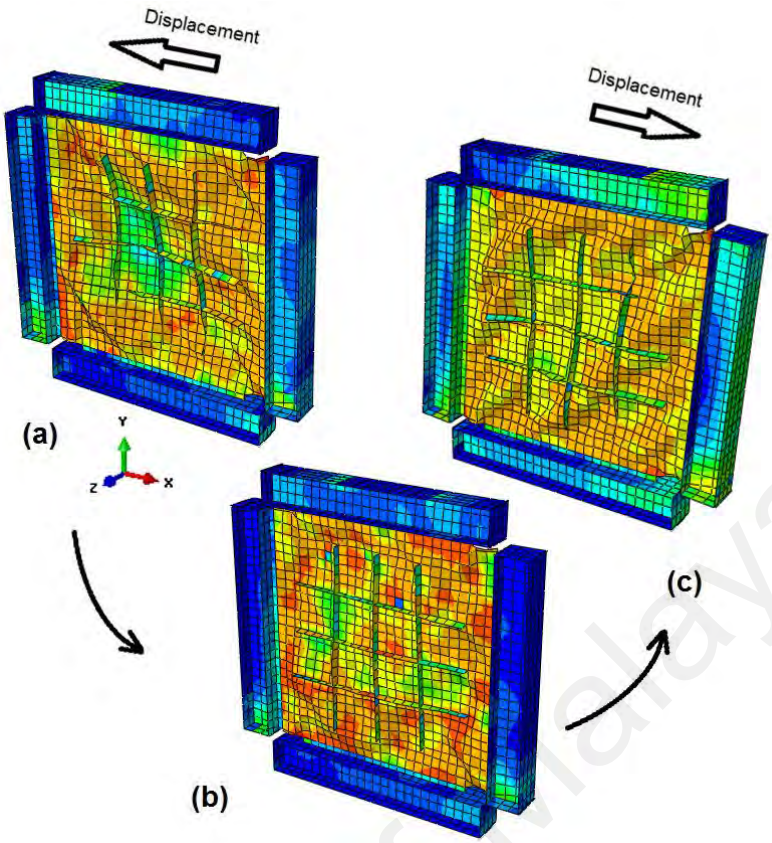

Figure 4-22 Deformed shape of CS-SPSW from quasi-static analysis, a) Loading, b)unloading and c)reloading

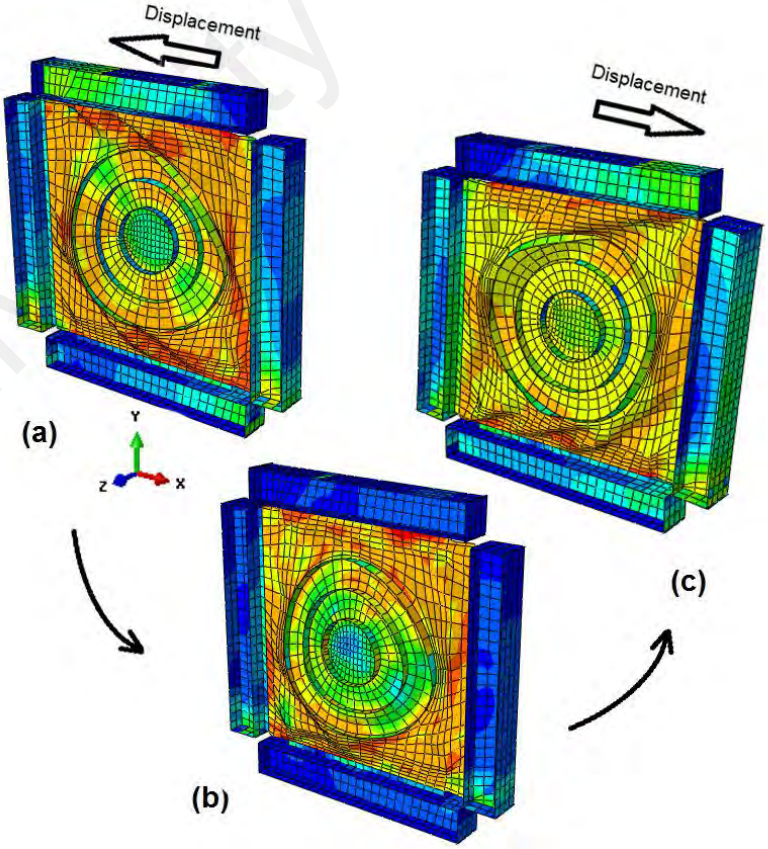

Figure 4-23 Deformed shape of CRS-SPSW from quasi-static analysis, a) loading, b)unloading and c)reloading

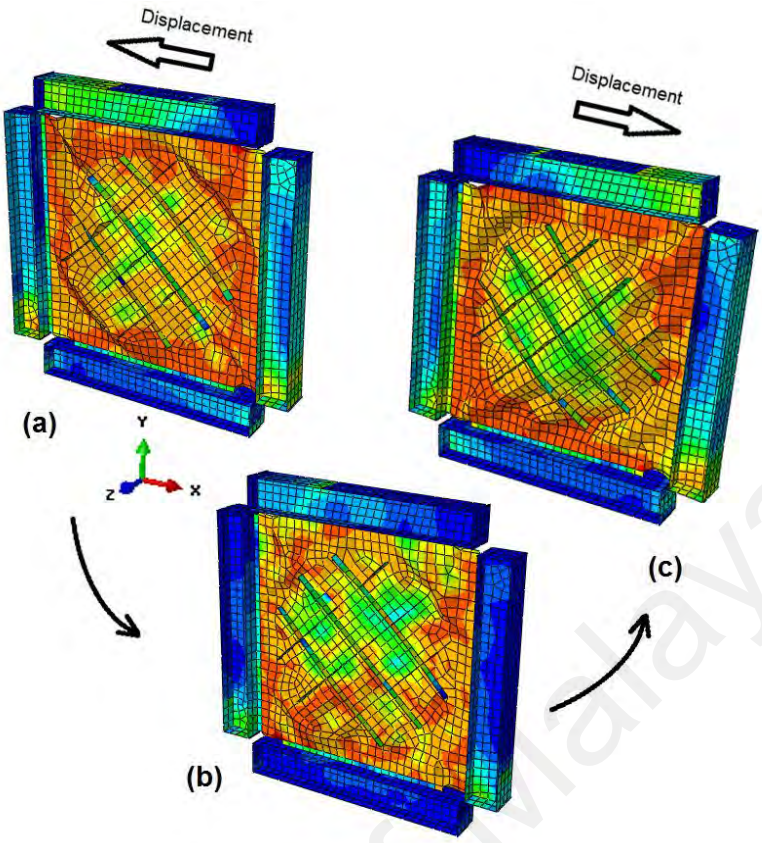

Figure 4-24 Deformed shape of DS-SPSW from quasi-static analysis, a) loading, b)unloading and c)reloading

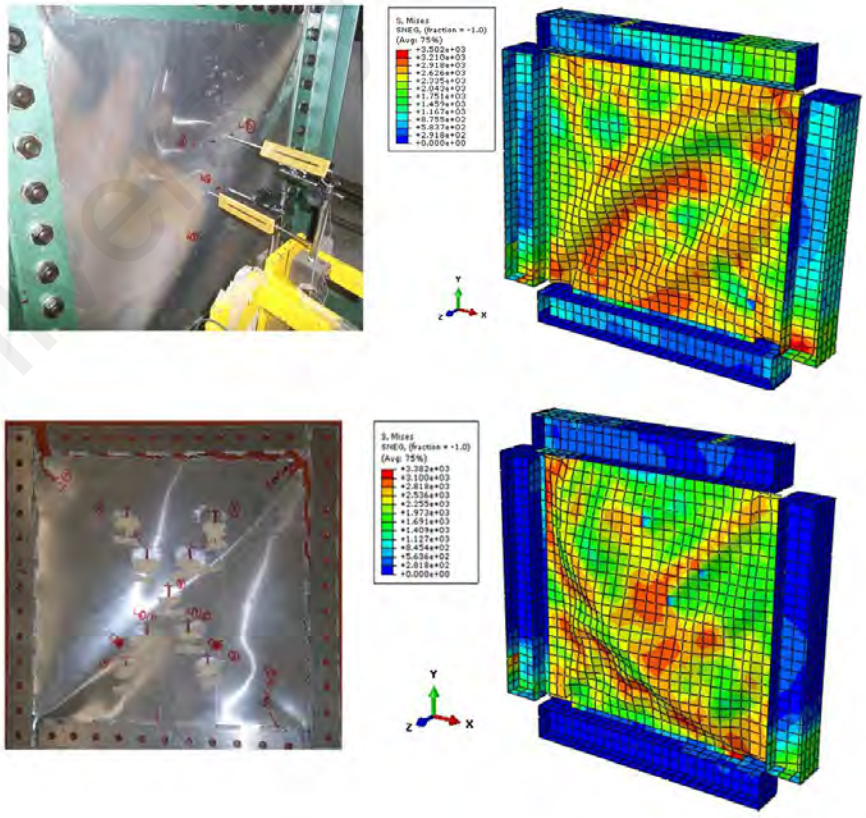

Figure 4-25 Comparison of buckling of test and quasi-static analysis for AL-SPSW, (top) during loading and (bottom) at the end of loading

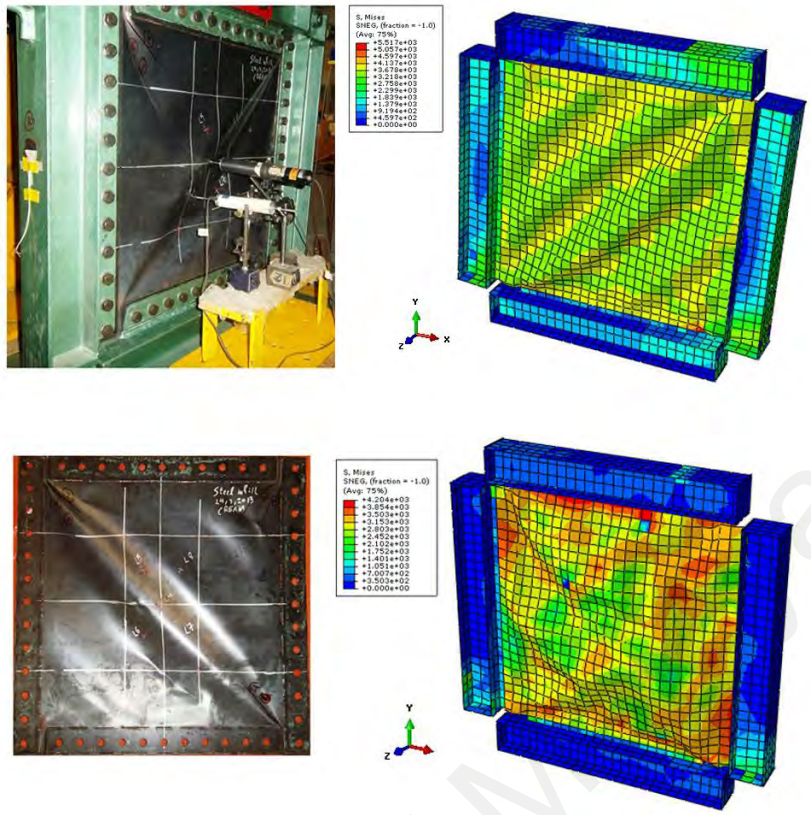

Figure 4-26 Comparison of buckling of test and quasi-static analysis for US-SPSW, (top) during loading and (bottom) at the end of loading

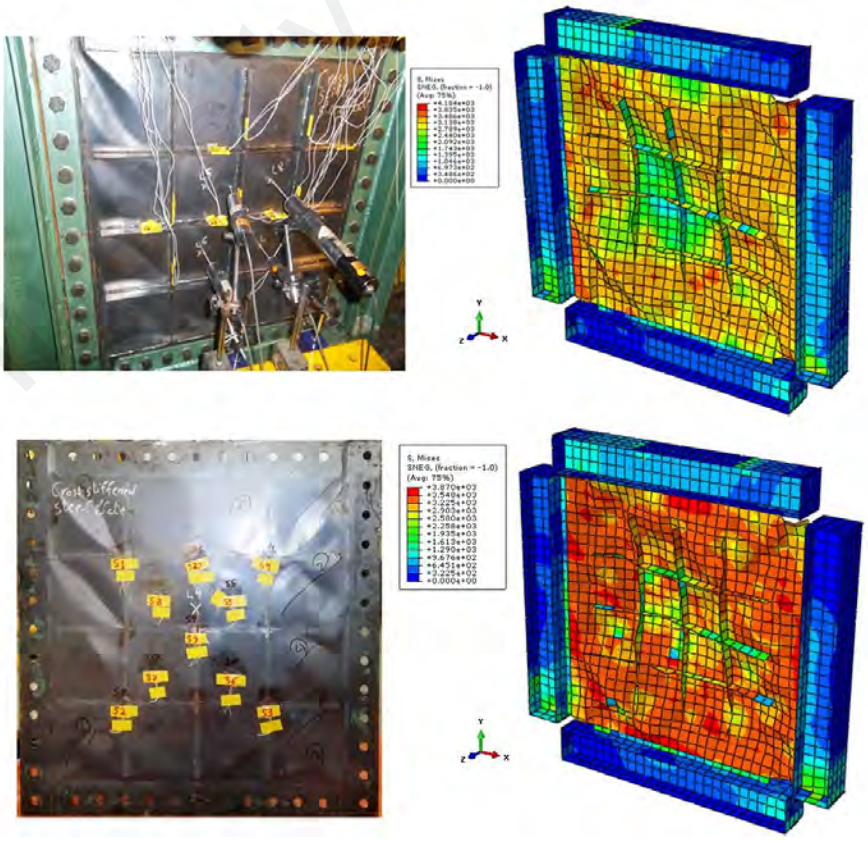

Figure 4-27 Comparison of buckling of test and quasi-static analysis for CS-SPSW, (top) during loading and (bottom) at the end of loading

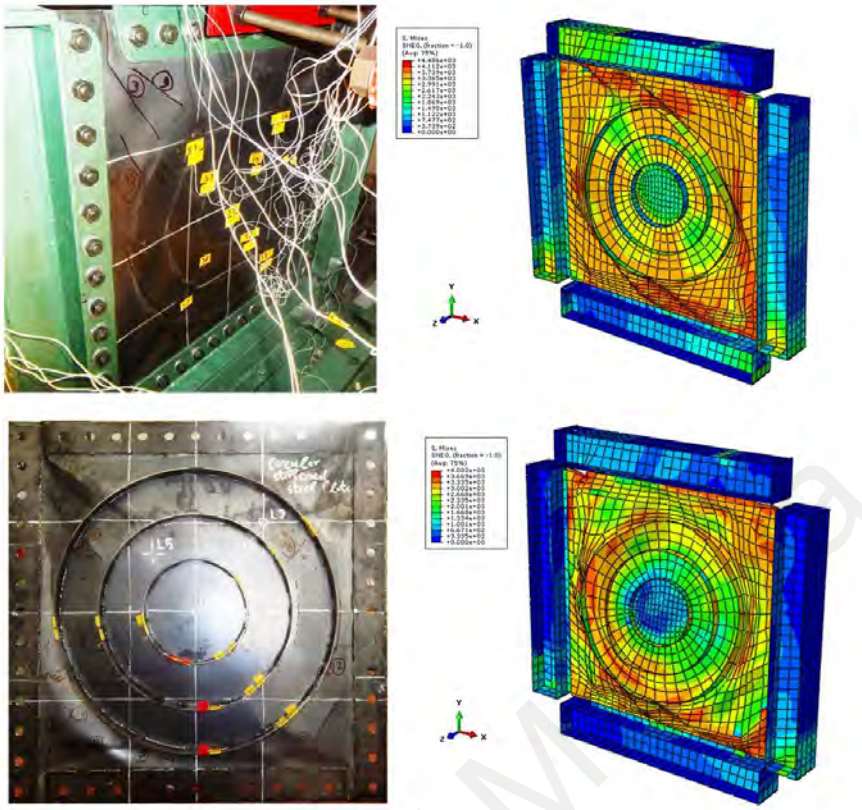

Figure 4-28 Comparison of buckling of test and quasi-static analysis for CS-SPSW, (top) during loading and (bottom) at the end of loading

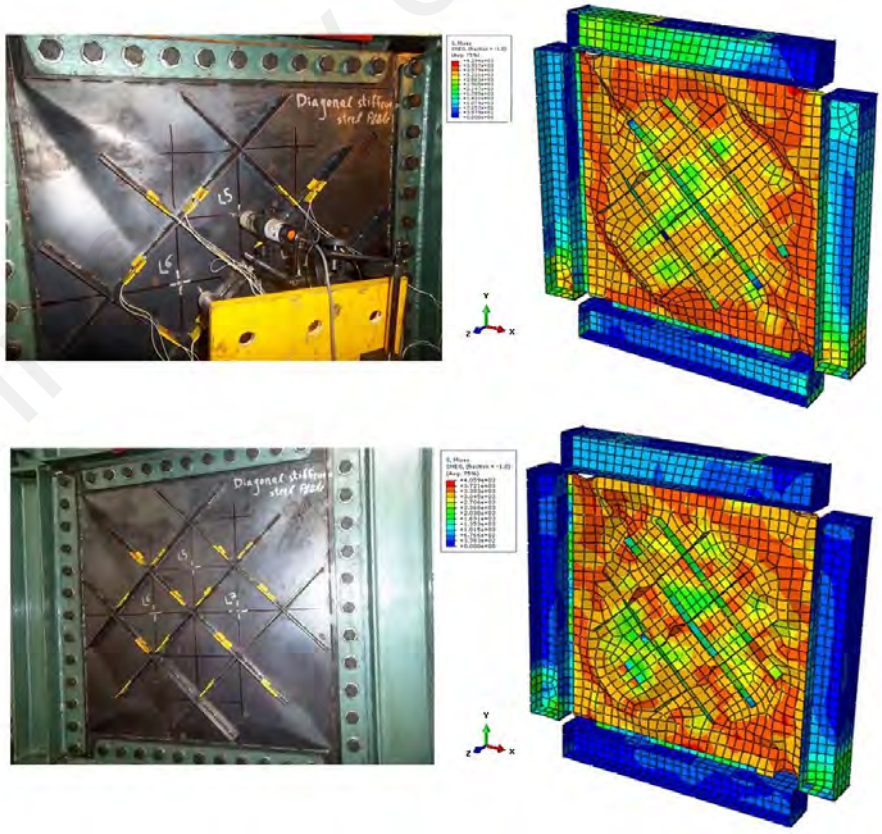

Figure 4-29 Comparison of buckling of test and quasi-static analysis for DS-SPSW, (top) during loading and (bottom) at the end of loading

4.4.4 Energy Dissipation

The amount of energy absorbed during the cycle was obtained by measuring the enclosed area through the hysteresis curve of quasi-static analysis. Figure 4-30 presents the cumulative amount of energy dissipated by FE models as a function of drift levels. The dissipation arrangement of FE models is similar to that observed in the test program. In general, good agreement was observed between the test and the FE analysis. However, the FE model overestimates the dissipated energy in all the panels because the pinching of the hysteresis loops is not simulated accurately.

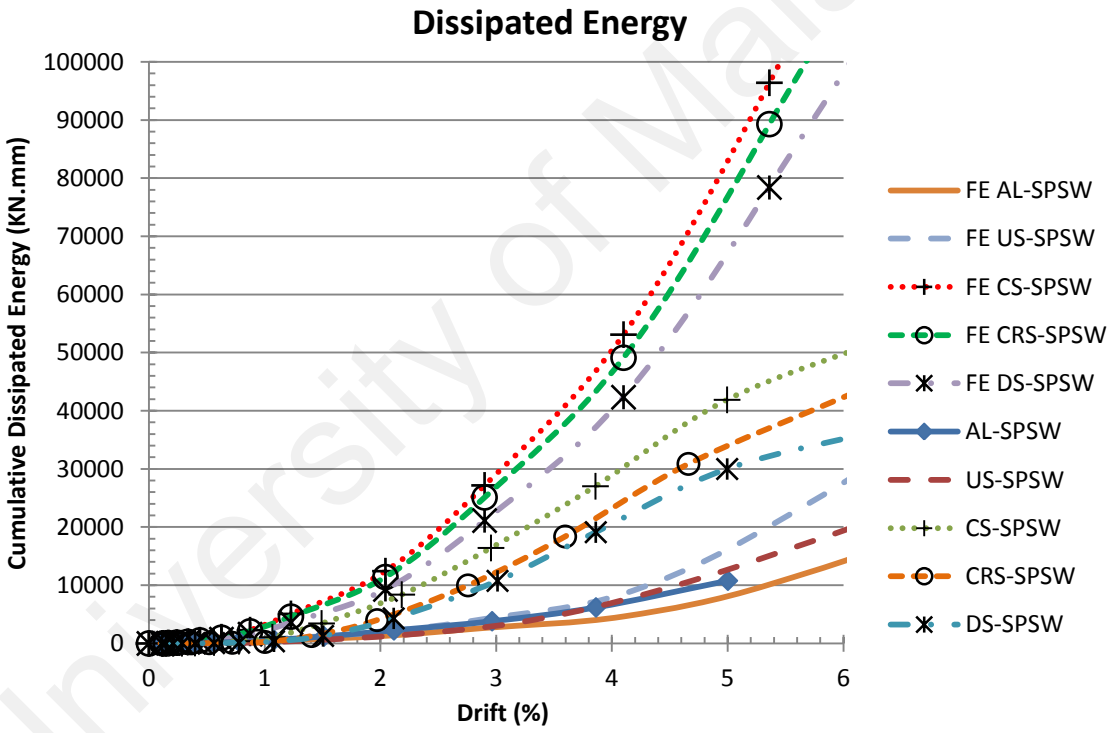

Figure 4-30 Energy Dissipated by FE models and tested specimens

4.5 SUMMARY

A comparison of the predicted behavior of five FE models with test results indicated that the FE method developed throughout this chapter provided a reliable prediction of the strength, stiffness, yielding point, pinching of hysteresis curve, and energy absorption of the SPSWs subjected to cyclic

loading. This validated procedure will be used to conduct the study in Chapter 5.

CHAPTER 5: PARAMETRIC STUDY

5.1 INTRODUCTION

A series of FE models was developed in Chapter 4 to analyze stiffened and unstiffened SPSWs. A comparison of the predicted behavior between the five FE models and the test results indicated that the FE method developed can predict the cyclic and monotonic behavior of SPSWs accurately. The validated procedure will be used to conduct the parametric studies.

The main objective of the present chapter is to examine the cyclic performance of SPSWs with extended geometric properties. The models selected for this investigation include a set of SPSWs with different thicknesses of infill and stiffeners, which are attached on one or both sides of the infill plates. The aspect ratio, overall dimension of boundary frame, stiffener configurations, and other specifications of FE models and their boundary condition are maintained constant. To compare the results of the present research universally, the standard E modules of materials were used through this chapter.

5.2 DESCRIPTION OF SELECTED PARAMETERS

Beyond the various configurations of stiffeners, the sensitivity of cyclic performance to the value of different slenderness of infill plate, thickness of stiffeners, and their position on the SPSWs were investigated. FEMA450 (F.E.M.A, 2003-2006) classified the slenderness of SPSWs using the following equation:

$$\boldsymbol{\lambda} = \frac{\boldsymbol{min(d,b)}}{\boldsymbol{tp}} \leq \mathbf{25}\sqrt{\frac{\boldsymbol{E}}{\boldsymbol{Fy}}} \qquad (5\text{-}1)$$

Where d and b are infill's dimensions, E and F_y are modules of elasticity and yielding stress, respectively. Equation 5-1 shows that the infill plates with a thickness of 1.2, 1.6, and 2.0 millimeters were considered for further investigation. These thicknesses were classified as slender, medium, and thick using a slender classification. In addition, two types of stiffeners on the infill plate were considered, namely, stiffeners attached on one side and on both sides. The thickness of stiffeners attached on one or both sides of the infill plate was designed to ensure that the shear strength of SPSWs was achieved.

All other modeling parameters were identical to the studies presented in Chapter 4. Figure 5-1 shows the overall selected configuration of the models. The shear strength of SPSWs was evaluated using the plate frame interaction (PFI) method. To anchor the stresses associated with tension field action without changing the aspect ratio of the models, only the thickness of the web and the flange of the boundary frame were increased. Table 5-1 summarizes the details of the selected models. The outputs of the FE models are presented in terms of hysteresis and displacement curves, energy dissipation, yield and ultimate strength, elastic stiffness, natural period of vibration, and seismic performance factors (SPF). The findings are discussed in the subsequent sections.

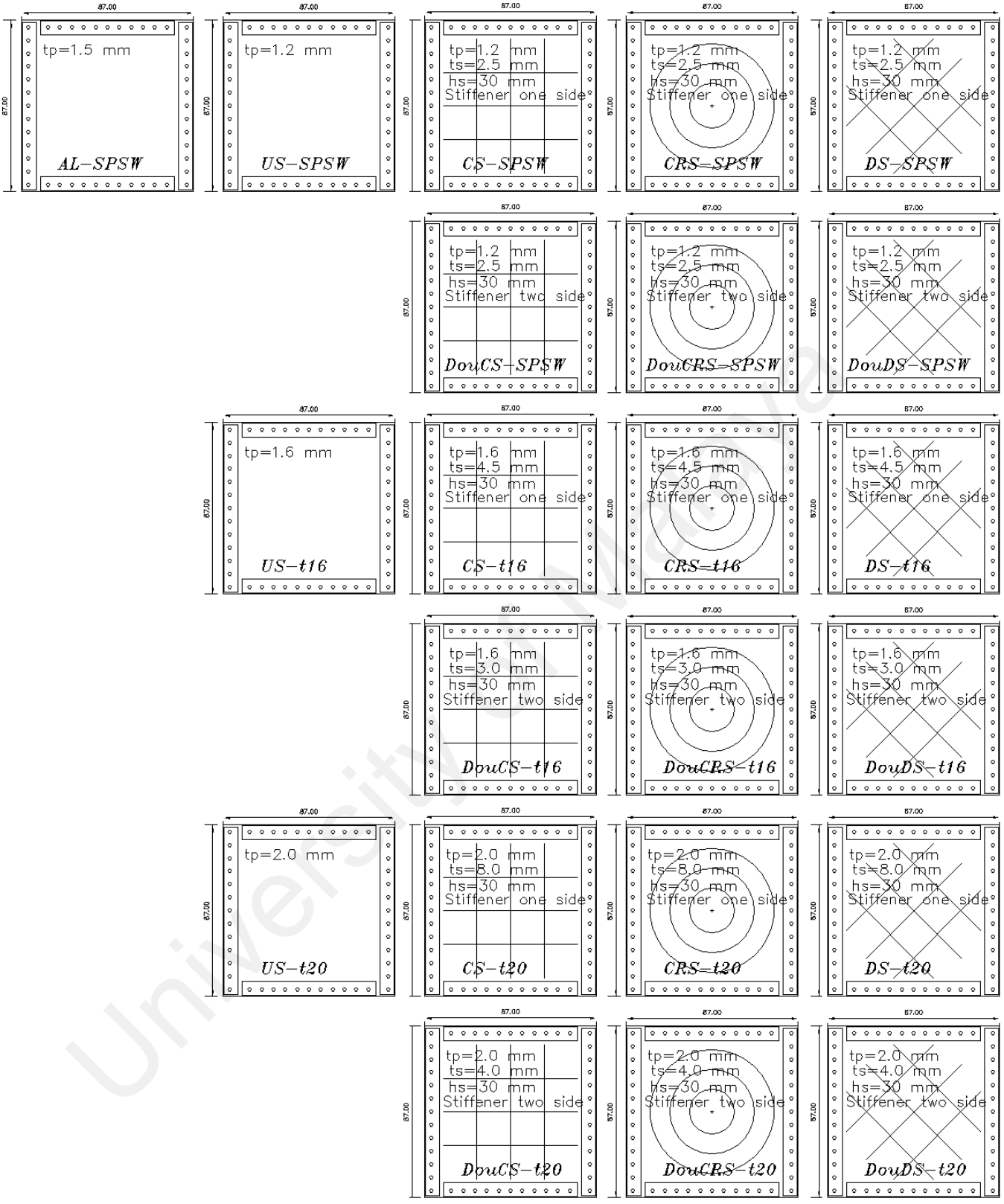

Figure 5-1 General configuration of selected models

Table 5-1 Detail of selected FE models

Model	Thickness of infill plate (mm)	Thickness of stiffeners (mm)	Height of stiffeners (mm)	Position of stiffeners	Sectional area of stiffeners (mm^2)	Expected yield strength by PFI method (KN)	Expected yielding displacement by PFI method (mm)	Expected elastic stiffness by PFI method (KN/mm)
AL-SPSW	1.5	-	-	-	0.0	166.5	10.85	15.3
US-SPSW	1.2	-	-	-	0.0	174.9	4.55	38.4
CS-SPSW	1.2	2.5	30	One Side	10200	200.1	2.0	100.1
CRS-SPSW	1.2	2.5	30	One Side	10131.6	-	-	-
DS-SPSW	1.2	2.5	30	One Side	9616	-	-	-
DouCS-SPSW	1.2	2.5	30	Both Sides	20400	200.1	2.0	100.1
DouCRS-SPSW	1.2	2.5	30	Both Sides	20236.2	-	-	-
DouDS-SPSW	1.2	2.5	30	Both Sides	19232	-	-	-
US-t16	1.6	-	-	-	0.0	225.2	4.5	50
CS-t16	1.6	4.5	30	One Side	18360	256.1	2.0	128.1
CRS-t16	1.6	4.5	30	One Side	18236.9	-	-	-
DS-t16	1.6	4.5	30	One Side	17308.8	-	-	-
DouCS-t16	1.6	3.0	30	Both Sides	24480	256.1	2.0	128.1
DouCRS-t16	1.6	3.0	30	Both Sides	24315.9	-	-	-
DouDS-t16	1.6	3.0	30	Both Sides	23078.4	-	-	-
US-t20	2.0	-	-	-	0.0	283.80	4.5	63
CS-t20	2.0	8.0	30	One Side	32640	320.2	2.0	168.1
CRS-t20	2.0	8.0	30	One Side	32421.2	-	-	-
DS-t20	2.0	8.0	30	One Side	30771.2	-	-	-
DouCS-t20	2.0	4.0	30	Both Sides	32640	320.2	2.0	168.1
DouCRS-t20	2.0	4.0	30	Both Sides	32421.2	-	-	-
DouDS-t20	2.0	4.0	30	Both Sides	30771.2	-	-	-

5.3 HYSTERSIS AND LOAD-DISPLACEMENT CURVES

The pushover and quasi-static analyses for all models were performed. The load–displacement and hysteresis curves of all models are shown in Figures 5-2 to 5-7. For models where the PFI method was applicable, a comparison between PFI results and FE output was conducted.

The pushover and cyclic analyses exhibited similar load–displacement curves, except for unstiffened steel infills. In the case of unstiffened SPSWs, the comparison of the load–displacement curve of pushover and cyclic analyses with the PFI results shows that cyclic analysis overestimated the strength of models. The comparison of the test results presented in Chapter 3 likewise confirmed such overestimation. The strength overestimation rates for

unstiffened infill plates with thicknesses of 1.2, 1.6, and 2.0 millimeters are equal to 9.7%, 11.7%, and 12.6%, respectively. By increasing the thickness of the unstiffened plate, results of the predicted strength by quasi-static analysis slightly increased. Good agreement was observed between the load–displacement curves obtained from the pushover analysis and PFI method.

The load–displacement curves obtained from the envelope of the hysteresis curve of all models are depicted in Figures 5-8 to 5-10. By neglecting the overestimation of the strength of unstiffened models, we see that one-sided diagonal stiffeners did not increase the strength of the SPSW. However, double-sided diagonal stiffeners considerably increased the strength of the SPSW. For all thickness values, this behavior could be seen clearly. This performance is related to the buckling and interaction of a subpanel with the stiffeners. In the one-sided diagonally stiffened specimens (DS-SPSW, DS-t16, and DS-t20) as observed during the test, because of the special rotation of stiffeners, the buckling and yielding of the subpanel could not be formed (Figure 4-28). In the double-sided stiffened models, (DouDS-SPSW, DouDS-t16, and DouDS-t20), the symmetric stiffeners lie along the direction of tension field stresses and act like diagonal braces. As shown in Figure 5-11, which shows the Misses stress distribution, the buckling and stresses are lower in the central subpanels than those in other parts.

Although double-sided circular stiffened models (DouCRS-SPSW, DouCRS-t16, and DouCRS-t20) displayed increases in the strength compared to the one-sided circular stiffened models (CRS-SPSW, CRS-t16, and CRS-t20), such increase is not considerable as observed in the diagonally stiffened models.

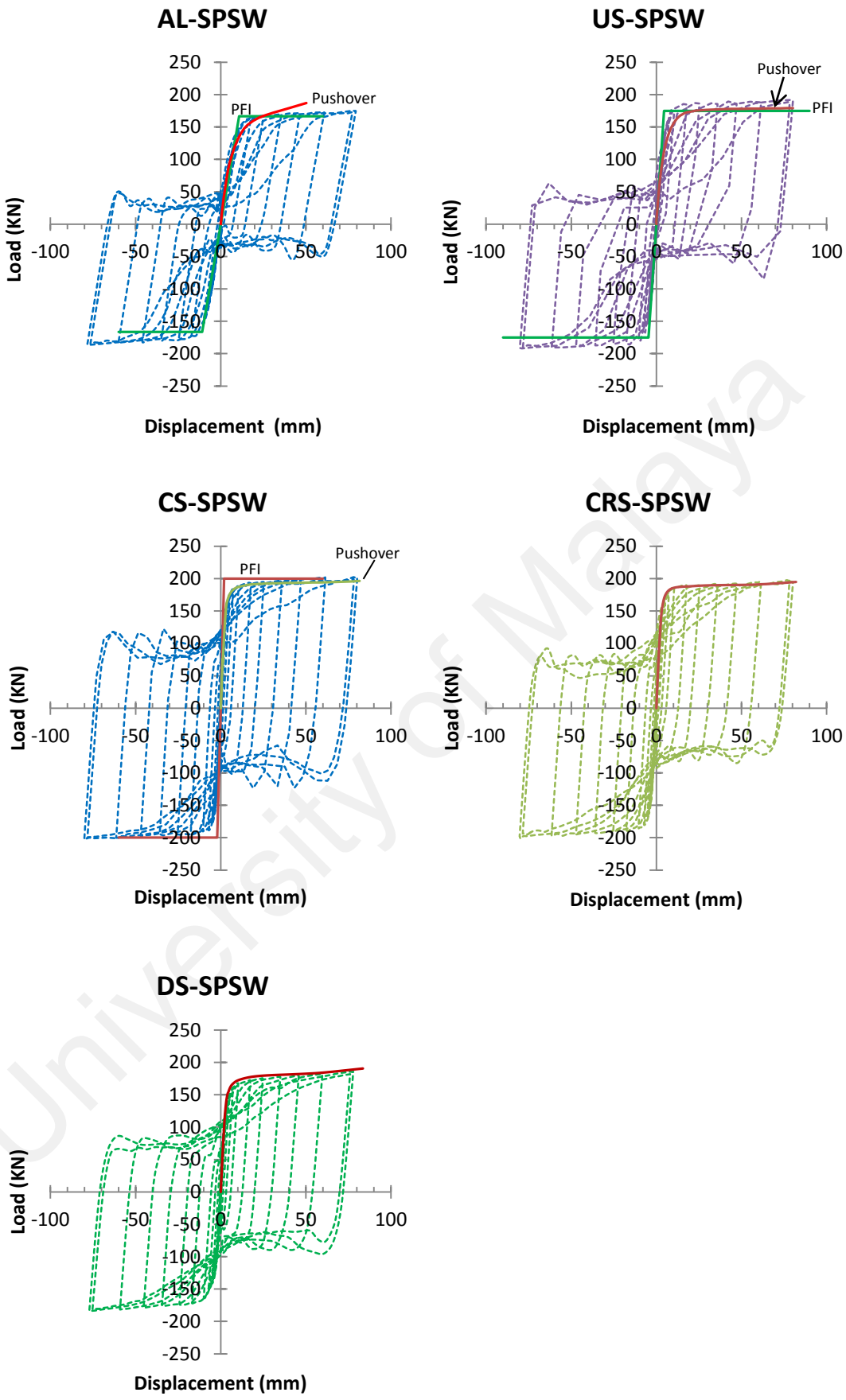

Figure 5-2 Hysteresis (quasi-static analysis) and load-displacement curve (pushover analysis) for Aluminum and for steel infill plate with thickness of 1.2 mm and one side stiffeners

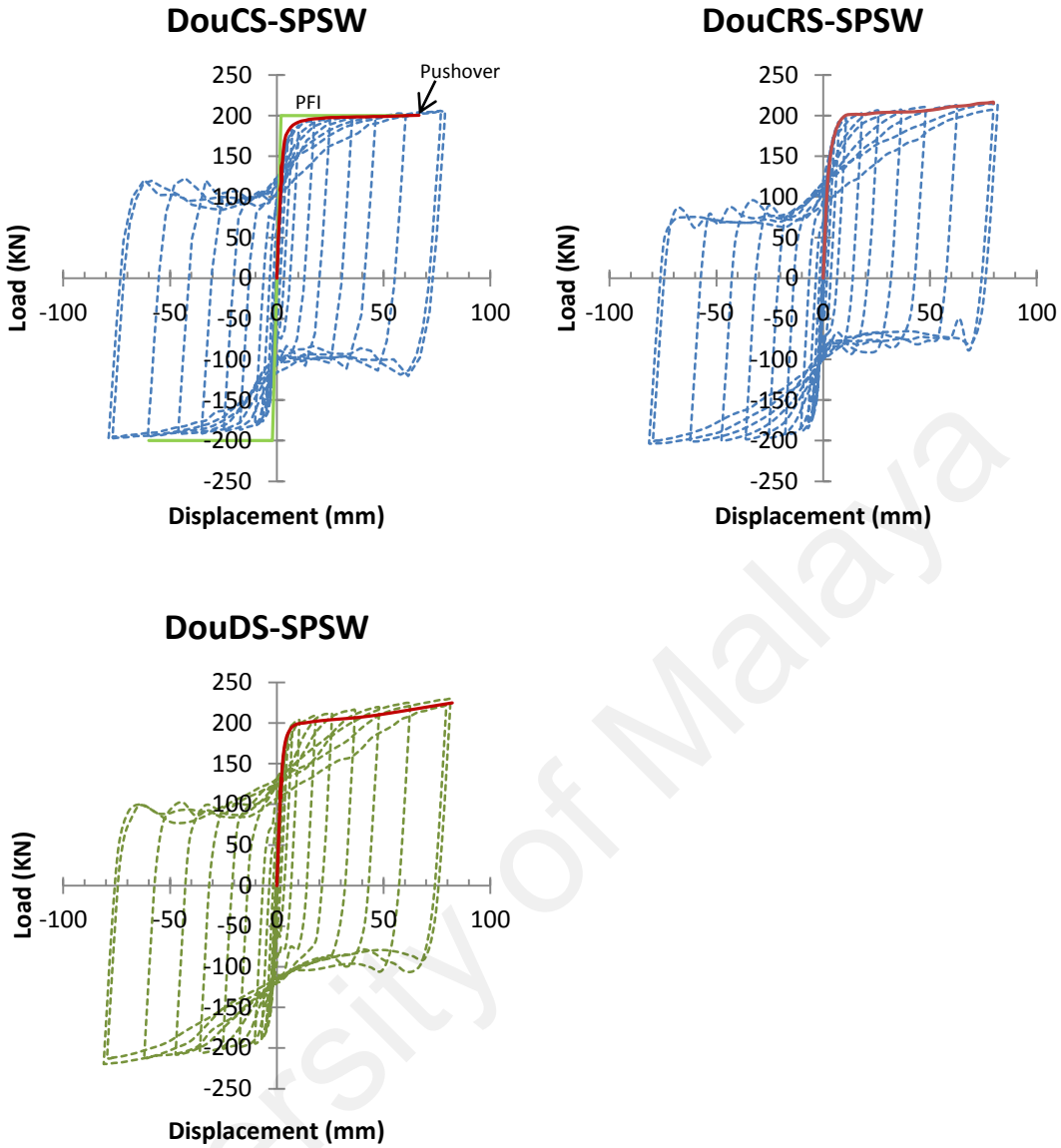

Figure 5-3 Hysteresis (quasi-static analysis) and load-displacement curve (pushover analysis) of steel infill plate with thickness of 1.2 mm and both side stiffener

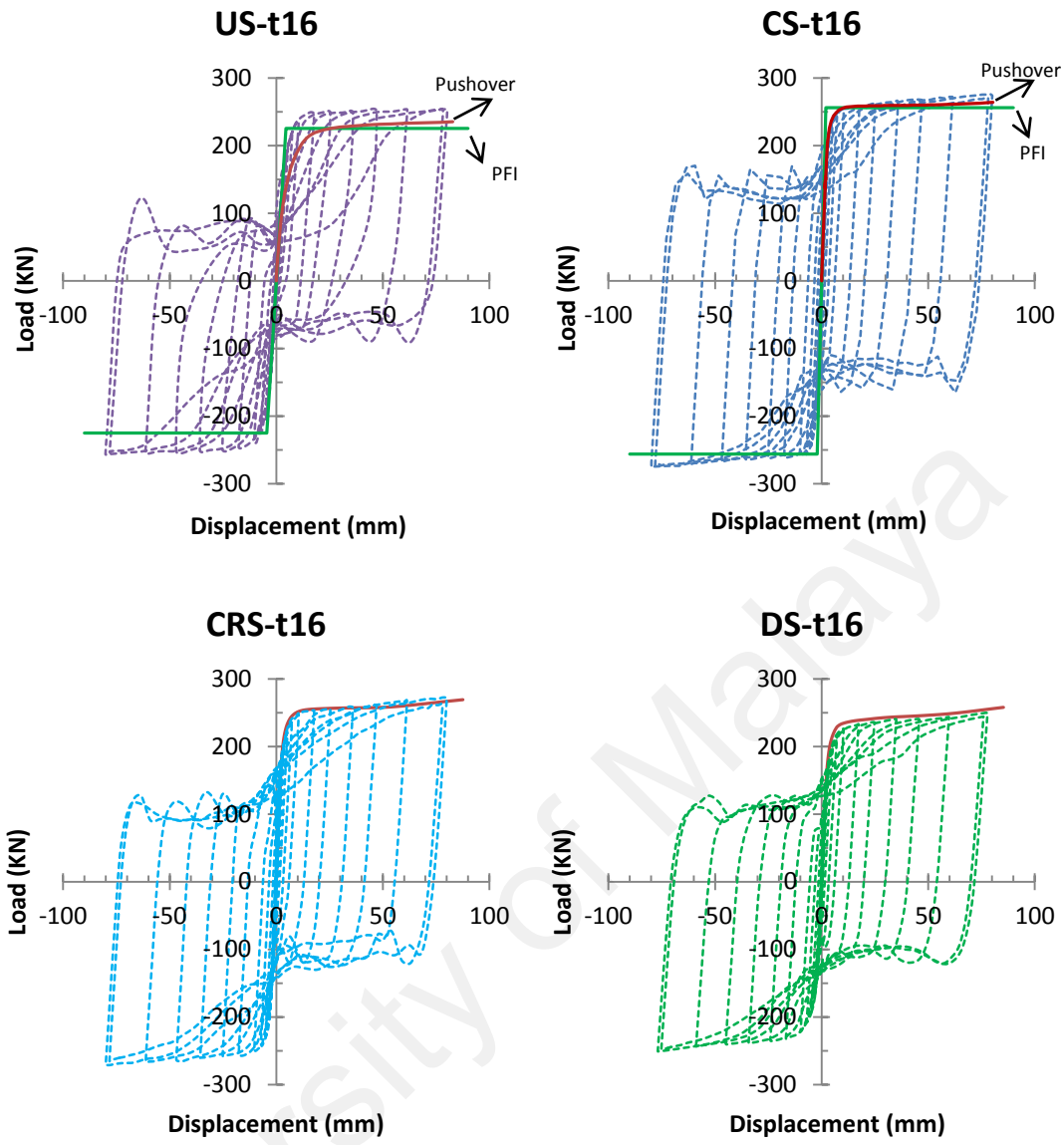

Figure 5-4 Hysteresis (quasi-static analysis) and load-displacement curve (pushover analysis) of steel infill plate with thickness of 1.6 mm and one side stiffener

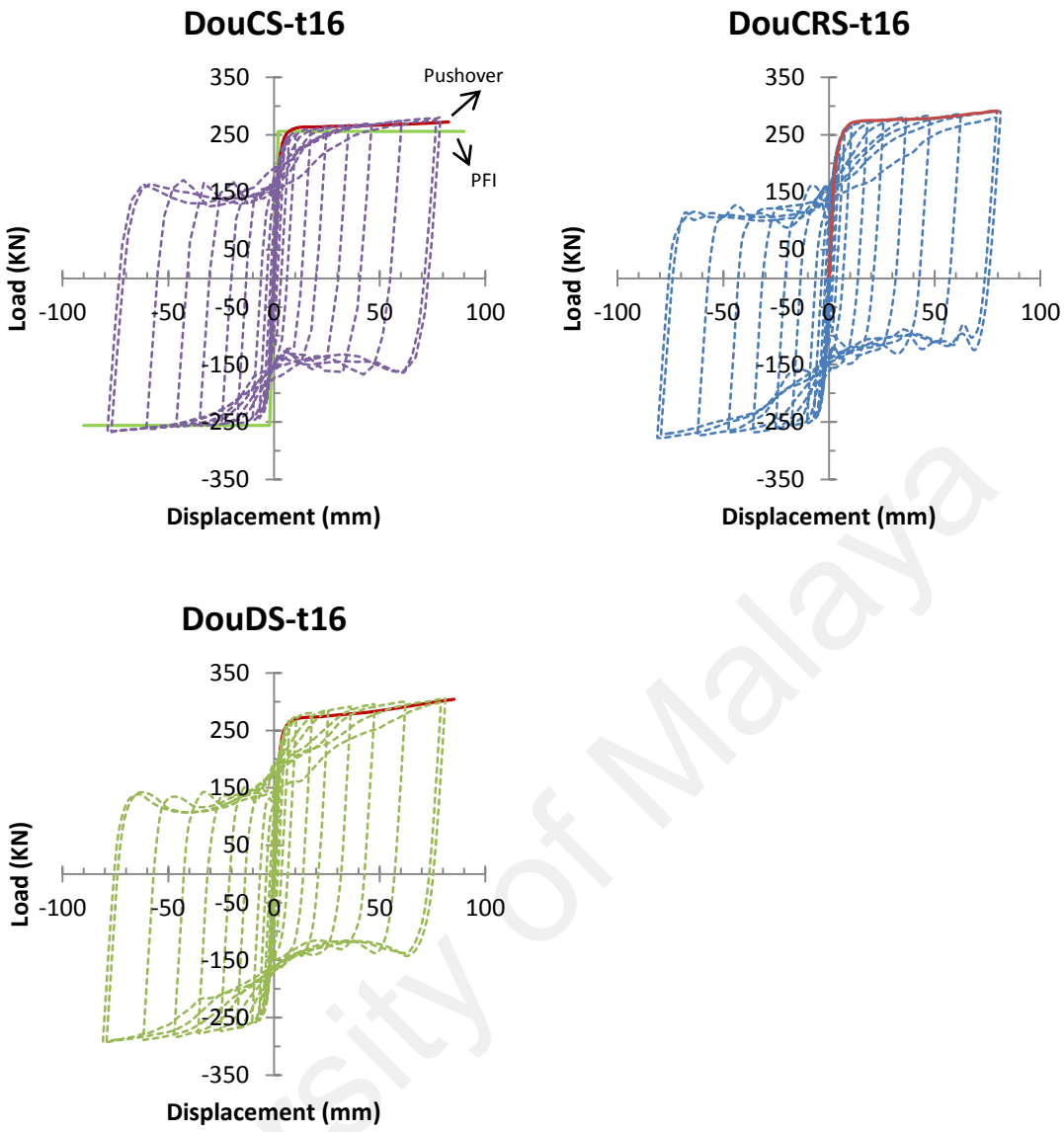

Figure 5-5 Hysteresis (quasi-static analysis) and load-displacement curve (pushover analysis) of steel infill plate with thickness of 1.6 mm and both side stiffener

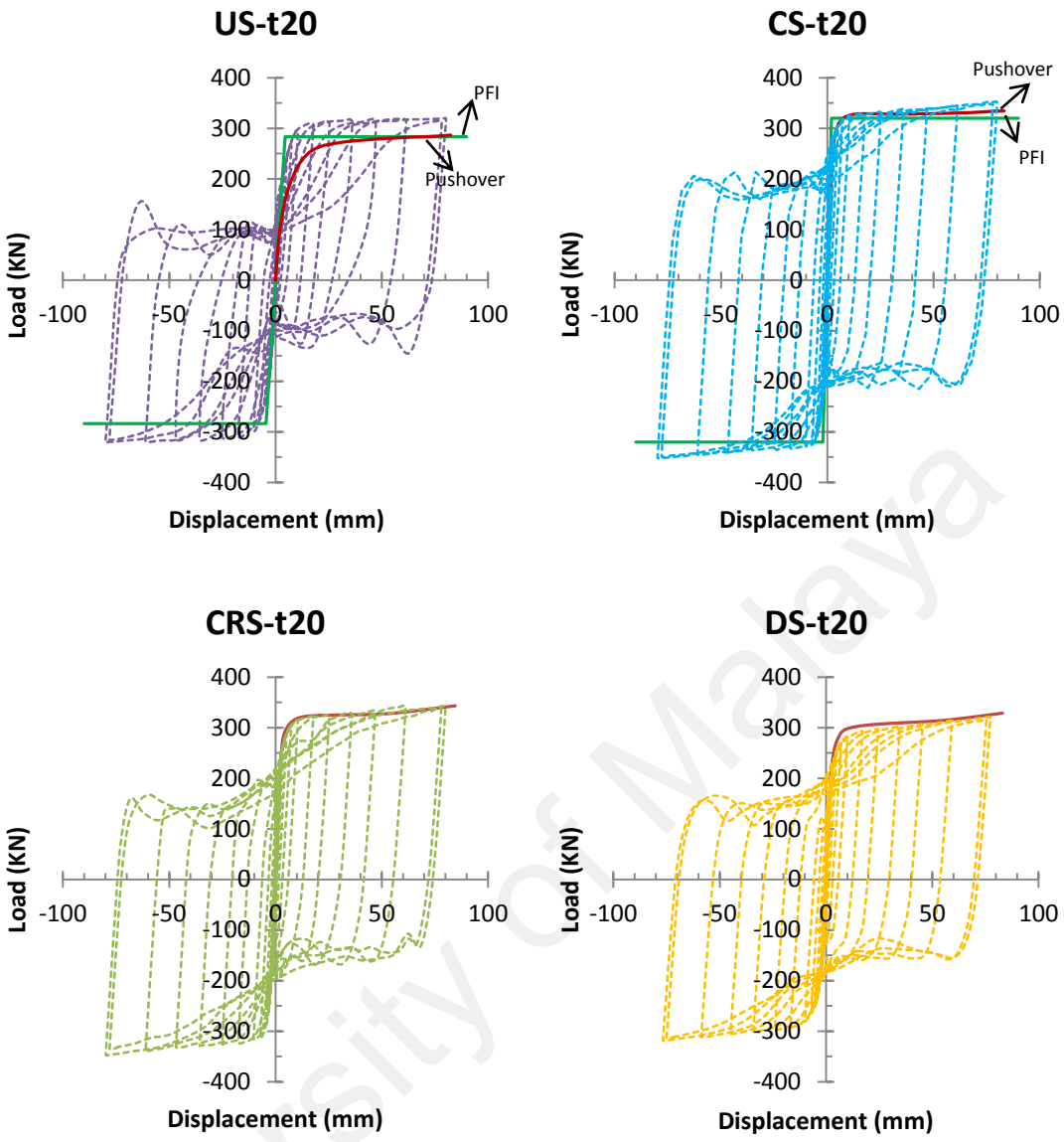

Figure 5-6 Hysteresis (quasi-static analysis) and load-displacement curve (pushover analysis) of steel infill plate with thickness of 2.0 mm and one side stiffener

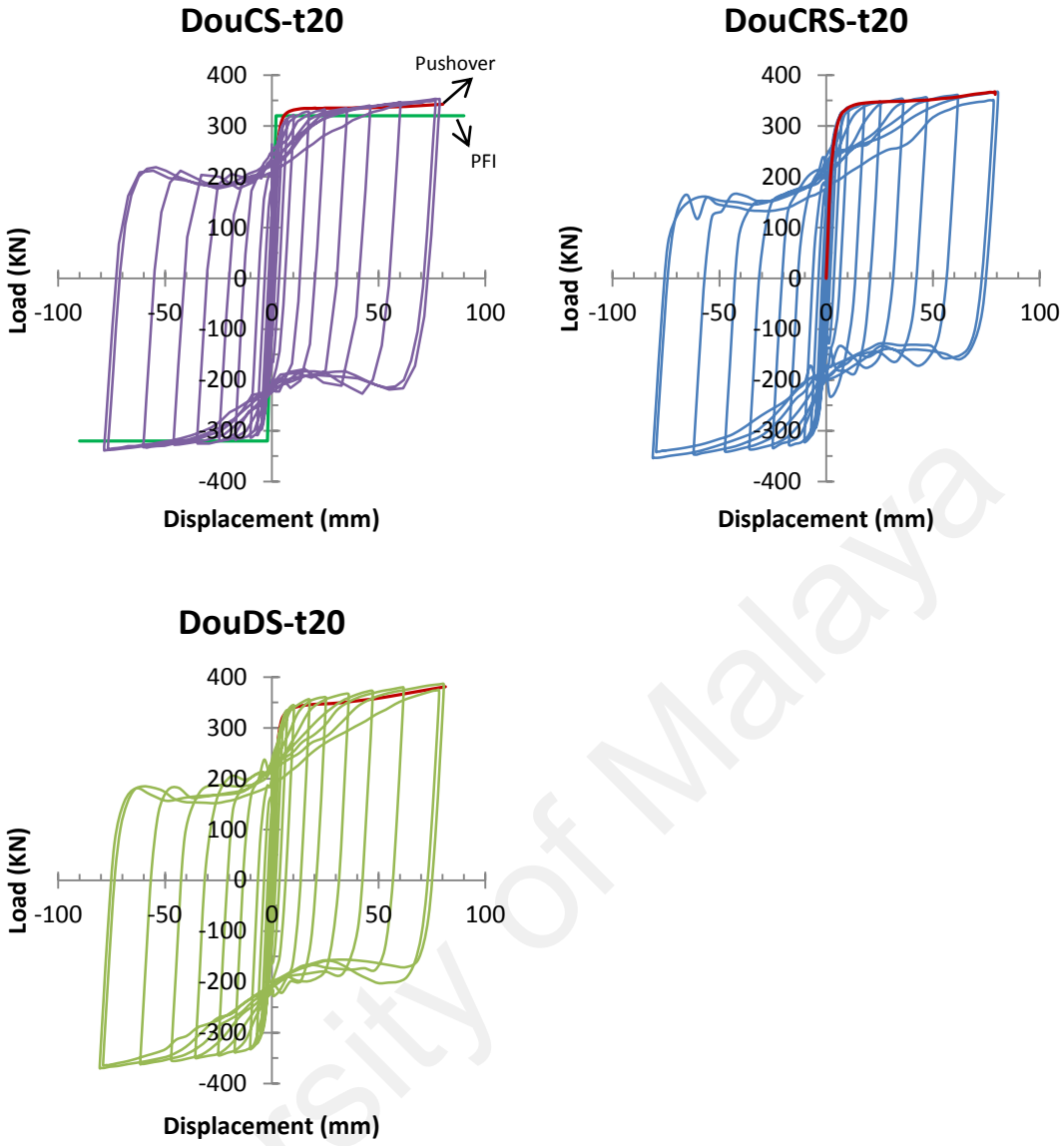

Figure 5-7 Hysteresis (quasi-static analysis) and load-displacement curve (pushover analysis) of steel infill plate with thickness of 2.0 mm and both side stiffener

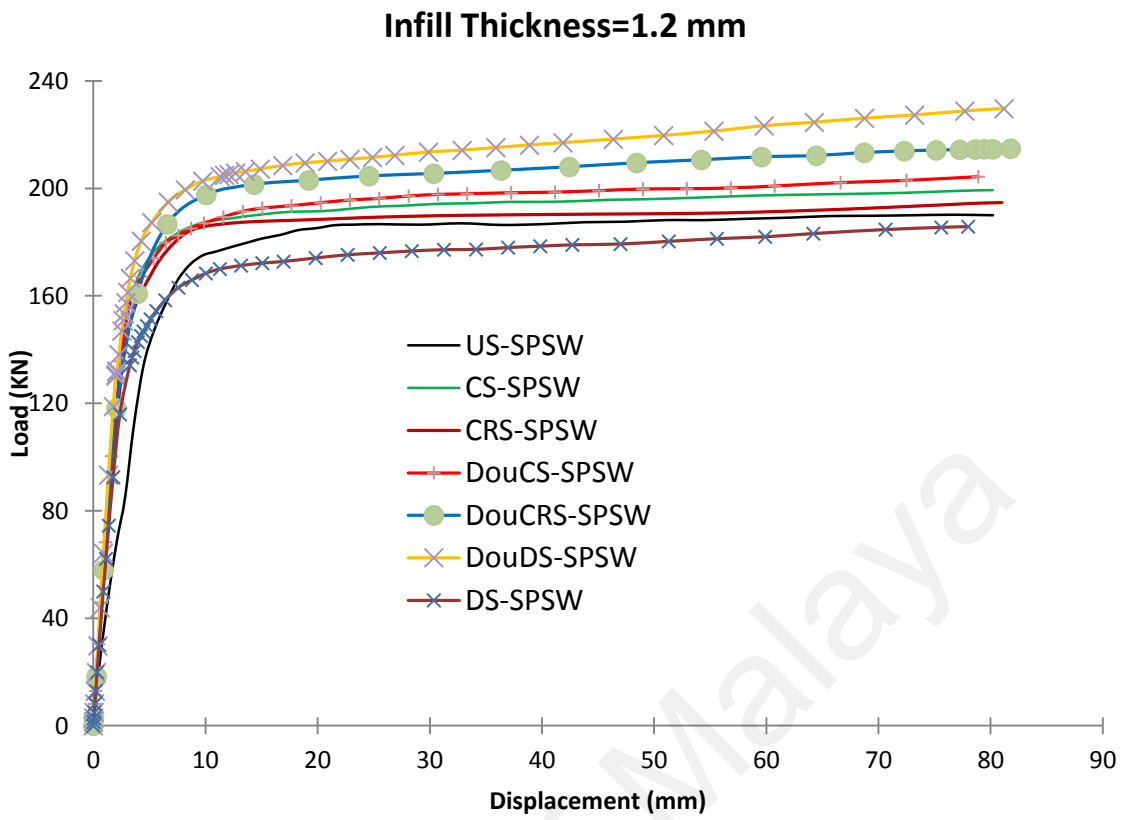

Figure 5-8 Comparison of envelope of hysteresis curves for infill thickness 1.2 mm

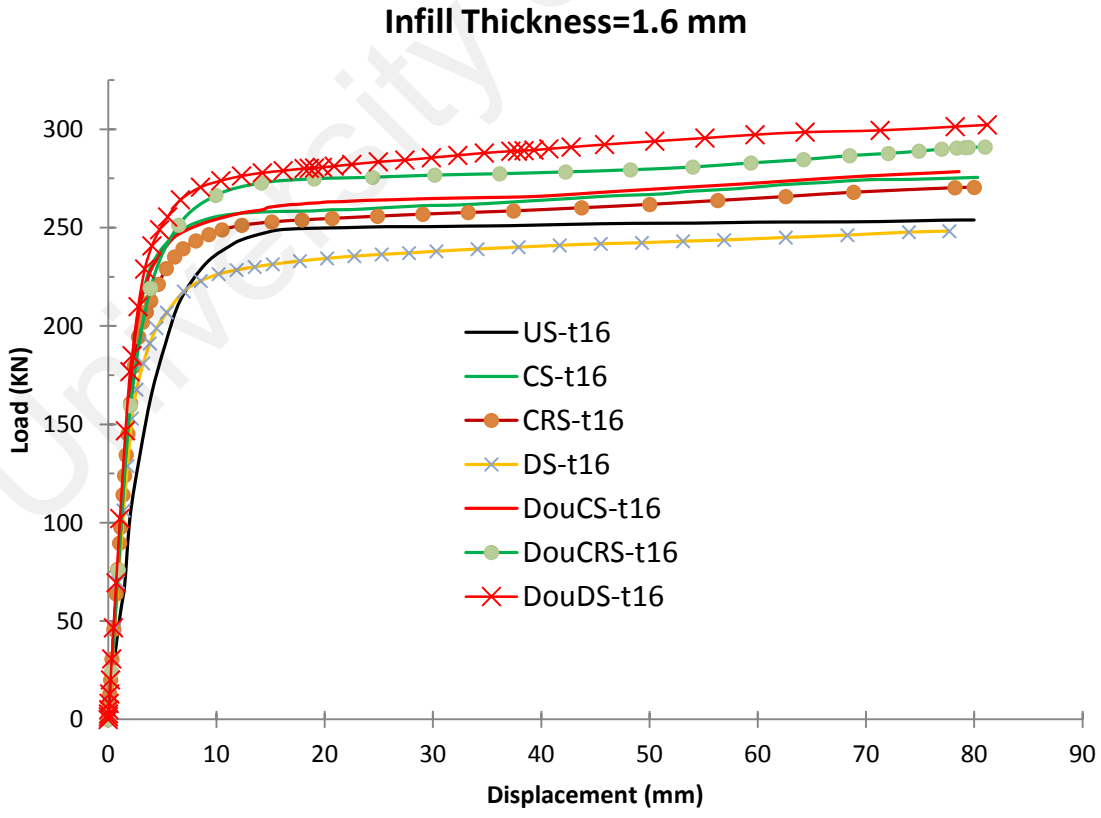

Figure 5-9 Comparison of envelope of hysteresis curves for infill thickness 1.6 mm

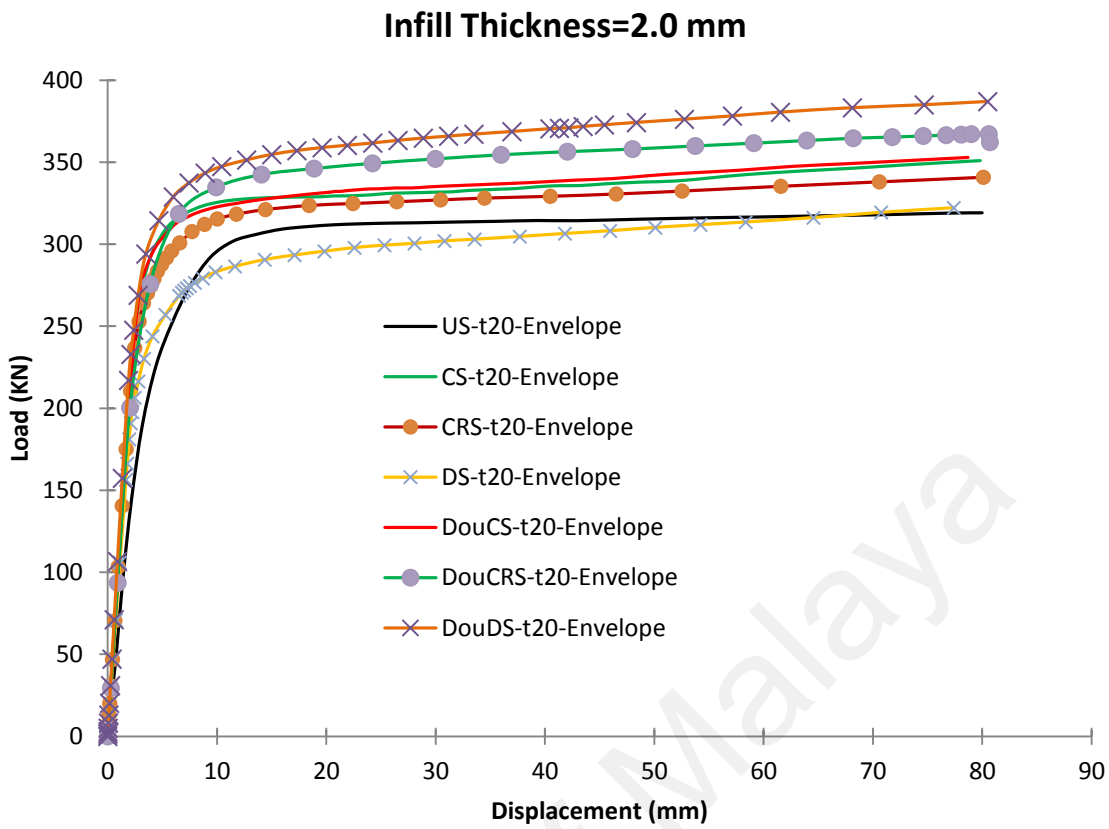

Figure 5-10 Comparison of envelope of hysteresis curves for infill thickness 2.0 mm

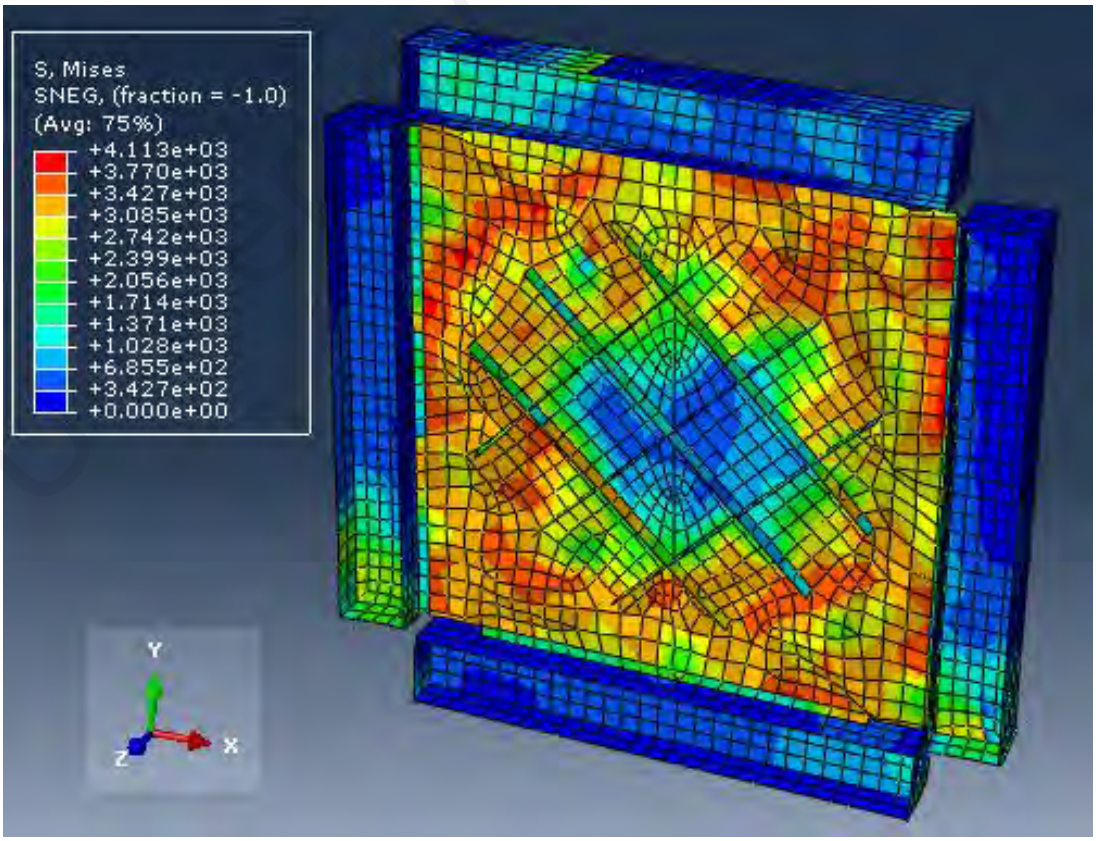

Figure 5-11 Buckling and Von Misses stress distribution in the DouDS-t16

Among the one-sided stiffened plates, cross-stiffened models (CS-SPSW, CS-t16, and CS-t20) exhibited considerable increases in the strength compared to the unstiffened infill plate. This finding means that cross-stiffened configuration is the optimum choice for increasing the strength and reducing the number of stiffeners. The comparison of double-sided cross-stiffened model with one-sided cross-stiffened model (Figures 5-8 to 5-10) shows that no considerable differences in strength were observed due to the conversion of one-sided stiffeners to double-sided stiffeners. Hence, from the aspect of the number of used materials, the double-sided cross stiffeners are not reasonable choices.

5.4 ENERGY DISSIPATION

The envelope of the whole hysteresis curves of all FE models is depicted in Figure 5-12. Such envelopes are useful for comparing the expansion of hysteresis curves, especially in quarters 2 and 4. For a convenient comparison, the envelope of hysteresis curves based upon the stiffener configuration was classified in Figures 5-13 to 5-16.

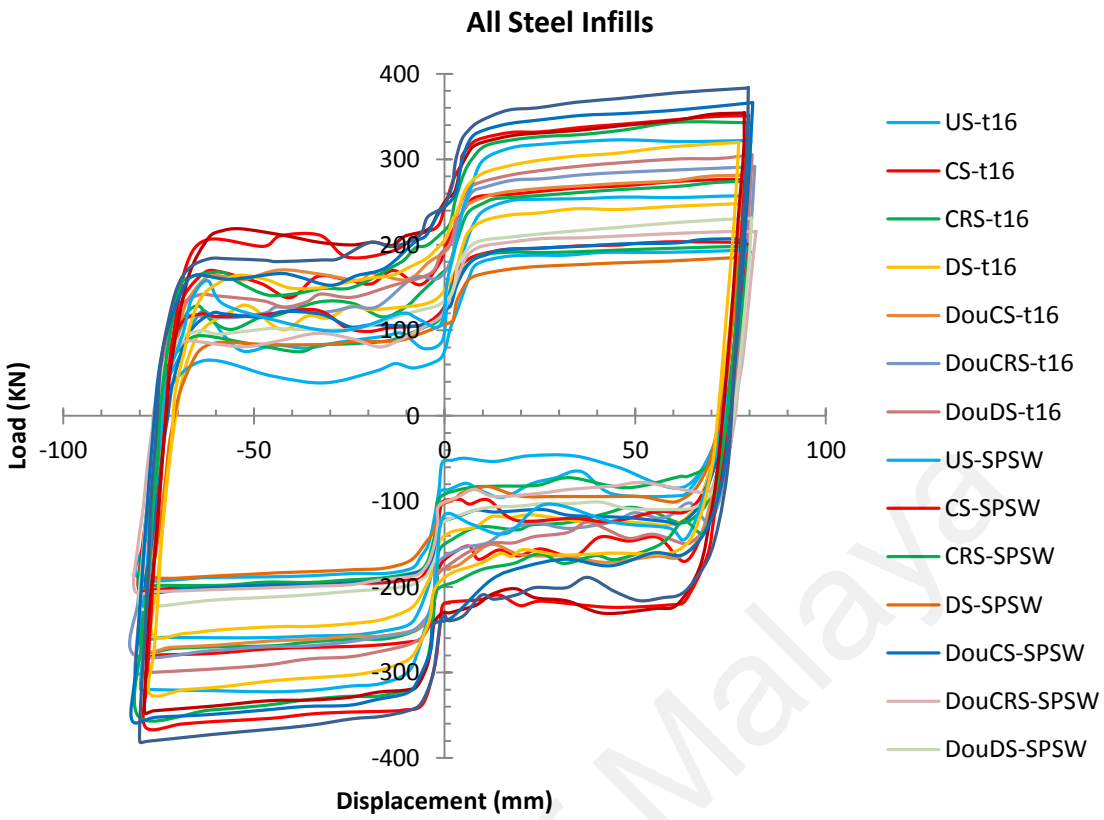

Figure 5-12 Envelope of hysteresis curve of models with steel infill plate

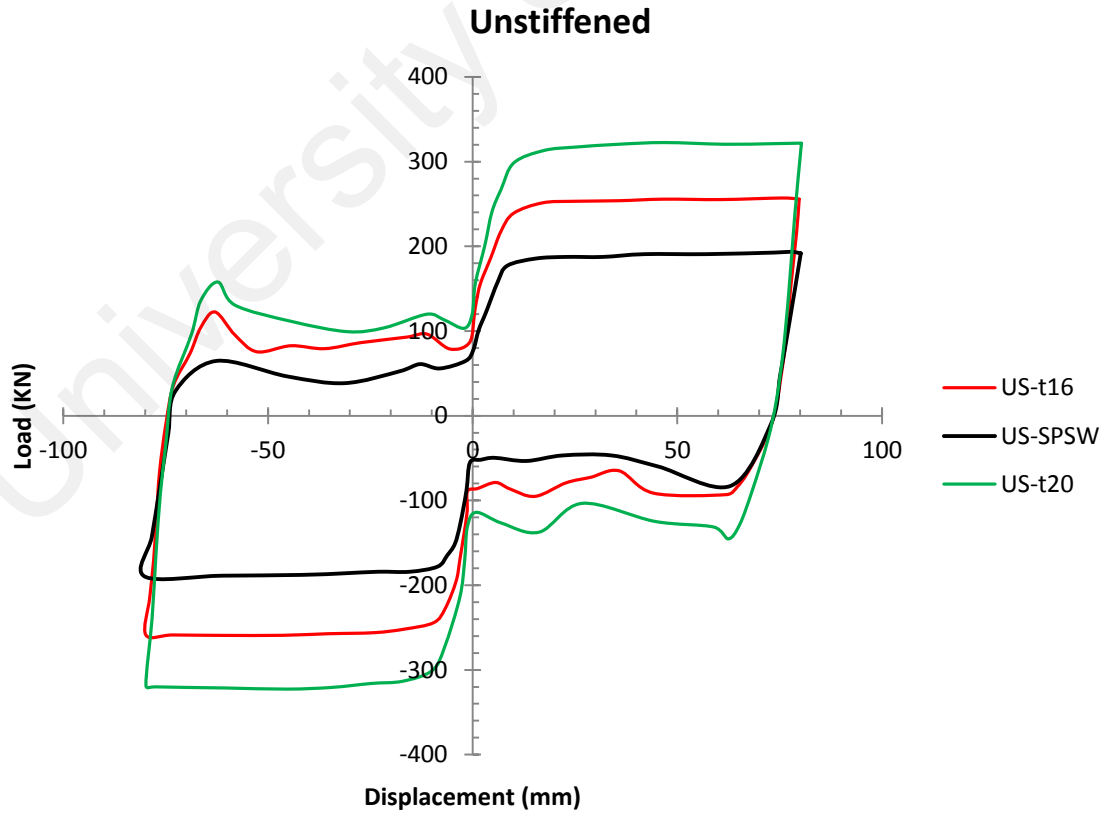

Figure 5-13 Envelope of hysteresis curve of models with un-stiffened infill

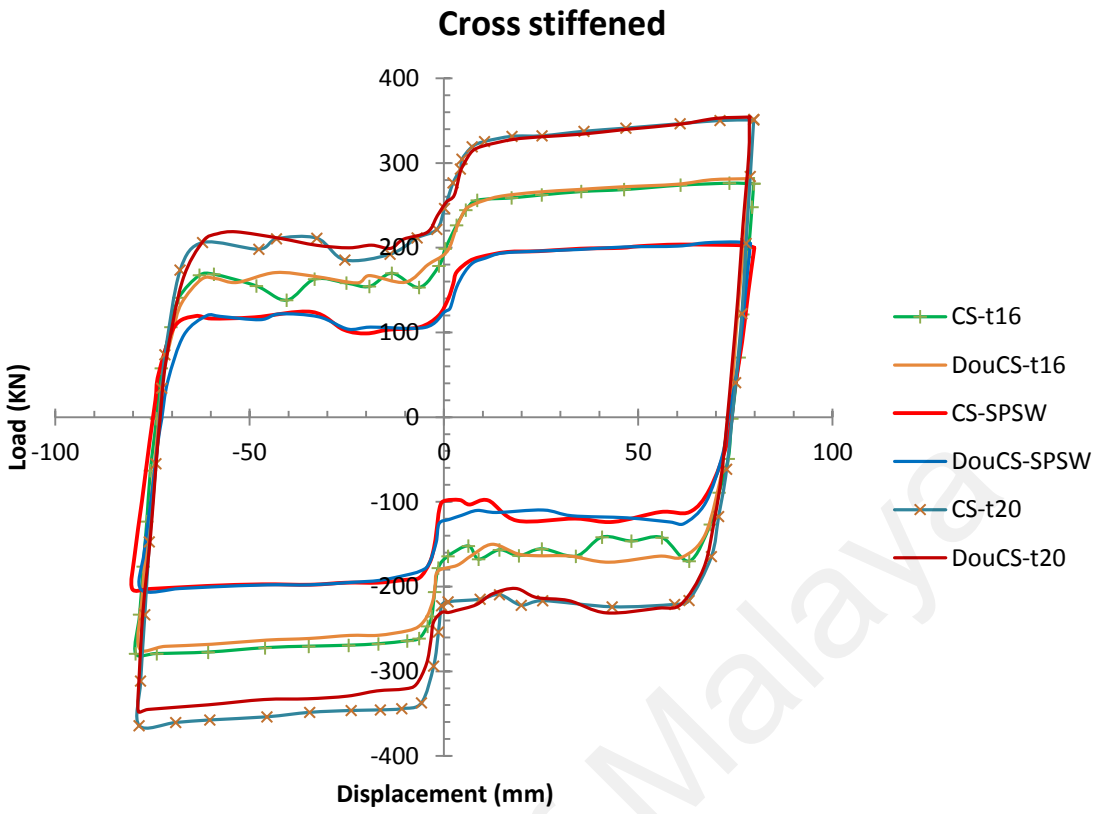

Figure 5-14 Envelope of hysteresis curve of models with cross stiffeners configuration

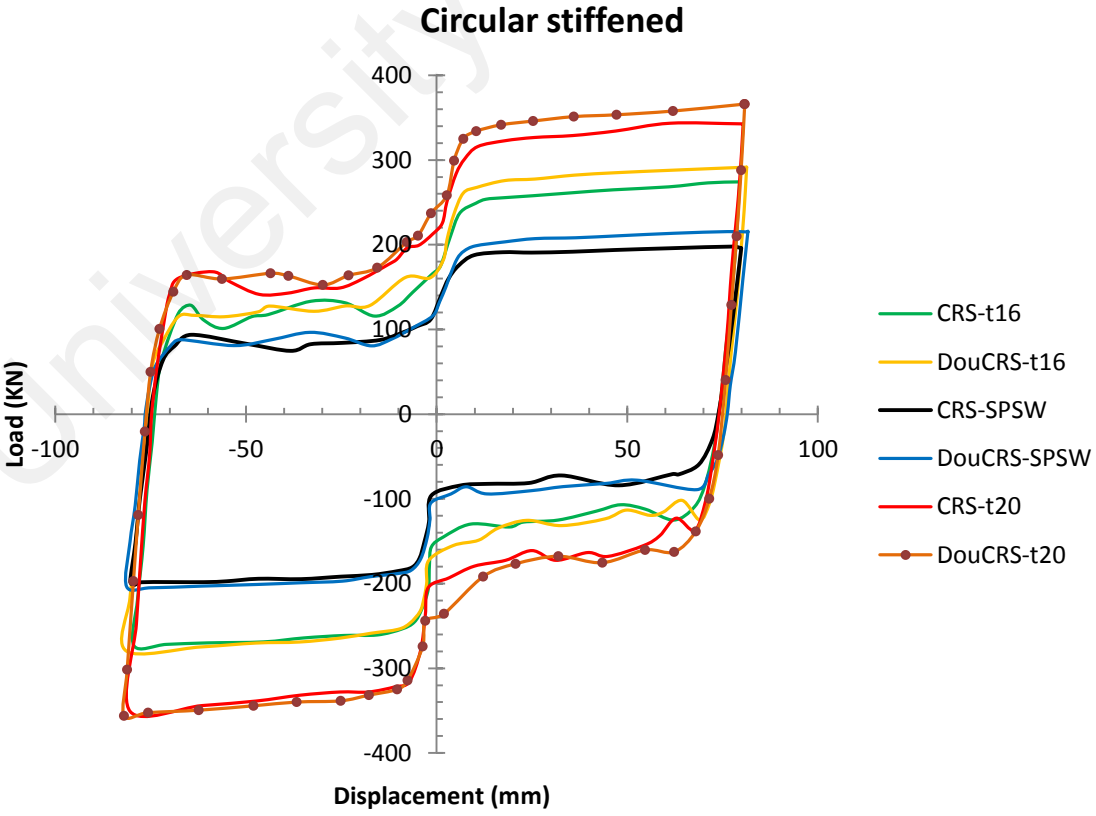

Figure 5-15 Envelope of hysteresis curve of models with circular stiffeners configuration

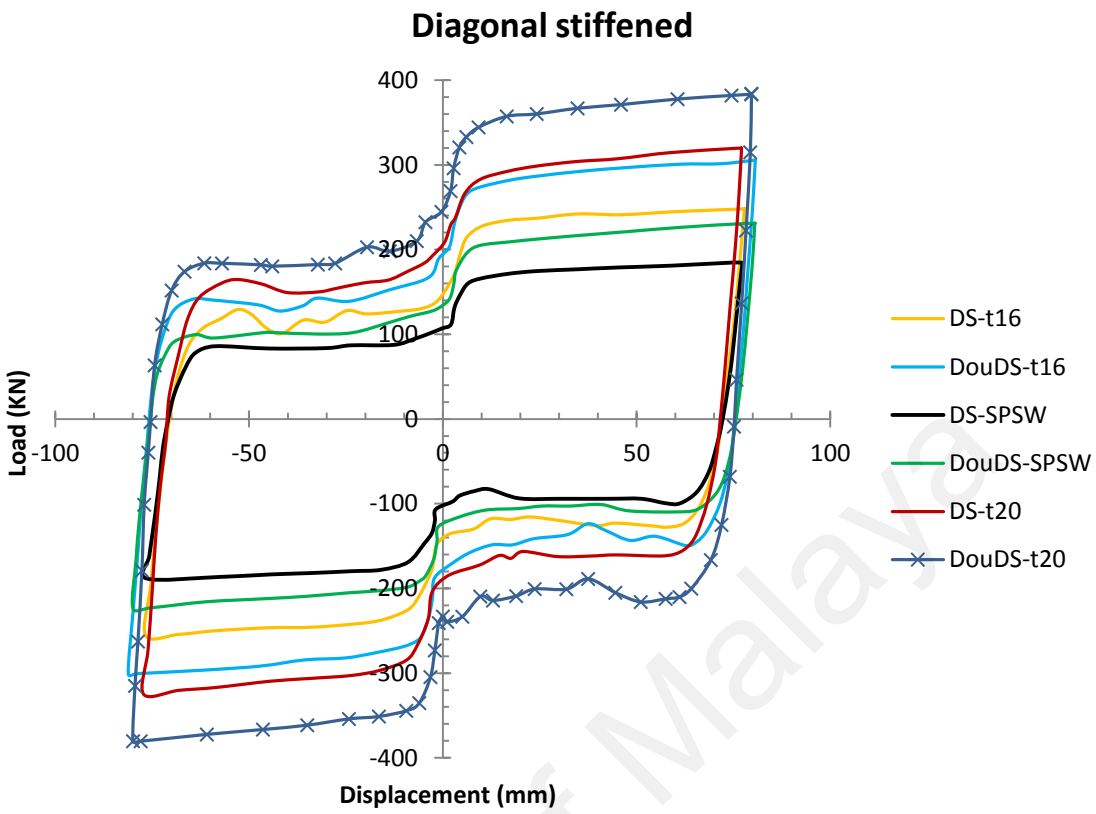

Figure 5-16 Envelope of hysteresis curve of models with diagonal stiffeners configuration

Pinching behavior, which is the characteristic behavior of unstiffened SPSWs, was observed in the envelope of hysteresis curves (Figure 5-13). The increase in thickness improved the pinching effect, which was also observed in all the hysteresis curves, even for the thick infill plate.

As indicated in Figure 5-14, the use of double-sided cross stiffeners created no considerable differences in the envelope of hysteresis curves compared to the one-sided cross stiffeners. This finding means that, by using one-sided cross stiffeners, the same envelope hysteresis curve was obtained. As mentioned in Section 5.3.1, such behavior classifies the one-sided cross-stiffened SPSWs as the most optimal selections by incorporating the accepted structural behavior with the minimum quantity of stiffeners.

However, for a circular stiffened configuration, no considerable expansion of the envelope of the hysteresis curve in quarters 2 and 4 occurs

(Figure 5-15). In the case of a diagonal stiffener configuration, a sensible difference between the envelope of the hysteresis curve of double- and one-sided stiffeners was observed. The expansion of the envelope due to the usage of double-sided stiffeners could be found in quarters 2 and 4, as shown in Figure 5-16.

To compare the effectiveness of each model and its stiffener configuration, the cumulative absorbed energy of FE models was calculated using the enclosed area under every hysteresis loop. The results are depicted in Figures 5-17 to 5-19. Based on the quantity of absorbed energy, the models displayed a similar trend, as shown in Figures 5-17 to 5-19. Although the double-sided diagonally stiffened model dissipated most of the energy, one-sided and double-sided cross-stiffened models were located within a negligible distance from the peak curve. Double- and one-sided circular stiffened models are found in the third position of Figures 5-17 to 5-19. The remarkable difference in the mentioned figures is that all one-sided stiffened models appeared superior to one-sided diagonally stiffened patterns. Among the one-sided stiffened models, the cross-stiffened model exhibited the best performance, and the diagonally stiffened model absorbed the least amount of the energy.

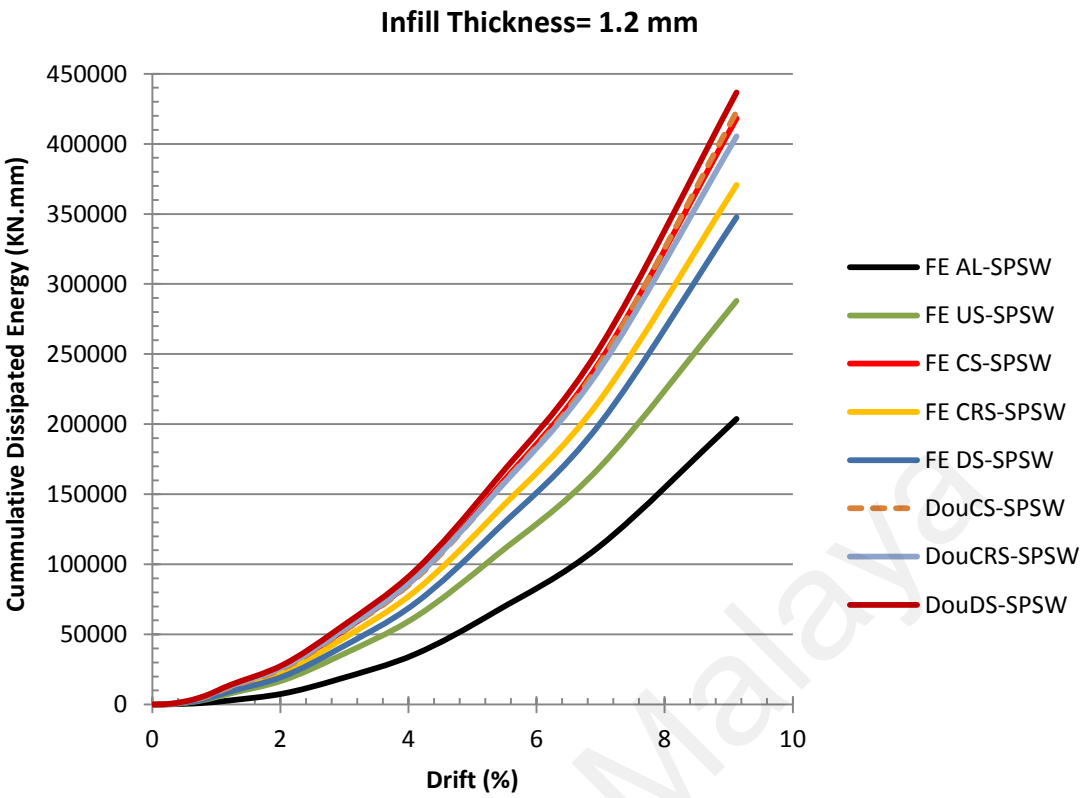

Figure 5-17 Cumulative dissipated energy of models with infill thickness 1.20 mm and AL-SPSW

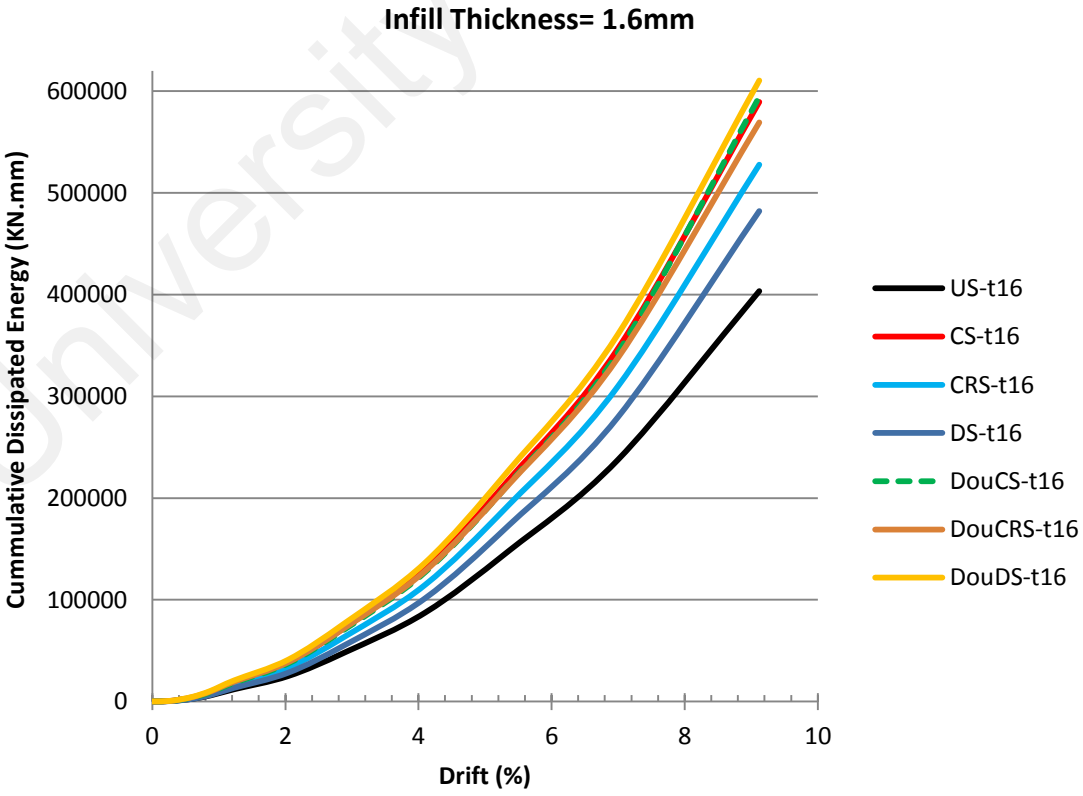

Figure 5-18 Cumulative dissipated energy of models with infill thickness 1.60 mm

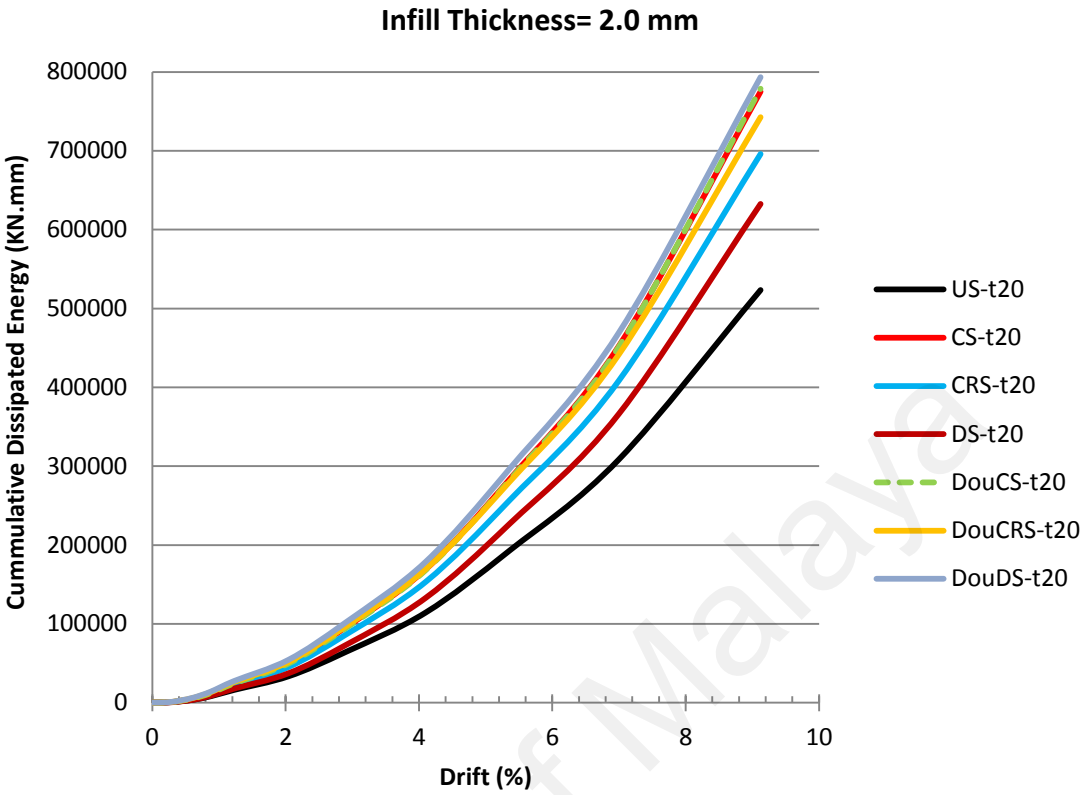

Figure 5-19 Cumulative dissipated energy of models with infill thickness 2.0 mm

To compare the relative effectiveness of stiffener configuration, the hysteretic dissipation per infill material volume was measured. Figures 5-20 to 5-22 show the variation of volumetric energy dissipation versus drift of models. For an infill thickness of 1.2 millimeters, the peak absorbed energy per volume of 0.3058, 0.294, 0.29, 0.29, 0.278, 0.267, 0.2536, and 0.179 were calculated for models CRS-SPSW, DouDS-SPSW, DS-SPSW, CS-SPSW, DouCS-SPSW, DouCRS-SPSW, US-SPSW, and AL-SPSW, respectively, as shown in Figure 5-20. In the case of models with medium thickness (1.6 mm), the peak dissipated energy per volume of 0.334, 0.333, 0.32, 0.306, 0.30, 0.2933, and 0.2787 were calculated for models CS-t16, US-t16, DouDS-t16, DouCS-t16, CRS-t16, DouCRS-t16, and DS-t16, respectively, as shown in Figure 5-21. For thick infill plate with a thickness of 2.0 millimeters, the maximum absorbed energy per volume of 0.345, 0.3255, 0.312, 0.311, 0.2986,

0.2799, and 0.2595 were calculated for models US-t20, DouDS-t20, DouCS-t20, CS-t20, DouCRS-t20, CRS-t20, and DS-t20, respectively, as shown in Figure 5-22. All volumetric energies were close together and no dramatic change could be observed, except for the aluminum infill plate.

As shown in Figures 5-20 to 5-22, the energy-absorbing performance of double-sided diagonally stiffened models was better than that of one-sided diagonally stiffened models. Hence, from a practical view, the use of double-sided diagonal stiffeners is preferable. In medium and thick infill plates, models with flat plate (without stiffeners) displayed superior behavior in absorbing volumetric energy, as one-sided cross-stiffened and double-sided diagonally stiffened models were performed. Moreover, in medium and thick infill plates, one-sided cross-stiffened models dissipated more volumetric energy compared to the double-sided cross-stiffened models. This finding means that, in the aspect of absorbed energy, the double-sided cross-stiffened configuration does not have any advantage. The best volumetric energy absorption performance of the circular stiffeners pattern can be observed in the thin infill plate, where, with the increase in the thickness of infill plate, the effectiveness of such stiffeners would be reduced.

Figure 5-20 Volumetric cumulative dissipated energy of models with infill thickness 1.2 mm and Aluminum infill

Figure 5-21 Volumetric cumulative dissipated energy of models with infill thickness 1.6 mm

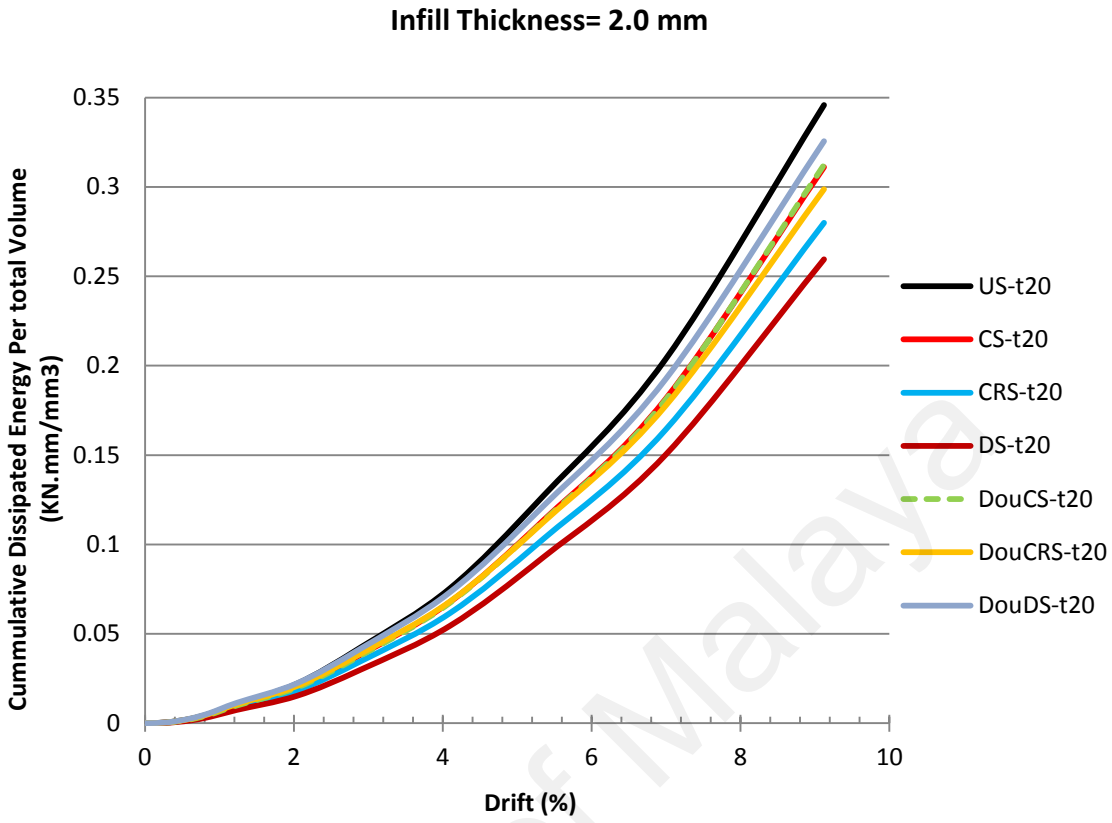

Figure 5-22 Volumetric cumulative dissipated energy of models with infill thickness 2.0 mm

5.5 SEISMIC PERFORMANCE FACTORS

Given that a new structural system is introduced, the certainty of the seismic capability should be quantified. The capability to use the nonlinear collapse simulation technique results in the linking of SPFs to the system performance capability in a probabilistic earthquake. In current building codes, SPFs are used to estimate the deformation and strength demands on seismic-force-resisting systems, which are designed using a linear method of analysis and respond in the nonlinear range. Although most of the structural design standards intend to allow the inelastic behavior of structural elements under severe earthquake ground motion, static analysis has protected its prevalence

for primary seismic design in practice. As a result, SPFs have preserved their importance.

All significant deterioration mechanisms that could lead to structural collapse should be included in the explicit simulation of the nonlinear system (F.E.M.A, 2009a). The representative nonlinear model of the seismic-force-resisting system requires detailed design information of its assemblies and comprehensive test data on the structural component. Such nonlinear models have substantially less uncertainty in their seismic performance and require a low safety margin against collapse compared to the system with less robust data in the equivalent level of safety.

The development of the representative models for assessing nonlinear behavior is discussed in Chapter 4. The FE models in Chapter 4 provide the basis for developing a corresponding finite number of idealized nonlinear models that represent the range of interested parameters.

The present research focused on quantifying SPFs, including over-strength factor (Ω_0), displacement amplification factor (C_d), and response modification coefficient (R), for stiffened SPSWs. Using the response modification factor can determine the reduced seismic forces through elastic analysis. The displacements determined through elastic method increase by the displacement amplification factor. The expected strength is estimated using design strength and over-strength factor. In fact, the over-strength factor accounts for the reserved strength from the first plastic hinge to the mechanism stage (instability) of the structural system.

For SPSWs, in accordance with the American Society of Civil Engineers (ASCE) (A.S.C.E, 2010), Table 12.2-1 lists the values of 7, 2, and 6 for R, Ω_0, and C_d, respectively. No reliable data, however, were provided for

the performance factor of stiffened SPSWs. The aim of this investigation is to explore the sensitivity of the SPF to the stiffener configuration and stiffener thickness and thus provide reliable SPFs for stiffened SPSWs.

5.5.1 Natural Vibration Period of Models

In this investigation, the SPFs were developed following the methodology described in Chapter 2. This methodology was outlined by Uang (Uang, 1991). Consequently, the SPFs would be obtained from the ductility reduction factor, and the values of the SPFs would depend directly on the fundamental natural period and target ductility of the system. Therefore, the reliable amounts for the natural period of models are necessary.

To acquire the natural period of FE models, relevant frequency analysis was conducted. Figure 5-23 depicts the frequency and deformation mode of the various models. Among the numerous shapes of vibration frequencies obtained from numerical analysis, those that possess similar lateral displacement and buckling to the deformed shape obtained during quasi-static analysis are selected. A comparison of the natural vibration period obtained from numerical investigation is presented in Figure 5-24.

The detailed numerical analysis of most of the SPSWs exhibited similar values for the natural period of vibration. The average natural period of one-sided diagonally stiffened models is 12.5% higher and that of double-sided diagonally stiffened models is 6% lower than other SPSWs. In general, the variations of the period for different SPSWs are negligible.

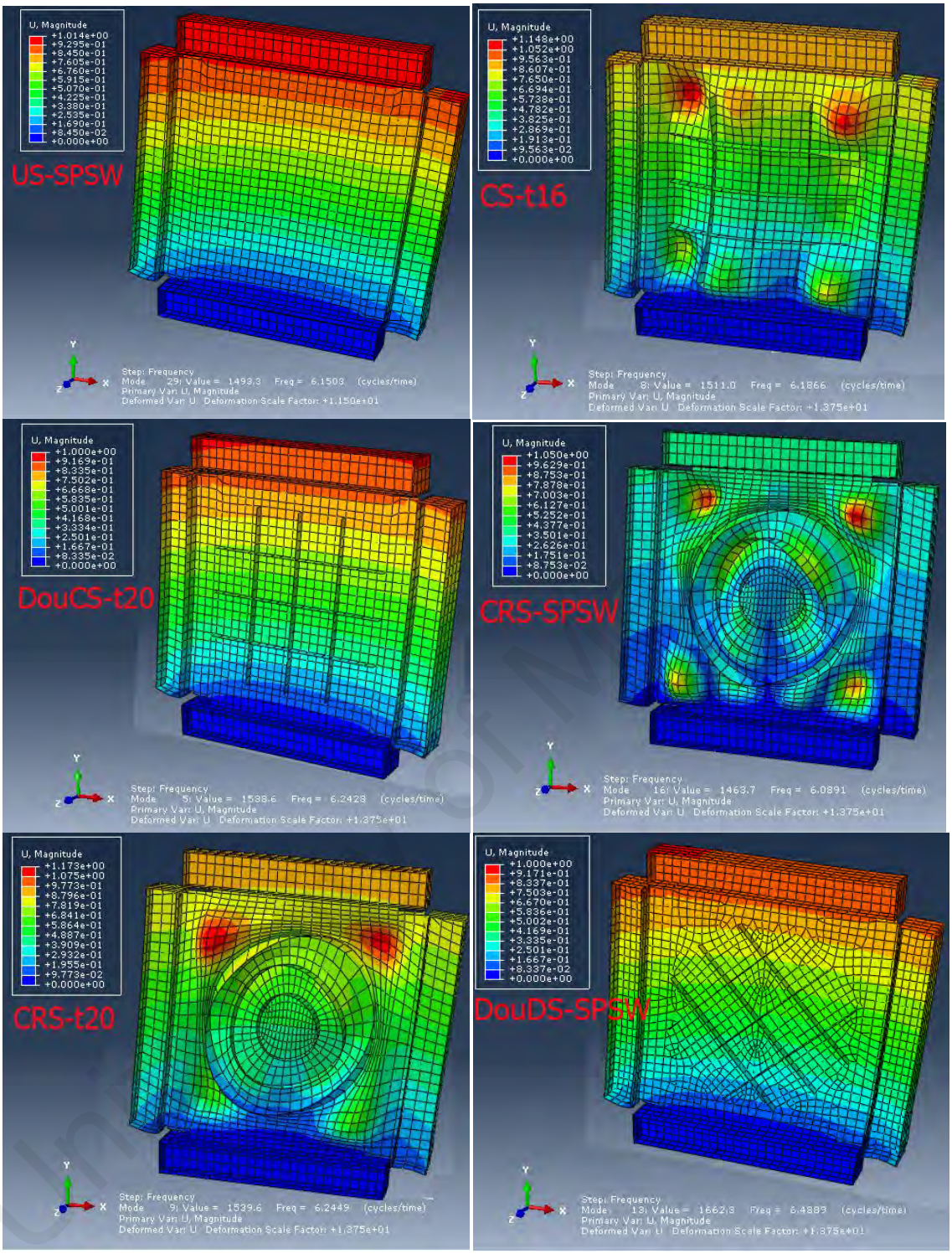

Figure 5-23 Natural frequencies of SPSWs with Steel infill plate

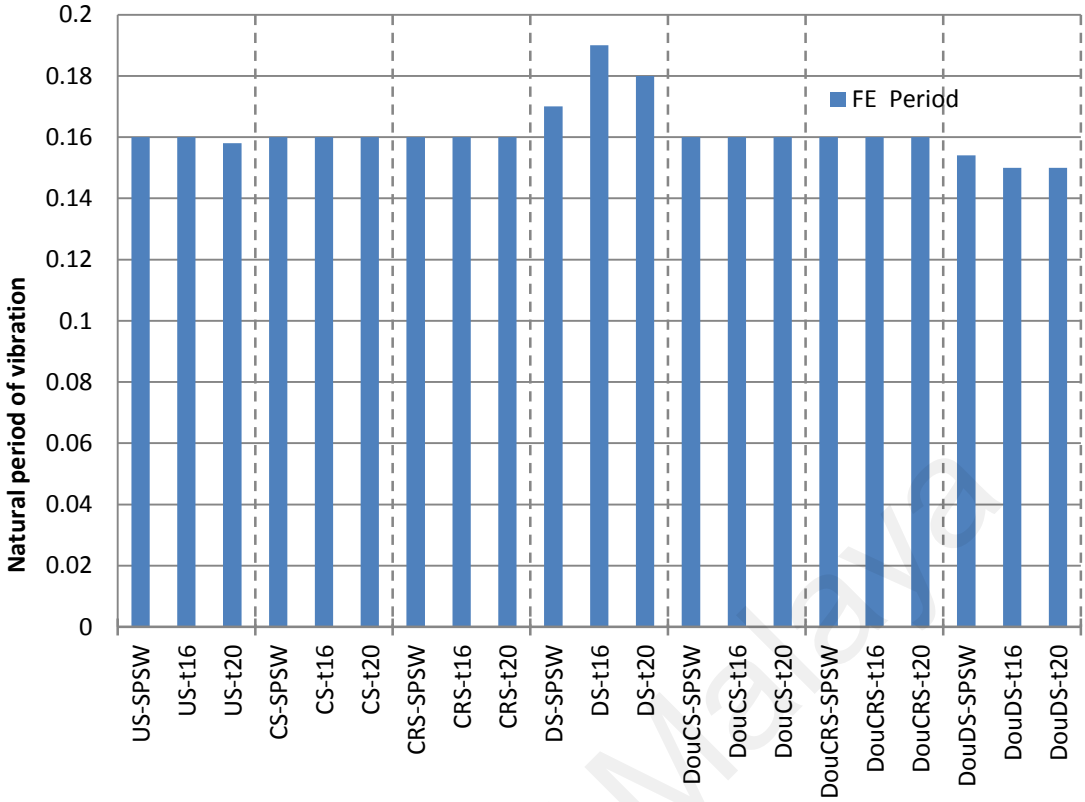

Figure 5-24 Natural period of vibration of FE models

5.5.2 Target displacement and envelope curves used for S.P.F

To perform the methodology outlined in Chapter 2, a reliable load–displacement curve for models should be obtained to enhance the quality of information. Figures 5-2 to 5-7 suggest that the load–displacement curves obtained from monotonic loading are close to those obtained from cyclic loading. However, owing to the realistic behavior of cyclic loading in accounting for cumulative damage effect and the advantages according to FEMA (2009b), the envelopes of hysteresis curves were selected for future investigation. All the abovementioned curves, material properties, cyclic behavior, and model components were calibrated and validated by experimental test data and described in Chapters 3 and 4.

Owing to the direct relationship between ultimate lateral drift to the ductility and ductility reduction factor, the determination of considered maximum lateral displacement is an important matter. An increase in the

ultimate lateral drift exaggerates the estimation of SPFs. According to FEMA (2009b), the deformation associated with a force value of 80% of the maximum strength would be considered the ultimate lateral deformation (Figure 2-32). As shown in the figure, such criteria are applicable for load–displacement curves, which involve degradation. In the present study, the horizontal line from 80% of the ultimate strength does not intersect the curve. Therefore, such rule could not be used here. The maximum lateral displacement applied to all models is equal to 97.7 millimeters, and the models tolerated 80 millimeters of displacement. As shown in Figures 5-2 to 5-7, no obvious deterioration appeared in the envelope curve.

In the numerical analysis, because the collapse behavior and deterioration mode are not simulated directly, the ultimate displacement could be evaluated using alternative limit state checks on structural response quantities. In some cases, ultimate displacement can be defined based on the failure of the structure component, but during the nonlinear simulation, no structural failure of model component was found. Based on the test data and median value of the response, the ultimate displacement could be estimated. As described in Chapter 3, the maximum drift observed during the test program was 4.99%, 8.94%, 4.99%, 5.85%, and 5.44% for the specimens of AL-SPSW, US-SPSW, CS-SPSW, CRS-SPSW, and DS-SPSW respectively. Therefore, based on the above values, the ultimate drift for all models was considered equal to 5%.

5.5.3 Calculation and Comparison of S.P.F

Several methods were found in the evaluation of SPFs. In the present section, the method proposed by Uang (Uang, 1991) was used to derive the trail value of SPFs. In this method, a bilinear relationship regarding the base

shear versus the lateral displacement (Figure 5-25) idealizes the actual load–displacement envelope curves, where V_y, V_u, Δ_y, and Δ_u represent the yielding and ultimate loads and yielding and ultimate displacements, respectively.

The bilinear idealized load–displacement curves were obtained based on the clearly defined elastic stiffness (which must cross from 0.6 V_y), ultimate displacement, and equal energy method. The slope of the tangent at the start of the actual curve was considered the initial stiffness. As shown in Figure 5-25, the equal energy method balances the areas between the actual and bilinear curves. Therefore, the area under the bilinear curve is equal to the area under the actual curve. The idealized load–displacement curves consist of two elastic portions up to the yield displacement (Δ_y) and inelastic part beyond the limit point of yield displacement. In other words, the yield displacement was estimated by bilinear idealization, and this approach provides the bases for the calculation of performance factors.

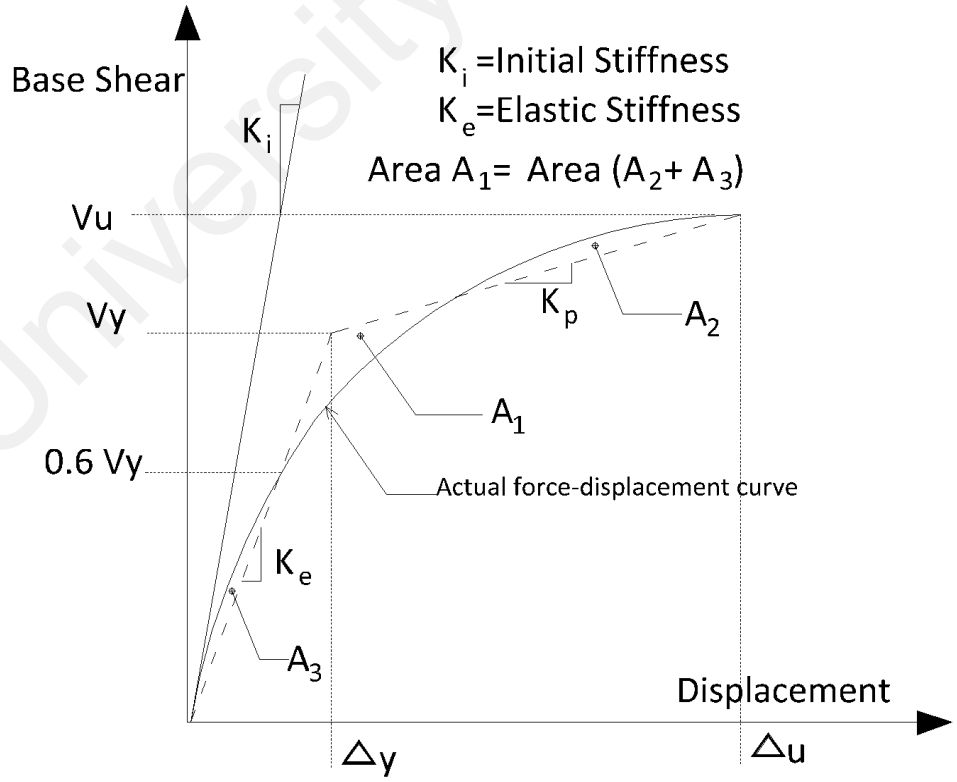

Figure 5-25 Bilinear methodology definition

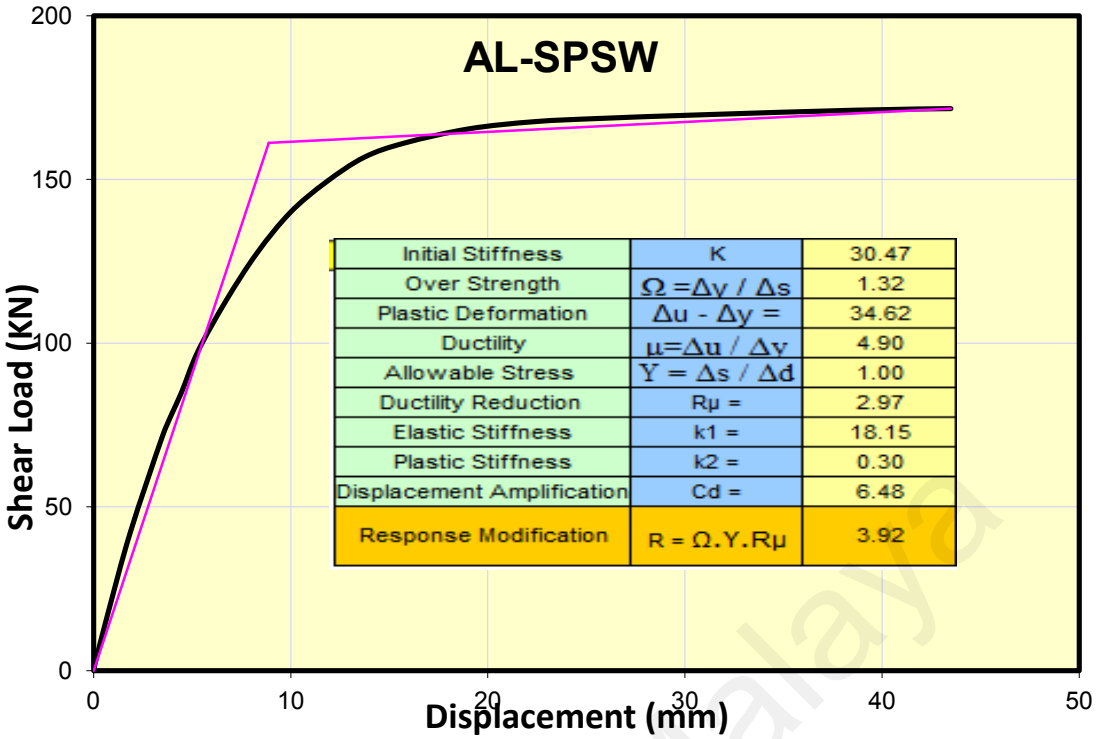

Figure 5-26 Bilinear idealization and seismic performance factors of AL-SPSW

The actual load–displacement response based on the envelope of the hysteresis curves defines the bilinear idealized load–displacement response, as shown for AL-SPSW in Figure 5-26 and for other models in Figures 5-27 to 5-32. The loading steps in both directions were symmetric with the excursions of equal displacement magnitude. Therefore, the differences of the envelope of the hysteresis curve were found to be negligible. Next, all required parameters were calculated by obtaining the idealized response. In this section, ductility and, consequently, ductility reduction factor and other relevant factors were obtained based on equations suggested by Newmark-Hall for the estimation of ductility. The performance factors obtained from Figures 5-27 to 5-32 are summarized in Table 5-2.

Table 5-2 Summary of the obtained seismic performance factor of FE models

FE model	FE natural period (sec)	K_i Initial Stiffness (KN/mm)	Ω Over Strength Factor	μ Ductility	Y Allowable stress Factor	$R\mu$ Ductility Reduction Factor	K_1 Elastic Stiffness (KN/mm)	K_2 Plastic Stiffness (KN/mm)	C_d Displacement Amplification Factor	V_u Ultimate strength (KN)	V_y Yield Strength (KN)	Δ_y Yield Displacement (mm)	$R = \Omega.Y.R_\mu$ Force Modification Factor
AL-SPSW	0.204	30.47	1.32	4.9	1	2.97	18.15	0.3	6.48	171.58	161.19	8.9	3.92
US-SPSW	0.16	56.83	1.32	7.33	1	3.7	30.82	0.12	9.7	187.4	182.93	5.94	4.89
CS-SPSW	0.16	56.16	1.18	12.95	1	4.99	56.41	0.15	15.28	195.357	189.49	3.36	5.89
CRS-SPSW	0.16	66.54	1.22	13.04	1	5.01	55.32	0.14	15.97	190.3518	184.54	3.34	6.13
DS-SPSW	0.17	54.15	1.19	13.03	1	5.01	50.87	0.23	15.48	179.06	169.82	3.34	5.95
DouCS-SPSW	0.16	54.99	1.13	14.22	1	5.24	61.09	0.3	16.11	198.97	186.84	3.05	5.93
DouCRS-SPSW	0.16	73.05	1.14	12.71	1	4.94	57.32	0.3	14.5	208.264	196.24	3.42	5.64
DouDS-SPSW	0.154	61.66	1.2	14.21	1	5.24	66.2	0.37	17.09	217.47	202.71	3.06	6.3
US-t16	0.16	75	1.31	7.85	1	3.83	43.99	0.21	10.28	251.77	243.8	5.54	5.02
CS-t16	0.16	75.98	1.15	14	1	5.2	81.3	0.31	16.05	265.05	252.56	3.1	5.96
CRS-t16	0.16	85.95	1.23	13.94	1	5.18	79.2	0.32	17.19	260.04	247.12	3.12	6.39
DS-t16	0.19	71.44	1.2	13.82	1	5.16	71.7	0.39	16.63	241.377	225.6393	3.15	6.21
DouCS-t16	0.16	71.67	1.21	14.26	1	5.25	83.06	0.34	17.28	267.2	253.44	3.05	6.36
DouCRS-t16	0.16	81.28	1.14	12.81	1	4.96	77.68	0.37	14.6	278.52	263.8	3.39	5.65
DouDS-t16	0.15	78.7	1.19	14.36	1	5.26	89.65	0.48	17.13	291	271.57	3.03	6.28
US-t20	0.158	92.14	1.31	8.75	1	4.06	60.52	0.35	11.45	314.38	300.9	4.97	5.31
CS-t20	0.16	99.63	1.22	14.08	1	5.21	103.22	0.42	17.13	335.94	318.97	3.09	6.34
CRS-t20	0.16	103.86	1.24	14.19	1	5.23	102.66	0.38	17.64	330	314.63	3.06	6.5
DS-t20	0.18	89.44	1.23	14.31	1	5.26	92.66	0.63	17.61	307.19	281.7	3.04	6.47
DouCS-t20	0.16	87.23	1.18	13.9	1	5.18	102.94	0.43	16.42	339.36	322.2	3.13	6.11
DouCRS-t20	0.16	101.41	1.17	12.85	1	4.97	97.94	0.63	15	356.89	331.62	3.38	5.8
DouDS-t20	0.15	94.99	1.26	14.47	1	5.29	114.3	0.7	18.26	371.8	343.46	3	6.67

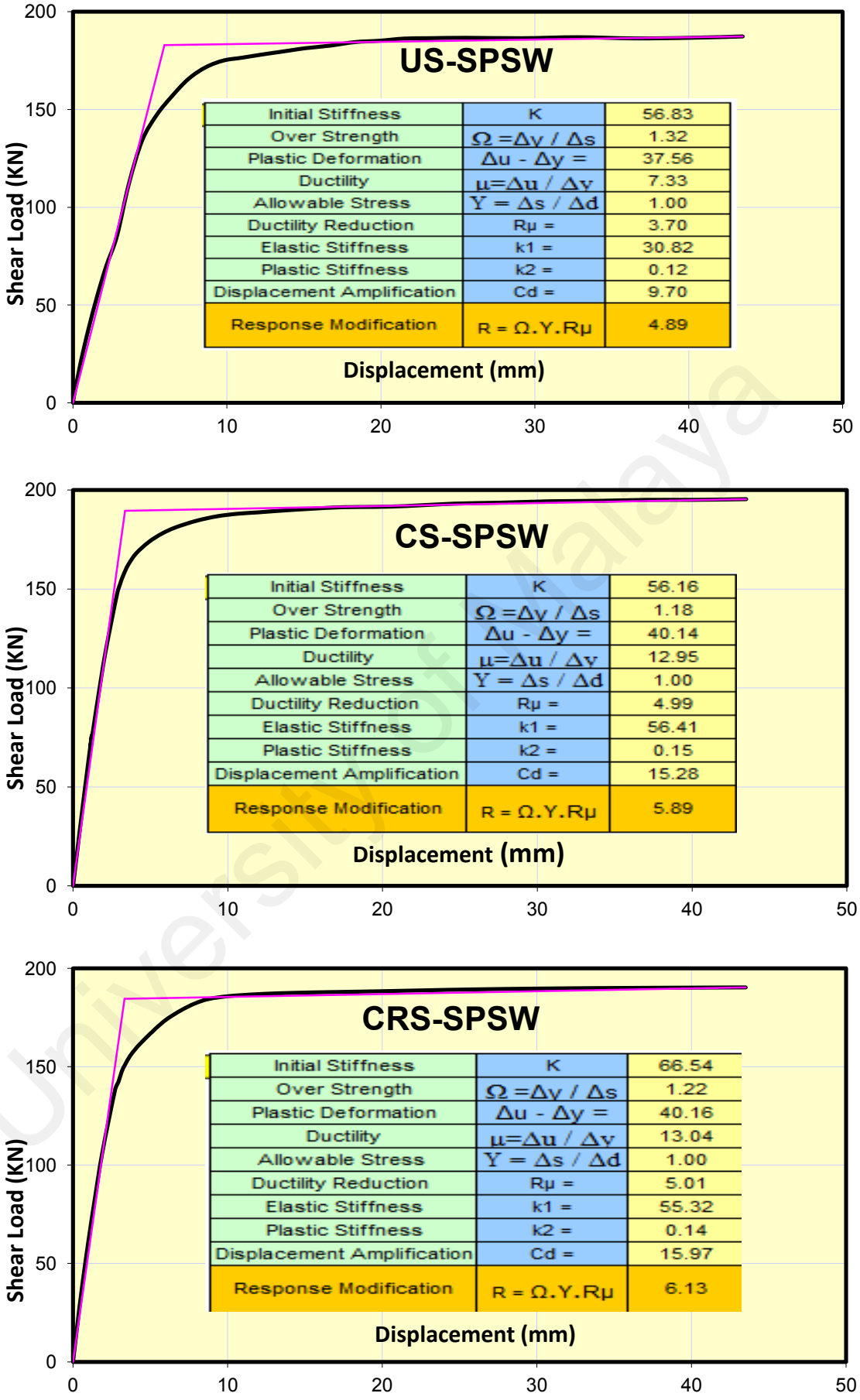

Figure 5-27 Bilinear idealization and seismic performance factors of models with 1.2 mm thickness of infill plate

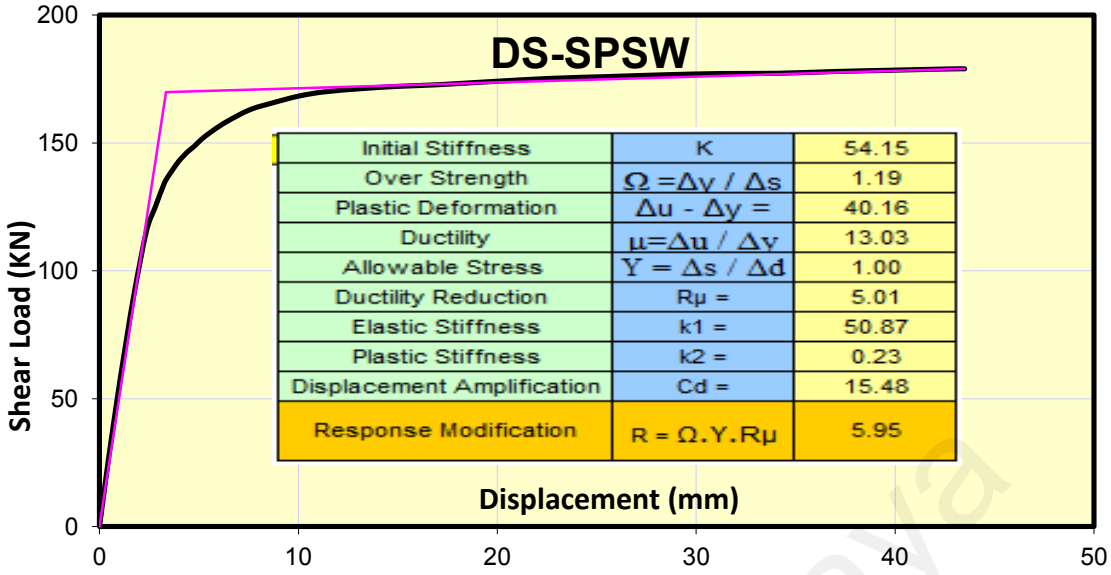

Continue Figure 5- 27 Bilinear idealization and seismic performance factors of models with 1.2 mm thickness of infill plate

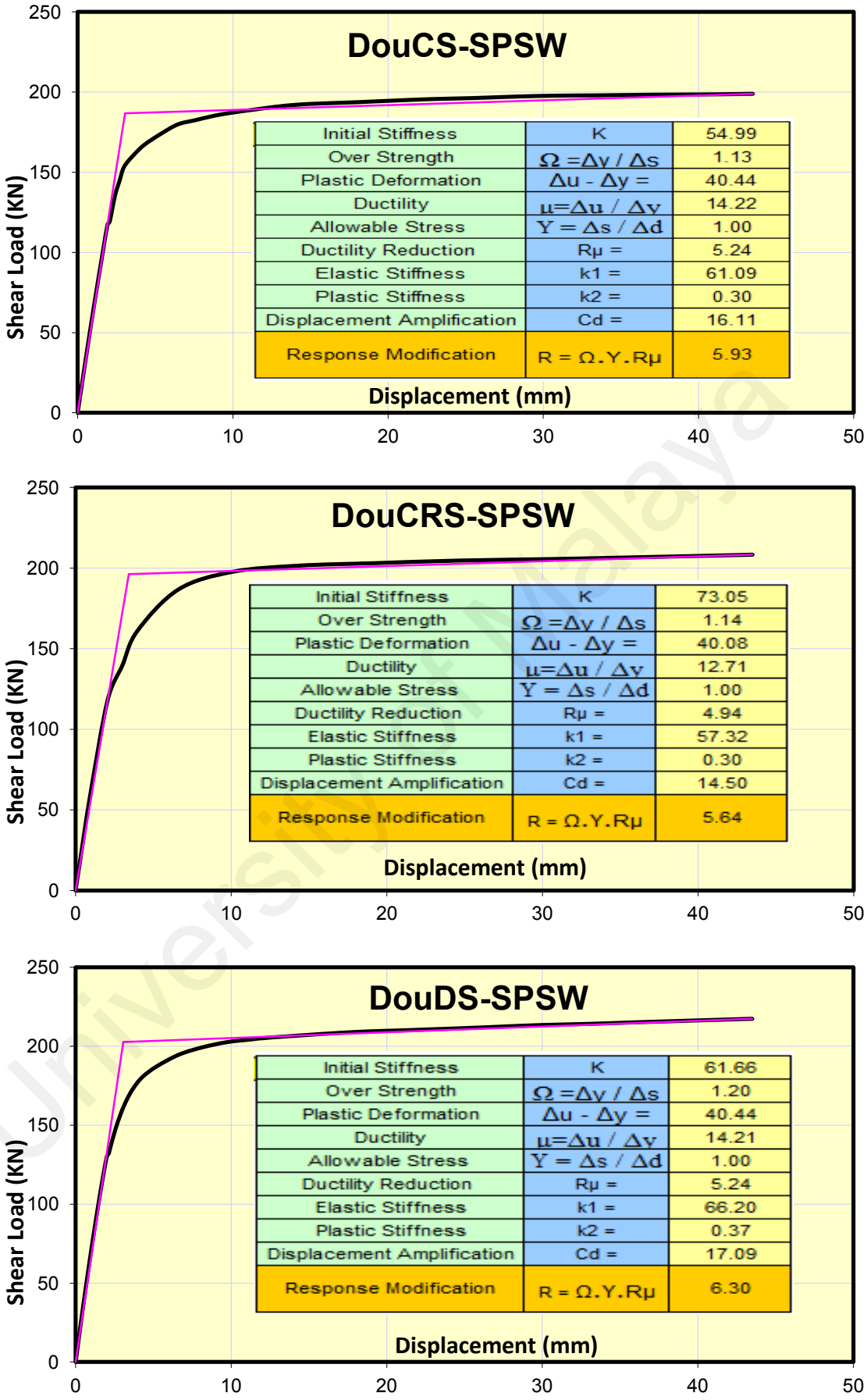

Figure 5-28 Bilinear idealization and seismic performance factors of models with 1.2 mm thickness of infill plate and double side stiffeners

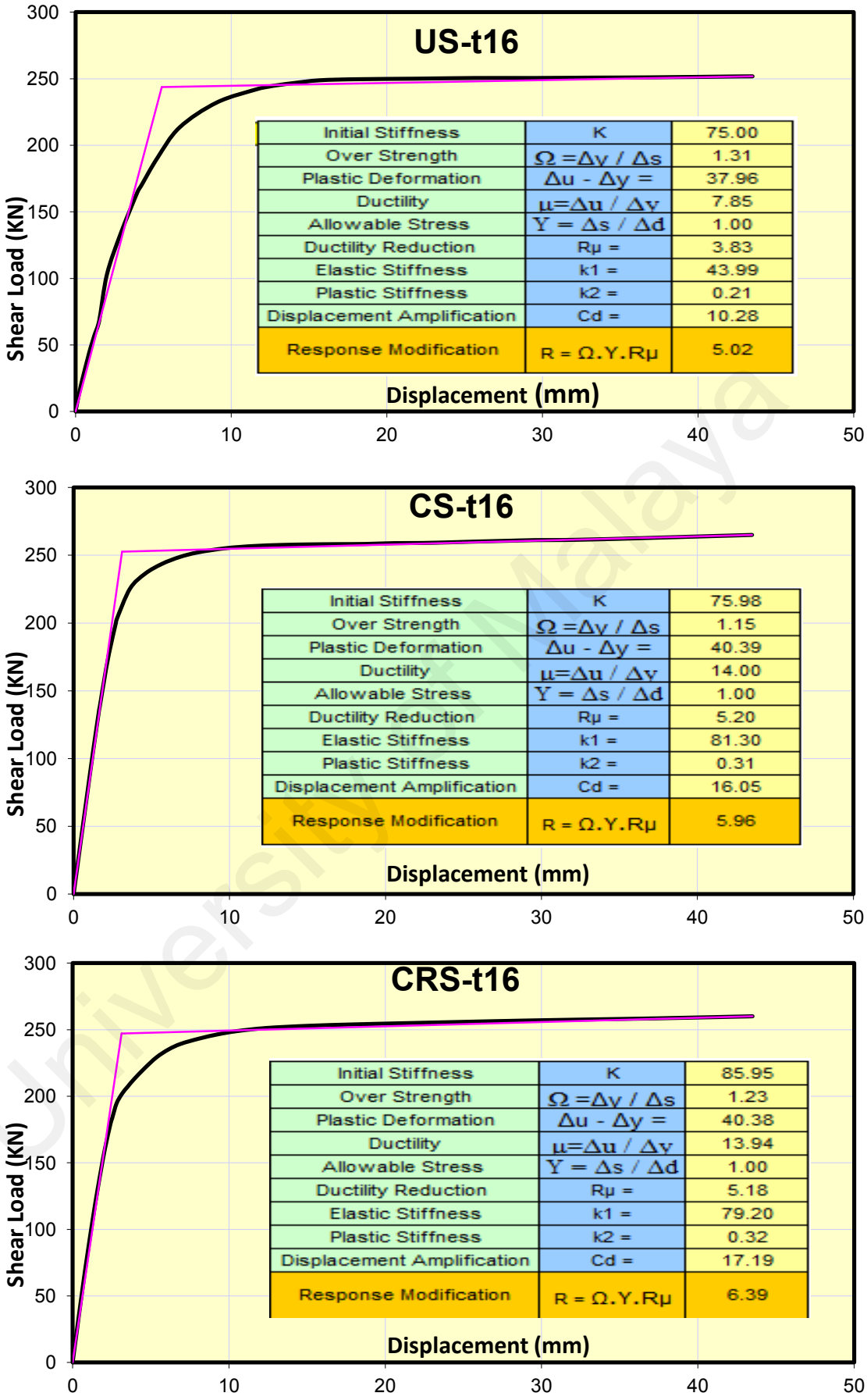

Figure 5-29 Bilinear idealization and seismic performance factors of models with 1.6 mm thickness of infill plate

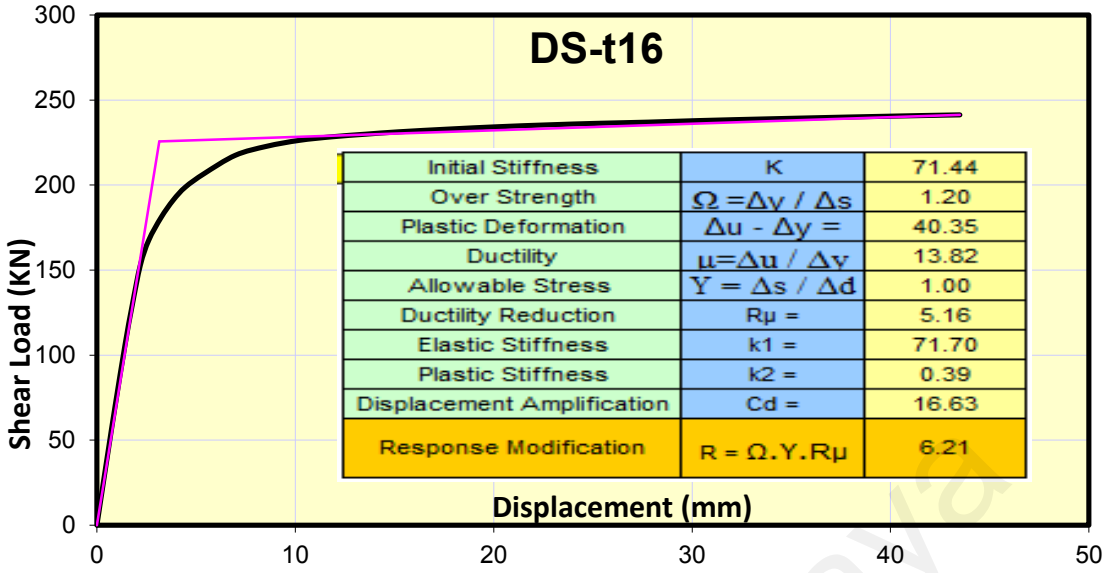

Continue Figure 5- 29 Bilinear idealization and seismic performance factors of models with 1.6 mm thickness of infill plate

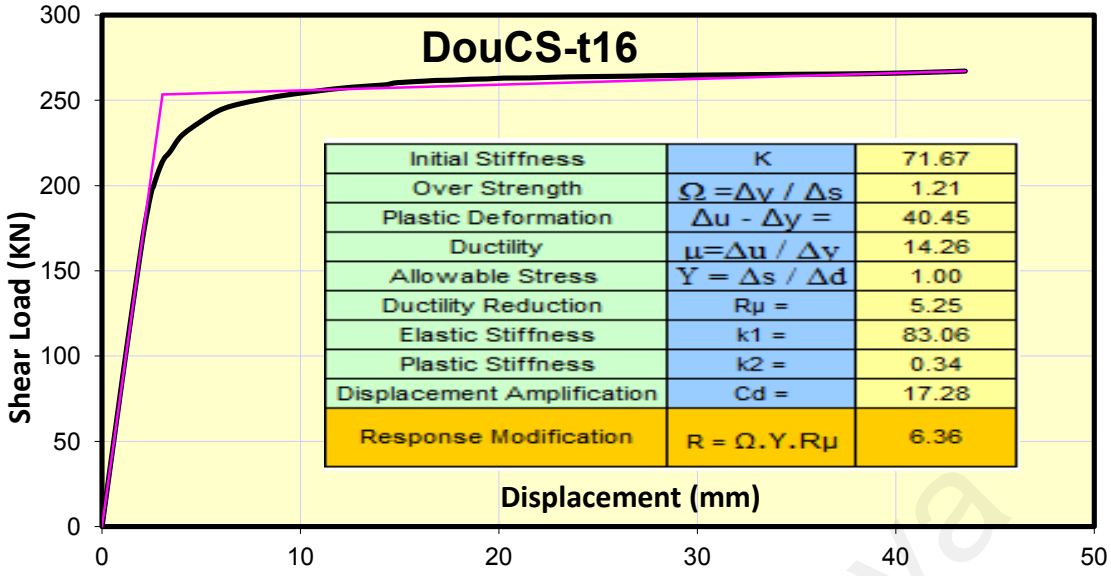

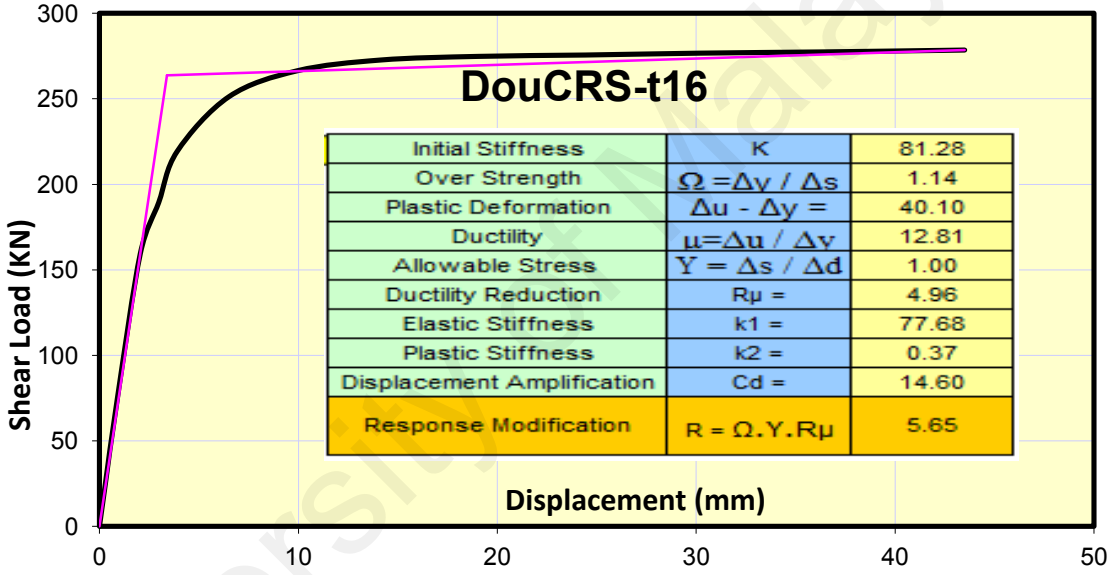

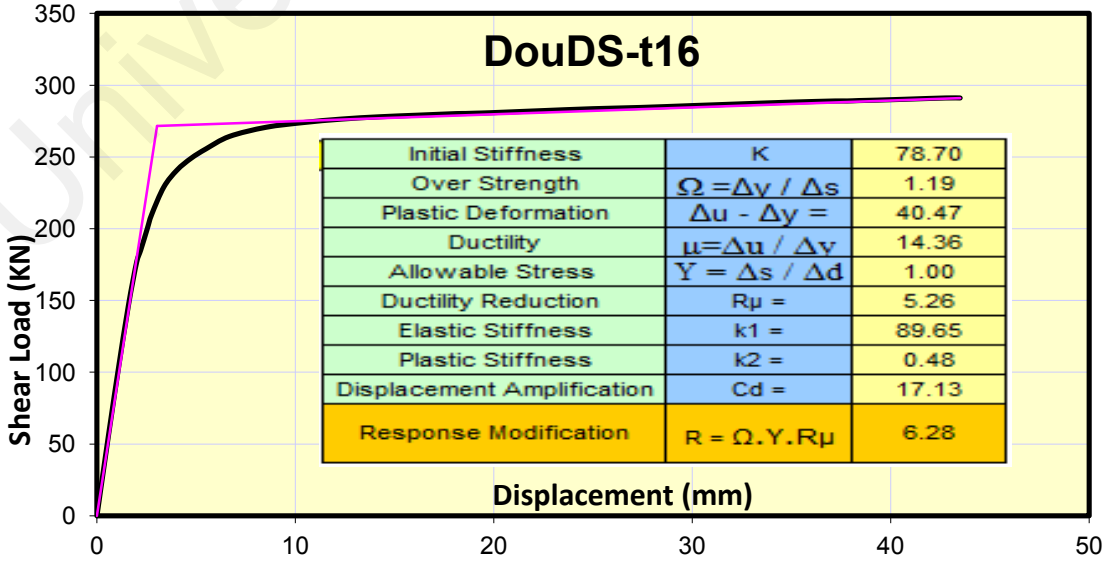

Figure 5-30 Bilinear idealization and seismic performance factors of models with 1.6 mm thickness of infill plate and double side stiffeners

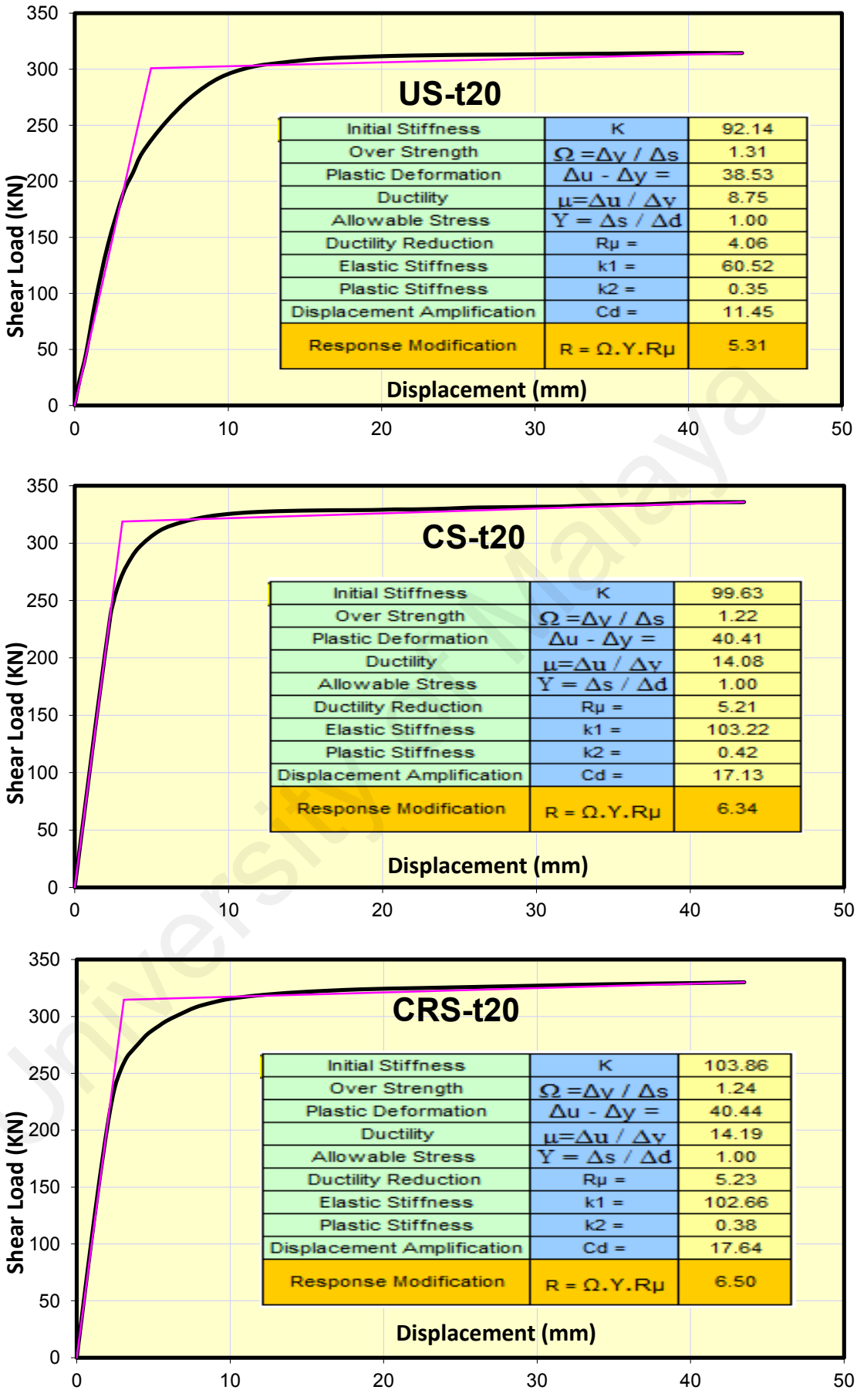

Figure 5-31 Bilinear idealization and seismic performance factors of models with 2.0 mm thickness of infill plate

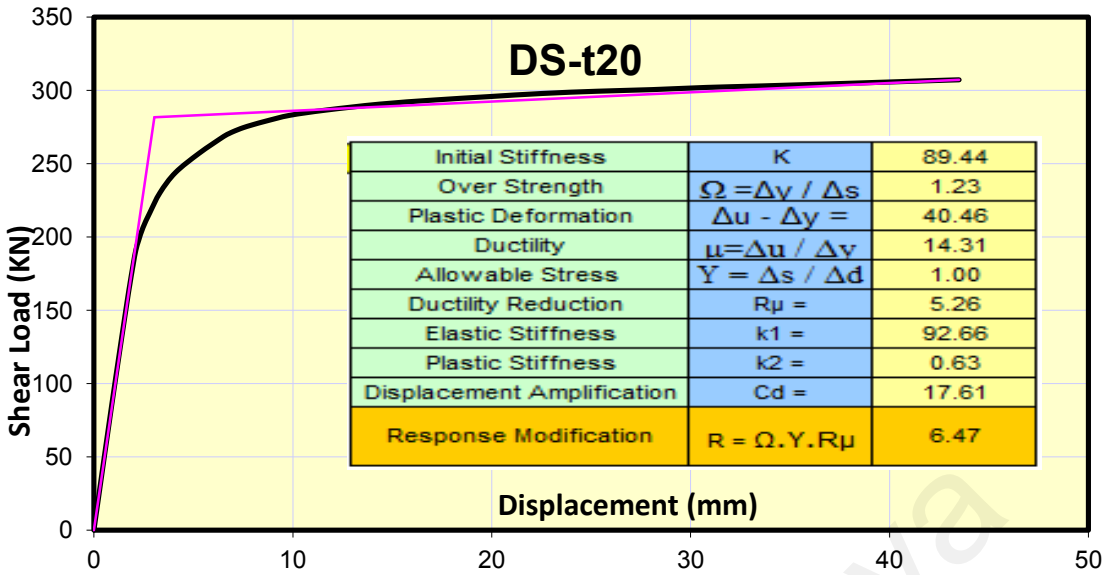

Continue Figure 5- 31 Bilinear idealization and seismic performance factors of models with 2.0 mm thickness of infill plate

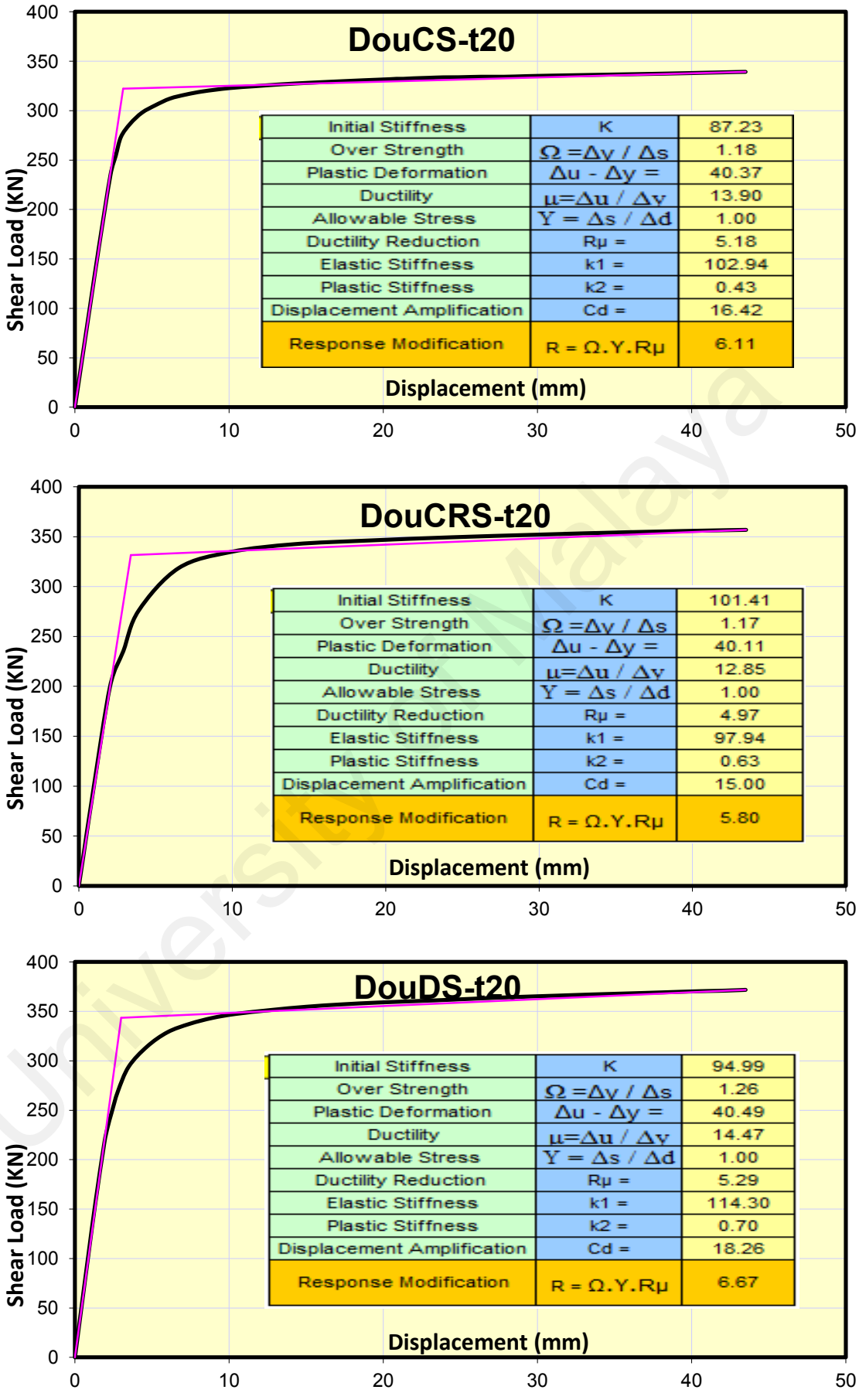

Figure 5-32 Bilinear idealization and seismic performance factors of models with 2.0 mm thickness of infill plate and double side stiffeners

5.5.3.1 Ductility and ductility reduction factor

As shown in Figure 5-33, a 29% increase of the infill thickness resulted in the ductility of unstiffened models with a 9% increase on average. Generally, comparing the unstiffened models, the use of stiffeners increased the ductility by approximately 46% (comparing the minimum stiffened model ductility to the highest ductility of un-stiffened model). The obtained ductility of the stiffened model showed a close range of value for all models. Specifically, no significant difference was found for the obtained ductility of stiffened models. Despite the increase of infill plate thickness and a small increase of ductility resulting in a one-sided stiffened model, in the case of double-sided stiffeners, the equal value of ductility was obtained for different infill plate thickness. This finding means that, for double-sided stiffened models, increasing the infill thickness has no effect on the ductility of SPSWs. Average values of ductility 8 and 13.7 were obtained for unstiffened and stiffened models, respectively. Among all stiffened models, the ductility of double-sided circular stiffened seems to be 8% lower than the average ductility of stiffened models.

The observed trend for the ductility reduction factor (Figure 5-34) is similar to that observed for the ductility. In the case of unstiffened models, due to the 29% increase in infill thickness, 3.5%–6% increase was observed for the ductility reduction factor. For stiffened models, generally, a similar value was obtained for the ductility reduction factor, and no considerable variation of values was found. On average, compared to the unstiffened models, the use of stiffeners resulted in a 30% increase in the ductility reduction factor. The variances of the ductility reduction factor of stiffened models are depicted in Figure 5-35. The negligible slope of the trend line, with a value of 5.0, can be

considered for all stiffened models, whereas 3.7 is the minimum value of the unstiffened ductility reduction factor. Through stiffened models, double-sided circular stiffened models exhibited the lowest value for the ductility reduction factor (4.94).

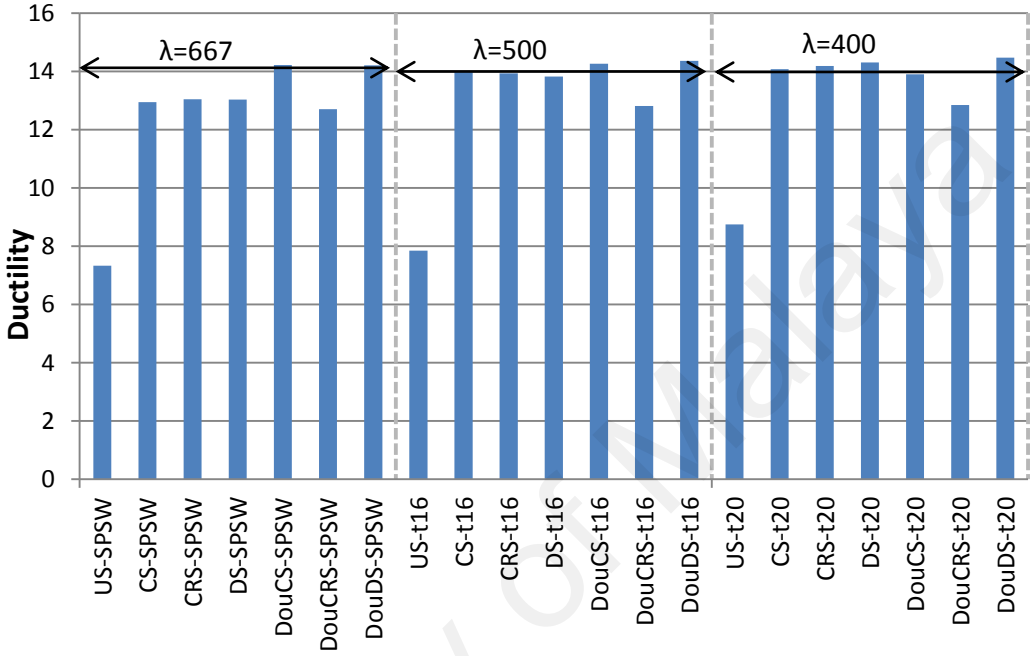

Figure 5-33 Ductility of FE models with steel infill plate

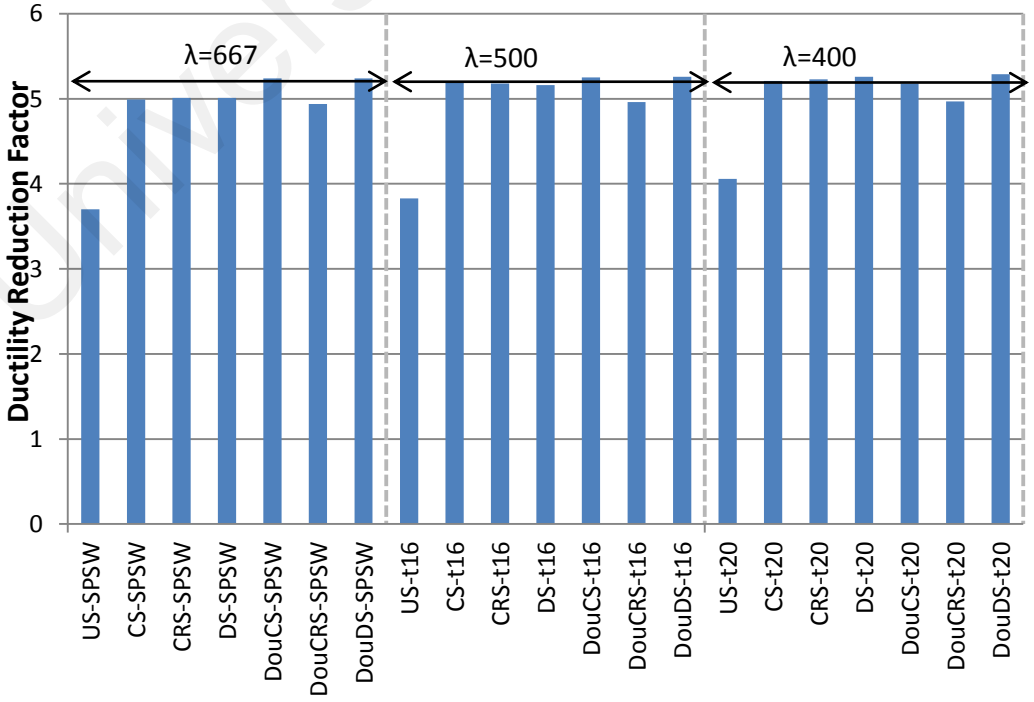

Figure 5-34 Ductility reduction factor of FE models with Steel infill plate

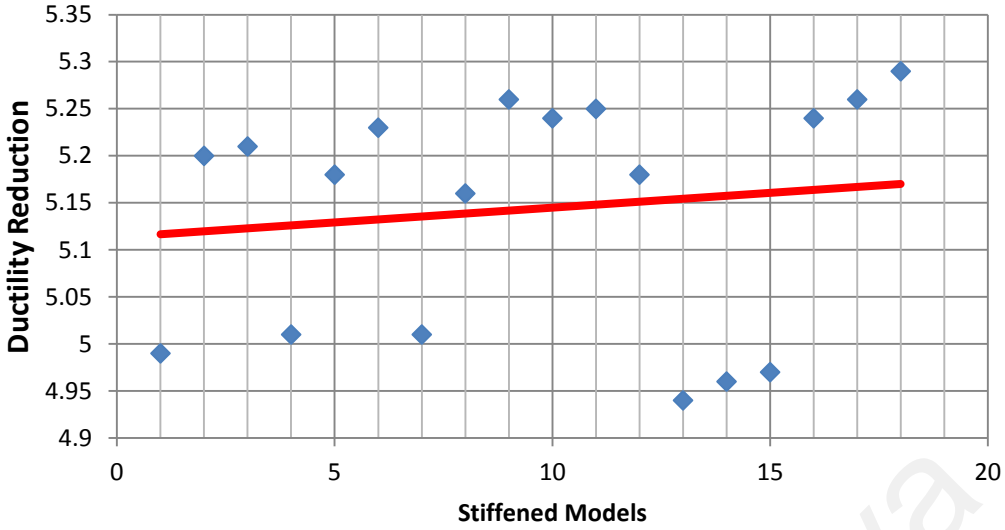

Figure 5-35 Trend line and scatter of ductility reduction factor for all stiffened models

5.5.3.2 Overstrength factor

For unstiffened models with different thicknesses of infill plate, a similar value with negligible differences was obtained for the over-strength factor. By contrast, in the case of a stiffened model, no meaningful trend was found, as shown in Figure 5-36. The average value obtained for unstiffened models is equal to 1.31, which is higher than the values obtained for stiffened models. The average obtained value of the over-strength factor of stiffened models is equal to 1.19. From the aspect of variation of the obtained value for stiffened models, as shown in Figure 5-37, the slope of the trend line is not considerable and the value of 1.20 can be used for the over-strength factor of all stiffened models. The values of 1.2 for stiffened models and 1.31 for unstiffened models improved with the use of stiffeners, leading to a 9% decrease in the over-strength factor of stiffened SPSWs. For the one-sided circular and diagonal configuration, the over-strength factor increased with the increase of infill plate.

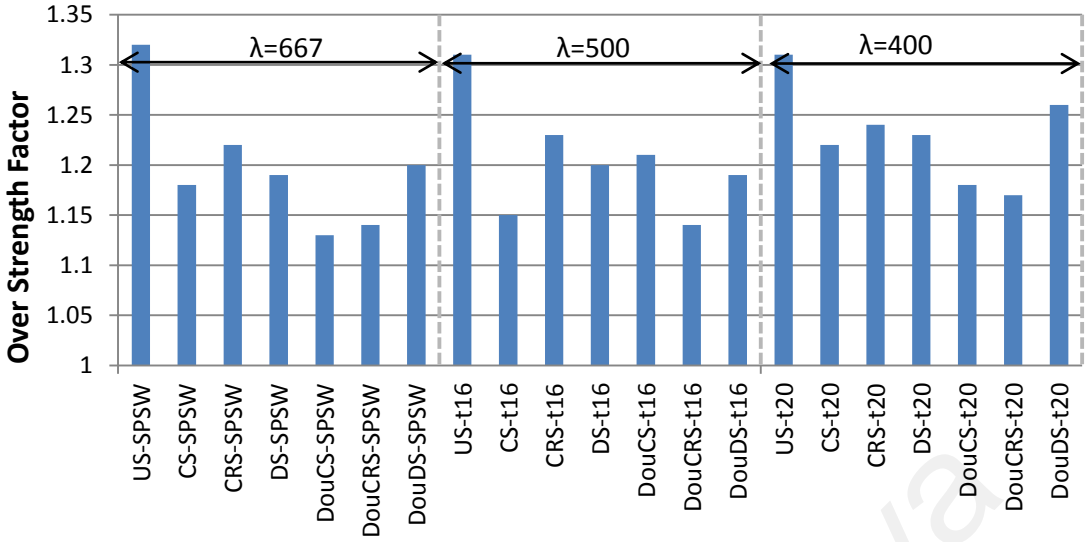

Figure 5-36 Over strength factor of FE models with steel infill plate

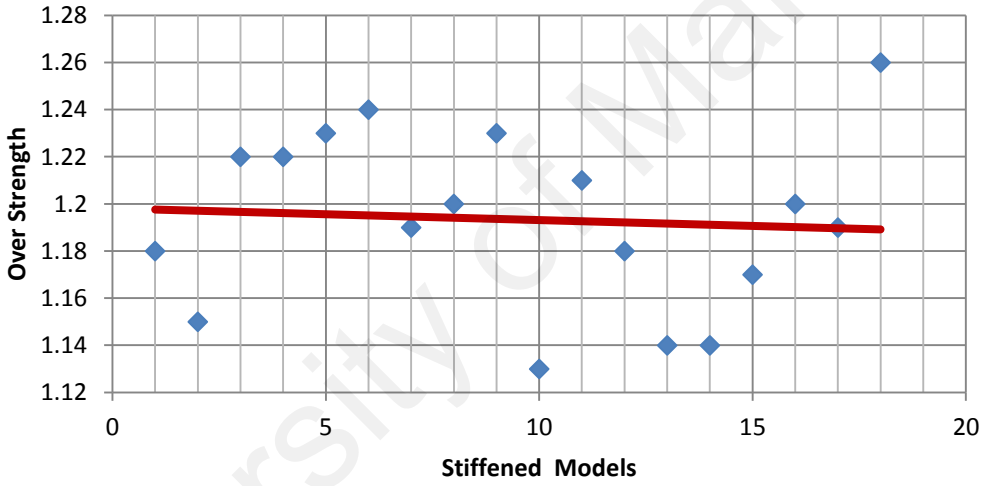

Figure 5-37 Trend line and scatter of over strength factor for all stiffened models

5.5.3.3 Displacement amplification factor

For unstiffened and one-sided stiffened models, a 29% increase of infill thickness resulted in a 6% increase of the displacement amplification factor. In a conservative estimation, the displacement amplification factor of stiffened models increased by 30% compared to the unstiffened models (Figure 5-38). Furthermore, the comparison between stiffened models showed that, for the double-sided stiffened model, the displacement amplification factor did not changed significantly, and for the double-sided circular stiffened model, this

factor decreased by 10%. The average preliminary values of 10 and 16.4 were obtained for the unstiffened and stiffened models, respectively. Figure 5-42 shows the scatter distribution of the displacement amplification factors of stiffened models. The horizontal trend line obtained for all stiffened models in Figure 5-39 indicates that the value of 16.4 could be selected as the preliminary value of the displacement amplification factor for stiffened models.

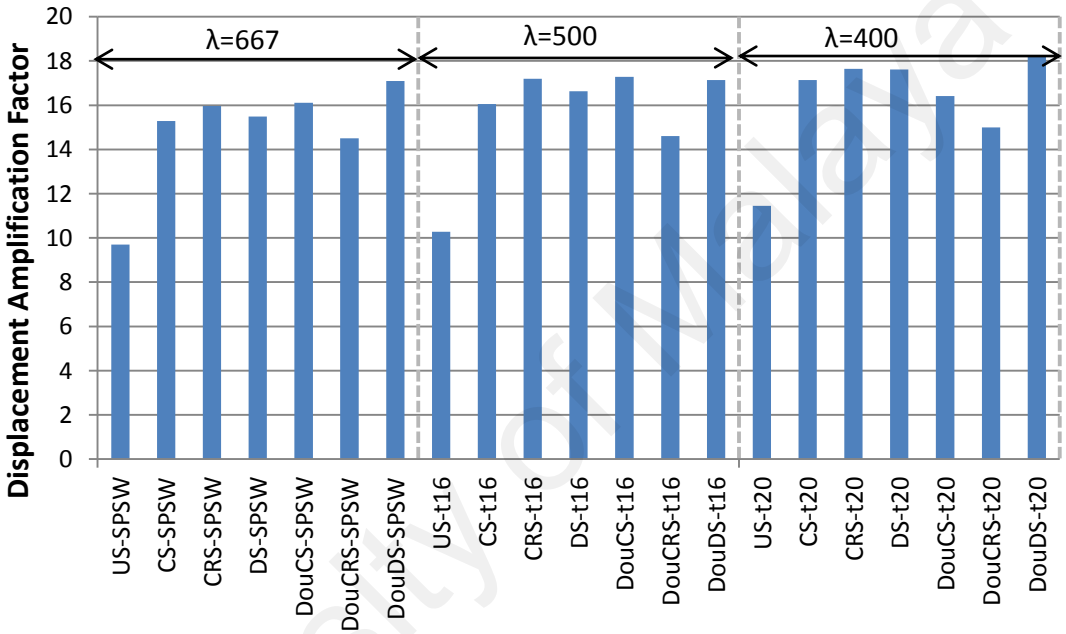

Figure 5-38 Displacement amplification factor of FE models with steel infill plate

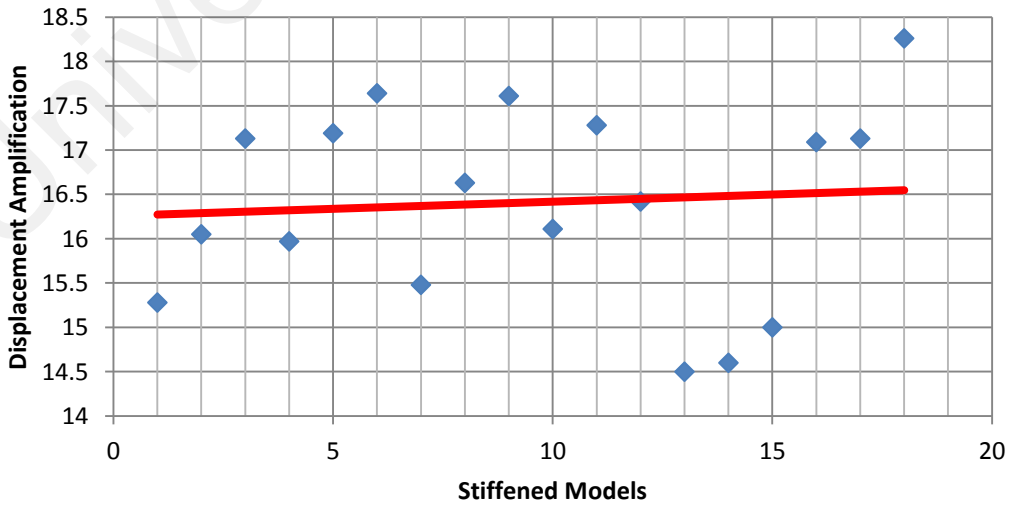

Figure 5-39 Trend line and scatter of displacement amplification factor for all stiffened models

5.5.3.4 Response (or Force) modification factor

As shown in Figure 5-40, owing to the increase in thickness of the infill plate, no substantial changes were found in the response modification factor of unstiffened and stiffened models. The use of stiffeners caused an increase in the response modification factor from an average of 5.0 to a value of 6.0. The comparison of the response modification factors of stiffened models with equal cross section of stiffeners improved that different configurations of stiffeners had a negligible effect on the variation of the obtained values. Among the stiffened models, the lowest value of the response modification factor was obtained for the double-sided circular stiffened models. Figure 5-41 exhibits the scatter of the values of response modification factors for all stiffened models. Considering the horizontal trend line of this figure, the value of 6.1 can be selected for the response modification factor of all stiffened models. As shown in Table 5-2, the value of the allowable stress factor (Y) was set to a unit. Therefore, the obtained value can be used according to the strength design method. For allowable stress design method, the obtained value should be multiplied by 1.4.

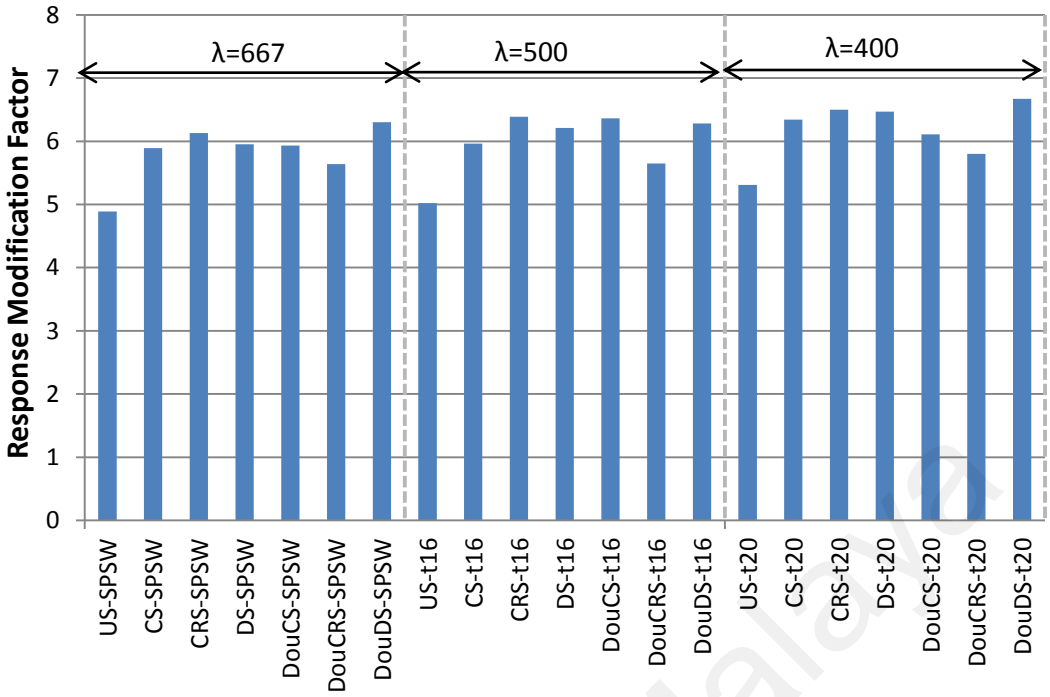

Figure 5-40 Response modification factor of FE models with steel infill plate

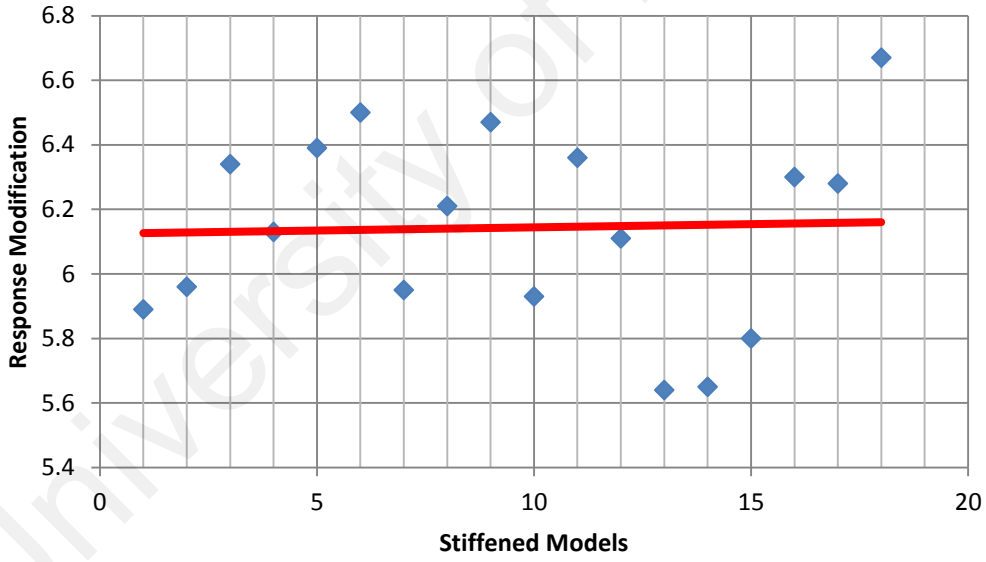

Figure 5-41 Trend line and scatter of response modification factor for all stiffened models

5.5.3.5 Calibration of the obtained S.P.F of stiffened SPSW

This part of the study evaluates the preliminary obtained value of the SPF using the methodology outlined in FEMA (2009b). In applicable cases, the obtained value was calibrated by comparing it to the valid available data.

Base on the FEMA (2009b), the system over-strength factor needs to be conservatively larger than the average calculated value. Meanwhile, the system over-strength factor is not allowed to exceed 1.5 times the response modification factor and must be defined in 0.5 increments. The maximum practical limit of the over-strength factors is 3.0. When such limitation is considered, the over-strength factor is selected to be equal to 1.5 for stiffened SPSWs with every stiffener configuration discussed above.

Table 12.2-1 of ASCE (2010) listed the value 7.0 for the response modification factor of special un-stiffened SPSWs. Astaneh-Asl (2001) suggested a value of 6.5 for the SPF of unstiffened SPSWs. In this study, the average values of 5 and 6 were obtained for the response modification factor of unstiffened and stiffened SPSWs, respectively. In particular, the obtained value should increase by 30% to be equal to the prescribed value of the response modification factor of unstiffened SPSWs. If such interpretation is considered true, then applying a 30% increase in the response modification factor (R=6) results in a value of 7.8 for stiffened SPSWs. The value of 7.8 for response modification factor of stiffened SPSWs is close to the value of R=7.0, as suggested by (Astaneh-Asl, 2001).

The displacement amplification factor could not be greater than the acceptable R value (F.E.M.A, 2009b). The damping effect also needs to be considered on the basis of the suggested equation by ASCE (2010).

$$C_d = R/B_I \qquad (5\text{-}2)$$

Where B_I is the damping factor

According to the table 18.6-1 of ASCE(2010), for a damping ratio equal to 5% and a period of structure greater than (To=0.1 sec), the B_I is equal to the unit. Therefore, the value of 7.8 is selected for stiffened SPSWs with any stiffener configuration discussed throughout this study.

5.6 ELASTIC STIFFNESS AND INITIAL STIFFNESS

For all infill thicknesses, the elastic stiffness of cross-stiffened and circular stiffened SPSW was equal and, among the stiffened models, the diagonally stiffened SPSW presents the minimum elastic stiffness (Figure 5-42). Except for the double-sided diagonally stiffened model, the comparison between one-sided to the same configuration double-sided stiffeners shows that using double-sided stiffness did not increase the elastic stiffness of relevant models considerably. The stiffness of the double-sided cross-stiffened model at an average of 6% is greater than that of double-sided circular stiffened model. Through the double-sided stiffened models, the diagonal configuration showed the highest increase in the stiffness and the circular pattern indicated the lowest increase in elastic stiffness compared to the same one-sided stiffener configuration.

As shown in Figure 5-42, in an opposite trend to the elastic stiffness, which is discussed above, the initial stiffness of the double-sided diagonally stiffened model does not possess the highest value of initial stiffness. Furthermore, except for the thin infill plate, the circular stiffener configuration (one and double side) showed the maximum initial stiffness. As shown in Figure 5-42, except for the unstiffened model, no significant differences exist between the initial and elastic stiffness of models. The initial stiffness of un-stiffened SPSWs was found to be higher than its elastic stiffness. In the case of one-sided circular stiffened SPSWs, the initial stiffness was larger than the elastic stiffness and, as the thickness of infill plate increased, the differences between initial and elastic stiffness decreased. For double-sided diagonally stiffened models, by increasing the thickness of the infill plate, the rise of

elastic stiffness value appears higher than the initial stiffness. Therefore, the difference between initial and elastic stiffness increased.

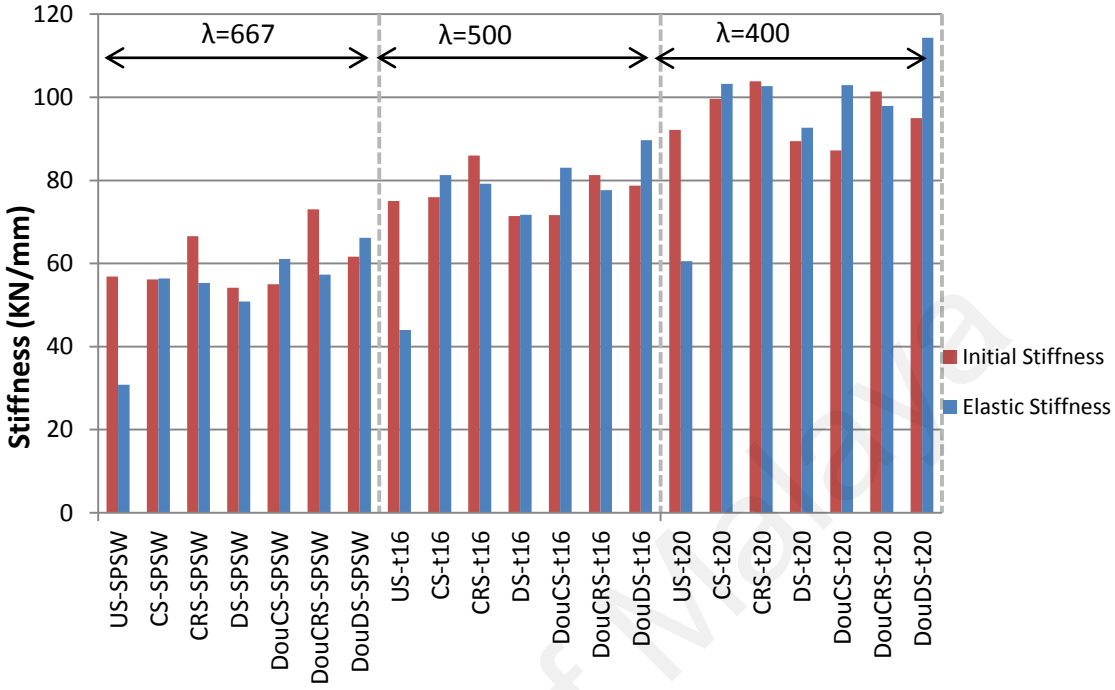

Figure 5-42 Initial and elastic stiffness of FE models with steel infill plate

5.7 SUMMARY

The main objective of the present chapter is to extend the results of the cyclic performance of SPSW with different geometric properties by adopting the validated FE model developed in Chapter 4. The models selected for this investigation include a set of SPSWs with different thicknesses of infill and slenderness of stiffener plate and with stiffeners attached on both sides of the infill plates. The aspect ratio, overall dimension of boundary frame, stiffener configurations, and other specifications of FE models and their boundary condition were kept constant and identical to the models described in Chapter 4. From the slender classification aspect, the infill plate thickness of the FE models was classified as the slender, medium, and thick infill plates. The

thickness of stiffeners that were attached on one or both sides of the infill plate was designed to ensure the achievement of shear strength of SPSWs.

The performance of the FE models, including strength, hysteresis behavior, energy dissipation, stiffness, natural periods of vibration, and SPFs, was investigated. Based on the investigation performed in this study, the conclusions could be summarized as follows:

- One-sided diagonal stiffeners did not increase the strength of the SPSW. However, for all infill thicknesses, double-sided diagonal stiffeners increased the strength of the SPSW considerably.
- Double-sided circular stiffened models displayed an increase in the strength compared to the one-sided circular stiffened models. Meanwhile, such increase was not considerable compared to the diagonally stiffened models. Among one-sided stiffened plates, the cross-stiffened models exhibited considerable increases in strength compared to the unstiffened infill plate.
- Comparing the double-sided cross-stiffened models with one-sided cross-stiffened models, no considerable differences in strength were found. Hence, from an economical aspect, the double-sided cross stiffeners are not reasonable choices.
- Increasing the thickness of the infill plate of unstiffened SPSWs improved the pinching effect. However, this effect still existed in all the hysteresis curves of unstiffened models, even for the thick infill plate.
- The double-sided diagonally stiffened model dissipated the highest amount of energy, but the one-sided and double-sided cross-stiffened models had negligible difference in the amount of absorbed energy, compared to the double-sided diagonally stiffened model.

- Among the one-sided stiffened models, the cross-stiffened model exhibited the best performance, and the diagonally stiffened model absorbed the least amount of energy.
- No significant changes were found in the absorbed energy per volume of unstiffened SPSWs with different infill thickness.
- In the medium and thick infill plates, models with flat plate (without stiffeners) displayed superior behavior in absorbing volumetric energy and were comparable with the one-sided cross-stiffened and double-sided diagonally stiffened models.
- The detailed numerical analysis of most SPSW models exhibited similar values for the natural period of vibration. For short SPSWs, this study found that the prescribed code formula exhibited a low estimation of the natural period.
- The ductility, ductility reduction factor, over-strength, and displacement amplification factor of stiffened SPSWs were not sensitive to the stiffener configuration.
- Compared to the unstiffened models, using the stiffeners resulted in a 30% increase on average in the ductility reduction factor.
- For unstiffened models with different thickness of infill plate, a similar value with negligible differences was obtained for the over-strength factor.
- The comparison of the stiffened and unstiffened models proved that using stiffeners led to a 9% decrease in the over-strength factor of the stiffened SPSWs.
- The displacement amplification factor for the stiffened models increased by 30% compared to the unstiffened models.

- Owing to the increase of the infill plate thickness, no substantial change was found in the response modification factor of the unstiffened and stiffened models. The use of stiffeners caused a 20% increase in the response modification factor for the stiffened SPSWs compared to the unstiffened SPSWs.
- The comparison of the response modification factors of stiffened models with an equal cross-section area of the stiffeners demonstrated that the differences in stiffener configuration had a negligible effect on the variation of the obtained values.
- The energy dissipation, SPFs, and cyclic performance of stiffened steel shear walls were not sensitive to the stiffener thickness and their configuration.
- For all stiffened steel shear walls with equal infill thickness and different stiffener configuration, the values of 7.8, 1.5, and 7.8 were suggested for the response modification factor, displacement amplification factor, and over-strength factor, respectively.
- The elastic stiffness values of cross-stiffened and circular stiffened SPSW were equal, and, among the stiffened models, the diagonally stiffened SPSW possessed the minimum elastic stiffness.
- Except for the double-sided diagonally stiffened model, the comparison between one-sided stiffeners to the same configuration of double-sided stiffeners showed that the former did not increase the elastic stiffness of the models considerably.

CHAPTER 6: CONCLUSIONS

6.1 CONCLUSIONS

A literature study was carried out to review the research on the steel plate shear walls. An extensive amount of research was found on the performance of un-stiffened steel plate shear walls. Comparing to the other lateral load resisting system, the distinctive behavior of SPSWs demonstrated its advantages in the aspect of energy absorption, strength and ductility, stable hysteresis curves and stiffness. Relatively limited research was found for the stiffened steel plate shear walls. Within those researches, no attention was paid on comparing the stiffeners configuration. Considering such information shortcoming, the main objective of this research which is to study the behavior and energy absorption of stiffened steel plate shear wall under lateral loading has been successfully investigated and comprehensively attained in this study. The conclusions addressing each specific objectives listed in Chapter 1 are as follows:

1. To examine experimentally the behavior of stiffened SPSWs with different stiffeners configuration, five specimens were designed and prepared. Considering the available facility in the location of research, the quasi-static cyclic loading is selected for the present investigation. From five test specimens, two specimens were un-stiffened aluminum and steel plate, whereas another three specimens were stiffened with cross, circular and diagonal stiffeners on one side of the steel infill plate. The cross section area of the stiffeners was kept constant. Two unstiffened specimens were fabricated for comparison purpose. The results of the stiffened specimens showed that installation of stiffeners has increased the stiffness considerably rather than the shear strength.

Comparing with the un-stiffened specimens, the buckling behaviors of all stiffened specimens were improved and the buckling mode was governed by the stiffener configuration. The stiffeners has increased the shear stiffness, energy dissipation and ductility considerably, especially for the cross-stiffened (CS-SPSW). The highest amounts of stiffness, dissipated energy and ductility belong to the CS-SPSW, while its stiffness degradation is not favorable.

2. Using commercial software ABAQUS, finite element models of the tested specimens were developed. A comparison of the predicted behavior of five FE models with the test results indicated that the developed finite element model is able to provide a reliable prediction of the strength, stiffness, yielding point, pinching of hysteresis curve and energy absorption of the SPSWs subjected to cyclic and monotonic loading. To conduct the parametric study, the validated FE procedure was used.
3. To investigate the effect of geometric properties of stiffened SPSWs with different stiffeners configurations on the cyclic behavior of stiffened SPSWs, a series of parametric studies was conducted. It was found that the energy dissipation, seismic performance factors and cyclic performance of stiffened steel shear walls were not sensitive to the stiffeners thickness and their configuration. One-sided cross-stiffened models and double-sided diagonally stiffened models exhibited considerable increases in the strength compared to the un-stiffened infill plate.
4. For all stiffened steel shear walls with equal infill plate thickness and different stiffeners configuration, the value of 7.8, 1.5 and 7.8 were

suggested for the response modification factor, displacement amplification factor and the over strength factor respectively (Ω=1.5 R=7.8 C_d= 7.8). Furthermore, comparing to the un-stiffened SPSWs, the utilization of stiffeners has resulted in 30% increase in the ductility reduction factor, 9% decrease in the over strength factor and 20% increasing in the response modification factor for stiffened SPSWs.

6.2 FUTURES RESEARCH RECOMMENDATIONS

Based on the limitations of the present study and other existing gaps, some recommendations for future research are described in this section.

- The aspect ratio influences the behavior of the SPSWs. In this study, the aspect ratio was equal to one. To obtain optimum performance of the stiffened SPSWs, based on the specific aspect ratio, special stiffeners configuration could be proposed.
- During the fabrication of the stiffened SPSWs, due to the welding of stiffeners to infill plate, extensive deformation of the infill plate were observed. Such deformation affected the overall behavior of the specimens. Studying the residual stresses seems to be crucial in this case.
- To obtain reliable results, the performance of the stiffened SPSWs needs to be investigated in the multi-story SPSWs in the presence of the gravity loads.
- Owing to the thin thickness, SPSWs are vulnerable in the fire incident and the fire protection of the SPSWs needs to be study.
- The performance of the stiffened SPSWs under the effect of the explosion loads requires more investigation.

- The test results of the aluminum infill plate showed that low-rapture material did not behave ideally. The revision and modification factor can be proposed based on the material properties of the infill plate of SPSWs.
- Hinged boundary frame was used in this investigation. The result of the stiffened SPSWs requires verification for moment connection in the boundary frames.

REFERENCES:

A. T. C. 1996. Seismic Evaluation and Retrifit of Concrete Buildings Volume 1 (ATC-40). California: Seismic Safety Commision.

A.A.S.H.T.O 2007. LRFD Bridge design specification, 4th edition SI unit. American Association of State Highway and Transportation Officials.

A.I.S.C 2005. Seismic provisions for structural steel buildings (including supplement no. 1). ANSI/AISC 341-05 and ANSI/AISC 341s1-05. Chicago, Illinois: American Institute of Steel Construction.

A.I.S.C 2010. Specification for structural steel buildings. ANSI/AISC 360-10. Chicago, Illinois: AISC 2010.

A.S.C.E 2010. Minimum design loads for buildings and other structures (ASCE/SEI 7-10). Reston, Virginia: American Society of Civil Engineers.

A.T.C 1978. Tentative provisions for the developement of seismic regulations for buildings. ATC 3-06.

A.T.C 1992. Guidline for cyclic seismic testing of components of steel structures (ATC 24). Redwoodcity, CA.: Applied Technology Council.

A.T.C 1995. Structural response modification factors ATC 19. California: Applied Technology council.

Abdollahzadeh, G. & Malekzadeh, H. 2013. Response modification factor of coupled steel shear walls. Civil Engineering Infrastructures Journal, 46, 15-26.

Alavi, E. & Nateghi , F. 2012. Experimental study of diagonally stiffened steel plate shear walls. Journal of Structural Engineering (ASCE), 139.

Alavi, E. & Nateghi , F. 2013. Experimental study on diagonally stiffened steel plate shear walls with central perforation. Journal of Constructional Steel Research, 89, 9-20.

Alinia, M. M. & Dastfan, M. 2007. Cyclic behaviour, deformability and rigidity of stiffened steel shear panels. Journal of Constructional Steel Research, 63, 554-563.

Alinia, M. M. & Sarraf Shirazi, R. 2009. On the design of stiffeners in steel plate shear walls. Journal of Constructional Steel Research, 65, 2069-2077.

Astaneh-Asl, A. 2001. Seismic Behavior and design of steel shear walls. SEOANC Seminar. Northern California, San Francisco.

B.S. 2001. Metallic materials - Tensile testing Part 1: Method of test at ambient temperature. British Standard.

Bakhshi, A. & Aslani, J. 2012. Study on Response modification factor for stiffened steel shear wall systems. 15 WCEE. Lisboa.

Bathe, K. J. 1996. Finite element procedures, New Jersy, Prentice Hall.

Behbahanifard, M. R., Gordin, G. Y. & Elwi, A. E. 2003a. Experimental and numerical investigation of steel plate shear walls. PhD Structural Engineering Report No .254, University of Alberta.

Behbahanifard, M. R., Grondin, G. Y. & Elwi, A. 2003b. Cyclic behaviour of unstiffened steel plate shear walls. Phd Dissertation, University of Alberta.

Berman, J. W. & Bruneau, M. 2003. Plastic analysis and design of steel plate shear walls. Journal of Structural Engineering ASCE, November, 1448-1456.

Bhowmick, A. K., Driver, R. G. & Grondin, G. Y. 2009. Seismic analysis and design of steel plate shear walls. PhD Dissertation, University of Alberta.

Caccese, V., Elgaaly, M. & Chen, R. 1993. Experimental study of thin steel plate shear walls under cyclic load. Journal of Structural Engineering ASCE, 119, 573-587.

Choi, I. & Park, H. 2008. Cyclic test for framed steel plate walls with various infill plate details. The 14 th World Conference on Earthquake Engineering. Beijing, China.

Choi, I. R. & Park, H. G. 2009. Steel plate shear walls with various infill plate designs. Journal of Structural Engineering ASCE, JULY, 785-796.

Driver, R. G. 1997. Seismic Behaviour of steel plate shear walls. PhD Dissertation University of Alberta.

Dubina, D., Dinu, F. & Neagu, C. 2012. Global performance of steel frames of shear walls. Stessa 2012 – Mazzolani & Herrera (eds). Taylor & Francis Group, London, ISBN 978-0-415-62105-2.

F.E.M.A 2003-2006. NEHRP recommended provisions for seismic regulations for new buildings and other structures (FEMA 450). Part 1: Provisions. National Institute of Building Sciences.

F.E.M.A 2005. Improvement of nonlinear static seismic analysis procedures. FEMA 440. Redwood City, California: Applied Technology Council (ATC-55 Project).

F.E.M.A 2007. Interim testing protocols for determining the seismic performance characteristics of structural and nonstructural component. FEMA 461. Redwood City, California: Applied Technology Council.

F.E.M.A 2009a. Quantification of building seismic performance factors. FEMA P695. Redwood City, California: Applied Technology Council.

F.E.M.A 2009b. Quantification of building seismic performance factors (FEMA P695-ATC 63). Redwood City, California.

Gholhaki, M. & Sabouri-Ghomi, S. 2009. Effect of ductility factor on force modification factor of thin steel plate shear walls. Journal of Structure & Steel, 5, 52-63.

Gholipour, M. & Alinia, M. M. 2016. Behavior of multi-story code-designed steel plate shear wall structures regarding bay width. Journal of Constructional Steel Research, 122, 40-56.

Guo, H., Hao, J. & Liu, Y. 2015. Behavior of stiffened and unstiffened steel plate shear walls considering joint properties. Thin-Walled Structures, 97, 53-62.

Guo, H., Li, Y., Liang, G. & Liu, Y. 2017. Experimental study of cross stiffened steel plate shear wall with semi-rigid connected frame. journal of Constructional Steel Research, 135, 69-82.

Hibbitt, Karlsson & Sorenson 2000. ABAQUS/Explicit user's manual, Hibbitt, Karlsson & Sorensen, Inc. 2000.

Hosseinzadeh, S. A. A. & Tehranizadeh, M. 2012. Introduction of stiffened large rectangular openings in steel plate shear wall. Journal of Constructional Steel Research 77, 180-192.

Hunter, D. A. N. 2010. Welding of light gauge infill panels for steel plate shear walls. Msc, University of Alberta.

Ibarra, L. F., Medina, R. A. & Krawinkler, H. 2005. Hysteretic models that incorporate strength and stiffness deterioration. Earthquake Engineering and Structural Dynamics, 34, 1489-1511.

Jiang, L., Zheng, H. & Hu, Y. 2017. Experimental seismic performance of steel- and composite steel-panel wall strengthened steel frames. Archives of Civil and Mechanical Engineering, 17, 520-534.

Kharazi, M. H. K., Ventura, C. E. & Prion, H. 2005. Rational method for analysis and design of steel plate walls. PhD Dissertation, British Columbia.

Kharazi, M. H. K., Ventura, C. E., Prion, H. G. L. & Sabouri-Ghomi, S. 2004. Bending and shear analysis and design of ductile steel plate walls. 13th World Conference on Earthquake Engineering. Vancouver, B.C., Canada.

Kurban, C. O. & Topkaya, C. 2009. A numerical study on response factors for steel plate shear wall systems. Msc, Middle East Thechnical University.

Lubell, A. S., Prion, H. & Ventura, C. E. 1997. Performance of unstiffened steel plate shear walls under cyclic quasi-static loading. Msc, British Colombia University.

Lubell, A. S., Prion, H. G. L., Ventura, C. E. & Rezai, M. 2000. Unstiffened steel plate shear wall performance under cyclic loading. Journal Of Structural Engineering, april, 453-460.

Meng, W., Weiguo, Y., Yongjiu, S. & Jian, X. 2015. Seismic behaviors of steel plate shear wall structures with construction details and materials. Journal of Constructional Steel Research, 107, 194-210.

Mimura, H. & Akiyana, H. 1977. Load-deflection relationship of earthquake-resistant steel shear walls with a developed diagonal field (in Japanese). Transactions of the Architectural Institute of Japan, 260, 109-114.

Newmark, N. M. & Hall, J. 1982a. Earthquake engineering Spectra and design, El Cerrito.

Newmark, N. M. & Hall, W. J. 1982b. Earthquake spectra and design., University of Illinois at Urbana Champaign, Earthquake Engineering Research Institute.

Nie, J. G., Zhu, L., Fan, J. S. & Mo, Y. L. 2013. Lateral resistance capacity of stiffened steel plate shear walls. Thin-Walled Structures, 67, 155-167.

Nooralizadeh, A., Naghipour, M., Nematzadeh, M. & Zamenian, H. 2017. Experimental evaluation of steel plate shear walls stiffened with folded sheets. International Journal of Steel Structures, 17, 291-305.

Pubra, R. H. & Bruneau, M. 2006. Design Recommendations for Perforated Steel Plate Shear Walls. Msc thesis, State University of New York.

Qu, B., Gua, X., Pollino, M. & Chi, H. 2013. Effect of column stiffness on drift concentration in steel plate shear walls. Journal of Constructional Steel Research, 83, 105-116.

Rezai, M., Ventura, C. E. & Prion, H. G. L. 1999. Seismic behaviour of steel plate shear walls by shake table testing. Phd Dissertation, University of British Colombia.

Roberts, T. M. & Ghomi, S. S. 1991. Hysteretic characteristics of unstiffened plate shear panels. Thin-Walled Structures, 12, 145-162.

Roberts, T. M. & Sabouri-Ghomi, S. 1992. Hysteretic characteristics of unstiffened perforated steel plate shear panels. Thin-Walled Structures, 14, 139-151.

Sabelli, R. & Bruneau, M. 2007. (AISC 820-06) Steel design guide- steel plate shear walls American Institute of Steel Construction.

Sabouri-Ghomi, S. & Asasd-Sajadi, S. R. 2008. Experimental investigation of force modification factor and energy absorption ductile steel plate shear walls with stiffeners and without stiffener (in Persian). Journal of Structure & Steel, 4, 13-25.

Sabouri-Ghomi, S. & Mamazizi, S. 2015. Experimental investigation on stiffened steel plate shear walls with two rectangular openings. Thin-Walled Structures, 86, 56-66.

Sabouri-Ghomi, S. & Roberts, T. M. 1991. Nonlinear dynamic analysis of thin steel plate shear walls. Computers & Structures, 39, 121-127.

Sabouri-Ghomi, S. & Roberts, T. M. 1992. Nonlinear dynamic analysis of steel plate shear walls including shear and bending deformations. Engineering Structures, 14, 309-317.

Sabouri-Ghomi, S. & Sajjadi, R. A. 2012. Experimental and theoretical studies of steel shear walls with and without stiffeners. Journal of Constructional Steel Research, 75, 152-159.

Sabouri-Ghomi, S., Ventura, C. E. & Kharrazi, M. H. K. 2005. Shear analysis and design of ductile steel plate walls. Journal of Structural Engineering ASCE, June, 878-889.

Schumacher, A., Gordin, G. Y. & Kulak, G. L. 1999. Connection of infill panels in steel plate shear walls. Canadian journal of Civil Engineering, 26, 549-563.

SEAOC 2008. SEAOC Blue book: Seismic design recommendations. Sacramento, CA: Structural Engineering Association Of California, Seismology Commitee.

Sigariyazd, M. A., Joghataie, A. & Attari, N. K. A. 2016. Analysis and design recommendations for diagonally stiffened steel plate shear walls. Thin-Walled Structures, 103, 72-80.

Simulia, D. S. 2009a. ABAQUS Analysis users manual- volume I: introduction, spatial modeling, execution & output, providence, RI, USA., Dassault Systèmes Simulia Corp.

Simulia, D. S. 2009b. ABAQUS Analysis users manual- volume II: analysis, providence, RI, USA., Dassault Systèmes Simulia Corp.

Simulia, D. S. 2009c. ABAQUS Analysis users manual- volume III: materials, providence, RI, USA., Dassault Systèmes Simulia Corp.

Simulia, D. S. 2010. ABAQUS Getting started with abaqus-interactive edition, providence, RI, USA., Dassault Systèmes Simulia Corp.

Takahashi, Y., Takemoto, Y., Takeda, T. & Takagi, M. 1973. Experimental study on thin steel shear walls and particular bracings under alternative horizontal load, preliminary report, IABSE Symposium on Resistance and Ultimate Deformability of Structures Acted on by Well-defined Repeated Loads. Lisbon, Portugal.

Thorburn, L. J., KULAK, G. L. & MONTGOMERY, C. J. 1983. Analysis of steel plate shear wall (Structural engineering report No.107). PhD thesis Structural engineering report No.107, University of Alberta.

Timler, P. A. 1983. Experimental study of steel plate shear walls (Structural Report No.114). Msc thesis Master Thesies, University of Alberta.

Timler, P. A. & Kulak, G. L. 1983. Experimental study of steel plate shear walls (Structural Engineering Report No. 114). PhD Structural Engineering Report No. 114, University of Alberta.

Tromposch, E. W. 1987. Cyclic and static behaviour of thin panel steel plate shear walls. Msc Thesies, University of Alberta.

Uang, C. M. 1991. Establishing R (or Rw) and Cd factors for building seismic provisions Journal of Structural Engineering ASCE, 117, 19-28.

Uang, C. M. & Maarouf, A. 1996. Evaluation of displacement amplification factor for seismic design provisions. Boston: Northeastren University.

Valizadeh, H., Sheidaii, M. & Showkati, H. 2012. Experimental investigation on cyclic behavior of perforated steel plate shear walls. Journal of Constructional Steel Research, 70, 308–316.

Veladi, H., Armaghani, A. & Davaran, A. 2007. Experimental investigation on cyclic behavior of steel shear walls. Asian Journal Of Civil Engineering, 8, 63-75.

Vian, D. & Bruneau, M. 2005. Steel plate shear walls for seismic design and retrofit of building structures. PhD thesis, University of Buffalo.

Zhang, X. & Guo, Y. 2014. Behavior of steel plate shear walls with pre-compression from adjacent frame columns. Thin-Walled Structures, 77, 17-25.

Zhao, Q. & Qiu, J. 2016. Nonlinear analyses of stiffened steel plate shear walls considering gravity effects. Proceedings of the Annual Stability Conference Orlando, Florida: Structural Stability Research Council.

LIST OF PUBLICATIONS

Haddad, O., N. H. Ramli, et al. (2018). "Cyclic performance of stiffened steel plate shear walls with various configuration of stiffeners." Journal of Vibroengineering 20(1): 459-476, DOI: https://doi.org/10.21595/jve.2017.18472.

Haddad, O., Ramli, N.H.R. and Ibrahim, Z. “Characterizing the cyclic behavior of stiffened SPSWs.” Accepted paper, KSCE journal, Manuscript No. KSCE-D-18-01038.

Haddad, O., Ramli, N.H.R. and Ibrahim, Z. The effect of axial loads on the behavior of steel plate shear walls. Under review paper.